University of Alberta

QUANTIFICATION OF SOIL HETEROGENEITY

By

Tamer M. Elkateb

©

A thesis submitted to the Faculty of Graduate Studies and
Research in partial fulfillment of the requirements for the
degree of Doctor of Philosophy

in

Geotechnical Engineering

Department of Civil and Environmental Engineering

Edmonton, Alberta

Spring 2003

National Library
of Canada

Bibliothèque nationale
du Canada

Acquisitions and
Bibliographic Services

Acquisisitons et
services bibliographiques

395 Wellington Street
Ottawa ON K1A 0N4
Canada

395, rue Wellington
Ottawa ON K1A 0N4
Canada

The author has granted a non-exclusive licence allowing the National Library of Canada to reproduce, loan, distribute or sell copies of this thesis in microform, paper or electronic formats.

L'auteur a accordé une licence non exclusive permettant à la Bibliothèque nationale du Canada de reproduire, prêter, distribuer ou vendre des copies de cette thèse sous la forme de microfiche/film, de reproduction sur papier ou sur format électronique.

The author retains ownership of the copyright in this thesis. Neither the thesis nor substantial extracts from it may be printed or otherwise reproduced without the author's permission.

L'auteur conserve la propriété du droit d'auteur qui protège cette thèse. Ni la thèse ni des extraits substantiels de celle-ci ne doivent être imprimés ou aturement reproduits sans son autorisation.

Canada

University of Alberta

Library Release Form

Name of Author: Tamer Mohamed Elkateb

Title of Thesis: Quantification of Soil Heterogeneity

Degree: Doctor of Philosophy

Year This Degree Granted: 2003

Permission is hereby granted to the University of Alberta Library to reproduce single copies of this thesis and to lend or sell such copies for private, scholarly or scientific research purposes only.

The author reserves all other publication and other rights in association with the copyright in the thesis, and except as herein before provided, neither the thesis nor any substantial portion thereof may be printed or otherwise reproduced in any material form whatever without the author's prior written permission.

506 Michener Park
Edmonton, Alberta
Canada, T6H 4M5

Date: April 10th, 2003

University of Alberta

Faculty of Graduate Studies and Research

The undersigned certify that they have read, and recommended to the Faculty of Graduate Studies and Research for acceptance, a thesis entitled *Quantification of Soil Heterogeneity* submitted by **Tamer Elkateb** in partial fulfillment of the requirements for the degree of Doctor of Philosophy in Geotechnical Engineering.

Rick Chalaturnyk, Assistant Professor
(Supervisor)
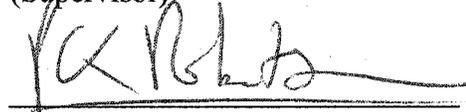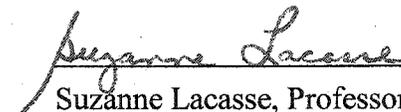
Peter K. Robertson, Professor
(Co-supervisor)

Norbert R. Morgenstern, Professor
Emeritus

Clayton V. Deutsch, Professor

Vadim Kravchinsky, Assistant
Professor

Suzanne Lacasse, Professor
(External Examiner)

Date: February 25th, 2003

ABSTRACT

Almost all natural soils are highly variable and rarely homogeneous. Soil heterogeneity can be classified into two main categories. The first category is lithological heterogeneity, which can be manifested in the form of soft/stiff small soil volumes embedded in a stiffer/softer larger media of different soil types. The second source of heterogeneity can be attributed to soil inherent spatial variability, which is the variation of soil properties from one point to another in space due to variation of deposition conditions and loading history.

The main objective of this study is to clearly understand the design consequences of soil heterogeneity and to investigate different ways to incorporate it into geotechnical engineering design framework. This has been applied to static problems, such as shallow foundation settlement, and dynamic problems, such as liquefaction assessment.

The effect of different types of heterogeneity on the macro behavior of soil under static loading has been investigated through deterministic numerical analysis with stochastic input soil parameters. A shallow foundation resting on heterogeneous soil media was adopted as a consistent example for demonstrating the influence of ground heterogeneity on static geotechnical field problems. In addition, co-depositional fine tailings – sand embankments were analysed to assess the impact of lithological heterogeneity on the stability of such innovative tailings disposal systems.

Dynamic problems have been addressed through analysis of well-documented case histories of potentially liquefiable sites in California, USA. Empirical techniques were adopted in the analyses of these sites. Cone penetration test (CPT) data recorded at these sites were used to identify different lithologies and to assess different elements of soil inherent spatial variability. These elements were applied to perform liquefaction analyses of these sites in a probabilistic analysis framework.

This research study indicated that the influence of soil heterogeneity on its engineering behavior is problem-dependent. Quantitative assessment of this influence can be obtained by separate comprehensive analyses of each geotechnical field problem. Using mean values of soil properties in deterministic geotechnical analyses was found to be on the unsafe (non-conservative) side. In addition, a list of characteristic risk-based soil parameters for different applications is provided for use in engineering design.

ACKNOWLEDGMENT

Thanks are due to many people who, over the course of this study, provided me with an enormous help and encouragement. This acknowledgment is but a small appreciation for their priceless support.

The guidance, enthusiasm and encouragement of Dr. Rick Chalaturnyk, my main supervisor, were instrumental in achieving the goals of this work. It was really a wonderful experience working with such nice individual. I thank him for his support, for the unique mentoring environment he provided and for the valuable discussions we had.

I also thank Professor Peter K. Robertson, my co-supervisor, for his assistance and vision. His ideas, comments and thorough review of the thesis have greatly contributed towards the completion of this research study.

The Geotechnical Engineering Group at the University of Alberta, both staff and colleagues, provided an exceptionally cooperative and friendly environment. I also thank Dr. Hassan Elramly, my former office mate, for the helpful discussions we had during the progress of this research. Appreciation is extended to Dr. Clayton Deutsch, mining group, for his help in geostatistics aspects and for the guidance he provided me. Thanks are also extended to the geotechnical staff at Ain Shams University, Cairo, Egypt for the quality of education they provided me in my undergraduate and my master studies.

I would also like to express my gratitude to my wife Rehab for being such a wonderful, supportive, and caring person during these long years of study. I am greatly indebted to my parents and my brother Mahmoud for their continuous support, love and encouragement.

Finally, I'd like to dedicate this work to God and to my home country Egypt.

TABLE OF CONTENTS

LIST OF TABLES

LIST OF FIGURES

CHAPTER 1

INTRODUCTION

1.1. STATEMENT OF THE PROBLEM

Almost all natural soils are highly variable in their properties and rarely homogeneous. Soil heterogeneity can be classified into two main categories. Lithological heterogeneity, which can be manifested in the form of thin soft/stiff layers embedded in a stiffer/ softer media or the inclusion of pockets of different lithology within a more uniform soil mass. The second source of heterogeneity can be attributed to soil inherent spatial variability, which is the variation of soil properties from one point to another in space due to different deposition environment and loading history.

Early attention to the problem of soil non-homogeneity emerged from the field of petroleum engineering where efforts were devoted towards assessing the effect of heterogeneity on the production of oil fields. This was prominently applied to estimate representative hydraulic conductivity values for the field of interest that honored detailed ground heterogeneity. On the other hand, geotechnical practice has generally relied on increased safety factors and experiential judgment to deal with different types of ground heterogeneity. Deterministic analyses have usually been conducted on simplified ground profiles with the selection of single-valued soil parameters to represent each lithological unit.

Early attempts to rationally deal with the variability of soil properties in geotechnical engineering involved the introduction of reliability-based design methods that combined limit equilibrium analysis with Monte Carlo simulation technique. This was followed by the introduction of different types of stochastic finite element analysis as an effective way to incorporate soil spatial variability into a numerical analysis

- 1 -

framework. It is worth noting that almost no attention has been given to assess the effect of lithological heterogeneity on the macro (overall) behavior of heterogeneous soil media. The treatment of such heterogeneity has been exclusively left to local experience and engineering judgment.

It has been readily acceptable, recently, that unavoidable degrees of uncertainty are usually involved in geotechnical design and that the main source of such uncertainty is the difficulty associated with selecting design parameters for different field problems. As a result, implementation of statistical techniques into geotechnical analysis has become a valuable tool to assess the implications of ground variability on engineering behavior of soils under different loading conditions. Since geotechnical engineers usually have limited statistical backgrounds, there has been a need to ascertain whether methods can be developed to obtain risk-based representative soil parameters for use in simplified deterministic analysis, while continuing to honor detailed ground heterogeneity.

1.2. OBJECTIVES OF THE RESEARCH PROGRAM

The main objective of this research study is to quantify the effect of ground heterogeneity on the macro behavior of soil under static and dynamic loadings. This is accomplished by:

1. Assessing the consequences of lithological heterogeneity and inherent spatial variability of soil properties on the engineering behavior of soil;
2. Providing methods to obtain risk-based characteristic (representative) design parameters of soil that honors detailed ground heterogeneity;
3. Examining the safety level associated with the current state of practice in some geotechnical applications, such as shallow foundation and liquefaction assessment;
4. Studying the applicability of up-scaling techniques and homogenization theories in geotechnical design scheme; and

- 2 -

5. Developing a risk-based design approach for co-depositional sand – fine tailings embankments, where lithological heterogeneity is manifested in fine tailings pockets spatially distributed in a bigger uniform sand mass.

1.3. THESIS OUTLINE

In order to achieve the objectives mentioned in the previous section, this study has passed through several stages as outlined below.

In Chapter 2, a detailed review of literature is provided. This covers various topics in petroleum engineering literature relevant to the scope of this study, such as up-scaling techniques and homogenization theories. Basic principles of geostatistics necessary to identify different elements of soil spatial variability are summarized. Attempts made by geotechnical engineers to incorporate soil spatial variability into probabilistic analysis framework are discussed together with their implementation into geotechnical field problems, such as shallow foundation and liquefaction assessment. In addition, different decision making algorithms are presented with examples of their applications in the field of geotechnical engineering.

In Chapter 3, the effect of lithological heterogeneity on the macro behavior of soil is investigated. This has been carried out through numerical analysis of a theoretical model consisting of a thin soft clay layer embedded into a uniform rectangular mass of sand under plane strain conditions. The applicability of up-scaling techniques commonly used in petroleum engineering literature to the theoretical model is examined. In addition, the results obtained from the theoretical model are applied to a shallow foundation problem to investigate their applicability to geotechnical field problems.

In Chapter 4, the effect of a different form of lithological heterogeneity is investigated. The engineering behavior of co-depositional sand - fine tailings

embankments, where pockets of fine tailings are randomly distributed in a bigger mass of medium dense sand is assessed. This has been carried out using numerical analysis and implementing multiple realizations of the spatial distribution of the fine tailings pockets within the sand mass. The safety level of this tailings disposal system is investigated in terms of failure probability and associated vertical displacements.

In Chapter 5, the effect of inherent spatial variability of soil properties on the macro behavior of soil is studied in a probabilistic analysis framework. This has been carried out through stochastic numerical analysis of a theoretical model of spatially variable rectangular sand mass under plane strain conditions. The effect of different elements of soil spatial variability on soil mechanical behavior under static loading is quantified. In addition, attempts have been made to develop risk-based characteristics (equivalent) elastic modulus of sand that can be used in engineering design.

In Chapter 6, the effect of inherent spatial variability of soil properties on the behavior of shallow foundation is investigated in a probabilistic analysis framework. This has been carried out through stochastic numerical analysis of a strip footing resting on a spatially variable sand medium. An attempt is made to assess the safety level associated with the current state of practice and to obtain a risk-based characteristic elastic modulus that can be used in simplified deterministic analyses while continuing to honor detailed ground heterogeneity. The stochastic analyses outcomes are compared with the results obtained in Chapter 5 to examine the sensitivity of stochastic analyses to changes in stress path and boundary conditions.

In the Chapter 7, a simplified geostatistical analysis of liquefaction-induced ground response at the Wildlife site, California, is presented. Cone penetration test (CPT) results are implemented into a geostatistical analysis framework to assess the effect of ground heterogeneity on soil behavior under dynamic loading. Different criteria used to quantify liquefaction-induced damage are examined and attempts are made to obtain risk-

based characteristic CPT parameters that can be used in simplified deterministic liquefaction analyses.

In Chapter 8, a geostatistical analysis of earthquake-induced ground response at the Treasure Island site, California, is provided in a fashion similar to Chapter 7. An attempt is made to examine the applicability of the results obtained in the previous chapter to other liquefaction case histories.

In Chapter 9, a geostatistical analysis of liquefaction-induced ground response at the Marina district, California, is presented in a fashion similar to the previous two chapters. In addition, the results obtained in this chapter are used to verify and refine the outcomes of the stochastic analyses carried out in Chapters 7 and 8.

In Chapter 10, the outcomes of the analyses performed in the previous chapters are integrated and the main conclusions of this research study are summarized together with recommendations for future research.

CHAPTER 2

AN OVERVIEW OF SOIL HETEROGENEITY: QUANTIFICATION AND IMPLICATIONS ON GEOTECHNICAL FIELD PROBLEMS

2.1 INTRODUCTION

Almost all natural soils are highly variable in their properties and rarely homogeneous. Soil heterogeneity can be classified into two main categories. Lithological heterogeneity, which can be manifested in the form of thin soft/stiff layers embedded in a stiffer/softer media or the inclusion of pockets of different lithology within a more uniform soil mass. The second source of heterogeneity can be attributed to soil inherent spatial variability, which is the variation of soil properties from one point to another in space due to different deposition conditions and loading history.

Early attention to the problem of soil non-homogeneity emerged from the field of petroleum engineering where efforts were devoted towards assessing the effect of heterogeneity on the production of oil fields. Geostatistical theories and up-scaling techniques were implemented to estimate equivalent permeabilities for the fields of interest that honored detailed reservoir heterogeneity.

In the field of geotechnical engineering, relying on high safety factors and local experience have been the conventional tools to deal with ground heterogeneity. Morgenstern (2000) introduced case histories for different geotechnical applications where relying solely on engineering judgment resulted in poor to bad predictions in up to 70% of the cases considered. As a result, it has been readily accepted that there is a need to develop more reliable tools to incorporate ground heterogeneity in a rather quantitative

---

A version of this chapter has been published in the Canadian Geotechnical Journal, Vol. 40, No. 1: 1-15.

scheme amenable to engineering design. Early attempts to rationally deal with the variability of soil properties in geotechnical engineering involved the introduction of reliability-based design methods that combined limit equilibrium analysis with Monte Carlo simulation technique. In addition, the stochastic finite element method was introduced as an effective way to incorporate soil variability into a numerical analysis framework. Recently, attempts have been made to incorporate spatial correlation between soil properties into a statistical design scheme using either of the above approaches or through implementing the outcome of Monte Carlo simulation into deterministic numerical analysis schemes. It is worth noting that almost no attention has been given to assess the effect of lithological heterogeneity on the macro (overall) behavior of heterogeneous soil media. The treatment of such heterogeneity has been exclusively left to local experience and engineering judgment.

The main objective of this chapter is to discuss the different techniques developed to deal with soil heterogeneity in both petroleum and geotechnical engineering and their applicability to geotechnical field problems. In addition, attempts will be made to identify the difficulties associated with obtaining representative parameters that honor detailed ground heterogeneity. In the following sections, techniques developed in the petroleum literature to deal with lithological heterogeneity are discussed. Then, different elements of inherent soil variability will be presented along with their implications on geotechnical field problems, such as settlement of shallow foundation, liquefaction susceptibility, and seepage flow. Limitations of current practice will be addressed and potential trends for future studies will be suggested. Finally, different decision algorithms will be discussed together with examples of their applications in geotechnical analyses.

2.2 LITHOLOGICAL HETEROGENEITY

The impact of lithological heterogeneity of the ground on the production of oil and gas reservoirs has been a major area of study in petroleum engineering practice.

Several up-scaling techniques were developed to deal with complex ground profiles, such as the sand shale sequence shown in Figure 2.1. The main aim of these techniques was to scale up fine scale permeability to coarser scales amenable to flow simulation and engineering calculations. These averaging techniques can be classified into:

1. Empirical techniques, such as the power averaging technique (Deutsch 1989). These are the simplest forms of up-scaling laws;

2. Semi-empirical methods, such as the renormalization (King 1989) and the REV-Renormalization (Norris et al. 1991). They are more sophisticated than the previous type but have limited theoretical basis; and

3. Analytical techniques, such as that proposed by Warren and Price (1961). These methods are rather cumbersome to implement in practice.

The power averaging method was obtained through non-linear regression of the results obtained from a 3-dimensional numerical simulation of flow through sandstone-shale formations. The analysis was carried out under different target shale volumes and the equivalent permeability was regarded as that of a homogeneous soil mass producing similar flow under the same head difference and boundary conditions. This equivalent permeability, k_e, was found to satisfy the relation:

$$k_e = [V_{sh}k_{sh}^\omega + (1 - V_{sh})k_{ss}^\omega]^{1/\omega}$$
(2-1)

where: k_{sh} and k_{ss} are the permeabilities of the shale and sandstone, respectively;

V_{sh} is the volume fraction of shale; and

ω is an averaging power.

The value of ω was suggested to range from -1 to 1 depending on the direction of flow and the geometrical anisotropy of shale, i.e. the ratio between the vertical to the lateral extent of shale. The major advantage of this method is its simplicity while the main drawback is that the shale blocks were assumed to be uncorrelated to each other.

- 8 -

In the renormalization technique (King 1989), a simulation grid is generated across the analysis domain and a constant value of soil permeability is assigned to each element of the simulation grid. Then, these elements are grouped into blocks of four and assigned an effective (equivalent) permeability value, k_e, as illustrated in Figure 2.2. This effective permeability was obtained based on the analogy between water flow through soils of different permeabilities and electric current flow through a network of resistors:

$$k_e = \frac{4(k_1 + k_3)(k_2 + k_4)[k_2 k_4 (k_1 + k_3) + k_1 k_3 (k_2 + k_4)]}{[k_2 k_4 (k_1 + k_3) + k_1 k_3 (k_2 + k_4)][\sum_{i=1}^{4} k_i] + 3(k_1 + k_2)(k_3 + k_4)(k_1 + k_3)(k_2 + k_4)}$$ (2-2)

where k_e is the equivalent permeability of four soil blocks of permeabilities k_1, k_2, k_3, and k_4, as shown in Figure 2.2

The above procedure can be applied to the new grid and repeated several times depending on the scale of interest. This method was originally developed for uncorrelated permeability fields, but it is also valid to correlated fields. It is worth noting that only isotropic media, of equal permeabilities in vertical and horizontal directions, were considered during the development of this technique. However, the method can be extended to anisotropic media by applying the up-scaling procedure to both vertical and horizontal directions. In spite of the theoretical basis implemented in this technique, it can be regarded as a relatively complicated method compared with the empirical formula presented in Equation 2-1.

The REV-Renormalization approach (Norris et al. 1991), for up-scaling of sand-shale formations for flow simulation, combined the representative elementary volume (REV) theory with the renormalization technique. The REV theory defines a specific averaging volume at which all microscopic variations are averaged out producing a representative single macroscopic value, which is usually referred to as the representative elementary property (REP), (Norris et al. 1991). The REV technique was originally developed to assess representative property of porous materials, where the representative

property at the smallest scale represents the property of either a void or a solid. By gradually increasing the averaging volume, more voids and solids are included in the averaging volume resulting in fluctuation in the representative property, as shown in Figure 2.3. The REV can be defined as a critical averaging volume beyond which there is no significant fluctuation in the representative property, as the addition of extra voids or solids has a minor effect on the averaged property. In the REV-Renormalization technique, subsurface soil is discretized into exclusive geological units characterized by a specific type of sedimentary structure. Within each unit, the spatial distribution of sand and shale is translated into binary maps. The renormalization technique is, then, employed to determine soil permeabilities at different averaging volume scales to determine the REV and the associated equivalent permeability, which is regarded in this case as the REP. It was concluded from the results obtained using this approach that effective permeability was mainly dependant on the relative volume and connectivity of different lithologies rather than their inherent spatial variability.

The first rational attempt to provide an analytical solution to the problem of soil lithological heterogeneity and its effect on flow was proposed by Warren and Price (1961). They combined the results of physical modeling with that of numerical simulation and suggested the geometric mean as an estimate of the effective permeability of a heterogeneous medium. Afterwards, several studies were carried out to develop enhanced measures of effective permeability. Two main approaches were adopted in these studies, the effective medium theory and the perturbation expansion, as discussed by King (1989). In either case, the effective permeability estimates were considered accurate only for small ranges of permeability fluctuations.

In the field of geotechnical engineering, almost no attempt has been made to assess the effect of lithological heterogeneity on the macro behavior of soil mass in spite of the need to develop such algorithms for certain geotechnical applications. An example of these applications is co-depositional sand - fine tailings embankments, shown in Figure 2.4. The basic idea of this tailings disposal system is to mix fine tailings, which

behave as very soft clay, with sand to obtain relatively steeper embankments, compared with conventional thickened tailings embankments (Robinsky 1999). The heterogeneous nature of these embankments requires an estimation of equivalent engineering parameters that take into consideration the effect of spatial distribution of fine tailings pockets on the overall behavior of these embankments.

2.3 INHERENT SPATIAL VARIABILITY OF SOIL PROPERTIES

Most geotechnical analyses are deterministic in the sense that average soil parameters are given to each distinct layer. The uncertainties in these properties and their variation from one point to another in space have been accounted for, qualitatively, by the use of safety factors and by implementing local experience and engineering judgment. The selection of these design parameters, however, has contained some degree of uncertainties and consequently a degree of unavoidable risk. These uncertainties can be attributed to the following factors (Phoon and Kulhawy 1999):

1. Soil inherent spatial variability due to variation in deposition conditions and stress history from one point to another in space;

2. Measurement errors due to insufficient control of testing procedure and equipment;

3. Deterministic trends in soil properties such as the increase in soil strength with depth due to the increase in confining pressure; and

4. Collection of field data over long time periods.

This study will focus primarily on soil spatial variability, where stochastic analysis can be employed to assess its influence on engineering design. To proceed with a stochastic analysis, the main elements of soil inherent spatial variability have to be identified, such as:

1. Classical statistical characteristics, such as the mean, coefficient of variation (COV), and probability distribution of soil data;

- 11 -

2. The spatial correlation structure that describes the variation of soil properties from one point to another in space;

3. The limit of spatial continuity, beyond which no or small correlation between soil data exists; and

4. The volume-variance relations, which help assess the reduction in the variance of field data upon averaging over a certain volume of interest.

Details of the above elements are discussed in the following sections.

2.3.1. Classical Statistical Characteristics of Soil Properties

Several attempts have been made to obtain classical statistical properties of soil, such as the mean value, coefficient of variation, and probability distribution, throughout geotechnical engineering practice. These statistical characteristics have been discussed by several authors, such as Lumb (1970), Schultze (1975), and Griffiths and Fenton (1993). Phoon and Kulhawy (1999) provided an excellent summary of different statistical characteristics for different soil types and field tests. Generally, it was found that high variability, expressed in terms of high coefficient of variation, was usually associated with strength parameters, and that undrained shear strength was usually highly variable compared to drained friction angle. It is worth noting that different probability distributions models such as normal, lognormal, and beta distributions have been implemented by different authors to curvefit the results of field data. This implies that these distributions are probably site and parameter specific and that there is no generic distribution pattern for soil properties.

2.3.2. Spatial Correlation between Soil Properties

Soil properties do not vary randomly in space; rather such variation is gradual and follows a pattern that can be quantified using spatial correlation structures, where soil

- 12 -

properties are treated as random variables. Spatial correlation structure is often expressed in terms of the variogram (Deutsch 2002) or the covariance function (Vanmarcke 1977).

The variogram is a measure of dis-similarity between two points in space separated by a distance h, according to the relation:

$$2\gamma(h) = Var[Z(u + h) - Z(u)] \tag{2-3}$$

where: $2\gamma(h)$ is the variogram value at a separation distance h;

Z (u) is the value of the random variable at location u;

Z (u+h) is the value of the random variable at distance h from Z (u); and

Var [ ] is the variance operator.

On the other hand, the covariance is a measure of similarity between the above two points and can be obtained through:

$$C(h) = E[Z(u).Z(u + h)] - m^2 \tag{2-4}$$

where: C(h) is the value of the covariance function at a separation distance h;

m is the mean value of Z; and

E [ ] is the mean operator.

Variogram and covariance functions are correlated through the variance of field data, σ^2, in the form:

$$\gamma(h) = \sigma^2 - C(h) \tag{2-5}$$

It should be emphasized that the above variogram and covariance relations are only valid for stationary random fields where both the mean and standard deviation are constants across the domain of interest. Most soil mechanical properties, however, are

- 13 -

expected to exhibit spatial trends especially in the vertical direction due to their sensitivity to change in confining pressure. An example of these vertical trends is shown in Figure 2.5.a where the tip resistance, q_c, of cone penetration test data tends to increase with depth. To satisfy stationarity condition, these trends must be removed (detrended) in a process often referred to as detrending of field data. The detrending process is usually carried out by identifying deterministic trends in field data implementing regression analysis (Deutsch 2002), as shown in Figure 2.5.a. It should be realized that the linear variation of cone tip resistance with depth, shown in Figure 2.5, is a simplifying assumption for practical application; as such variation can take other forms especially for sandy soils. Spatial trends in field data, however, should be kept as simple as possible to minimize the uncertainty associated with the assessment of these trends (Baecher 1987). This uncertainty in spatial trends may have a significant influence on the outcomes of stochastic geotechnical analyses especially in the presence of limited field data. Neter et al. (1996) and El-Ramly (2001) provided an excellent discussion on the assessment of this uncertainty and its implications on statistical analyses. The detrending process results in generating detrended field data, as shown in Figure 2.5.b, which can be considered as stationary random variables using the relation:

$$q = q_c - q_o(z) \tag{2-6}$$

where q is the detrended cone tip resistance and $q_o(z)$ is the deterministic vertical trend.

Spatial correlation structures are usually characterized by their model types and the limit of spatial correlation between field data. Spatial correlation models are parametric relationships used to curvefit the experimental variograms, or covariance functions, obtained from analysis of field data. Deutsch (2002) has provided an excellent summary of common variogram models used in practice. Examples of these models, such as spherical, exponential, and gaussian models, are shown in Figure 2.6. These models help determine the spatial correlation between field data at any separation distance and in different directions. In addition, they can incorporate other geological information such

- 14 -

as direction of maximum continuity and maintain numerical stability of stochastic simulation (Deutsch 2002). The limit of spatial continuity is discussed in more details in the following section.

2.3.3. Limit of Spatial Continuity between Field Data

The limit of spatial continuity is defined as the separation distance between field data at which there is no, or insignificant, spatial correlation. This limit can be expressed in terms of the spatial range (Deutsch 2002), the scale of fluctuation (Vanmarcke 1977), or the autocorrelation distance (DeGroot and Baecher 1993). The spatial range, a, can be defined as the separation distance at which the variogram reaches the sill (variance) and correlation between data no longer exists, as shown in Figure 2.6. For variogram models where the variogram is asymptotic to the sill (σ^2), as the case for exponential and gaussian models, an effective range can be considered as the separation distance at which the variogram reaches a value equal to 0.95 the sill. The scale of fluctuation, θ, estimates the distance within which soil properties show relatively strong correlation and data become either above or below the mean value. Vanmarcke (1977) developed a simplified procedure to estimate the scale of fluctuation for different spatial correlation structure models. The autocorrelation distance, R, is the separation distance at which the covariance function decays to a value of σ/e, where e is the base of natural logarithm, and correlation between field data can be considered relatively weak. A relationship between these different measures was developed in this study, as illustrated in Appendix 2-A and summarized in Table 2.1.

2.3.4. Volume-variance Relations

The volume-variance relationships are analytical expressions used to obtain the variance of spatial averages of field data over certain volumes of interest. These spatial averages usually have a narrower probability distribution function than those associated with field data (Vanmarcke 1977) and consequently a smaller variance. The variance of

these spatial averages can be correlated to the point variance using the variance reduction factor, Γ_v^2, as discussed by Vanmarcke (1984) through:

$$(\sigma)_\Gamma = \Gamma_v \cdot \sigma \qquad (2\text{-}7)$$

where: σ is the standard deviation of field data (point statistics);

σ_Γ is the standard deviation of the spatial average of data over volume v; and

Γ_v is the square root of the variance reduction factor.

The variance reduction factor depends on the averaging volume, type of correlation structure, and the limit of spatial correlation between field data. Several analytical expressions for the variance reduction factor were introduced by Vanmarcke (1984), in the form:

$$\Gamma_T^2 = 2 \cdot (\frac{R}{T})^2 \cdot (\frac{T}{R} - 1 + e^{-T/R}) \qquad \text{for exponential correlation structures} \qquad (2\text{-}8\text{-}a)$$

$$\Gamma_T^2 = 2 \cdot (\frac{R}{T})^2 \cdot [\sqrt{\pi} \frac{T}{R} \cdot \xi(\frac{T}{R}) - 1 + e^{-T/R}] \qquad \text{for gaussian correlation structures} \qquad (2\text{-}8\text{-}b)$$

where: Γ_T^2 is the one-dimensional variance reduction factor;

R is the autocorrelation distance;

T represents the size of the average volume; and

$\xi(\frac{T}{R})$ is the error function, which varies from 0 to 1 as T increases from o to ∞.

The above expressions are based on the assumption that the averaging process occurs in one direction only. These expressions can be easily extended to the three-dimensional case by assuming separable correlation structures (Vanmarcke 1984). Such an assumption implies that the three-dimensional variance reduction factor could be expressed as the product of its one-dimensional components in the form:

- 16 -

$$\Gamma_v = \Gamma_{Tx} \cdot \Gamma_{Ty} \cdot \Gamma_{Tz} \qquad\qquad (2\text{-}9)$$

where: $\Gamma_{Tx}, \Gamma_{Ty}, \Gamma_{Tz}$ are the one-dimensional variance reduction factors in x, y and z directions, respectively.

The variance reduction factor tends to 1 when the parameter T is small compared to the spatial range. For many geotechnical applications, the size of the averaging volume in the horizontal direction is usually small compared to the horizontal spatial range. As a result, it has been a common practice in many geotechnical implementations of the variance reduction factor to assume that its value is affected only by the size of the averaging volume in vertical direction, i.e. layer thickness. This is because the variance reduction factor in the horizontal direction can be reasonably assumed equal to one.

In a similar fashion, the variance reduction factor for spherical correlation structures was developed in this study, as explained in Appendix 2-B, and could be expressed in the form:

$$\Gamma_T^2 = 1 - \frac{T}{2a} + \frac{T^3}{20a^3} \qquad\qquad (2\text{-}10)$$

Spatial averages of random variables are spatially correlated in a way similar to point (field data) statistics. This correlation can be quantified in a pair wise manner by assessing the coefficient of correlation between any couple of one-dimensional spatial averages, as shown in Figure 2.7, through the relationship (Vanmarcke 1977):

$$\rho_{12} = \frac{D_0^2 \cdot \Gamma^2(D_0) - D_{01}^2 \cdot \Gamma^2(D_{01}) - D_{02}^2 \cdot \Gamma^2(D_{02}) + D_{012}^2 \cdot \Gamma^2(D_{012})}{2 \cdot D_1 \cdot \Gamma(D_1) \cdot D_2 \cdot \Gamma(D_2)} \qquad (2\text{-}11)$$

where: ρ_{12} is the correlation coefficient between the spatial averages over the depths D_1 and D_2;

$\Gamma^2(D_0)$, $\Gamma^2(D_{01})$, $\Gamma^2(D_{02})$, and $\Gamma^2(D_{012})$ are the variance reduction factor over averaging thickness equal to D_0, D_{01}, D_{02} and D_{012}, respectively; and

$\Gamma(D_1)$ and $\Gamma(D_2)$ are the square roots of variance reduction factor over averaging thickness equal to D_1 and D_2, respectively.

2.4 STOCHASTIC ANALYSIS TECHNIQUES IN GEOTECHNICAL ENGINEERING

Stochastic analysis provides an excellent tool to account for the variability of soil properties and to develop rational algorithms to estimate soil design parameters on a probabilistic basis, where the associated risk level can be quantified. Several approaches have been adopted by geotechnical practitioners to implement stochastic analyses in geotechnical field problems, such as liquefaction assessment, slope stability analysis, and foundation settlement. Examples of these approaches are:

1. Application of reliability principles to limit equilibrium analysis;
2. Stochastic finite element analysis; and
3. Application of stochastic input soil parameters into deterministic numerical analysis.

Detailed discussion of the above approaches is provided in the following sections together with examples of their applications to geotechnical field problems.

2.4.1. Application of Reliability Principles to the Limit Equilibrium Analysis

Statistical analysis of limit equilibrium problems was primarily developed to perform probabilistic slope stability analysis using different techniques, such as analytical approaches, approximate solutions, and Monte Carlo simulation.

Analytical approaches, such as those proposed by Tobutt and Richards (1979), were primarily concerned with obtaining closed form solutions for the statistical properties of earth slopes factors of safety. These solutions do not provide information about the output probability distribution and become cumbersome when considering different sources of uncertainty.

Approximate solutions of probabilistic slope stability analysis, such as the first order second moment (FOSM) and the point estimate method (PEM), have been advocated by several authors, such as Christian et al. (1994). The basic idea of the FOSM method (Harr 1987) is to express factor of safety as a function of different random variables considered in the statistical analysis. This function is then expanded about the mean values of these random variables using Taylor expansion, retaining only linear (first order) terms, where the mean and variance of safety factor can be assessed through:

$$E[F.S] = F(E(x_1), E[x_2], \ldots\ldots\ldots E[x_n])$$ (2-12-a)

$$Var[F.S] = \sum_{i=1}^{i=n} \left(\frac{\partial F}{\partial x_i} \cdot \sigma_{x_i} \right)^2 + 2 \cdot \sum_{i=1}^{i=n} \sum_{j=1}^{j=n} \left(\frac{\partial F}{\partial x_i} \frac{\partial F}{\partial x_j} \right) \cdot C[x_i, x_j]$$ (2-12-b)

where: E[F.S] and Var[F.S] are the mean and variance of factor of safety, respectively;

C[x_i, x_j] is the covariance between the random variables x_i and x_j; and

n is the number of random variables

The major advantage of this technique is its simplicity, especially when considering different sources of uncertainty, as it provides direct estimation of the mean and variance of factors of safety. However, the accuracy of this technique is questionable, especially when dealing with highly non-linear relations and large soil variability, due to the truncation of high order terms in Taylor expansion.

In the PEM (Rosenblueth 1975 and 1981), the probability distribution of each of the random variables is represented by two points estimates x+ and x- with probability

- 19 -

densities of p+ and p-, respectively. This is based on the analogy between probability distributions and distributed vertical loads on a horizontal rigid beam resting on two pin supports (Harr 1987). For symmetrical probability distributions, p+ and p- are taken equal to 0.5; while x+ and x- are taken one standard deviation above and below the mean value of the random variable, respectively. The mathematical details of this method are complicated enough to be beyond the scope of this study and interested reader can refer to Harr (1987) for more details. This technique is quite useful when it is difficult, or even impossible, to obtain derivatives of the factor of safety with respect to different random variables to apply the FOSM method. The main limitation of this technique is the complexity in calculations when considering multiple random variables in the assessment of safety factors. An excellent summary of the accuracy and limitations of this method has been provided by Christian and Baecher (1999).

The early implementation of Monte Carlo simulation to limit equilibrium analysis considered soil, or rock, properties as uncorrelated random variables (Kim and Major 1978). Several realizations of soil design parameters were obtained and used to develop a histogram for the factor of safety of earth slopes. Recently, the effect of spatial correlation between soil properties has been accounted for through the application of geostatistics principles and volume-variance relationships (El-Ramly 2001). A complete probability distribution of output variables, such as the factor of safety, can be obtained and the failure probability can be reasonably assessed. This is a major advantage over other analysis technique where some assumptions have to be made about the probability distribution of output variables. It should be noted, however, that Monte Carlo simulation has its own limitations, which can be summarized as follows:

1. The need to define a reliable input reference distribution, which requires a considerable number of field data. In addition, older versions of Monte Carlo simulation algorithms used to deal only with parametric probability distribution functions, i.e. probability distributions that can be defined through mathematical relationships such as normal and lognormal distribution. Field data, however, do not necessarily fit into any of these parametric distributions. This problem has been

overcome by recent versions of Monte Carlo simulations, such as that of Deutsch and Journel (1998), which are capable of dealing with non-parametric distribution functions directly inferred from field data;

2. Clustering of the simulation outcome into a limited zone of the input probability distribution, as the drawn samples are more likely to be in areas of higher probability, as shown in Figure 2.8. This problem mainly arises in cases where insufficient number of realizations (number of iterations in Monte Carlo algorithm) is used in the simulation process (Palisade Corporation 1996). This may result in sampling values of the random variable away from the tails of the input probability distribution, which can be on the unsafe (non-conservative) side. This problem, however, can be overcome by using a number of realizations large enough to reproduce the input probability distribution; and

3. Depending on the number of variables involved in the simulation process, Monte Carlo simulation may require a significantly large number of iterations and consequently a considerable computational effort. However, the author believes that this problem has been overcome by the new generation of fast computers.

2.4.2. Stochastic Finite Element Analysis

The stochastic finite element method (SFEM) is a modification of the traditional finite element method to capture the effect of soil spatial variability on numerical analysis. This is carried out by using finite element discretization to obtain direct assessment of the mean and variance of nodal displacements together with the covariance between displacements at different nodes of the numerical analysis mesh (Baecher and Ingra 1981). This assessment is usually accomplished by calculating a covariance matrix, whose value depends on the characteristics of spatial correlation between soil properties, such as variogram model and spatial range. These characteristics are captured into the finite element scheme by introducing the matrix of differentials, which assesses the effect of the variation of mechanical soil properties from one element to another on the global stiffness matrix. For more details about SFEM, the reader can refer to Baecher and Ingra

- 21 -

(1981); and Auvinet et al. (1996). Different modifications of SFEM have been developed by introducing different numerical techniques to capture soil spatial variability. Examples of these modifications are the probabilistic finite element method (Righetti and Harrop-Williams 1988) and stochastic integral formulations (Zeiton and Baker 1992).

The major advantage of the SFEM is the direct assessment of statistical characteristics of output variables, such as the mean and variance. This helps avoid long computational time associated with incorporating several realizations of spatially variable soil parameters into deterministic analysis scheme, as discussed in the following section. On the other hand, different limitations of the SFEM have been discussed by several authors, such as Baecher and Ingra (1981); and Auvinet et al. (1996), and they can be summarized as follows:

1. The analysis results are not affected by the probability distribution of input random variables. Furthermore, a distribution has to be assumed for output variables as SFEM provides only an assessment of the mean and standard deviation;

2. Element variance and covariance matrices are functions of element shape and geometry and their determination becomes quite tedious for irregular element shape and complicated boundary conditions;

3. Limited to small variability due the error associated with the truncation of higher order terms in Taylor expansion, which is used for the determination of mean values of the response variables, such as surface settlement;

4. Integration of the random variable field over each element may result in a change in the anisotropy ratio of the correlation structure of soil properties;

5. Usually limited to linear elastic behavior of soil to avoid extreme complexity in the computation process; and

6. Does not adequately capture the behavior of soil properties with skewed probability distributions.

Due to the above limitations, the use of stochastic finite element analysis has received limited attention from geotechnical practitioners and researchers.

- 22 -

2.4.3. Application of Stochastic Input Parameters into Deterministic Numerical Analysis

Deterministic numerical analysis with stochastic input soil parameters has been recently adopted by many researchers, such as Paice et al. (1994), and Popescu et al. (1998), as a technique to incorporate soil spatial variability in geotechnical design. Monte Carlo based simulation techniques have been used to generate several realizations of soil properties that vary from one point to another across the domain of interest, as shown in Figure 2.9. This spatial variation is usually employed into the numerical analysis scheme by assessing soil properties at the center of each element of the numerical simulation grid, and assuming them to be constant within that element. By analyzing several realizations of the spatially variable soil medium, histograms of response (output) variables can be obtained. Examples of the simulation algorithms commonly used in practice are the Sequential Gaussian and the Sequential Indicator simulations (Deutsch 2002), and the Local Average Subdivision technique (Fenton and Vanmarcke 1990).

The Sequential Gaussian Simulation (SGS) is the most commonly used technique, especially in the field of petroleum engineering. The basic idea of this technique is illustrated in Figure 2.10. Input random variables are transformed into standardized normally distributed random variables with zero means and unit variances, for which different variogram characteristics are assessed. Simulated values of a standardized variable, Z, can be determined at any node of the simulation grid through:

$$Z_s(u) = Z^*(u) + R(u) \qquad (2-13)$$

where: $Z_s(u)$ is the simulated value of the variable Z at location u;

$Z^*(u)$ is the krigged estimate of the variable Z at location u; and

$R(u)$ is a random residual.

The krigged estimate is a linear estimator of the variable Z at location u in space, where the value of Z is unknown, using the krigging interpolation techniques (Journel and Huijbregts 1978). This estimate depends on different characteristics of spatial correlation structure (variogram) and does not vary from one realization to another, and can be assessed through:

$$Z^*(u) = \sum_{i=1}^{n} \lambda_i \cdot Z(u_i) \qquad (2\text{-}14)$$

where: $Z(u_i)$ is a known value of Z at location u_i in space, either from field data at that location or previously simulated nodes; and

λ_i is a weight given to field data at location u_i that depends on the characteristics of the spatial correlation structure.

The random residual R(u) follows a normal distribution with zero mean and variance equal to the krigging variance (Deutsch 2002). A different value of R(u) is obtained in each realization of Monte Carlo simulation resulting in a variation of the simulated value of the random variable, Z(u), from one realization to another. A random path is followed to assess the value of the standardized random variable at each node of the numerical simulation grid. The simulated values are then back-transformed to their original probability distribution. By repeating the above procedure, several realizations of soil spatial variation across the analysis domain can be obtained.

2.5 APPLICATION OF STOCHASTIC ANALYSIS TO GEOTECHNICAL FIELD PROBLEMS

The stochastic analysis techniques discussed in the previous sections have been implemented in several applications throughout the history of geotechnical engineering practice to assess the impact of ground variability on geotechnical field problems. In the

following sections, an attempt is made to address the current state of practice in some of these applications and its limitations together with potential trends for future research.

2.5.1. Stochastic Analysis of Shallow Foundation Settlement

Early attempts to perform probabilistic analysis of foundation settlement started in the late 1960s. Wu and Kraft (1967) estimated the uncertainty in soil bearing capacity and foundation settlement through assessing the uncertainty in applied load, soil strength, and deformation parameters. The uncertainty in soil strength was estimated through assessing the variability of laboratory undrained shear strength for clayey soils and that of SPT data for sandy soils. Resendiz and Herrera (1969) carried out a probabilistic analysis of settlement and rotation of flexible and rigid footings over randomly variable compressible soils. A one-dimensional settlement model was adopted in which the coefficient of volume change was characterized as a normally distributed random variable. The analysis results were used to obtain design parameters that satisfied tolerable settlements and rotations criteria together with minimum expected monetary loss. These studies can be considered as a good start to address such complex problem. However, they were fairly primitive as some elements of soil inherent variability, such as spatial correlation between soil properties, were not adequately considered.

The modern approach to deal with uncertainty in foundation settlement started in the early 1980s with the pioneer work of Baecher and Ingra (1981). In their study, two-dimensional stochastic finite element analysis was carried out to assess the uncertainty in total and differential settlement. Soil elastic modulus was treated as a random variable, whereas Poisson's ratio was assumed to be constant across the soil mass. Two spatial correlation models, the exponential and the squared exponential (gaussian), were considered and the response variables (total and differential settlement) were assumed to be normally distributed. The uncertainty in total settlement was expressed in terms of the coefficient of variation of the maximum settlement and was found to increase with higher autocorrelation distance, as shown in Figure 2.11. Furthermore, the study proposed a

- 25 -

critical ratio of 0.75 to 1 between the autocorrelation distance, R, and footing width to be associated with maximum differential settlement. On the other hand, the type of correlation structure was found to have insignificant effect on both total and differential settlement. A limiting assumption of the study was the assumed linear elastic soil behavior, which implies, together with the use of SFEM, a small variation in soil properties to avoid the development of plastic zones and the onset of non-linear constitutive behavior. In addition, the effect of different probability distributions of soil properties on the expected uncertainty was not assessed.

Zeitoun and Baker (1992) proposed a stochastic approach for settlement prediction of shallow foundations using the stochastic integral formulation (SIF) technique, which is a modification to the SFEM. It was assumed that soil would exhibit linear elastic behavior under both axi-symmetrical and plane strain conditions. Soil shear modulus was treated as a random variable, whereas Poisson's ratio was assumed to be a deterministic constant throughout the soil medium. The Gaussian model was chosen to represent the spatial variation of shear modulus across the problem domain. Equations were obtained for the determination of the mean and standard deviation of total and differential settlement. The uncertainty in total and differential settlements was expressed in terms of the coefficient of variation (COV) and was found to be proportional to the increase in the autocorrelation distance. For the axi-symmetric case, the increase in COV of total settlement normalized to COV of shear modulus was found to increase gradually until reaching an asymptotic value smaller than one, as shown in Figure 2.12. This indicated that the variability in surface settlement was usually smaller than that of the underlying soil properties. The technique used in the study had serious limitations as unrealistic spatial correlations were assumed either through the use of a very high horizontal autocorrelation distance or by considering the soil medium to be in the form of concentric rings of constant elastic modulus. Furthermore, no information was provided about the probability distribution of output variables; and the effect of different spatial correlation structures was not accounted for. Finally, the use of SFEM implied some

restrictions on the range of soil variability used in the analysis to prevent development of plastic zones as discussed in the previous paragraph.

The effect of random soil stiffness on foundation settlement was reinvestigated by Paice et al. (1994) through the use of deterministic finite element analysis with stochastic input soil parameters. Poisson's ratio was presumed constant, whereas the elastic modulus was regarded as a spatially random variable resulting in a ground profile as previously shown in Figure 2.9. Soil elastic modulus was assumed to follow a lognormal probability distribution with a coefficient of variation (COV) ranged between 0.02 and 0.42 and exponential correlation structure. The settlement was expressed in terms of the influence coefficient (I) proposed by Poulos and Davis (1974). The mean of the influence coefficient (m_I) and its coefficient of variation (σ_I/m_I) were found to increase with higher scales of fluctuation (θ_E) and coefficients of variation of the elastic modulus (σ_E/m_E), as shown in Figure 2.13. It was, also, concluded that the effective mean elastic modulus, back-calculated from settlement below the footing centerline, showed close agreement with the geometric mean of the elastic modulus random field. This study has some limiting assumptions such as the linear elastic soil behavior, the isotropic correlation structure, and the symmetry of spatial distribution of elastic modulus around the footing centerline. In addition, the effect of different types of correlation structures and the sensitivity of the results to the number of realizations were not considered.

The effect of random fluctuations of the interface between soil layers on the uncertainty in foundation settlement has been accounted for by Brzakala and Pula (1996). This uncertainty in soil geometry was converted into a new random field expressed in terms of the interface fluctuation and was incorporated into stochastic finite element analysis. The mean settlements and the associated coefficients of variation were determined at several points on the ground surface together with the correlation between the computed settlements at these points. The analysis results showed smaller values for the coefficient of variation of surface settlement compared to that of soil layers interface. This indicated that the uncertainty in the interface between soil layers did not have a

profound effect on the uncertainty in settlement analyses. The limitations of the study lie in the linear elastic soil behavior and neglecting the inherent soil variability within layers. In addition, the effect of different types of probability distribution and correlation structure on the stochastic analyses outcomes was not adequately addressed.

It is worth noting that the above studies have not considered the effect of changing the state of stresses in subsurface layers on the outcome of geotechnical stochastic analyses. In other words, the sensitivity of the statistical characteristics of response (output) variables to wide ranges of applied vertical and horizontal stresses was not adequately addressed. In addition, these stochastic analyses have not been used to develop risk-based representative soil parameters that honor detailed ground variability.

2.5.2. Stochastic Analysis of Liquefaction Problems

Early attempts to quantify the stochastic nature of liquefaction problems were focused on developing analytical expressions to estimate the uncertainty in liquefaction potential assessment. Yegian and Whitman (1978) conducted a pioneer study to provide a statistical evaluation of annual probability of failure for potentially liquefiable sites. This was carried out by combining the annual probability of given earthquakes with the probability of ground failure under these earthquakes. In addition, an analytical expression was developed to assess the uncertainty in a limit state parameter, proposed to estimate the maximum shear resistance of the ground. A major limitation of that study was that the effect of spatial correlation between soil properties was not accounted for and that the uncertainty in the results were assumed to be insensitive to the probability distribution of the input random variables. Furthermore, the derivation of the expression for the limit state parameter was based on the assumption that soil shear resistance and vertical effective stress were two independent random variables.

Recently, the use of deterministic finite element analysis with stochastic input soil parameters has gained much popularity in the field of probabilistic liquefaction analysis.

Several attempts have been made to apply this technique to study case histories that involved potentially liquefiable ground conditions.

Fenton and Vanmarcke (1991) performed one-dimensional finite element analyses to assess the effect of spatial variability of soil properties on liquefaction potential at the Wildlife site, California. Soil properties, such as porosity, Poisson's ratio, elastic modulus, permeability, and the dilation angle, were considered as random variables. The first two properties were considered to be normally distributed, whereas the rest were assumed to follow a lognormal distribution. The effect of correlation structure was taken into consideration through the application of the variance reduction factor proposed by Vanmarcke (1977). Several realizations of soil properties were generated using the Local Average Subdivision technique, and were excited by various earthquake motion applied at the base of soil columns using DYNA1D software. The study introduced measures of liquefaction potential such as A_q that prescribes the lateral extension of zones associated with different values of normalized pore pressure (μ/σ_v') and ψ that depicts the connectivity of these zones. A critical threshold for A_q associated with high risk of liquefaction occurrence was proposed. Scale of fluctuation, θ, was found to have insignificant effect on A_q and substantial influence on ψ, as shown Figure 2.14. A main limitation of the study is that the sensitivity of the results to the number of realizations was not taken into consideration. Moreover, the effect of different probability distributions of soil properties was not accounted for together with the use of one-dimensional analysis, in which the analysis domain was divided into soil columns neglecting the coupling between soil elements. Finally, the study provided no basis for the critical threshold suggested to be associated with high risk of liquefaction and did not quantify the combined effect of the lateral extent of the liquefiable zones and their connectivity.

Popescu et al. (1996) carried out one of the pioneer investigations on the effect of soil spatial variability on liquefaction assessment using the results of cone penetration test, where cone tip resistance, q_c, and the cone index, I_c, were treated as random

- 29 -

variables. A simulation algorithm was developed for the simulation of non-gaussian multivariate random field. A non-linear regression algorithm was adopted to determine the probability distribution and the correlation structure of the random variables. The problem was analysed using the DYNAFLOW software, implementing stochastic input soil parameters obtained using the correlations between soil properties and CPT data. For comparison, a deterministic numerical analysis was carried out using the mean values of soil parameters. Increased pore pressure was predicted from the stochastic analysis due to the generation of loose sand pockets within the analysis domain that the deterministic analysis could not account for, as shown in Figure 2.15. A characteristic percentile of cone tip resistance was proposed for use in deterministic analyses to predict the same maximum pore pressure obtained from stochastic analysis. The effect of using different probability distributions to fit the field data was found to have a pronounced effect on the predicted pore pressure. The major limitation of the study lies in the use of only four realizations to quantify the effect of soil variability, which may not be sufficient to sample the expected range of response, as discussed earlier. In addition, the effect of spatial correlation range on the study outcomes was not accounted for. The author believes, however, that this spatial range may have a profound effect on liquefaction susceptibility and need to be considered in future stochastic liquefaction studies. In addition, the strength percentile proposed for use in deterministic analysis, to capture the effect of soil spatial variability, was subjectively assessed.

Popescu et al. (1998) extended the previous study to provide liquefaction potential measures through two-dimensional stochastic analysis where cone tip resistance was treated as a spatially random variable. The effect of inherent variability was assessed through 25 realizations of the spatial distribution of CPT data across the site. A series of deterministic finite element analysis was carried out, using different percentiles of the recorded CPT data, to estimate equivalent (representative) soil parameters that can capture the implications of soil spatial variability. These parameters were considered to be associated with the upper limit of Monte Carlo simulation response range. The A_{80} index was proposed as a measure of aerial extent of liquefiable layers, for which the

- 30 -

normalized induced pore pressure, μ/σ_v', exceeded a value of 0.80. Whereas, the liquefaction index, Q, was proposed as the average induced pore pressure ratio in the horizontal direction. Furthermore, the differential horizontal deformation between the ground surface and the base of the analysis domain was adopted as an estimate of the liquefaction induced deformations. It was concluded from the results shown in Figure 2.16 that the initiation of soil liquefaction can not be accurately predicted by deterministic models employing average soil parameters, which can not account for the presence of loose pockets within soil masses. Moreover, the variability of cone tip resistance data, expressed in terms of their coefficient of variation, was found to have a significant effect on selecting representative soil parameters for use in liquefaction analysis. This study, as the case of the previous one, did not take into consideration the sensitivity of the analysis to the number of realizations of soil properties. In addition, the proposed equivalent parameters could be considered over-conservative, as they were associated with the most critical response of the stochastic analysis. Moreover, the effect of the type of correlation structure and its spatial limit was not accounted for.

Once again, the effect of changing the state of stresses in soil mass on the outcome of stochastic analyses has not been adequately considered in any of the above studies. For example, more investigation is needed to ascertain whether or not the same values of the representative cone tip resistance percentiles of Popescu et al. (1998) would be obtained if potentially liquefiable layers were to be at different depths below ground surface. In addition, no decision making approach was adopted to provide representative soil parameters that depend on the risk level of the problem considered.

2.5.3. Stochastic Analyses of Seepage Flow and Retaining Walls

The problem of water flow through heterogeneous porous media has been studied thoroughly along the history of petroleum engineering and water resources research. One of the pioneer attempts to apply the principles of geostatistics into the geotechnical engineering practice to study the effect of soil spatial variability on seepage flow was

- 31 -

made by Griffiths and Fenton (1993). In their study, the Local Average Subdivision simulation technique was used to generate 1000 realizations of spatially variable hydraulic conductivity below a water retaining structure. The resulting field was then mapped onto a finite element mesh in order to perform numerical analysis of the problem under deterministic boundary conditions. The hydraulic conductivity, k, was assumed to follow lognormal probability distribution and the effect of spatial correlation structure was accounted for through quantifying the influence of the scale of fluctuation on different response (output) variables. It was found that the variation of the permeability field, expressed in terms of its COV, had a substantial influence on the mean value of flow rate and exit hydraulic gradient, and an insignificant effect on the mean uplift force. The scale of fluctuation was found to have a profound effect on the mean value of the exit gradient rather than other response variables. The uncertainty in these variables was found to increase with higher values of COV and scale of fluctuation. The limitations of the study lie in the use of an isotropic correlation structure where the vertical and horizontal ranges were assumed equal, and that the effect of different probability distributions and correlation structure model were not accounted for. Furthermore, the sensitivity of the analysis to the number of realizations of the random variable, hydraulic conductivity, was not considered.

Duncan (2000) conducted a stochastic analysis to assess the uncertainty associated with the factor of safety against sliding for cantilever retaining walls backfilled with compacted silty sand. In the study, soil unit weight, concrete unit weight, and friction angle between the wall and soil were considered as random variables. The coefficient of variation of the safety factor against sliding was estimated using the Taylor series techniques (United States Army, Corps of Engineers 1994). The probability of failure was assessed assuming that the factor of safety would follow a lognormal distribution. Furthermore, it was assumed that the probabilistic analyses results were not sensitive to the probability distribution of the input random variables. The main limitation of that study was ignoring the effect of spatial correlation between soil data on the calculated failure probability. In addition, there was not any evidence to support the

- 32 -

assumption that the factor of safety was log-normally distributed. In addition, the author believes that the soil friction angle should have been considered as a random variable due to its significant effect on the assessment of active earth pressure.

2.6 DECISION MAKING IN GEOTECHNICAL ENGINEERING

One of the major challenges that face geotechnical engineers is to make decisions regarding the soil parameter to be used in engineering analysis. These decisions have to be based on information that invariably has a certain degree of uncertainty. Consequently, the decision making process is considered to be governed by two factors, the uncertainty in the decision variables and the risk level of the project. Several decision making algorithms have been used throughout the history of geotechnical engineering practice, such as the worst case and quasi worst case approaches, reliability-based techniques, confidence interval approach, and Bayesian decision analyses. Details of these algorithms will be discussed in the following paragraphs.

The worst case approach aims at achieving absolute safety of the project and relies on the notion of maximum loss and maximum expected hazards, often referred to as the maxi-max criterion (Ang and Tang 1984). For example, if the range of the measured friction angle of a sandy deposit at a certain site ranges from 30 to 40 degrees, the design value will be assessed as 30 degree. This approach is over conservative and rarely used in practice.

On the other hand, the quasi worst case approach (Pate-Cornell 1987) tries to apply some kind of engineering judgment into the above approach to provide an upper bound for the risk level. Revisiting the above example, the sandy soil at the site is classified (say medium dense sand) and the minimum value associated with such classification (say 33 degree) will be used as the design value. A common problem of the

- 33 -

two approaches is that no information can be obtained about the risk level associated with the design value.

The reliability-based approach relies on selecting design parameters that satisfy a desired degree of reliability or a certain probability of failure. This approach has been commonly used in slope stability analysis. Wolff (1996) proposed soil design parameters to be associated with reliability index, β, of 3 for routine slopes and β of 4 for critical slopes such as dams. The reliability index can be obtained through:

$$\beta = \frac{m_{FS} - L}{\sigma_{FS}} \tag{2-15}$$

where: m_{FS} is the mean factor of safety;

L is a limit state value usually equal to 1; and

σ_{FS} is the standard deviation of the factor of safety.

In a similar fashion, the US Corps of Engineers (1995) proposed an assessment of the performance level of embankments depending on the target reliability index and the corresponding failure probability, as shown in Table 2.2. Comparing the recommendation presented in Table 2.2 with the suggested values of reliability index of Wolff (1996) implies that the selection of design parameters for earth slopes should be associated with critical failure probabilities no more than 0.1%. British Columbia (BC) Hydro developed a similar approach for dam design based on a thorough review of different potential hazards (Whitman 2000). In their criterion, critical failure probabilities were assessed as a function of potential number of fatalities, as shown in Figure 2.17. On the other hand, El-Ramly (2001) concluded that critical failure probabilities developed in geotechnical literature were over-conservative and that a critical failure probability of (1-2)% could be regarded as an upper bound for satisfactory performance of earth slopes. This critical value was assessed based on extensive probabilistic slope stability analyses of several case histories in North America and Hong Kong.

In the confidence interval approach (Harr 1987), soil parameters associated with the upper and lower limits of a certain level of confidence are proposed as design parameters. The selection of design parameters associated with 90% level of confidence, commonly used in practice, is illustrated in Figure 2.18. Using these design parameters provides a range for output (response) variables, such as the factor of safety, with only a 5% chance that the actual value of these variables will be either larger than the upper limit or smaller than the lower limit of this range.

The most robust decision making algorithm is the Bayesian decision analysis (Benjamin and Cornell 1970, and Deutsch 2002), where the impact of making mistakes in estimating design parameters is expressed in terms of monetary values. This approach utilizes loss functions and histograms of soil parameters to obtain optimal estimates of these parameters associated with minimum expected monetary loss. The loss functions are mathematical relations used to quantify the effect of making mistakes in selecting design parameters. These functions can take different forms, such as linear, quadratic, and exponential, as shown in Figure 2.19 for linear loss functions. For more details of the application of this approach, the reader can refer to Deutsch (2002). The main limitation of this approach is the difficulty associated with its application in cases where loss of human lives may be expected.

Along the history of geotechnical engineering, few attempts have been made to implement the above approaches into field problems. One of the pioneer works in this area was that by Folayan et al. (1970), where the Bayesian decision analysis was applied to settlement prediction analysis. In their study, the compression index, C_c, was treated as a random variable and the results of 27 one-dimensional consolidation tests were used to obtain a histogram for C_c. In addition, an exponential loss function was adopted to assess a value of C_c that produced the minimum expected loss. The main limitation of the study was ignoring the effect of spatial correlation characteristics of C_c on the analysis results.

- 35 -

2.7 CONCLUSIONS

A thorough review of the different techniques developed to deal with soil heterogeneity has been presented in this chapter. Different approaches developed to handle lithological heterogeneity of the ground in the petroleum engineering field were briefly addressed. Different elements of soil inherent spatial variability, such as mean, variance, spatial correlation characteristics, and volume-variance relationships were discussed together with their implications in geotechnical design. Different approaches adopted throughout the geotechnical engineering history to perform stochastic analyses of different geotechnical applications were thoroughly reviewed and criticized. In addition, an expression for the variance reduction factor of spherical spatial correlation structures (variograms) was developed in this chapter. Examples of the applications of stochastic analysis to field problems such as shallow foundation settlement, liquefaction assessment, and seepage flow were presented with emphasis on the limitations of the current practice. Finally, different decision making algorithms are discussed together with comments regarding their applicability in the field of geotechnical engineering.

From this chapter, it can be concluded that there is a need for a comprehensive study of soil heterogeneity that takes into consideration different sources of non-homogeneity and their implications on different geotechnical applications. Furthermore, there is a need to ascertain whether or not the outcomes of stochastic geotechnical analyses are sensitive to changes in in-situ state of stresses. Finally, the risk level of geotechnical projects should be incorporated in a decision-making framework to provide estimates of representative soil parameters that honor detailed ground heterogeneity.

2.8 REFERENCES

Ang, A. H. S. and Tang, W. H. 1984. Probability concepts in engineering planning and design. Vol. 2: Decision, risk, and reliability. Wiley, New York.

Auvinet, G., Bouayed, A., Orlandi, S., and Lopez, A. 1996. Stochastic finite element method in geomechanics. In Proceeding of the 1996 Conference on Uncertainty in the Geologic Environment, Uncertainty 96, Vol. 2, Madison, WI, USA, pp. 1239-1253.

Baecher, G. 1987. Statistical analysis of geotechnical data. Contract Report GL-87-1 prepared for the Department of the Army, US Army Corps of Engineers, Washington, DC.

Baecher G. B., and Ingra, T. S. 1981. Stochastic FEM in settlement predictions. Journal of the Geotechnical Engineering Division, ASCE, 107 (GT4): 449-463.

Benjamin, J. R. and Cornell, C. A. 1970. Probability, statistics, and decision for civil engineers. McGraw-Hill Book Company, New York.

Brzakala, W. and Pula, W. 1996. A probabilistic analysis of foundation settlement. Computers and Geotechnics, 18 (4): 291-309.

Christian, J. T. and Baecher, G. B. 1999. Point estimate method as numerical quadrature. Journal of the Geotechnical and Geoenvironmental Engineering Division, ASCE, 125 (GT9): 779-786.

Christian, J. T., Ladd, C. C., and Baecher, G. B. 1994. Reliability and probability in stability analysis. Journal of the Geotechnical Engineering Division, ASCE, 120 (GT2): 1071-1111.

DeGroot, D. J., and Baecher, G. B. 1993. Estimating autocovariance of in-situ soil properties. Journal of the Geotechnical Engineering, ASCE, 119 (GT1): 147-166.

Deutsch, C. 1989. Calculating effective absolute permeability in sandstone/shale sequences. SPE Formation Evaluation, 4: 343-348.

Deutsch, C. V. 2002. Geostatistical reservoir modeling. Oxford University press, New York.

Deutsch, C. V. and Journel A. G. 1998. GSLIB geostatistical software library. Oxford University Press, Oxford, New York

El-Ramly, H. 2001. Probabilistic and quantitative risk analysis for earth slopes. Ph.D. thesis, University of Alberta, Edmonton, Alberta, Canada.

Fenton G. A., and Vanmarcke. E. 1990. Simulation of random fields via local average subdivision. Journal of Engineering Mechanics, 116 (8): 1733-1749.

Fenton, G. A., and Vanmarcke, E. H. 1991. Spatial variation in liquefaction risk assessment. Proceeding of the geotechnical Engineering Congress, Boulder, Colorado, USA. Geotechnical Special Publications, No. 27, Vol.1, pp. 594-607.

Folayan, J. I., Hoeg, K, and Benjamin, J. R. 1970. Decision theory applied to settlement predictions. Journal of Soil Mechanics and Foundation Division, ASCE, 96 (SM4): 1127-1141.

Griffiths, D.V., and Fenton, A. 1993. Seepage beneath water retaining structures founded on spatially random soil. Geotechnique, 43 (4): 577-587.

Harr, M. E. 1987. Reliability-based design in civil engineering. McGraw-Hill Book Company, New York.

Hutcheson, H. 2000. Depositional and geotechnical characteristics of mineral sands thickened/paste tailings. Transportation and Deposition of Thickened/Paste Tailings Learning Seminar. Edmonton, Alberta, Canada.

Journel, A. G. and Huijbregts, C. J. 1978. Mining geostatistics. Academic Press, New York.

Kim, H., and Major, G. 1978. Application of Monte Carlo techniques to slope stability analysis. Proceeding of the 19th US Symposium on Rock Mech., Nevada, USA, pp. 28-39.

King, P. R. 1989. The use of renormalization for calculating effective permeability. Transport in Porous Media, 4: 37-58

Lumb, P. 1970. Safety factors and the probability distribution of soil strength. Canadian Geotechnical Journal, 7 (3): 225-242.

Morgenstern, N. R. 2000. Performance in geotechnical engineering. The first Lumb Lecture, Hong Kong.

Neter, J., Kutner, M. H., Nachtsheim, C. J., and Wasserman, W. 1996. Applied linear statistical models. McGraw-Hill Book Company, New York.

Norris, R.J., Lewis, J. M., and Heriot-Watt, U. 1991. The geological modeling of effective permeability in complex heterolithic facies. Proceeding of the 66th Annual Technical Conference and Exhibition, SPE 22692 Dallas, Texas, USA, Vol. W, pp. 359-374.

Paice, G. M., Griffiths, D. V., and Fenton, G. A. 1994. Influence of spatially random soil stiffness on foundation settlement. Proceeding of the Conference on Vertical and Horizontal Deformation of Foundations and Embankments, Part 1 (of 2), College Station, Texas, USA, pp. 628-639.

Palisade Corporation. 1996. @Risk: Risk analysis and simulation add-in for Microsoft Excel or Lotus 1-2-3. Palisade Corporation, NY, USA.

Pate-Cornell, M. E. 1987. Risk uncertainties in safety decisions. Reliability and Risk Analysis in Civil Engineering. Proceedings of the ICASP5, the 5th International Conference on Application of Statistics and Probability in Soil and Structural Engineering, Vancouver, BC, Canada. Vol.1, pp. 538-374.

Phoon, K. K. and Kulhawy, F. H. 1999. Characterization of geotechnical variability. Canadian Geotechnical Journal, 36 (4): 612-624.

Popescu, R., Prevost, J. H., and Deodatis, G. 1996. Influence of spatial variability of soil properties on seismically induced liquefaction. Proceeding of the 1996 Conference on Uncertainty in the Geologic Environment, Uncertainty 96, Part 2 (of 2), Madison, WI, USA, pp. 1098-1112.

Popescu, R., Prevost, J. H., and Deodatis, G. 1998. Characteristic percentile of soil strength for dynamic analysis. Proceeding of the 1998 Conference on Geotechnical Earthquake Engineering and Soil Dynamics III, Part 2 (of 2), Seattle, WA, USA, pp. 1461-1471.

Resendiz, D. and Herrera, I. 1969. A probabilistic formulation of settlement control design. Proceeding of the 6th International Conference on Soil Mechanics and Foundation Engineering, Mexico City, Mexico, pp. 217-225.

Righetti, G., and Harrop-Williams, K. 1988. Finite element analysis for random soil media. Journal of the Geotechnical Engineering Division, ASCE 114 (GT1): 59-75.

Robinsky, E. I. 1999. Thickened tailings disposal in the mining industry. E.I. Robinsky Associates, Toronto.

Rosenblueth, E. 1975. Point estimate for probability moments. Proceedings of National Academy of Science, USA, 72 (10): 3812-3814.

Rosenblueth, E. 1981. Two-point estimates in probabilities. Applied Mathematical Modeling, 5: 329-335.

Schultze, E. 1975. Some aspects concerning the application of statistics and probability to foundation structures. Proceeding of the 2nd International Conference on Applications of statistics and probability in soil and structure Engineering, Aachen, Germany, pp. 457-494.

Tobutt, D. C., and Richards, E. 1979. The reliability of earth slopes. International Journal for Numerical and Analytical Methods in Geomechanics, (3): 323-354.

US Army Corps of Engineers. 1995. Introduction to probability and reliability methods for use in geotechnical engineering. Engineering Technical Letter No.1110-2-547, Washington DC, USA.

Vanmarcke, E. 1977. Probabilistic modeling of soil profiles. Journal of the Geotechnical Engineering Division, ASCE, 103 (GT11): 1227-1245.

Vanmarcke, E. H. 1984. Random fields, analysis and synthesis. MIT Press, Cambridge, MA.

Warren, J. E., and Price, H. S. 1961. Flow in heterogeneous porous media. Society of Petroleum Engineering Journal: 153-169.

Whitman, R. V. 2000. Organizing and evaluating uncertainty in geotechnical engineering. Journal of the Geotechnical Engineering Division, ASCE, 126 (GT7): 583-593.

Wolff, T. F. 1996. Probabilistic slope stability in theory and practice. Proceeding of the 1996 Conference on Uncertainty in the Geologic Environment, Uncertainty 96, Part 1 (of 2), Madison, WI, USA, pp. 419-433.

Wu, T. H., and Kraft, L. M. 1967. The probability of foundation safety. Journal of Soil Mechanics and Foundation Division, ASCE, 93 (SM5): 213-231.

Yegian, M. K. and Whitman, R. V. 1978. Risk analysis for ground failure by liquefaction. Journal of the Geotechnical Engineering Division, ASCE, 104 (GT7): 921-937.

Zeitoun, D. G. and Baker, R. 1992. A stochastic approach for settlement predictions of shallow foundations. Geotechnique, 42 (4): 617-629.

APPENDIX 2-A

COMPARISON BETWEEN DIFFERENT MEASURES OF LIMIT OF SPATIAL CONTINUITY BETWEEN FOELD DATA

For exponential correlation structure models, variogram, $\gamma(h)$, and covariance functions, $C(h)$, of standardized random variable of zero mean and unit variance can be expressed in the form:

$$\gamma(h) = 1 - e^{-3h/a} \qquad \text{(2-A-1.a)}$$

$$C(h) = e^{-3h/a} \qquad \text{(2-A-1.b)}$$

The autocorrelation distance is the separation distance at which the covariance functions decays to a value equal to σ/e, i.e. $1/e$ for standardized variables.

$$e^{-1} = e^{-3R/a} \Rightarrow 1 = \frac{3R}{a} \qquad \text{(2-A-2)}$$

$$\therefore R = \frac{a}{3} \qquad \text{(2-A-3)}$$

On the other hand, Vanmarcke (1984) provided an estimation of scale of fluctuation for exponential and gaussian correlation structure models in the form of $\theta = 2a/3$ and $\theta = (\sqrt{\pi}/\sqrt{3})$ a, respectively.

Applying similar procedure to Gaussian correlation structure models:

$$\gamma(h) = 1 - e^{-3h^2/a^2} \qquad \text{(2-A-4.a)}$$

$$C(h) = e^{-3h^2/a^2} \qquad \text{(2-A-4.b)}$$

$$e^{-1} = e^{-3R^2/a^2} \Rightarrow 1 = \frac{3R^2}{a^2} \qquad (2\text{-}A\text{-}5)$$

$$\therefore R = \frac{a}{\sqrt{3}} \qquad (2\text{-}A\text{-}6)$$

For spherical correlation structure models, DeGroot and Baecher (1993) suggested that R would be equal to θ for all practical purposes. While, the scale of fluctuation can be assessed using the mathematical expression proposed by Vanmarcke (1984) through:

$$\theta = \lim_{T \to \infty} T \cdot \Gamma^2(T) \qquad (2\text{-}A\text{-}7)$$

Since spherical correlation structure models decay to zero at a separation distance equal to the spatial range, not at infinity as the case for exponential and Gaussian models, it was suggested in this study that Equation 2-A-7 should be in the form:

$$\theta = \lim_{T \to a} T \cdot \Gamma^2(T) \qquad (2\text{-}A\text{-}8)$$

where $\Gamma^2(T)$ is the variance reduction factor for spherical correlation structures derived in Appendix 2-B.

Mathematical manipulation of Equation 2-A-8 would result in a scale of fluctuation, θ, in the form:

$$\theta = 0.55\,a \qquad (2\text{-}A\text{-}9)$$

DERIVATION OF VARIANCE REDUCTION FACTOR FOR SPHERICAL CORRELATION STRUCTURE

The variance reduction factor, Γ^2, can be determined according to the following relation proposed by Vanmarcke (1984):

$$\Gamma_T^2 = \frac{2}{T}\int_0^T (1-\frac{h}{T}).C(h)dh \qquad (2\text{-}B\text{-}1)$$

where: h is the separation distance; and

C(h) is the standard covariance, i.e. covariance with a unit variance.

The standard covariance of spherical correlation structure can be expressed in the form:

$$C(h) = 1 + 0.5(\frac{h}{a})^3 - 1.5(\frac{h}{a}) \qquad (2\text{-}B\text{-}2)$$

Substituting in Equation 2-A-1 provides

$$\Gamma_T^2 = \frac{2}{T}\int_0^T (1-\frac{h}{T}).[1 + 0.5(\frac{h}{a})^3 - 1.5(\frac{h}{a})]dh \qquad (2\text{-}B\text{-}3)$$

Integrating and rearranging results, provides the following expression for the variance reduction factor for spherical correlation structures:

$$\Gamma_T^2 = 1 - \frac{T}{2a} + \frac{T^3}{20a^3} \qquad (2\text{-}B\text{-}4)$$

Table 2.1. Comparison between different measures of the limit of spatial continuity between field data.

Type of correlation structure model	Spatial range	Scale of fluctuation	Auto-covariance distance
Exponential	a	$2a/3$	$a/3$
Gaussian	a	a	$0.58\,a$
Spherical	a	$0.55\,a$	a

Table 2.2. Assessment of performance of earth slopes and the associated failure probability as proposed by the US Corps of Engineers (1995).

Expected Level of Performance	β	Probability of Failure
High	5	$3*10^{-5}$ %
Good	4	0.003 %
Above average	3	0.1 %
Below average	2.5	0.6 %
Poor	2	2.3 %
Unsatisfactory	1.5	7 %
Hazardous	1	16 %
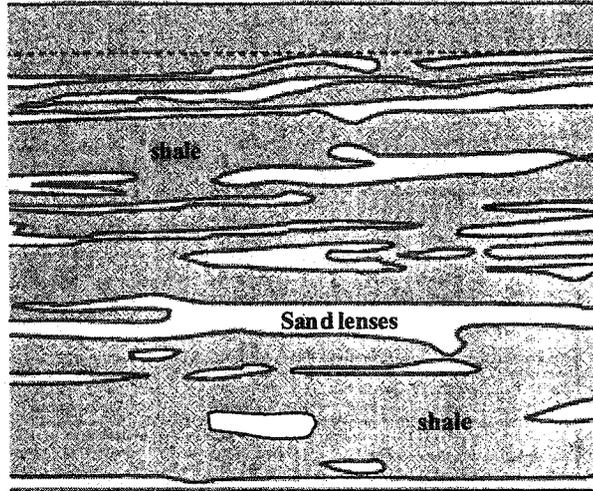
Figure 2.1. Sand-Shale sequence in a petroleum field, WY, USA (modified from Norris et al. 1991)
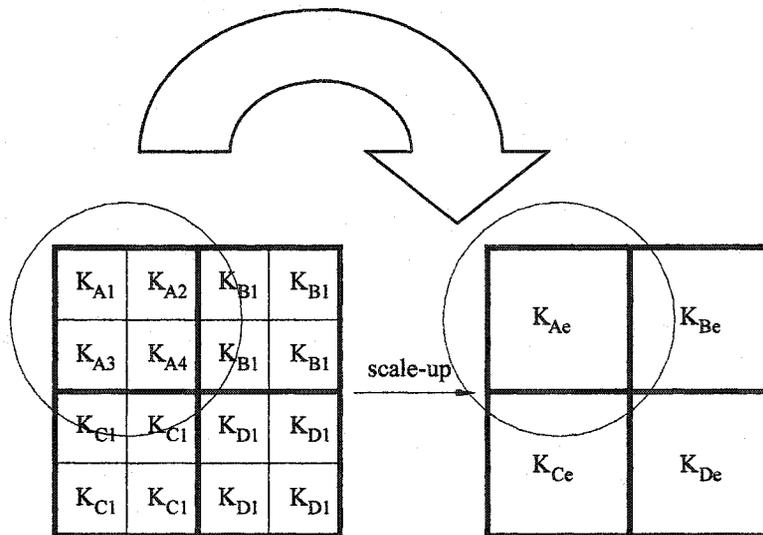
Figure 2.2. Schematic diagram of up-scaling using the Renormalization technique (modified from King 1989)
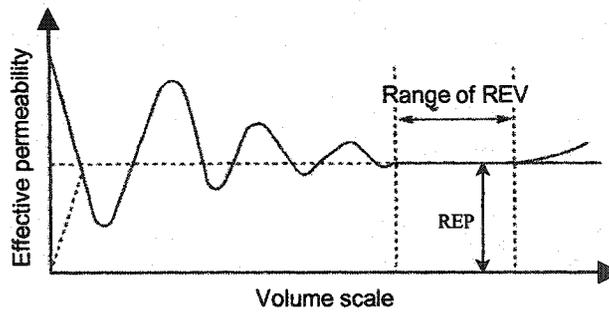
Figure 2.3. Representative Elementary Volume concept (modified from Norris et al. 1991)
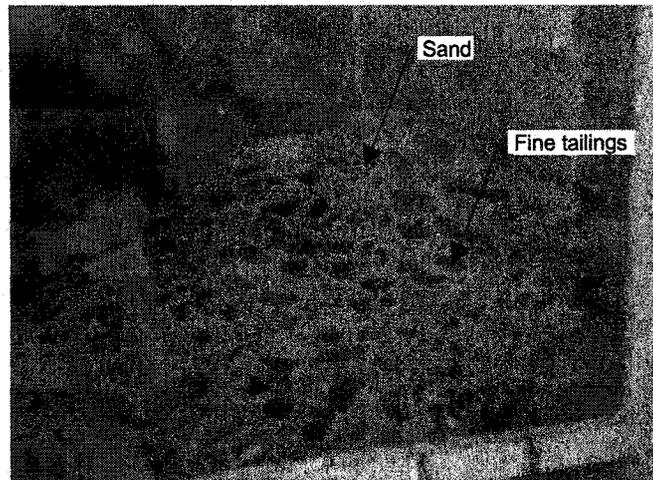
Figure 2.4. Sand-fine tailings mixture in a laboratory model of co-depositional sand - fine tailings embankments. (modified from Hutcheson 2000)
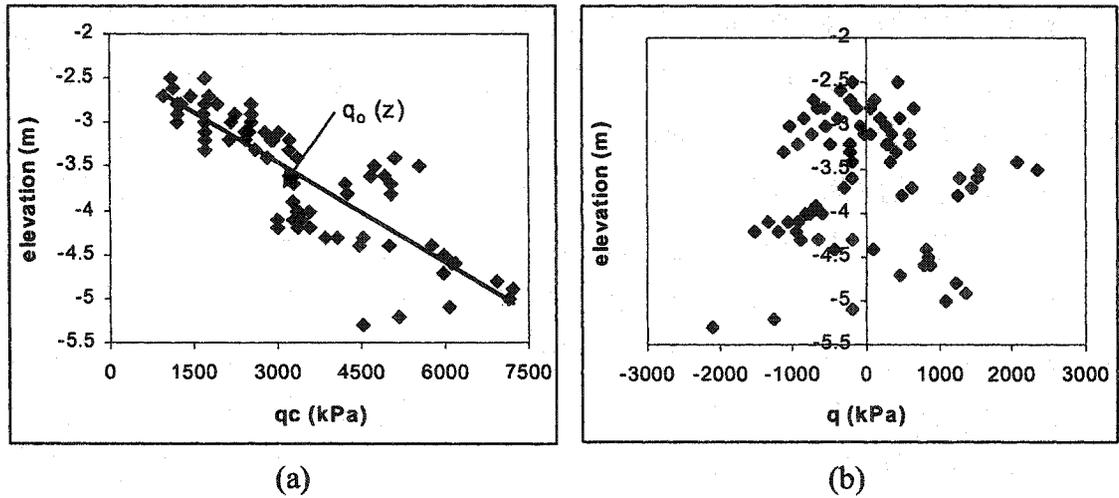
Figure 2.5. Detrending of CPT tip resistance data. a) identifying linear vertical trend; and
b) detrended data.
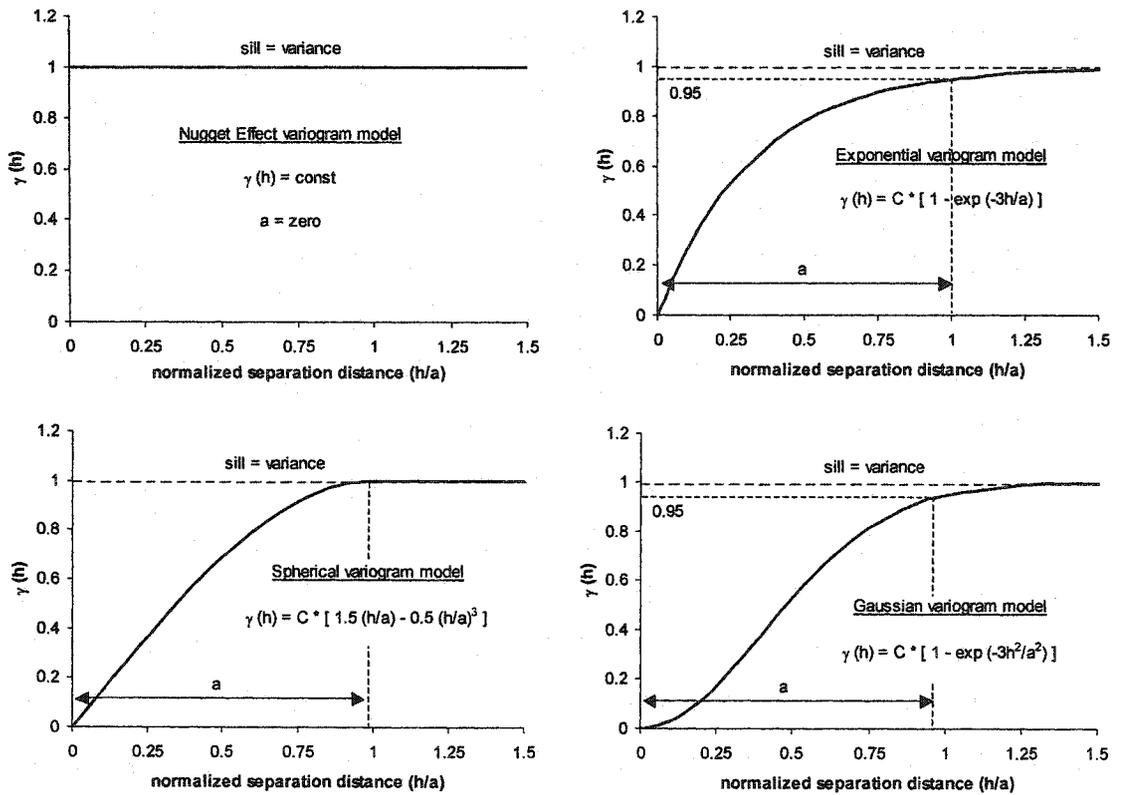
Figure 2.6. Examples of variogram models commonly used in practice
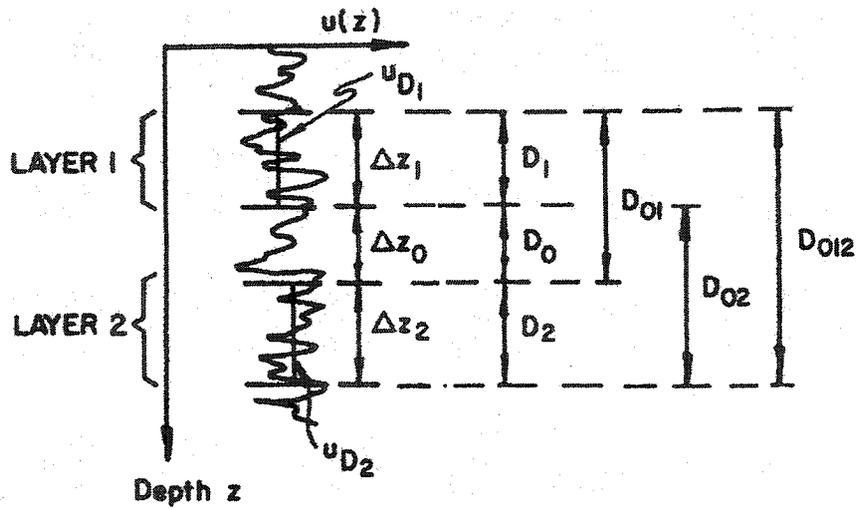
Figure 2.7. Schematic diagram illustrating different terms used to obtain correlation between spatial averages of random variables (modified from Vanmarcke 1977)
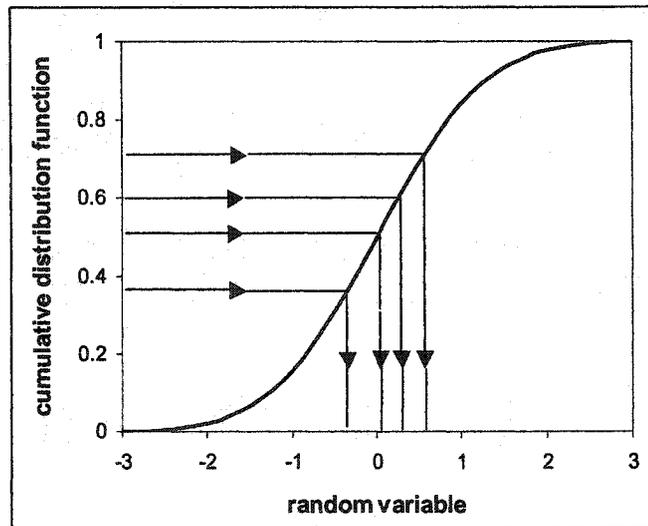
Figure 2.8. Clustering of the outcome of Monte Carlo simulation due to using insufficient number of realizations (modified from Palisade Corporation 1996).
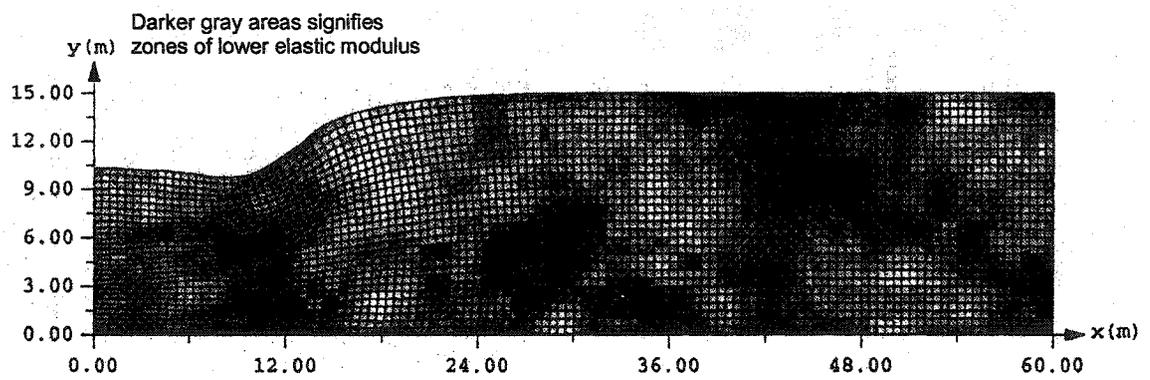
Figure 2.9. Deformed mesh with spatially variable elastic modulus below flexible strip footing (modified from Paice et al. 1994)
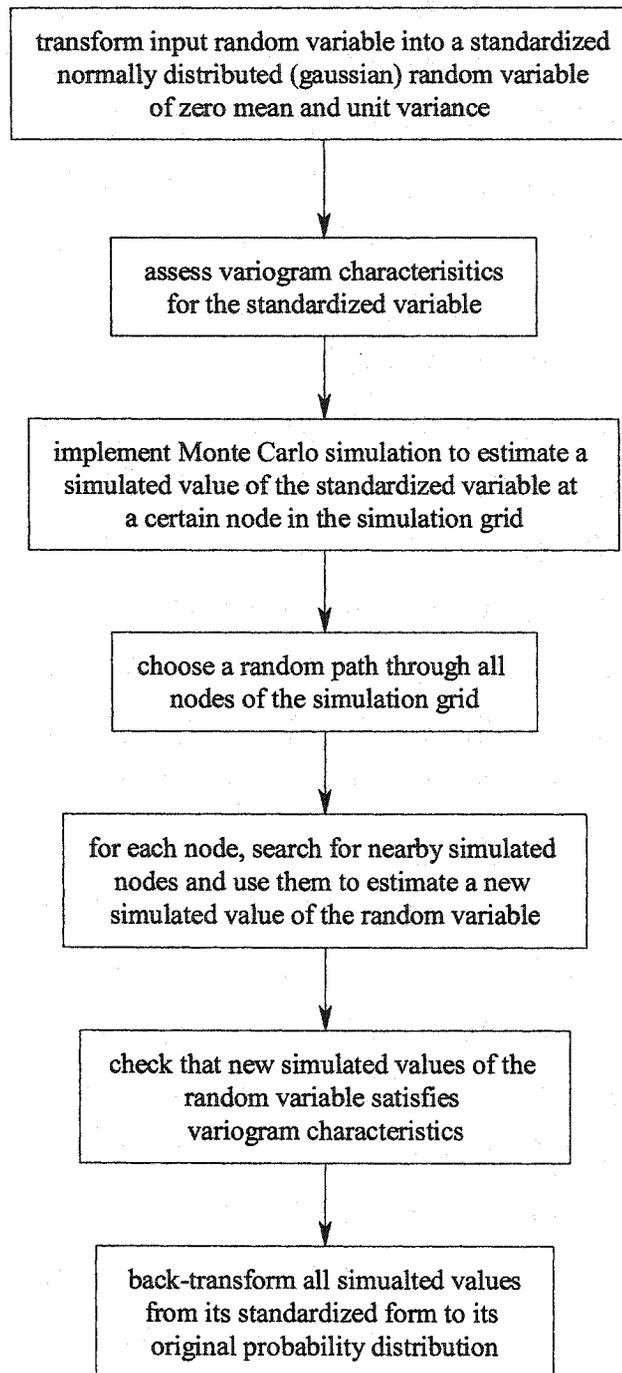
Figure 2.10. The basic idea of the sequential Gaussian simulation.
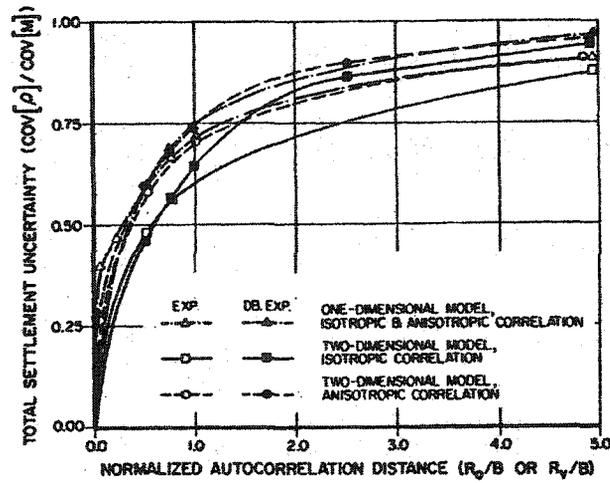
Figure 2.11. Increase in settlement uncertainty with the increase in normalized autocorrelation distance of soil elastic modulus. (modified from Baecher and Ingra 1981)
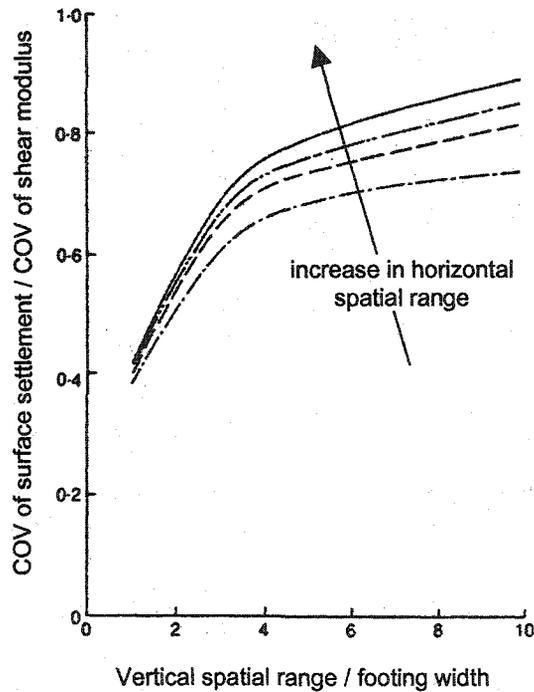
Figure 2.12. Increase in the uncertainty of surface settlement with higher ranges of spatial correlation between field data. (modified from Zeitoun and Baker 1992)

- 51 -
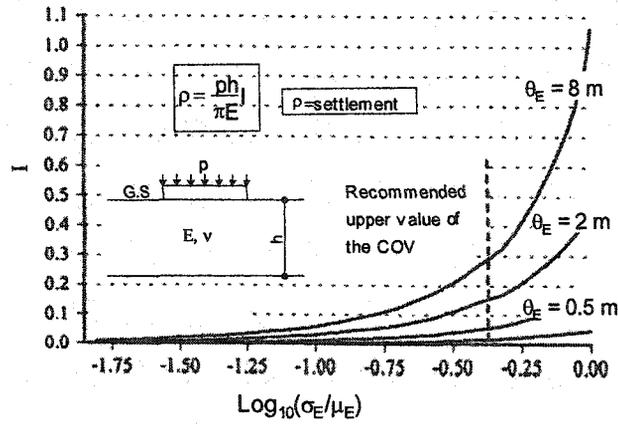
Figure 2.13. Increase in settlement uncertainty (expressed in terms of the influence factor standard deviation σ_I) with the increase in COV and auto correlation distance (θ_E) of soil elastic modulus. (modified from Paice et al. 1994)
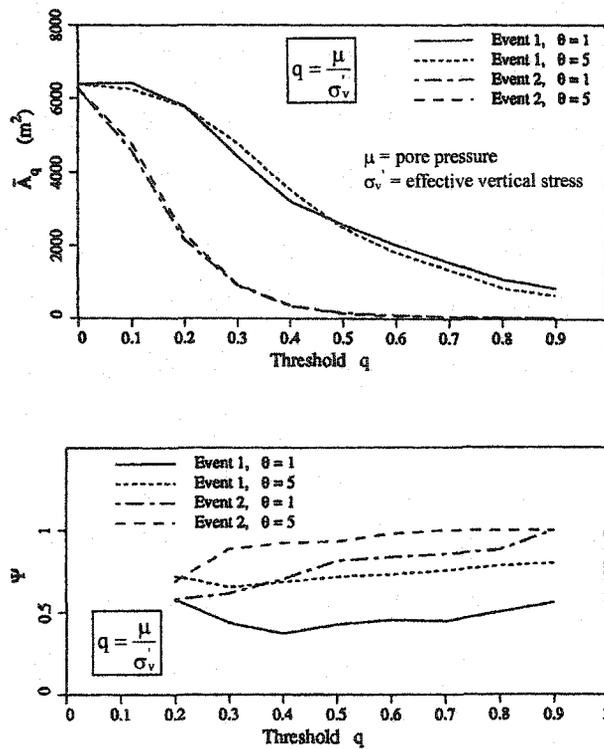
Figure 2.14. Effect of scale of fluctuation, θ, on different liquefaction potential measures. (event 1 and event 2 represent different input ground accelerations). (modified from Fenton and Vanmarcke 1991)

- 52 -

Stochastic input – #1

Stochastic input – #2

Stochastic input – #3

Stochastic input – #4

Deterministic using
mean values
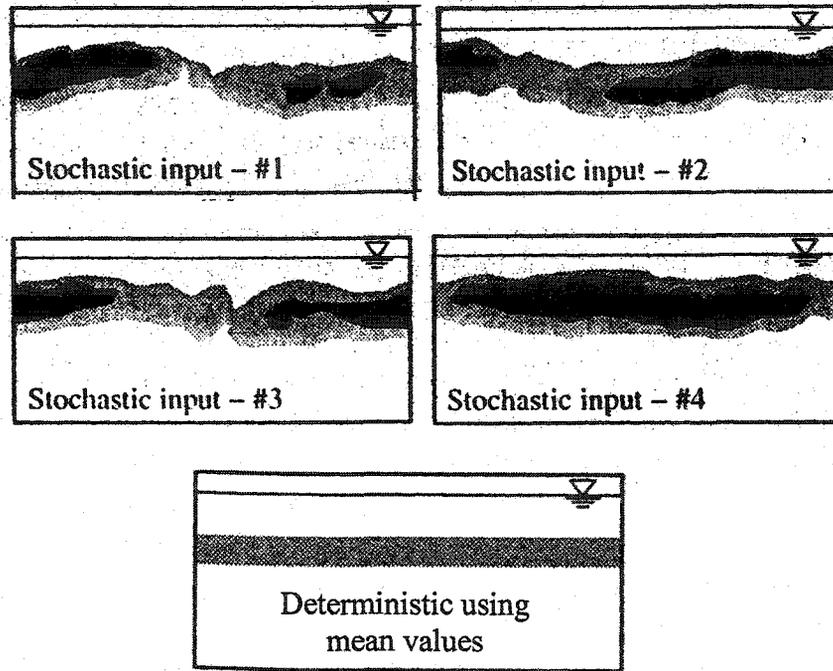
(darker gray scale indicates higher pore pressure)

Figure 2.15. Normalized induced pore pressure profiles obtained from different realizations of the soil strength. (modified from Popescu et al. 1996)
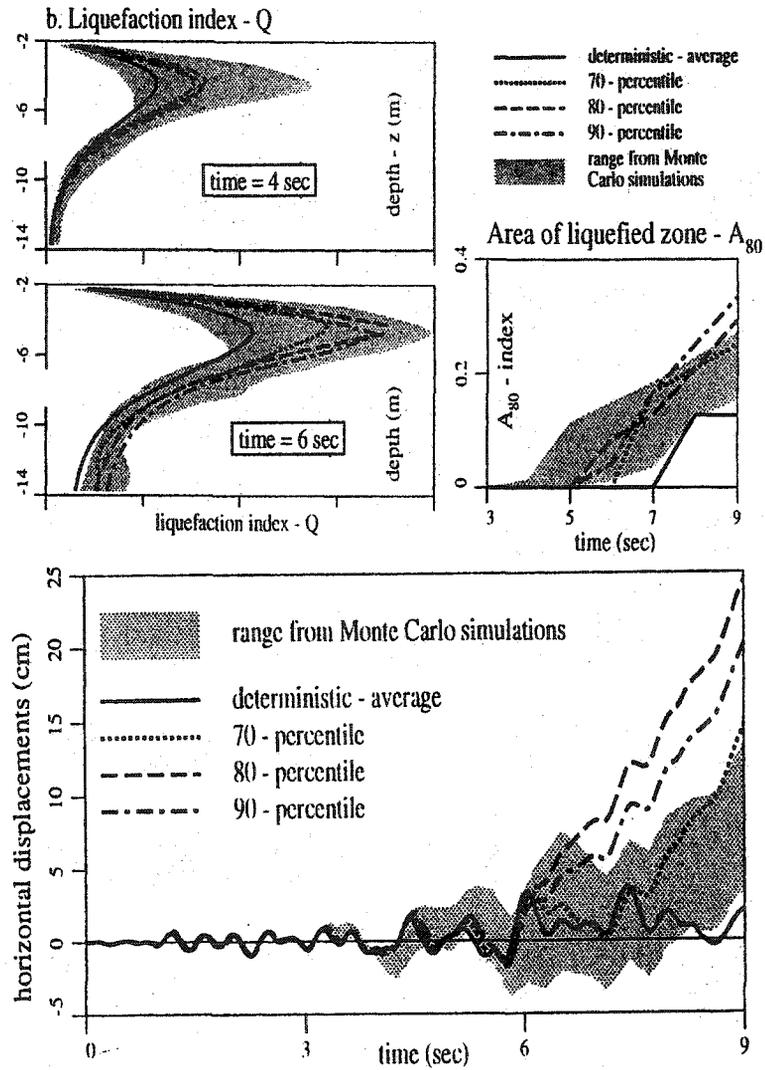
Figure 2.16. Stochastic assessment of liquefaction potential measures compared with values obtained from different characteristic percentiles of CPT data. (modified from Popescu et al. 1998)
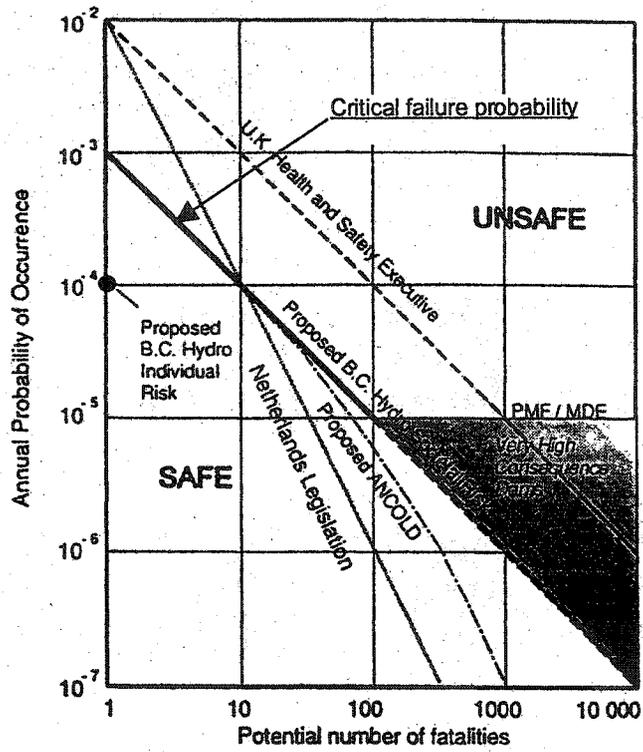
Figure 2.17. Critical probabilities of failure for dam design in terms of expected number of fatalities (modified from Whitman 2000)
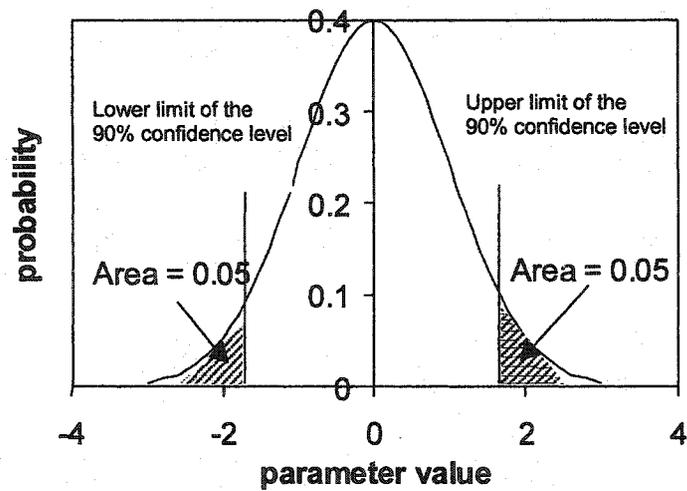
Figure 2.18. Selection of design parameters associated with 90% confidence level.
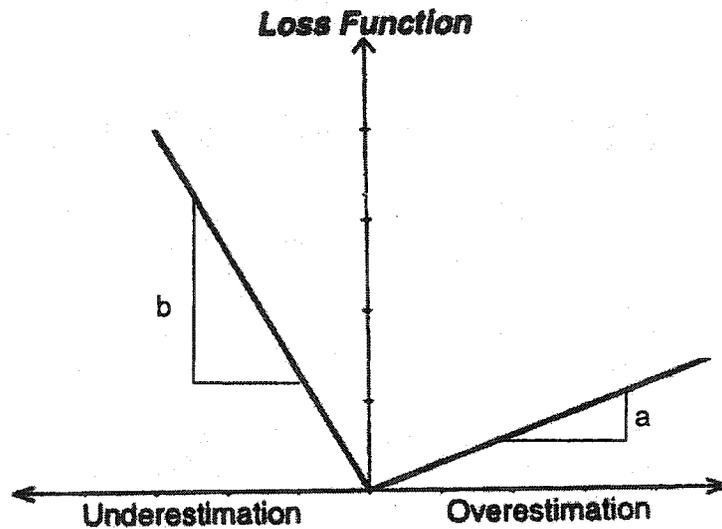
Figure 2.19. Linear loss functions to quantify the effect of making mistakes in estimating soil design parameters

- 56 -

CHAPTER 3

BEHAVIOR OF SAND WITH INTERCALATED CLAY SEAMS
UNDER PLANE STRAIN CONDITIONS

3.1. INTRODUCTION

Almost all natural soils are heterogeneous in nature. Soil heterogeneity can be classified into two main categories. The first type of soil heterogeneity can be attributed to soil inherent spatial variability, which is the variation of soil properties from one point to another in space due to difference in deposition conditions and loading history. The second category of soil heterogeneity is lithological heterogeneity, which can be manifested in the form of pockets of a certain soil type within a more uniform larger mass of different lithology and thin soft/stiff layers embedded in a stiffer/softer media. The latter type of lithological heterogeneity is commonly found in fluvial soil deposits where intercalated clay seams can be found in larger sand masses.

Early attention to the problem of soil heterogeneity emerged from the field of petroleum engineering. Several studies have been carried out to assess the impact of lithological heterogeneity, and the associated variation in hydraulic conductivity from one lithology to another, on the production of oil and gas reservoirs. This was accomplished by using homogenization theories and up-scaling (averaging) techniques to scale up fine scale permeability to coarser scales amenable to flow simulation and engineering calculations. These up-scaling techniques can be classified into 3 main categories, as discussed in Chapter 2:

1. Empirical techniques such as the power averaging technique (Deutsch 1989). These are the simplest forms of up-scaling laws;

2. Semi-empirical methods such as the Renormalization technique (King 1989), and the Representative Elementary Volume (REV) - Renormalization (Norris et al. 1991). They are more sophisticated than the previous type but have limited theoretical basis; and

3. Analytical techniques such as that proposed by Warren and Price (1961). These methods are rather cumbersome to implement in practice.

Dealing with lithological heterogeneity in geotechnical engineering has been exclusively left to local experience and engineering judgment. Nevertheless, few attempts have been made to assess the impact of this heterogeneity on engineering behavior of soils. Oda and Win (1990) investigated the effect of clay seams on the macro behavior of sand under plane strain conditions. This was carried out using lab models where a remolded thin clay layer was placed at several depths in a sand mass below a strip footing. The presence of the clay seam was found to have a significant impact on the ultimate bearing capacity of the heterogeneous soil media. However, no attempt was made to quantify the effect of the clay seam on the deformability of the sand mass. Niemunis et al. (2000) proposed an averaging technique for layered materials under plane strain conditions for use in finite element analysis. An equivalent stiffness matrix was derived for elements composed of layered materials based on the volume fraction of each of these materials, their constitutive relationships, and state of stresses. The proposed methodology has some limitations, as it is limited to elastic analysis. In addition, no justification was given for the assumption that layered materials can be replaced by a periodic microstructure, which preserved the laminar structure of the original element and the volume fraction of different materials. Generally, this approach can be considered relatively complicated to apply in practice and its applicability is limited to finite element codes that allow for user-defined stiffness matrix.

The main focus of this chapter is to quantify the effect of intercalated soft to medium clay seams on the macro behavior of sand under plane strain conditions. This was assessed in a numerical analysis framework using the FLAC software (Itasca

Consulting Group Inc. 2000) to obtain simplified representative (average) values for soil friction angle and elastic modulus that took into consideration the presence of the clay seams. In addition, an expression for average elastic modulus of heterogeneous soil media was developed in this study based on theory of elasticity and was compared to the numerical analysis results and different theoretical solutions in petroleum engineering literature. Finally, the results obtained in this chapter were applied to a shallow foundation problem to examine their applicability to geotechnical field problems.

3.2. DESCRIPTION OF THE USED MODEL

The effect of a thin layer of medium to soft clay on the macro (overall) behavior of a medium dense sand mass under plane strain condition was assessed numerically using the FLAC software (Itasca Consulting Group Inc. 2000). A clay layer of thickness T was inserted at the mid height of a rectangular sand mass of height H and width equal to H/2, as shown in Figure 3.1.a. A typical mesh used in the analyses is shown in Figure 3.1.b, where only one quarter of the physical model was analysed due to the similarity of the problem around horizontal and vertical axes. Soil was assumed to exhibit elastic perfectly plastic constitutive behavior applying Mohr-Coulomb failure criterion, for simplicity. The rate of loading was assumed to be rapid enough that the clay layer would behave under undrained conditions, while the sand was assumed to exhibit drained behavior. In addition, the soil was assumed to be weightless, i.e. the effect of body forces on the analysis results was not taken into account. This simplified model was chosen due its analogy with geotechnical laboratory tests with simple boundary and loading conditions, such as the triaxial and biaxial tests.

Soil properties used in the numerical analyses were obtained from the typical values cited in geotechnical engineering literature for soft to medium clay and medium sand, as shown in Table 3.1. Sand friction angle, elastic modulus, and Poisson's ratio were assumed to be 34 degree, 50 MPa and 0.30, respectively. Undrained shear strength

of the clay seams was varied between 15 and 35 kPa. Values of 200, 600, and 1200 for the ratio between the undrained elastic modulus of the clay seams and their undrained shear strength (E_u/S_u) were chosen for the analyses while Poisson's ratio was held constant at a value of 0.49.

3.3. ANALYSES RESULTS

A series of analyses was carried out applying the model discussed in the previous section for values of volumetric clay fraction (T/H) of 2.5%, 5.0%, and 10.0%. Confining pressures were varied between 25 kPa and 100 kPa to cover the typical range of in-situ horizontal stresses commonly encountered in geotechnical practice.

The failure deviator stress $(\Delta\sigma)_f$ of the heterogeneous sand-clay mass was found to decrease with increasing the clay seam volume under different applied confining pressures, resulting in the development of 3 heterogeneity zones. Examples of these heterogeneity zones are shown in Figure 3.2 for an applied confining pressure of 50 kPa. In zone I, the clay seam was found to have insignificant influence on the overall (macro) behavior of the sand mass as it resulted in a decrease in ultimate (failure) stress of uniform sand by values less than 10%. In addition, no change in the failure mode from that of a homogeneous sand mass was observed, as shown in Figure 3.3. In zone II, the presence of the clay layer had a significant impact on the overall performance of the heterogeneous mass and the failure stress was found to be highly sensitive to change in the clay layer volume. Furthermore, a dramatic change in the failure mechanism was observed, as shown in Figure 3.3, where yielding was concentrated in sand zones close to the clay layer. In zone III, the macro behavior of the sand-clay mass was mainly governed by the strength characteristics of the clay layer, which was manifested in a change in the failure mode in the form of yielded zones limited to the clay layer when failure occurred, as shown in Figure 3.3. Based on these results, it was postulated that zone II is the zone where efforts were needed to estimate representative average

properties for the sand-clay mass for use in engineering design, as explained in the following paragraphs.

The boundaries between zones I, II and III were assessed in a similar manner to the empirical technique used to estimate over-consolidation pressure for pre-consolidated clay (Casagrande graphical method). This was chosen because of the similarity between the curves presented in Figure 3.2 and one-dimensional consolidation curves for over-consolidated clay. As a result, the author believes that a considerable degree of uncertainty is associated with the values of these boundaries and that they should be used as approximate design guidelines.

The variation of the boundaries between different heterogeneity zones with undrained shear strength of the clay layer is presented Figure 3.4. As expected, the clay volumes associated with these boundaries increased for higher values of undrained shear strength, and this increase was found to be in a relatively linear fashion. These boundaries were, also, dependent on the applied confining pressure, as shown in Figure 3.4. The boundary between zones I and II was found to be highly sensitive to changes in confining pressure between 25 and 50 kPa and less sensitive for higher values of confining pressure. While, the boundary between zones II and III exhibited higher sensitivity to confining pressure values greater than 50 kPa.

An equivalent (average) friction angle, ϕ_e, was assessed as the friction angle of a homogeneous sand mass that would fail at the same failure deviator stress of the heterogeneous sand-clay mass. This equivalent angle was used to estimate the reduction in the overall friction angle of soil mass due to the presence of the clay seams ($\Delta\phi$), which is the difference between the friction angle of homogenous sand (ϕ_o) and the equivalent friction angle (ϕ_e). This reduction in friction angle, normalized to the friction angle of homogenous sand, was found to increase linearly with the increase in thickness of the clay layer, and became more significant for higher confining pressures, as shown in Figure 3.5.

- 61 -

Similarly, an equivalent elastic modulus, E_{eq}, for the heterogeneous sand-clay mass was obtained by assessing the value of elastic modulus of homogeneous sand that would reproduce the same average vertical displacement of the heterogeneous mass. It should be noted that the anisotropy in the clay elastic modulus and its implications on equivalent elastic modulus was not considered in this study, for simplicity. The variation of normalized equivalent elastic modulus (E_{eq}/E_o) with the increase in normalized deviator stresses, for $E_u/S_u = 200$, is presented through Figure 3.6.a to Figure 3.8.a and was found to be in a good agreement with a third degree polynomial. The normalized modulus was obtained by dividing the value of equivalent elastic modulus by the elastic modulus of sand, E_o. The normalized deviator stress was assessed as the value of applied deviator stress, $\Delta\sigma$, divided by the value of deviator stress at failure, $(\Delta\sigma)_f$.

Estimates of equivalent elastic modulus for E_u/S_u of 600 and 1,200 were obtained by multiplying the normalized value obtained from Figure 3.6.a to Figure 3.8.a by a correction factor (CF). This correction factor could be obtained from Figure 3.6.b to Figure 3.8.b and was developed by dividing the equivalent elastic modulus (E_{eq}) associated with (E_u/S_u) equal to 600 or 1,200 by its counterpart at (E_u/S_u) equal to 200. This factor was found to decrease with the increase in normalized undrained shear strength of the clay seam ((S_u/P_a)/tan ϕ) on a semi-log scale. The normalized undrained shear strength was defined as the ratio between the undrained shear strength of the clay seam, normalized to atmospheric pressure (P_a), and the tangent of the friction angle of sand. This normalized undrained shear strength was considered as an empirical non-dimensional factor to represent the relative strength between the clay seam and the medium dense sand.

3.4. COMPARISON WITH THEORETICAL SOLUTIONS

The results obtained in the previous section were compared with different theoretical solutions to examine their applicability. Examples of these solutions are:

- 62 -

1. A theoretical solution developed in this study based on theory of elasticity;

2. A modification of the power averaging technique (Deutsch 1989); and

3. A modification of the Renormalization technique (King 1989).

The theoretical elastic solution developed in this study aimed at assessing an equivalent elastic modulus for a rectangular heterogeneous mass of 2 different materials under plane strain conditions, as shown in Figure 3.9. A mathematical expression was obtained, as explained in Appendix 3-A, for the equivalent modulus in the form:

$$E_{eq} = \frac{[\sigma_1(1-\upsilon^2)-\upsilon\;\sigma_3(1+\upsilon)]\cdot\sum\limits_{i=A}^{B}H_i}{\sum\limits_{i=A}^{B}\dfrac{H_i}{E_i}[\sigma_1(1-\upsilon_i^2)-\upsilon_i\sigma_{3i}(1+\upsilon_i)]}$$

(3-1)

where σ_{3i} is the confining pressure affecting layer A and B (σ_{3A} and σ_{3B}), which can be assessed through:

$$\sigma_{3A} = \frac{\sigma_3\dfrac{H}{H_B}\cdot\dfrac{(1-\upsilon_B^2)}{E_B}+\sigma_1[\dfrac{\upsilon_A}{E_A}(1+\upsilon_A)-\dfrac{\upsilon_B}{E_B}(1+\upsilon_B)]}{\dfrac{1-\upsilon_A^2}{E_A}+\dfrac{1-\upsilon_B^2}{E_B}\cdot\dfrac{H_A}{H_B}}$$

(3-2-a)

$$\sigma_{3B} = \frac{\sigma_3\dfrac{H}{H_A}\cdot\dfrac{(1-\upsilon_A^2)}{E_A}+\sigma_1[\dfrac{\upsilon_B}{E_B}(1+\upsilon_B)-\dfrac{\upsilon_A}{E_A}(1+\upsilon_A)]}{\dfrac{1-\upsilon_B^2}{E_B}+\dfrac{1-\upsilon_A^2}{E_A}\cdot\dfrac{H_B}{H_A}}$$

(3-2-b)

The above equations were applied in two stages to obtain estimates of equivalent elastic modulus for different configurations of the heterogeneous sand-clay mass, as shown in Figure 3.10. These estimates were in good agreement with the numerical analysis outcomes for smaller values of applied deviator stresses where the behavior of the heterogeneous mass was mainly elastic, as shown in Figure 3.11. This agreement became less pronounced with increasing the thickness of the clay as it would result in

- 63 -

early deviation from elastic behavior and onset of plastic deformations at smaller deviator stress, as seen for the case of T/H = 10% in Figure 3.11. The author believes that the elastic solution presented in Equations 3-1 and 3-2 is cumbersome and difficult to apply in practice; and that reasonably good estimates of equivalent elastic modulus can be obtained from Figures 3-6, 3-7 and 3-8.

The power averaging method (Deutsch 1989) was obtained through non-linear regression of the results obtained from a 3-dimensional numerical simulation of flow through sandstone-shale formations. The analysis was carried out under different target shale volumes and the equivalent permeability was regarded as that of a homogeneous soil mass producing similar flow under the same head difference and boundary conditions. This equivalent permeability, k_e, was found to satisfy the relation:

$$k_e = [\frac{V_{sh}}{V_{total}} k_{sh}^{\omega} + \frac{V_{ss}}{V_{total}} k_{ss}^{\omega}]^{1/\omega}$$

(3-3)

where : k_{sh} and k_{ss} are the permeabilities of the shale and sandstone, respectively;

V_{sh} is the volume fraction of shale;

V_{total} is the total volume of the shale-sandstone heterogeneous medium; and

ω is an averaging power.

The value of ω was suggested to range from –1 to 1 depending on the direction of flow and the geometrical anisotropy of shale, i.e. the ratio between the vertical to the lateral extent of shale (Deutsch 1989). As an approximation for the application of the power averaging technique to the problem of sand with an intercalated clay seam, Darcy's law ($q_x = k \cdot dh/dx$) and the one dimensional stress analysis in solid mechanics ($\sigma_x = E \cdot du/dx$) were considered analogous. Consequently, it was concluded that hydraulic conductivity, k, in Equation 3-3 could be replaced by the elastic modulus, E, to provide an estimate of equivalent elastic modulus in the form:

- 64 -

$$E_{eq} = \left[\frac{V_{clay}}{V_{total}} \cdot (E_{clay})^{\omega} + \frac{V_{sand}}{V_{total}}(E_{sand})^{\omega}\right]^{1/\omega} \tag{3-4}$$

Estimates of equivalent elastic modulus were obtained by applying Equation 3-4 in 2 stages, in a way similar to the elastic solution, to different configurations of the heterogeneous sand-clay mass. These estimates were in poor agreement with the numerical analysis results, as shown in Figure 3.11, as they were considerably smaller than those obtained form numerical analyses. This could be attributed to two main factors:

1. Equation 3-4 does not take into consideration the effect of Poisson's ratio on the equivalent elastic modulus; and

2. The elastic modulus estimate does not depend on the applied state of stress in terms of confining pressures or change in deviator stresses.

In the Renormalization technique applied to fluid flow problems (King 1989), a simulation grid is generated across the analysis domain and a constant value of soil permeability is assigned to each element of the simulation grid. Then, these elements are grouped into blocks of four and assigned an effective (equivalent) permeability value, k_e, which can be assessed through.

$$k_e = \frac{4(k_1 + k_3)(k_2 + k_4)[k_2 k_4 (k_1 + k_3) + k_1 k_3 (k_2 + k_4)]}{[k_2 k_4 (k_1 + k_3) + k_1 k_3 (k_2 + k_4)][k_1 + k_2 + k_3 + k_4] + 3(k_1 + k_2)(k_3 + k_4)(k_1 + k_3)(k_2 + k_4)} \tag{3-5}$$

This effective permeability was obtained based on the analogy between water flow through soils of different permeabilities and electric current flow through a network of resistors. The above procedure can be applied to the new grid and repeated several times depending on the averaging scale of interest. In a fashion similar to the power averaging technique, the above equation was modified to produce an estimate of equivalent elastic modulus in the form:

- 65 -

$$E_{eq} = \frac{4(E_1 + E_3)(E_2 + E_4)[E_2 E_4 (E_1 + E_3) + E_1 E_3 (E_2 + E_4)]}{[E_2 E_4 (E_1 + E_3) + E_1 E_3 (E_2 + E_4)][E_1 + E_2 + E_3 + E_4] + 3(E_1 + E_2)(E_3 + E_4)(E_1 + E_3)(E_2 + E_4)}$$

<div align="right">(3-6)</div>

Estimates of equivalent elastic modulus were obtained using Equation 3-6 and were found to be in a relatively poor agreement with the numerical analysis results, as shown in Figure 3.11. This could be attributed to the same 2 factors discussed earlier in the power averaging technique. It is worth noting, however, that this method provided better estimates of equivalent elastic modulus than the power averaging technique due to the relatively theoretical bases employed in the development of Equations 3-5 and 3-6.

3.5. APPLICATION TO A SHALLOW FOUNDATION PROBLEM

The results obtained in the previous sections were applied to a shallow foundation problem to examine their applicability to geotechnical field problems with relatively similar stress path. This was carried out by performing a series of numerical analyses, using the FLAC software (Itasca Consulting Group Inc. 2000), of heterogeneous soil media composed of medium dense sand with intercalated clay layer at the layer center below a strip footing. A typical mesh used in the analyses is shown in Figure 3.12. The same soil properties presented in Table 3.1 were assigned to the sand and clay layers together with a unit weight of 20 kN/m^3 and coefficient of at rest earth pressure of 0.5. Soil thickness, H, was taken equal to 3, 6, and 12 m to provide average horizontal pressure of 25, 50, and 100 kPa, respectively, at the center of the heterogeneous mass. The thickness of the clay layers, T, was chosen to generate the same values of T/H used in the plane strain model, i.e. T/H equal to 2.5, 5.0, and 10%. The footing width, B, was taken equal to half the thickness of the soil mass, H, while the foundation depth was chosen equal to 2/3 the footing width. The footing load was simulated in terms of a uniform vertical stress applied at the top of the mesh and affecting an area equal to the footing width multiplied by a unit length. The effect of embedment depth was taken into account by applying vertical pressure, equal to the foundation depth multiplied by soil

- 66 -

unit weight, at the top of the mesh outside the footing area. Soil was assumed to exhibit elastic perfectly plastic behavior implementing Mohr-Coulomb failure criterion.

The above analyses were, then, repeated for homogenized soil sections using equivalent soil parameters obtained through Figure 3.5 to Figure 3.8. A comparison between the footing pressure – average displacement curves for both heterogeneous and homogenized sections together with that of uniform sand is provided in Figure 3.13, for $S_u = 25$ kPa, $E_u/S_u = 600$, $H = 6.0$ m, and $T/H = 5\%$. The presence of a clay seam at the center of the sand mass resulted in a dramatic decrease in ultimate footing pressure that it reached a value smaller than the allowable footing pressure, using a factor of safety equal to 3, of uniform sand. In addition, a poor agreement was observed between the behavior of the heterogeneous soil medium and the homogenized section with equivalent soil properties. A detailed comparison between the behavior of the heterogeneous and homogenized soil sections is provided in Figure 3.14 and Figure 3.15. Generally, using homogenized soil sections with equivalent soil properties resulted in over-estimated ultimate footing pressures by values up to 130%. This over-estimation decreased gradually with increasing horizontal pressure at the center of the soil mass and turned into under-estimated ultimate pressures for horizontal pressure of 100 kPa and T/H equal to 10%. In a similar fashion, using homogenized soil sections produced under-estimated average footing vertical displacements by values up to 40% of the displacements associated with heterogeneous soil sections. This under-estimation decreased gradually with the increase in average horizontal pressure resulting in over-estimated values for horizontal pressure of 100 kPa and T/H equal to 10%. As a result, it was concluded that using simplified equivalent soil parameters to homogenize heterogeneous soil media below a strip footing would probably result in unrealistic results mostly on the unsafe (non-conservative) side. This could be attributed to the following reasons:

1. Vertical stress distribution in heterogeneous soil media below strip footings is not uniform as the case for the simplified plane strain model;

2. Horizontal confining pressure is not uniform as the case for the simplified plane strain model. Rather, it increases with depth due to the weight of soil mass;

- 67 -

3. Soil elements within the Prandtl passive zone are likely to be subjected to unloading conditions in the vertical direction, which is different from the simplified uniform loading conditions in the plane strain model. This spatial variation in stress path may have contributed to the poor agreement between the footing and the plane strain models; and

4. Failure of the foundation system does not occur due to shear failure in both sand and clay layers, as the case for the plane strain model. Rather, this failure was a result of excessive deformation of the heterogeneous soil mass due to plastic flow of the clay layer, which is in a close agreement with the conclusion of Oda and Win (1990).

3.6. ASSESSMENT OF EQUIVALENT DESIGN PARAMETERS FOR HETEROGENEOUS SOIL MEDIA BELOW A STRIP FOOTING

The equivalent soil parameters obtained from simplified plane strain analyses were not applicable to the strip footing problem, as discussed in the previous section. As a result, an attempt was made to obtain equivalent parameters of heterogeneous soil media, composed of medium dense sand with intercalated horizontal clay layer at the center of the soil mass, below a strip footing. This was carried out numerically in a manner similar to the simplified ideal plane strain case. In other words, an equivalent friction angle, ϕ_e, was assessed as the friction angle of a homogeneous sand mass that would reproduce the same failure footing pressure of heterogeneous soil media. This equivalent angle was used to estimate the reduction in the soil friction angle, $\Delta\phi$, due to the presence of the clay layer. This reduction was found to decrease linearly with the increase in undrained shear strength of the clay layer, as shown in Figure 3.16.

Similarly, an equivalent elastic modulus, E_{eq}, was considered as the elastic modulus of a homogeneous sand mass of friction angle ϕ_e that would reproduce the same average vertical footing displacement of the heterogeneous soil medium. The average (mean) value of this equivalent modulus up to the limit of elastic behavior and its

- 68 -

coefficient of variation were assessed for different configurations of the heterogeneous sand - clay mass. The mean equivalent elastic modulus was defined as the mean value of different estimates of the equivalent elastic modulus of the heterogeneous sand - clay mass within the zone of elastic behavior. The variation of the mean equivalent elastic modulus, normalized to elastic modulus of uniform sand (E_o), with the change in undrained shear strength of the clay layer is shown in Figure 3.17, and was found to follow a linear relationship. The coefficient of variation of equivalent elastic modulus was assessed as the ratio between the standard deviation of different estimates of equivalent elastic modulus within the zone of elastic behavior and the mean equivalent elastic modulus. A list of the coefficients of variation for different configurations of heterogeneous sand -clay media is presented in Table 3.2. For practical application, soil equivalent elastic modulus was assumed constant, within the zone of elastic behavior, with a representative value equal to its mean value if the associated coefficient of variation was less than 0.1. As a result, estimates of mean equivalent elastic modulus provided in Figure 3.17 should be used with caution if the associated coefficients of variation are greater than 0.1, as the case for the hatched cells in Table 3.2.

3.7. CONCLUSIONS

Lithological heterogeneity can be manifested in intercalated soft to medium clay seams in a bigger sand mass, as commonly found in fluvial soil deposits. The main purpose of this chapter was to quantify the effect of this heterogeneity on the macro (overall) behavior of sand under plane strain conditions. This was carried out through numerical analyses of simplified heterogeneous sand-clay masses using the FLAC software (Itasca Consulting Group Inc. 2000) to obtain estimates of average (representative) friction angle and elastic modulus for these heterogeneous media. In addition, an expression for average elastic modulus was developed based on theory of elasticity and was compared with the numerical analysis results and different theoretical solutions in petroleum engineering literature. Finally, the results of the simplified

- 69 -

numerical analyses were applied to a shallow foundation problem to examine their applicability to geotechnical field problems with relatively similar stress path.

Design charts for equivalent friction angle and elastic modulus were developed based on the numerical analyses results. These results were in good agreement with the theoretical solution obtained based on theory of elasticity for small values of applied deviator stress, where the behavior of the heterogeneous mass was mainly elastic. Different averaging (up-scaling) techniques in petroleum engineering literature exhibited poor agreement with the numerical analyses results. This was expected as these techniques were originally developed to provide estimates of equivalent hydraulic conductivities of heterogeneous oil fields. As a result, they do not account for the effect of the state of stresses and Poisson's ration on equivalent soil parameters.

The numerical analyses results of the simplified plane strain model produced poor results when applied to a shallow foundation problem composed of a strip footing resting on medium dense sand with an intercalated clay seam at the center of the soil mass. This was attributed to several factors, such as differences in boundary conditions, stress path, and failure mechanism. As a result, it was concluded that the influence of lithological heterogeneity on sand behavior under plane strain conditions was problem dependent.

Estimates of equivalent friction angles and elastic modulus were obtained for different configurations of the shallow foundation problem. This was carried out by assessing the design parameters of uniform sand mass that would reproduce the same ultimate footing pressure and average vertical displacements of heterogeneous soil media. These equivalent parameters were found to vary linearly with changes in undrained shear strength of the clay seams.

It should be emphasized that the main purpose of this chapter is not to replace detailed analyses of non-uniform soil media. Rather, the average soil parameters developed in this chapter can be considered as design guidelines that can be applied to

relatively low risk projects where detailed numerical analysis is not economically feasible. In addition, more attention should be given to other factors that may influence the performance of heterogeneous sand media with intercalated clay layers, such as the location of these layers within the sand mass and their inclinations.

3.8. REFERENCES

Deutsch, C. 1989. Calculating effective absolute permeability in sandstone/shale sequences. SPE Formation Evaluation, 4: 343-348.

Itasca Consulting Group Inc. 2000. FLAC 4.0: fast lagrangian analysis of continua. Minneapolis, Minnesota, USA.

King, P. R. 1989. The use of Renormalization for calculating effective permeability. Transport in Porous Media, 4: 37-58.

Niemunis, A., Karcher, C., and Theile, T. 2000. An averaging procedure for layered materials. International Journal for Numerical and Analytical Methods in Geomechanics. 24: 837-851.

Norris, R.J., Lewis, J. M., and Heriot-Watt, U. 1991. The geological modeling of effective permeability in complex heterolithic facies. Proceeding of the 66th Annual Technical Conference and Exhibition, SPE 22692 Dallas, Texas, USA, Vol. W, pp. 359-374.

Oda, M. and Win, S. 1990. Ultimate bearing capacity tests on sand with clay layer. Journal of the Geotechnical Engineering Division, ASCE, 116 GT(12): 1902-1906.

Warren, J. E., and Price, H. S. 1961. Flow in heterogeneous porous media. Society of Petroleum Engineering Journal: 153-169.

APPENDIX 3-A

DERIVATION OF EQUIVALENT ELASTIC MODULUS OF TWO-LAYERED HETEROGENEOUS SOIL MASS BASED ON THEORY OF ELASTICITY

Assume vertical and horizontal stresses as principal stresses and that vertical normal stress is the same in both layers, L_A and L_B as shown in Figure 3.9, while the horizontal normal stress is layer dependant:

$$\varepsilon_{1A} = \frac{\sigma_1}{E_A} - \frac{\upsilon_A}{E_A} \cdot (\sigma_{2A} + \sigma_{3A})$$

$$\varepsilon_{1B} = \frac{\sigma_1}{E_B} - \frac{\upsilon_B}{E_B} \cdot (\sigma_{2B} + \sigma_{3B})$$

(3-A-1)

For plane strain conditions, the normal strain out of space (ε_2) is equal to zero resulting in:

$$\sigma_{2A} = \upsilon_A \cdot (\sigma_1 + \sigma_{3A})$$

$$\sigma_{2B} = \upsilon_B \cdot (\sigma_1 + \sigma_{3B})$$

(3-A-2)

Substituting in Equation 3-A-1, the vertical strains in layers A and B (ε_{1A} and ε_{1B}) can be obtained through:

$$\varepsilon_{1A} = \frac{1}{E_A} \cdot [\sigma_1 (1 - \upsilon_A^2) - \upsilon_A \sigma_{3A} (1 + \upsilon_A)]$$

$$\varepsilon_{1B} = \frac{1}{E_B} \cdot [\sigma_1 (1 - \upsilon_B^2) - \upsilon_B \sigma_{3B} (1 + \upsilon_B)]$$

(3-A-3)

The vertical displacements (δ_V) can be assessed by multiplying vertical strain by layer thickness:

- 72 -

$$\delta_{VA} = \frac{H_A}{E_A} \cdot [\sigma_1(1 - \upsilon_A^2) - \upsilon_A \sigma_{3A}(1 + \upsilon_A)]$$

$$\delta_{VB} = \frac{H_B}{E_B} \cdot [\sigma_1(1 - \upsilon_B^2) - \upsilon_B \sigma_{3B}(1 + \upsilon_B)]$$

(3-A-4)

The total displacement is the summation of the vertical displacement of the two soil layers, L_A and L_B, resulting in:

$$\frac{H_A}{E_A} \cdot [\sigma_1(1 - \upsilon_A^2) - \upsilon_A \sigma_{3A}(1 + \upsilon_A)] + \frac{H_B}{E_B} \cdot [\sigma_1(1 - \upsilon_B^2) - \upsilon_B \sigma_{3B}(1 + \upsilon_B)] = \frac{H}{E_{eq}} \cdot [\sigma_1(1 - \upsilon^2) - \upsilon \sigma_3(1 + \upsilon)]$$

(3-A-5)

Rearranging:

$$E_{eq} = \frac{[\sigma_1(1 - \upsilon^2) - \upsilon \sigma_3(1 + \upsilon)] \cdot \sum\limits_{i=A}^{B} H_i}{\sum\limits_{i=A}^{B} \frac{H_i}{E_i}[\sigma_1(1 - \upsilon_i^2) - \upsilon_i \sigma_{3i}(1 + \upsilon_i)]}$$

(3-A-6)

To satisfy equilibrium in horizontal direction:

$$\sigma_{3A} H_A + \sigma_{3B} H_B = \sigma_3 H$$

(3-A-7)

Assuming that both layers undergo similar displacements in the horizontal direction:

$$\varepsilon_{3A} = \varepsilon_{3B}$$

(3-A-8)

The horizontal strain of layers L_A and L_B can be expressed as:

- 73 -

$$\varepsilon_{3A} = \frac{\sigma_{3A}}{E_A} - \frac{\upsilon_A}{E_A} \cdot (\sigma_1 + \sigma_{2A})$$

$$\varepsilon_{3B} = \frac{\sigma_{3B}}{E_B} - \frac{\upsilon_B}{E_B} \cdot (\sigma_1 + \sigma_{2B})$$

(3-A-9)

Substituting Equation 3-A-2 into Equation 3-A-9 and rearranging

$$\varepsilon_{3A} = \frac{\sigma_{3A}}{E_A}(1 - \upsilon_A^2) - \frac{\sigma_1 \cdot \upsilon_A}{E_A}(1 + \upsilon_A)$$

$$\varepsilon_{3B} = \frac{\sigma_{3B}}{E_B}(1 - \upsilon_B^2) - \frac{\sigma_1 \cdot \upsilon_B}{E_B}(1 + \upsilon_B)$$

(3-A-10)

Substituting in Equation 3-A-7:

$$\frac{\sigma_{3A}}{E_A}(1 - \upsilon_A^2) - \frac{\sigma_1 \cdot \upsilon_A}{E_A}(1 + \upsilon_A) = \frac{\sigma_{3B}}{E_B}(1 - \upsilon_B^2) - \frac{\sigma_1 \cdot \upsilon_B}{E_B}(1 + \upsilon_B)$$

(3-A-11)

Substituting σ_{3B} from Equation 3-A-7 into Equation 3-A-11:

$$\frac{\sigma_{3A}}{E_A}(1 - \upsilon_A^2) - \frac{\sigma_1 \cdot \upsilon_A}{E_A}(1 + \upsilon_A) = \frac{(1 - \upsilon_B^2)}{E_B}[\frac{\sigma_3 H - \sigma_{3A} H_A}{H_B}] - \frac{(1 + \upsilon_B)}{E_B}\upsilon_B \sigma_1$$

(3-A-12)

Rearranging :

$$\sigma_{3A} = \frac{\sigma_3 \frac{H}{H_B} \cdot \frac{(1 - \upsilon_B^2)}{E_B} + \sigma_1[\frac{\upsilon_A}{E_A}(1 + \upsilon_A) - \frac{\upsilon_B}{E_B}(1 + \upsilon_B)]}{\frac{1 - \upsilon_A^2}{E_A} + \frac{1 - \upsilon_B^2}{E_B} \cdot \frac{H_A}{H_B}}$$

(3-A-13)

Substituting in Equation 3-A-7:

- 74 -

$$\sigma_{3B} = \frac{\sigma_3 \dfrac{H}{H_A} \cdot \dfrac{(1 - \upsilon_A^2)}{E_A} + \sigma_1 [\dfrac{\upsilon_B}{E_B}(1 + \upsilon_B) - \dfrac{\upsilon_A}{E_A}(1 + \upsilon_A)]}{\dfrac{1 - \upsilon_B^2}{E_B} + \dfrac{1 - \upsilon_A^2}{E_A} \cdot \dfrac{H_B}{H_A}} \qquad (3\text{-}A\text{-}14)$$

Substituting Equation 3-A-13 and 3-A-14 into Equation 3-A-6, the equivalent elastic modulus can be obtained.

- 75 -

Table 3.1. Soil properties used in the numerical analyses.

Soil type	Friction angle (degree)	Undrained shear strength (kPa)	Elastic modulus (kPa)	Dilation angle (degree)	Poisson's ratio
Medium sand	34.00	N/A	50,000	0.00	0.30
Soft to medium clay	N/A	15.00 – 35.00	(200-1200) S_u	N/A	0.49

Table 3.2. Coefficient of variation of equivalent elastic modulus of heterogeneous sand-clay soil mass below a strip footing.

Confining pressure (kPa)	S_u (kPa)	T/H = 5%			T/H = 10%		
		$E_u/S_u =$ 200	$E_u/S_u =$ 600	$E_u/S_u =$ 1200	$E_u/S_u =$ 200	$E_u/S_u =$ 600	$E_u/S_u =$ 1200
25	35	0.04	0.04	0.05	0.06	0.06	0.07
	25	0.04	0.05	0.06	0.05	0.06	0.07
	20	0.03	0.05	0.06	0.04	0.06	0.07
	15	0.01	0.05	0.07	0.04	0.04	0.06
50	35	0.04	0.06	0.07	0.03	0.07	0.08
	25	0.04	0.08	0.09	0.02	0.06	0.09
	20	0.05	0.10	0.11	0.03	0.08	0.10
	15	0.07	0.12	0.14	0.04	0.09	0.12
100	35	0.09	0.12	0.13	0.06	0.11	0.12
	25	0.11	0.15	0.16	0.06	0.12	0.14
	20	0.12	0.16	0.18	0.09	0.13	0.16
	15	0.13	0.18	0.19	0.10	0.15	0.17
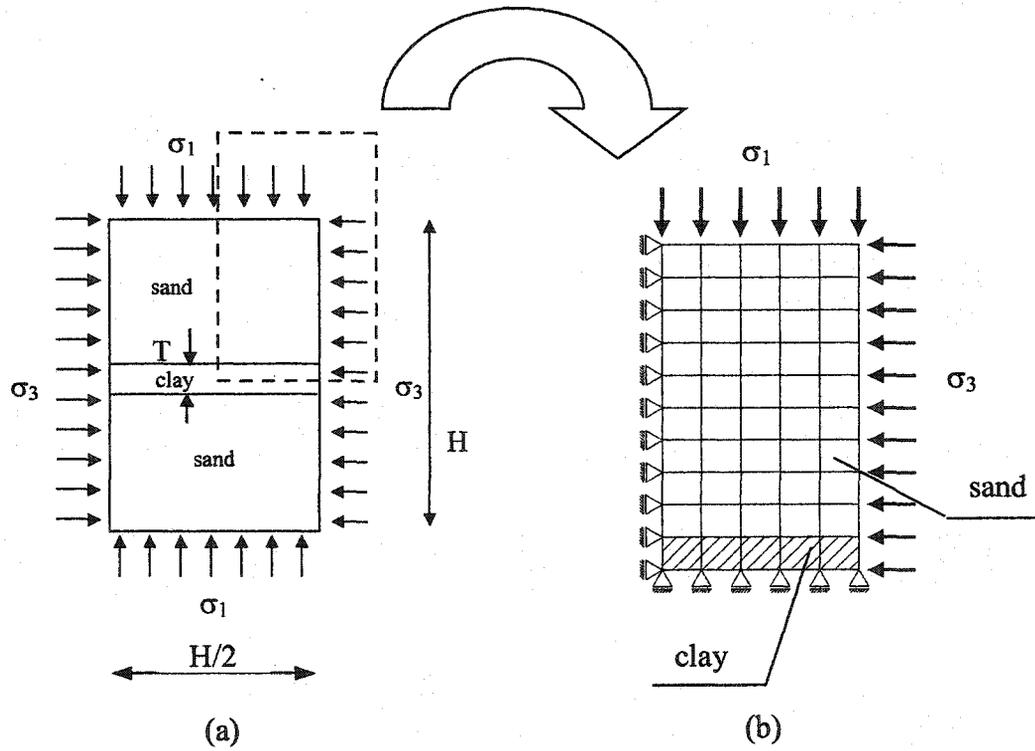
Figure 3.1. Description of the used model. a) a physical model; and b) a typical mesh used in the numerical analyses.
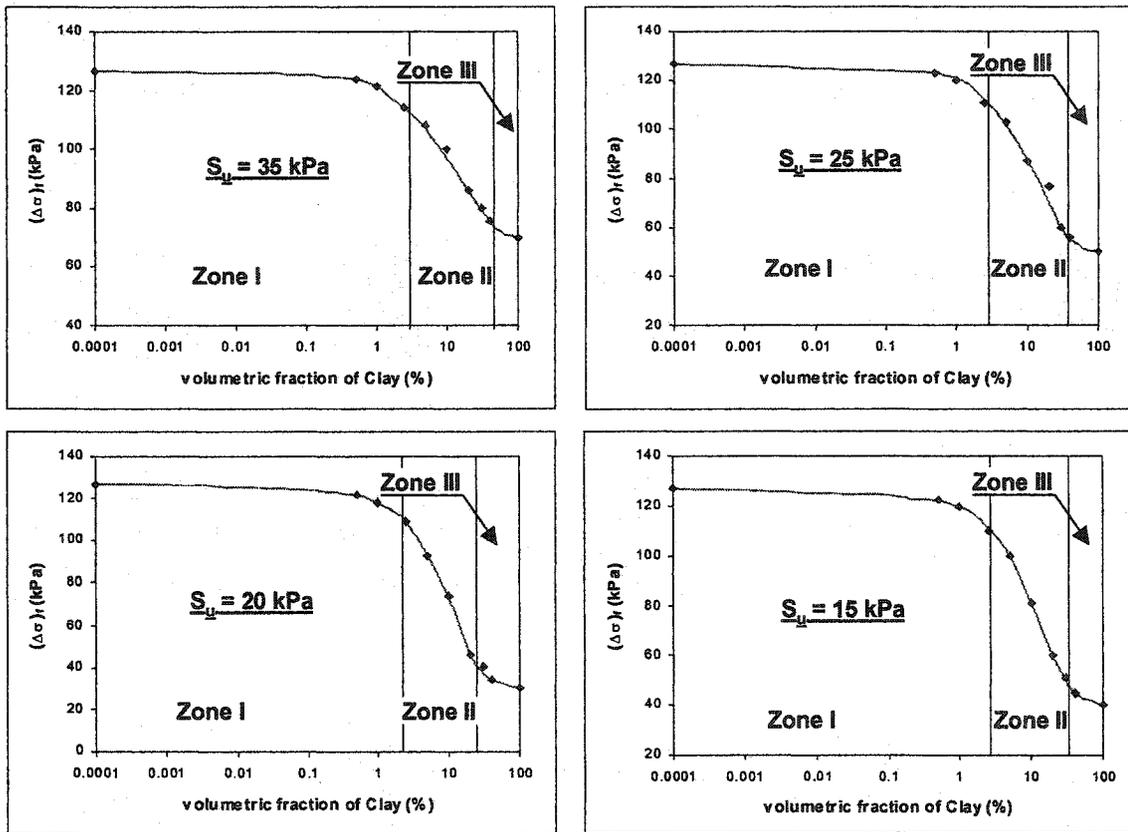
Figure 3.2. Decrease in failure stress of heterogeneous sand-clay mass with increasing the volume of clay seams for a confining pressure of 50 kPa.
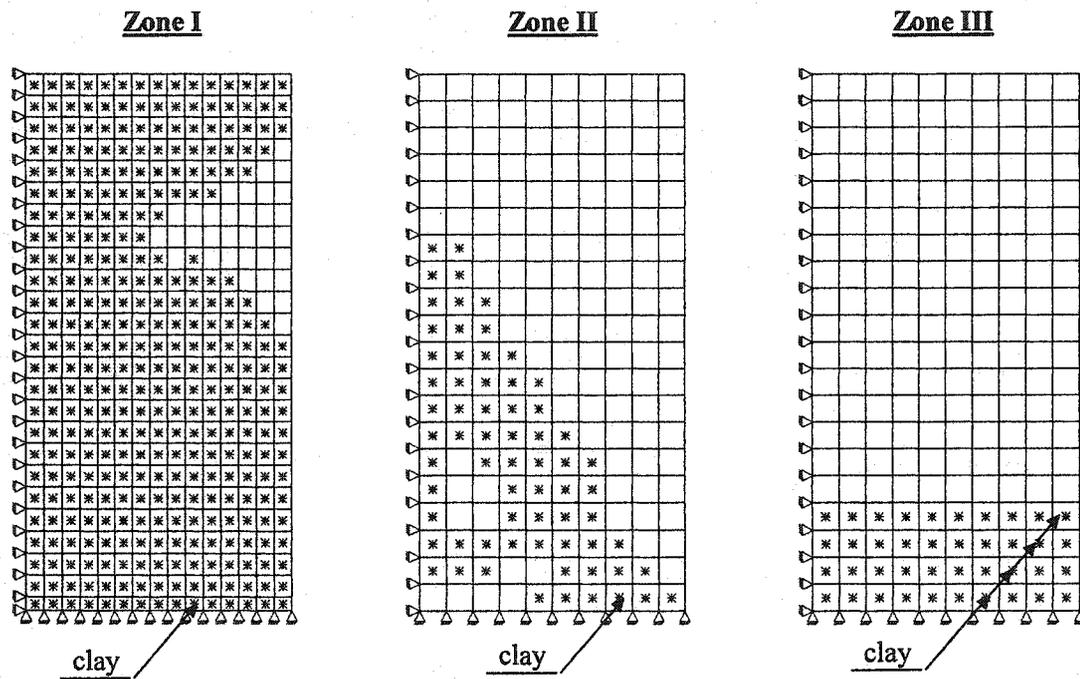
Figure 3.3. Failure modes associated with different heterogeneity zones deduced from Figure 3.2.
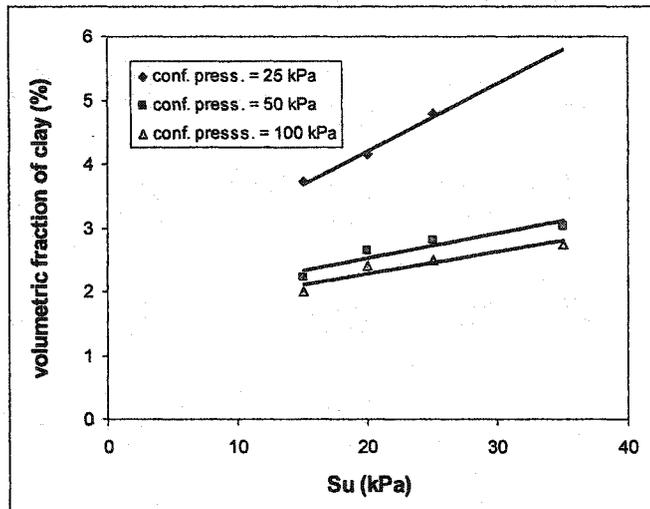
(a)
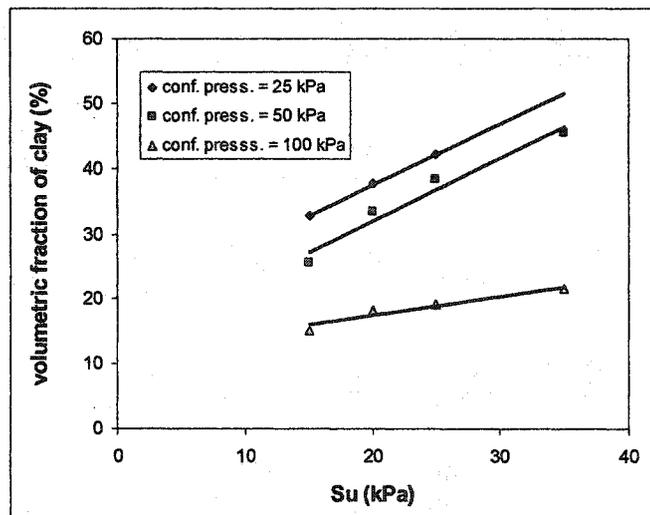
(b)

Figure 3.4. Variation of the boundaries between different heterogeneity zones with undrained shear strength of clay. a) boundary between zones I and II; and b) boundary between zones II and III.
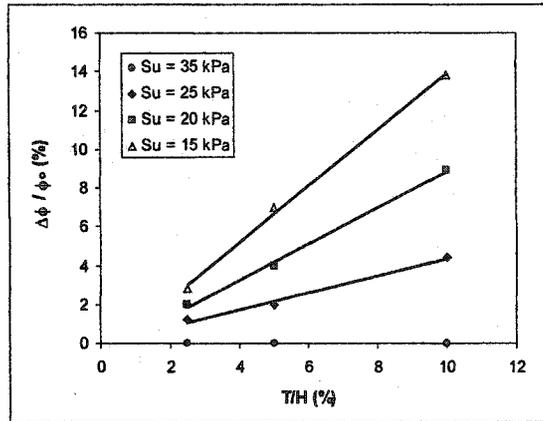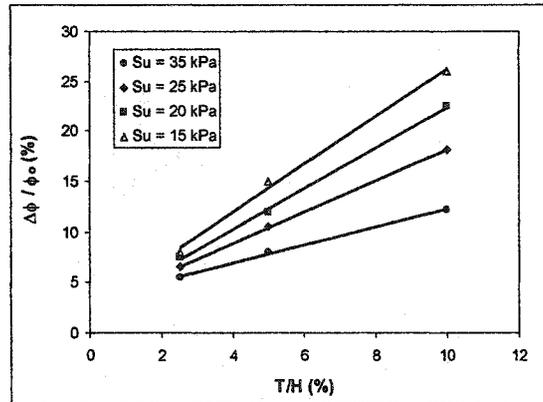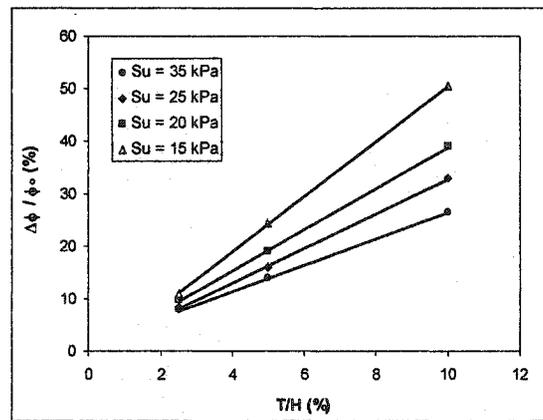
Figure 3.5. Assessment of the decrease in the friction angle of soil mass due to the presence of clay seams under different confining pressures (σ_3). a) $\sigma_3 = 25$ kPa; b) $\sigma_3 = 50$ kPa; and c) $\sigma_3 = 100$ kPa.

- 81 -
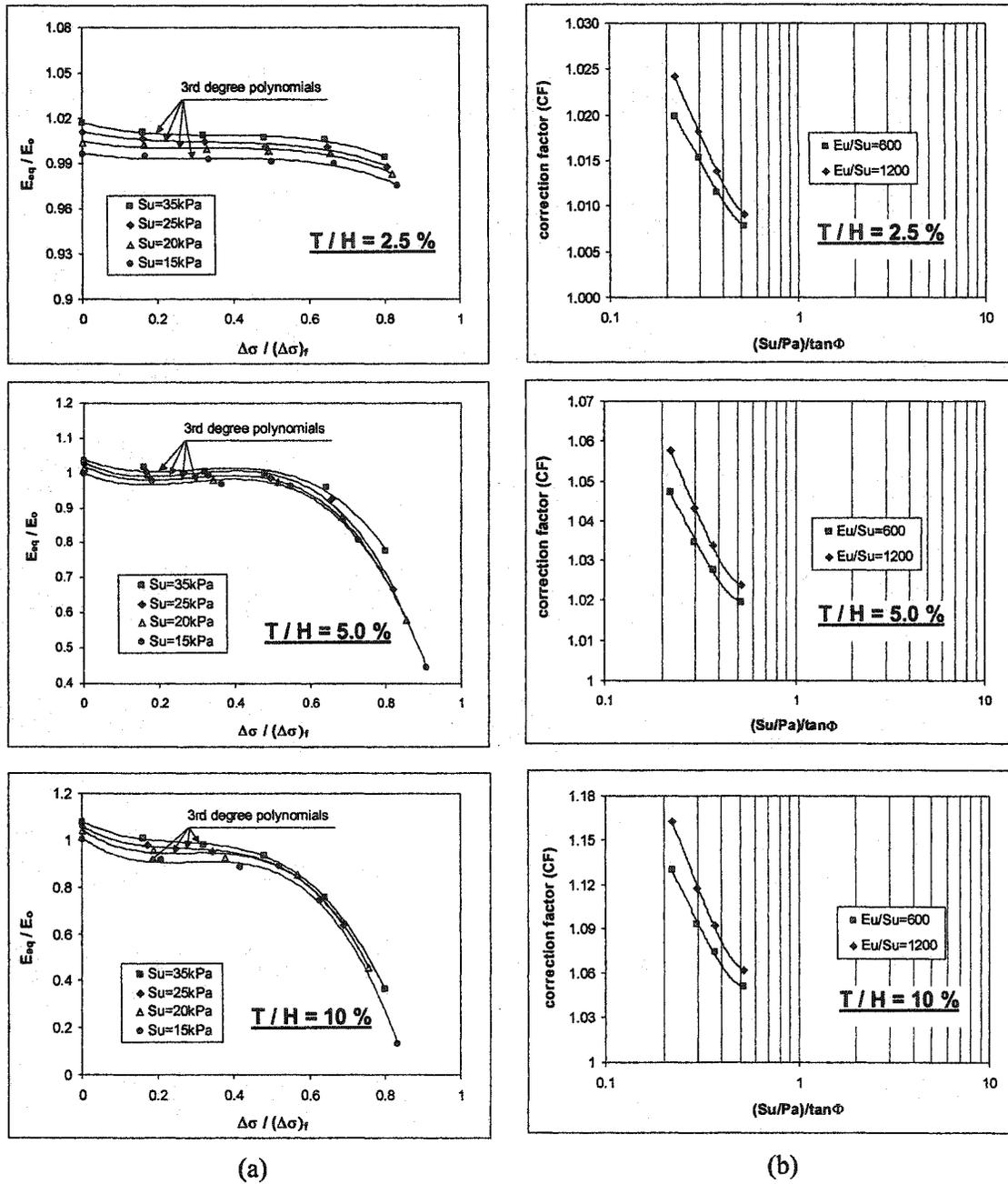
Figure 3.6. Estimation of normalized equivalent elastic modulus (E_{eq}/E_o) for heterogeneous sand-clay mass for confining pressure equal to 25 kPa. a) variation of E_{eq}/E_o with deviator stresses for $E_u/S_u = 200$; and b) correction factor for different values of E_u/S_u.

- 82 -
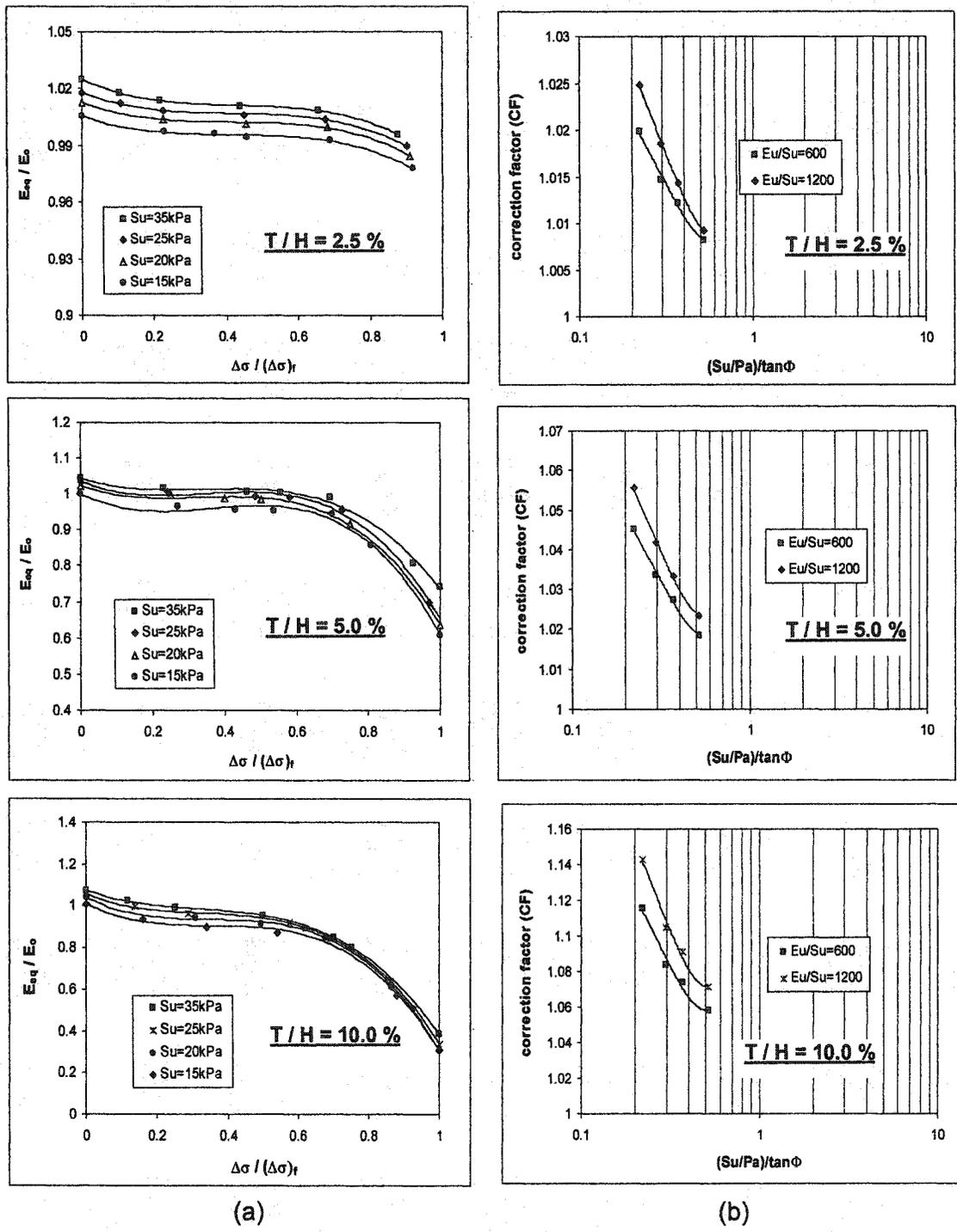
Figure 3.7. Estimation of normalized equivalent elastic modulus (E_{eq}/E_o) for heterogeneous sand-clay mass for confining pressure equal to 50 kPa. a) variation of E_{eq}/E_o with deviator stresses for $E_u/S_u = 200$; and b) correction factor for different values of E_u/S_u.
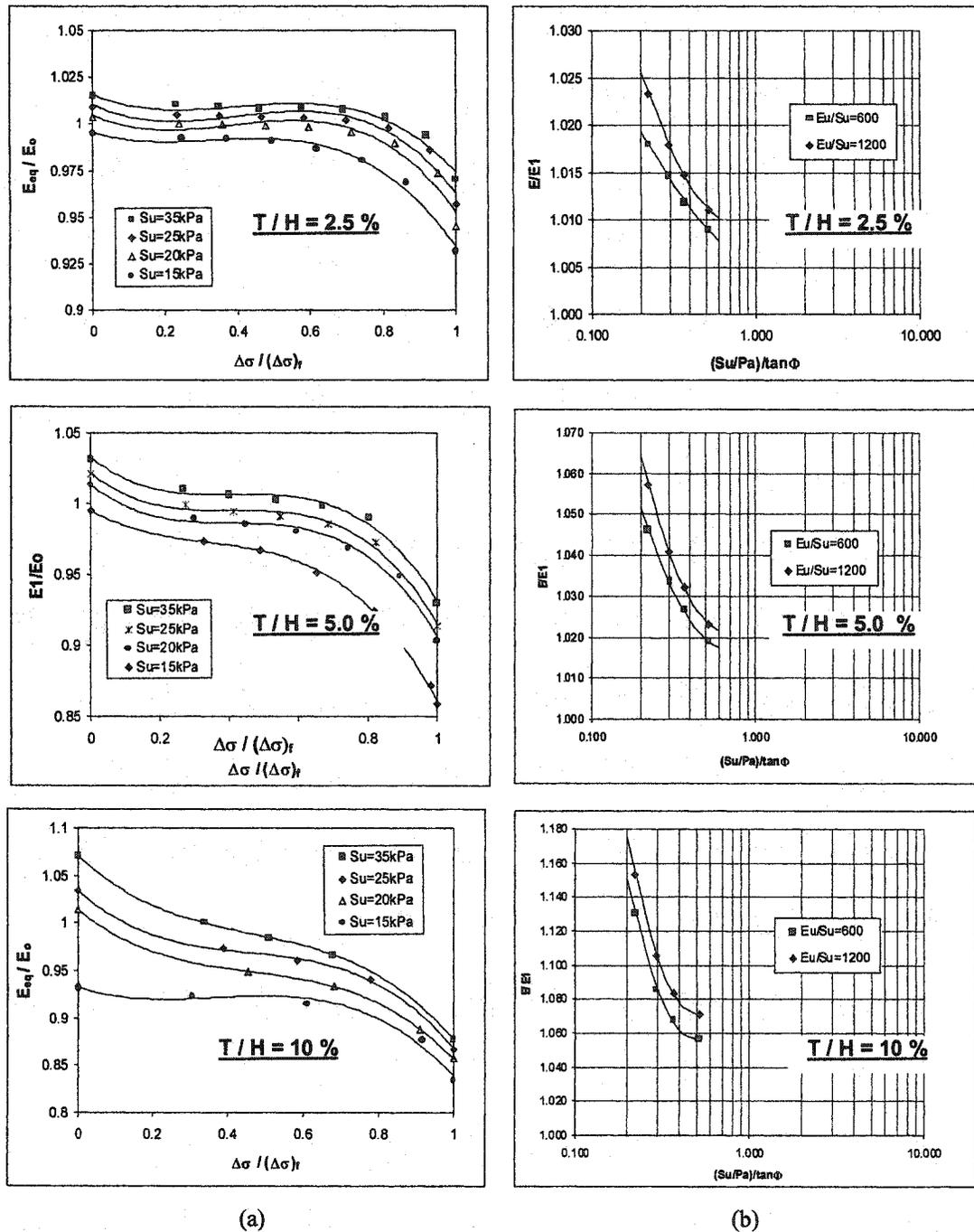
Figure 3.8. Estimation of normalized equivalent elastic modulus (E_{eq}/E_o) for heterogeneous sand-clay mass for confining pressure equal to 100 kPa. a) variation of E_{eq}/E_o with deviator stresses for $E_u/S_u = 200$; and b) correction factor for different values of E_u/S_u.

- 84 -
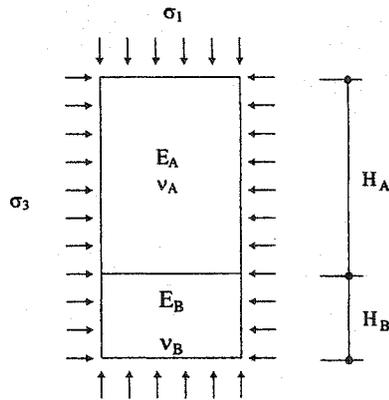
Figure 3.9. A simplified model used in the development of a mathematical expression for equivalent elastic modulusd of heterogeneous soil media based on theory of elasticity.
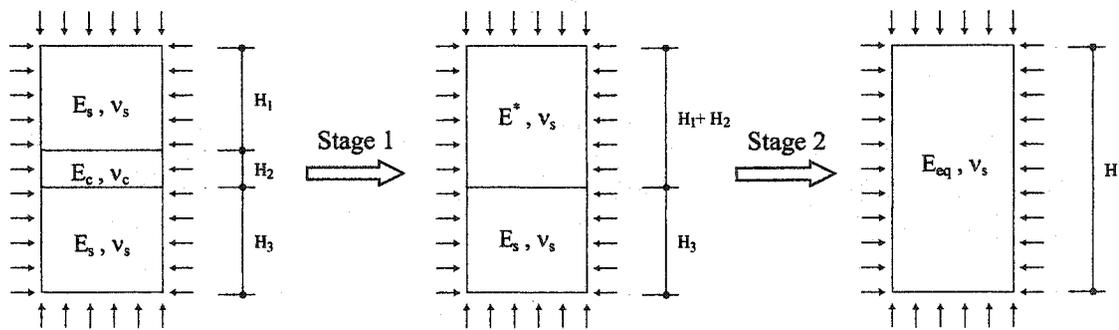
E_s, E_c = elastic modulus of sand and clay, respectively. N_s, v_c = Poisson's ratio of sand and clay, respectively.

E^* = intermediate elastic modulus that does not have any physical meaning

Figure 3.10. Assessment of equivalent elastic modulus for heterogeneous sand-clay mass in 2 stages using theory of elasticity.

- 85 -
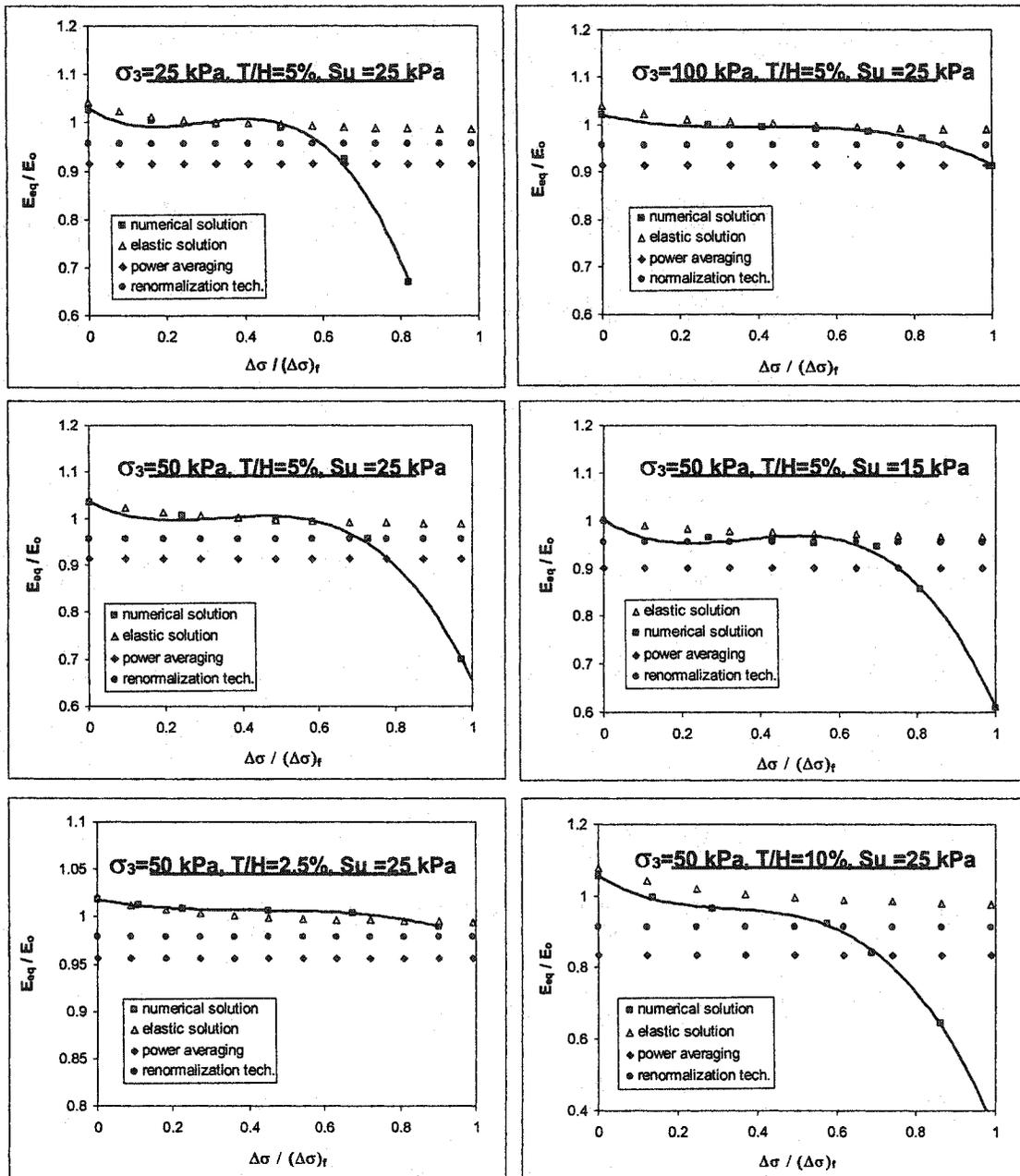
Figure 3.11. Comparison between numerical analyses results and other theoretical solutions (the solid lines represent the third degree polynomials that curvefit the numerical analyses results).
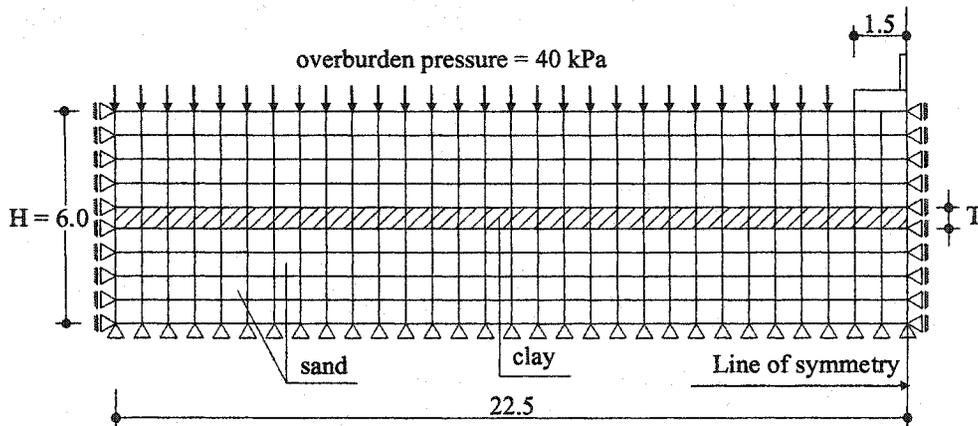
Figure 3.12. A typical mesh used in the analysis of heterogeneous soil media of 6 m thick below a strip footing placed at a foundation level 2 m below ground surface.
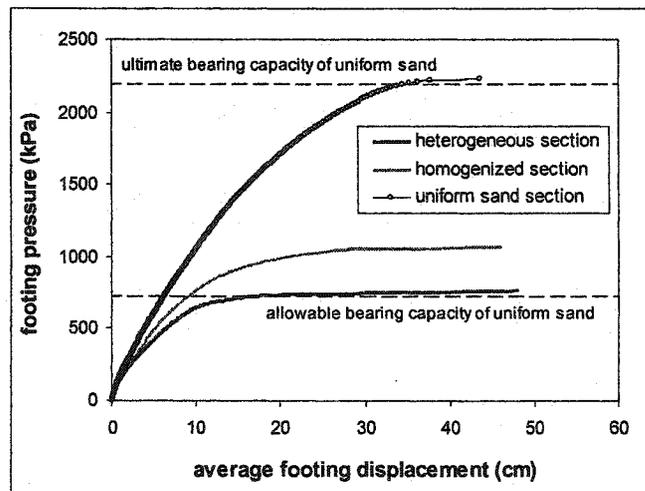
Figure 3.13. Comparison between footing pressure – average vertical displacement curves for different soil sections below a strip footing. (S_u = 25 kPa, E_u/S_u = 600, H = 6.0 m, and T/H = 5%).

- 87 -
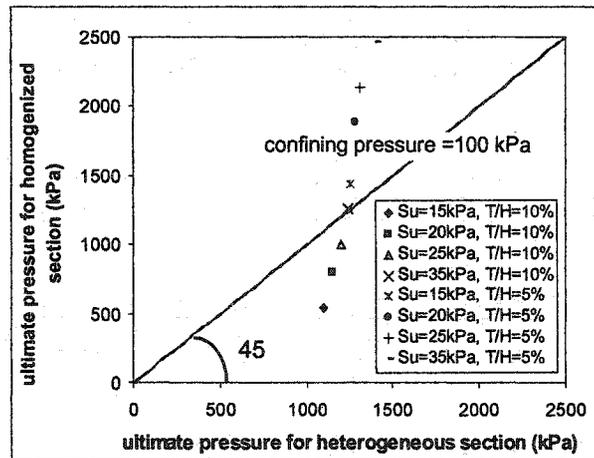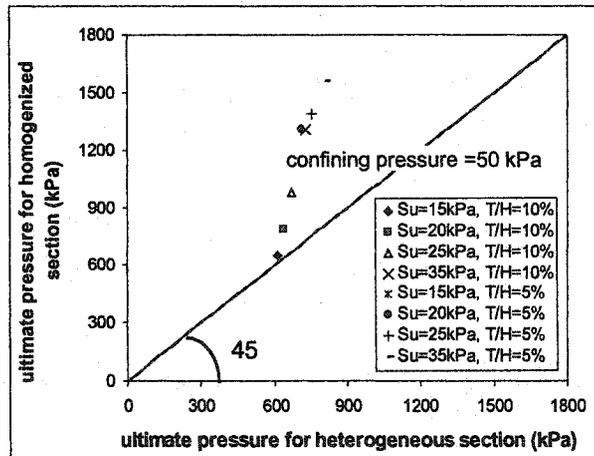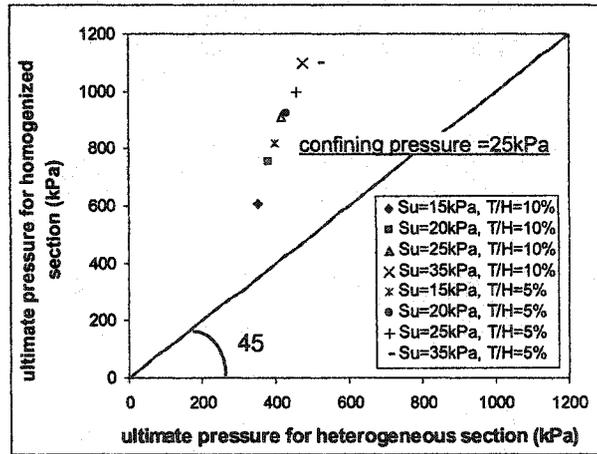
Figure 3.14. Comparison between ultimate footing pressures obtained from heterogeneous and homogenized soil sections. (confining pressure represents the in-situ horizontal stress at the centre of the soil mass)
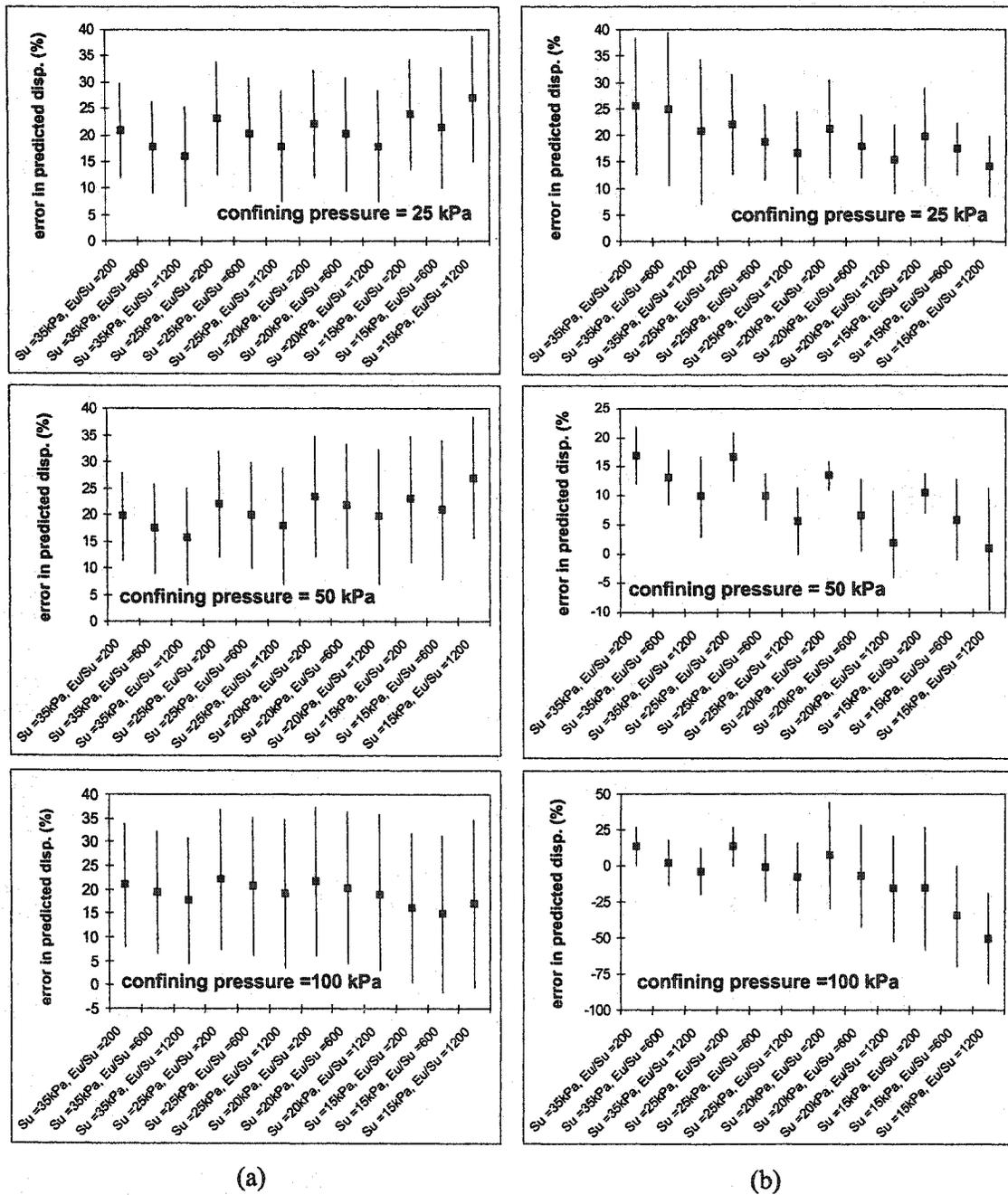
Figure 3.15. Error in average vertical footing displacements predicted using equivalent properties of homogenized soil section. a) T/H = 5%; and b) T/H = 10%. (solid squares represent average values and negative errors represent over-estimated displacements).

- 89 -
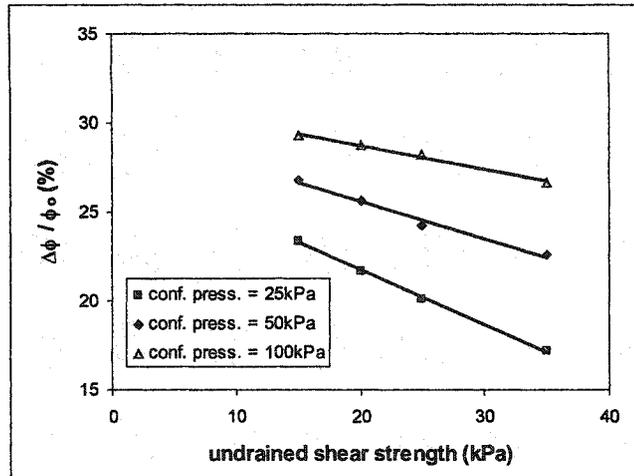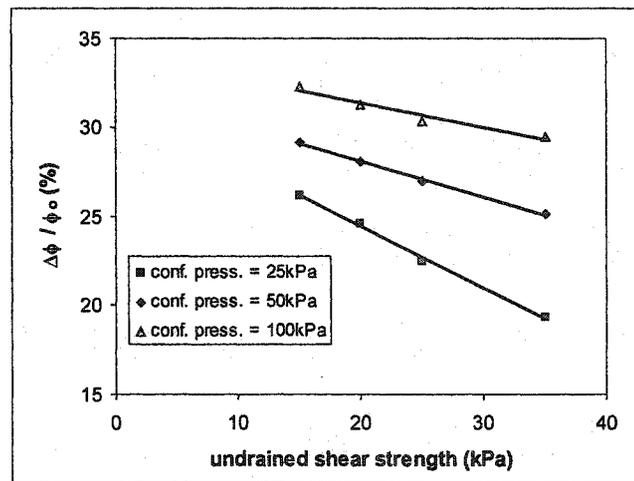
Figure 3.16. Assessment of reduction in equivalent friction angle of heterogeneous soil media below a strip footing under different volumes of clay seams. a) T/H = 5%; and b) T/H = 10%).
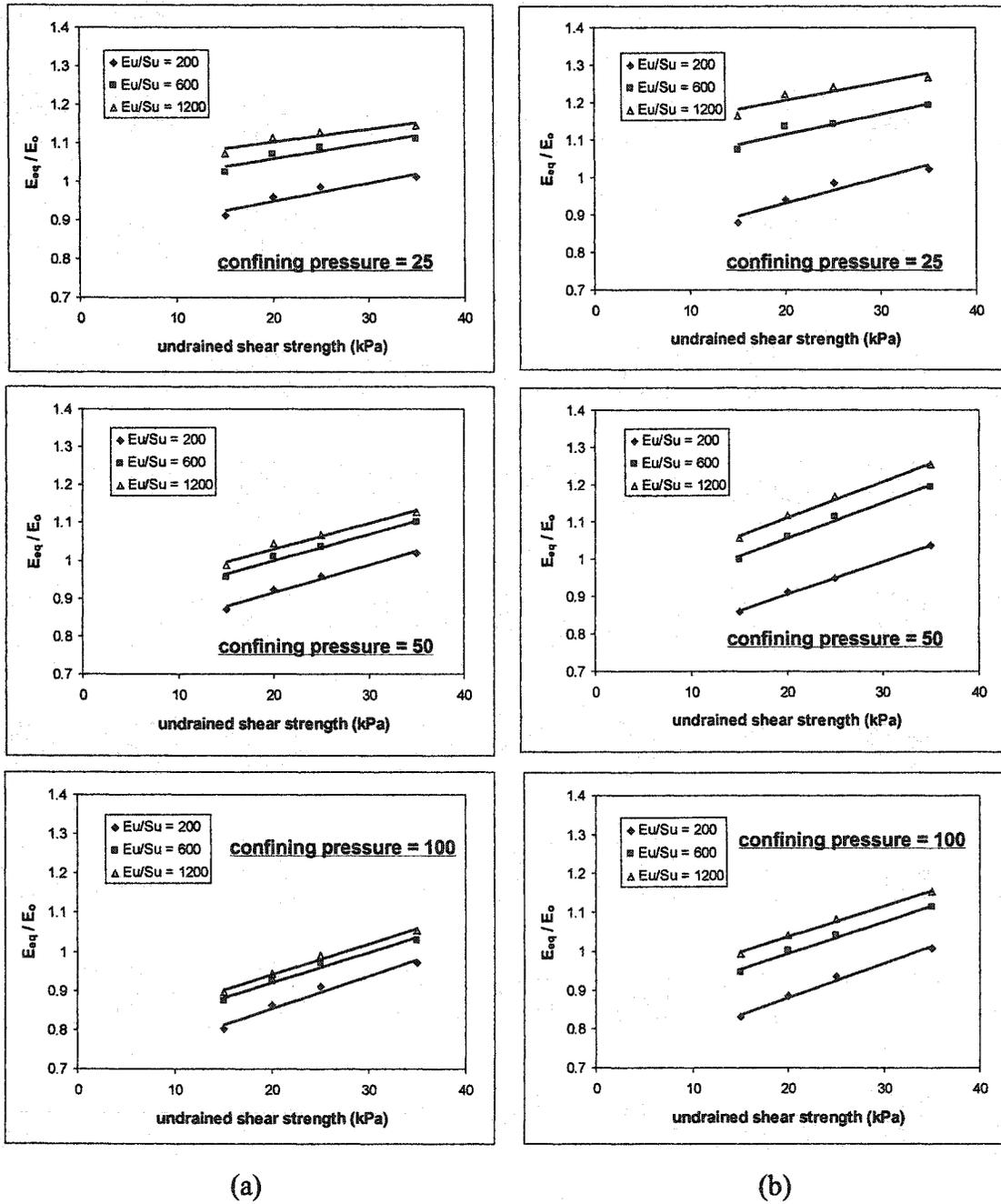
Figure 3.17. Estimation of equivalent elastic modulus for heterogeneous sand-clay mass below a strip footing. a) T/H = 5%; and b) T/H = 10%.

CHAPTER 4

GEOSTATISTICAL STABILITY ASSESSMENT OF CO-DEPOSITIONAL SAND - THICKENED TAILINGS EMBANKMENTS

4.1. INTRODUCTION

Tailings are by-products of processing different materials in the mining industry to extract economically valuable minerals. Tailings properties vary with raw ore characteristics and processing methodology. However, they are generally characterized by high water content, low shear strength and high compressibility. Tailings have minor economical value and are usually considered as waste materials that need to be disposed in a safe and economic manner. Several techniques have been developed for tailings disposal. The most common method of tailing disposal currently used in practice is conventional tailing dams (CTD), where tailings are placed in impoundments retained by engineered tailings dams (tailings dykes). Conventional tailing dams have proven to provide an effective technique for tailings management for different mining activities, such as the oil sand industry in northern Alberta.

Recently, the use of thickened tailings disposal systems (TTD) has captured some interest in the oil sand mining industry as a possible technique for the disposal of fine tailings. In this disposal technique, fine tailings are subjected to thickening using specific thickening vessels and flocculants that allow rapid dewatering and a considerable gain in shear strength. Thickened tailings are, then, discharged and dumped on the ground surface forming cone-shaped mounds at their angle of repose. This disposal system has several advantages over conventional tailings dams, such as:

A version of this chapter will be submitted for publication in the Canadian Geotechnical Journal.

1. Elimination of the need for settling ponds;

2. Reduction in the height of tailing dykes and associated hazards; and

3. A significant decrease in the amount of fluids that need to be removed from the disposal system.

A major limitation of the use of TTD in fine tailings disposal is the very flat slope angles of the deposited materials, usually in the range of 2 to 3.5 degrees (Poulos et al. 1985), due to the small shear strength of fine tailings. Several techniques have been developed to overcome this limitation, such as Scott and Cymerman (1984); and Carrier et al. (1987), through accelerating the dewatering and consolidation of fine tailings to improve their shear strength. However, these studies have resulted in little improvement in creating steeper deposition slope angles.

Recently, the idea of discharging thickened fine tailings into sand masses forming a thickened tailings - sand mixture with greater shear strength has arisen as a new technique to overcome the limitations of classical TTD. Employing these co-depositional mixtures of sand and thickened tailings, relatively steeper slopes are expected in comparison with those associated with conventional thickened tailings. Co-depositional embankments were investigated as early as 1988 through the pioneer trials of the CF industries in Florida (Minns 1988). More recently, Hutchinson (2000) carried out a laboratory testing program on the application of co-deposition technique for the mineral sand industry in Australia. Several laboratory models of co-depositional sand - thickened tailings embankments were constructed, as shown in Figure 4.1, in an attempt to investigate their engineering behavior. It should be realized, however, that the profile shown in this figure represented only one of many possible scenarios of thickened tailings- sand orientation in co-depositional embankments. Field application of co-depositional sand – thickened tailings is expected to have various scenarios of the spatial distribution of fine tailings within the sand mass that is hard to capture through a single laboratory model.

Few attempts have been made to quantify the properties of clay - sand mixtures. Townsend et al. (1989) compared sand-clay mixtures as a reclamation methodology with other reclamation approaches and developed closed form solutions for the unit weight and consolidation characteristics of these mixtures. This was done in the classical framework of the one-dimensional consolidation theory and did not take into account the effect of state of stresses on consolidation behavior. In addition, Dixon et al. (1984) conducted a study to assess the compaction and swelling characteristics of sand - clay mixtures. To the author's knowledge, all the above trials have not managed to establish solid design principles for these types of disposal systems.

In the current study, stability analyses of co-depositional sand - thickened tailings embankments were carried out in a probabilistic analysis framework. Geostatistical techniques were utilized to obtain several realizations of co-depositional embankments, where thickened tailings are spatially distributed within a larger mass of medium dense sand in a random fashion. These realizations were used to assess the stability of the disposal system expressed in terms of factor of safety against shear failure and the associated vertical deformations using the FLAC software. Different design parameters, such as the height and slope angle of the disposal system and shear strength of thickened tailings, were implemented in the proposed approach to quantify their implications on the stability of the disposal system. In addition, an attempt was made to estimate a critical probability of failure associated with significant damage, in terms of excessive displacements, in co-depositional embankments.

4.2. PROPOSED ANALYSIS METHODOLOGY

Thickened tailings – sand sequences in co-depositional embankments can take several forms, which can impact the stability of these structures, resulting in an unavoidable degree of uncertainty embedded in their engineering design. To account for

this uncertainty, a risk-based design methodology was developed in this study and passed through three main stages:

1. Generation of several realizations of random thickened tailings – sand sequences within the mass of co-depositional embankments;

2. Assessment of the number of these realization necessary to capture the statistical characteristics of these embankments; and

3. Implementation of different realizations of thickened tailings – sand sequences into deterministic elasto-plastic numerical analyses.

A detailed discussion of the above steps is provided in the following sections.

4.3. GENERATION OF RANDOM VARIABLES ACROSS THE ANALYSIS DOMAIN

The GSLIB geostatistical software library (Deutsch and Journel 1998) was utilized to generate several realizations of thickened tailings – sand sequences within the mass of the co-depositional embankment, as illustrated in Figure 4.2. Thickened fine tailings and sand were considered as categorical (discrete) random variables (Deutsch 2002) with a probability density function, as shown in Figure 4.3. The probability of occurrence of each discrete variable was considered equal to its volumetric ratio, which is the ratio between the volume of the discrete variable and the total volume of the tailings embankment. For the 1:10 ratio between thickened fine tailings and sand applied in this study, the probability of occurrence of thickened fine tailings and sand was assessed to be 0.091 (1/11) and 0.91 (10/11), respectively. The selection of a 1:10 volumetric ratio was in agreement with the ratio of the thickened tailings to sand used in the laboratory model of co-depositional embankments shown in Figure 4.1 (Hutchinson 2000). Consequently, the results presented in this study are limited to this ratio and should not be extended to other cases where different thickened tailings- sand mixtures are used.

The Sequential Indicator Simulation (SIS) technique (Deutsch and Journel 1998) was used to generate several realizations of random thickened tailings - sand sequences. The SIS technique is a simulation algorithm that deals with mutually exclusive lithological units, 2 units in this study: thickened tailings and sand, and employs Monte Carlo simulation to assign these units to different locations in the analysis domain, as shown in Figure 4.3. The assignment process is based on the probability that a specific lithological unit prevails at a certain location in space, which is usually governed by the probability distribution of categorical (discrete) variables and their indicator variograms (Deutsch 2002). Indicator variogram is a measure of transition probability at a separation distance h in space. In other words, if the value of the indicator variogram is equal to 0.20, for example, at a separation distance h, it implies that there is a 20% chance that there are two different lithological units at two points in space separated by a distance h. This imposes some restrictions on the simulated categorical variable as it will be affected by neighboring simulated points to fulfill variogram characteristics. It should be noted that the distribution of thickened tailings within the sand mass in this study was considered to be perfectly random, i.e. the simulation process was not influenced by the indicator variogram characteristics.

4.4. ASSESSMENT OF NUMBER OF REALIZATIONS

The number of realizations necessary for any statistical analysis is a function of the desired precision of the analysis, the greater the number of realizations the more precise the results are. In addition, extreme values statistics, i.e. values at the tails of the probability distribution function, may require a large number of realizations to be quantified with reasonable accuracy. Increasing the number of realizations beyond a certain limit, however, can be regarded as a tedious process with very little improvement in the numerical accuracy of the analysis results. To estimate the required number of realizations for each embankment geometry analysed in this study, a sensitivity analysis was carried out. This was accomplished by employing a material indicator, which

consisted of a binary code of material type for different elements of the numerical analysis grid. Material type indicators of 1 and 2 were used to denote thickened tailings and sand elements, respectively. For each realization, the arithmetic average (mean) of the material indicator of grid elements at the slope face was assessed and consequently a histogram of these averages was obtained by combining the results obtained from all realizations. The 0.05 percentile was determined as a measure of extreme values statistic, as it defines the values of the arithmetic average above which 95% of the histogram data occur. The optimum number of realizations was found to be 300 as it was considered as the number of realizations beyond which there was insignificant change in the value of the 0.05 percentile, as shown in Figure 4.4.

It should be noted that the results of this sensitivity analysis were based the assumption of shallow slope failure of co-depositional embankments, which was considered to be governed only by soil properties at the slope face. This assumption was verified through detailed numerical analyses of different realizations of co-depositional embankments, where a shallow mode of failure was encountered, as shown in Figure 4.5. The locations of these failure surfaces were found to be associated with zones of thickened fine tailings very close, or at, the slope face.

4.5. IMPLEMENTATION OF DIFFERENT REALIZATIONS OF THICKENED TAILINGS – SAND SEQUENCES INTO NUMERICAL ANALYSES

The FLAC software (Itasca Consulting Group Inc. 2000) was used to perform a series of deterministic numerical analyses implementing several realizations of thickened tailings – sand sequences in co-depositional embankments, as shown in Figure 4.2. The FLAC software adopts an explicit lagrangian finite difference scheme to simulate the engineering behavior of geotechnical materials. A typical mesh used in the analysis is shown in Figure 4.6, where a sloping mass of co-depositional embankment rests on a strong rock mass. Both the rock mass and the co-depositional embankment were assumed

to exhibit elastic perfectly plastic constitutive behavior, for simplicity, implementing Mohr-Coulomb failure criterion.

Thickened tailings pockets were considered to have the engineering characteristics of very soft clay with dimensions of 0.15m high and 0.40m wide, as assessed form visual examination of the laboratory models of Hutchinson (2000). These pockets were assumed to exhibit undrained behavior, with a ratio of undrained elastic modulus to undrained shear strength (E_u/S_u) of 600, which lies in the typical range of 200 to 1200 commonly used in geotechnical engineering literature. The sand elements were assumed to follow the purely frictional behavior of medium dense sand. A summary of material properties for the thickened tailings, sand and bedrock layers is provided in Table 4.1. These properties were chosen to represent the behavior of co-depositional embankment just after construction. It should be realized that there are two restrictive limitations imposed by the assumptions discussed above. Firstly, soil properties were assumed constants for each lithological unit, i.e. spatial variation of soil properties was not taken into account. Secondly, the analyses carried out in this study did not take into consideration the time dependent increase in shear strength of thickened tailings elements due to consolidation during and after embankment construction. These two limitations will be addressed in future studies.

Stability analyses carried out in this study utilized a subroutine invoked in FLAC 4.0 to assess the factor of safety of earth slopes using a bracketing approach based on the strength reduction technique (Dawson et al. 1999). The basic idea of the strength reduction method is to reduce soil shear parameters until failure occurs. The ratio between design shear parameters and their values at failure represents the slope factor of safety. Failure is usually detected in FLAC through a sharp increase in the unbalanced forces as shown in Figure 4.7. The unbalanced force is a measure of inertial forces developed in the analysis domain under applied loads. These forces tend to zero when equilibrium is satisfied, as FLAC invokes the full dynamic equation of motion into its formulation, even though static problems are addressed, to ensure numerical stability for

physically instable systems (Itasca Consulting Group Inc. 2000). The bracketing approach uses an iterative procedure to estimate shear strength parameters at failure in the following manner:

1. Initial lower and upper brackets for the expected factor of safety are assumed to be associated with the convergence and divergence of the numerical analysis model, respectively;

2. A mid point between these two brackets is tested. If the numerical model converges using the factor of safety represented by this point, the initial lower bracket is replaced by the new value of the mid point factor of safety. Otherwise, the upper initial bracket is replaced by the mid point value; and

3. This process is repeated until the difference between the upper and lower brackets is negligible.

A parametric study was carried out implementing undrained shear strength of thickened tailings between 0.25 kPa and 0.5 kPa, embankment heights in the range of 1.5 to 4.5 meters, and side slopes varying between 5.2:1 and 2:1. The results of these analyses are discussed in the following sections.

4.6. ANALYSIS RESULTS

The main output parameters considered in this study were the factor of safety against shear failure of co-depositional embankment and the associated vertical displacements at the embankment crest. The vertical displacements at embankment crest were expressed in terms of nominal vertical strains by dividing these displacements by embankment height. The statistics of these two output variables were used to obtain the probability of failure of co-depositional embankments and the vertical strains associated with the upper limit of the 90% confidence level, ε_{95}. The probability of failure, P_F, was assessed as the probability of occurrence of a factor of safety against shear failure less than unity. The ε_{95} was considered as the value of vertical strain at the embankment crest,

with only a 5% chance that the actual vertical strain would exceed this value, as shown in Figure 2.18 in Chapter 2. ε_{95} provides a risk-based measure of vertical deformations of co-depositional embankments with the following advantages over other deformation measures:

1. Takes into consideration statistical characteristics of vertical deformations, such as probability distribution and variance;

2. More realistic and less conservative deformation measure than maximum displacement as can be seen from Table 4.3; and

3. The consequences of failure can be quantified and employed into a decision making process.

An attempt was made in this study to assess the sensitivity of P_F and ε_{95} to different embankment characteristics, such as undrained shear strength of thickened fine tailings and embankment height and slope angle. It should be realized, however, that the engineering behavior of co-depositional embankments can be affected by other factors, such as thickened tailings – sand ratio and shear strength of sand. Quantification of the effects of these factors was considered to be beyond the scope of this study and need to be addressed in future studies.

Different combinations of soil properties and embankment characteristics applied in this study together with a summary of factors of safety and displacements statistics are presented in Table 4.2 and Table 4.3, respectively. A detailed discussion of the analyses results is provided in the following sections. In addition, these results were used to ascertain whether or not a critical probability of failure could be identified, above which excessive displacements in co-depositional embankments were likely to occur.

4.6.1. Effect of Undrained Shear Strength of Thickened Fine Tailings

The effect of undrained shear strength of thickened fine tailings on the probability of failure of co-depositional embankment for various embankment slope angles and

heights is shown in Figure 4.8.a and Figure 4.8.b, respectively. In general, probability of failure was found to decrease exponentially with increasing undrained shear strength. A critical threshold of 0.23 kPa for the undrained shear strength was identified at which the probability of failure approaches 100%. This implies that it is unlikely to obtain a stable co-depositional embankment if the thickening process results in undrained shear strength smaller than 0.23 kPa. The curves shown in Figure 4.8 provide risk-based design charts for the assessment of side slopes of these embankment based on the value of undrained shear strength obtained from the thickening process and the desired probability of failure.

The effect of undrained shear strength on vertical strain associated with the upper limit of the 90% confidence level, ε_{95}, is presented in Figure 4.9. Generally, ε_{95} tended to increase with smaller undrained shear strength of thickened tailings. This increase became abrupt and sharp at a critical threshold of undrained shear strength. This critical threshold varied from 0.50 kPa for embankment height of 4.50m to a value smaller than 0.25 kPa for embankment height of 1.50m. It should be realized that there is some uncertainty associated with the determination of these thresholds due to the limited number of data points used to develop the curves shown in Figure 4.9. This limited number of points was due to the time required to obtain the results for the 300 realizations required to assess the statistical characteristics of the output variables. For example, up to 4 weeks of continuous computational efforts was needed for geostatistical analysis co-depositional embankments of 4.5 m high.

4.6.2. Effect of Embankment Slope Angles

The effect of embankment slope angles on their probability of failure and the vertical strain associated with the upper limit of the 90% confidence level, ε_{95}, is shown in Figure 4.10. As expected, the probability of failure tended to decrease with smaller slope angles, or larger cot (B), and the rate of such decrease followed a quadratic relationship when plotted on a semi-log scale, as shown in Figure 4.10.a. Similarly, ε_{95} was found to decrease with smaller slope angles but the rate of such decrease was more

rapid following an exponential relationship, as seen in Figure 4.10.b. It is worth noting that vertical strains greater than 100% are not realistic, but they were presented in Figure 4.10.b to illustrate the nature of variation of ε_{95} with the change in slope angles. An abrupt increase in ε_{95} was noticed at a slope angle of 20 degrees (cot B of 2.7), which questioned the stability of these embankments for slope angles greater than 20 degrees. It should be noted that the curves shown in Figure 4.10.b were developed for an embankment height of 3 m and undrained shear strength of 0.50 kPa for the thickened tailings. Further investigation would be required to ascertain whether or not these relationships are valid for other embankment heights and different values of the undrained shear strength.

4.6.3. Effect of Embankments Heights

The effect of embankment height on the probability of failure of a co-depositional embankment with side slopes 4.4:1 is shown in Figure 4.11.a. Third degree polynomials were found to curvefit the variation of probability of failure with embankment height on a semi-log scale with a marginal error no more than 5%, expressed in terms of coefficient of determination (R^2) greater than 0.95. As a result, the probability of failure of these embankments could be expressed in the form:

$$\text{Log} \, [P_F \, (\%)] = a * H^3 + b * H^2 + c * H + d \qquad (4.1)$$

where: P_F is the probability of failure in percentage;

H is the embankment height in meters; and

a, b, c, and d are polynomial constants.

The third degree polynomial constants (a, b, c, and d) can be determined from Figure 4.12, where they were found to vary linearly with undrained shear strength of thickened tailings. Probability of failure curves were divided into 3 zones, as shown in Figure 4.11.a. In zone A, the geometrical effect of thickened tailings pockets was found

- 102 -

to have a significant impact on the overall stability of co-depositional embankments, which was manifested in increased probabilities of failure near the left tails of these curves. This geometrical effect was a result of small embankment heights where fine thickened pockets close or at the slope face represented a relatively large portion of the total height. Further increase in the probability of failure was noticed with increasing embankment heights as a result of generating higher state of stresses within the embankment and possible yielding of thickened tailings pockets close to the embankment base. In zone B, the geometrical effect decreased gradually and the overall performance became governed by the state of stresses within the embankment. It is worth noting that the geometrical effect was generally insignificant for thickened tailings with small undrained shear strength, such as $S_u = 0.25$ kPa. This could be attributed to the fact that the overall behavior of co-depositional embankments was mainly governed by the yielding of the thickened tailing pockets under applied stresses, which was manifested in increased probabilities of failure shown in Figure 4.11.a. In zone C, a sharp increase in failure probability was noticed due to the yielding of thickened tailings pockets close or at the slope face. Embankment heights associated with the boundary between zone A and zone B were found to decrease with smaller undrained shear strength of thickened tailings, as the case of the probability of failure curves associated with $S_u = 0.25$ kPa in Figure 4.11.a. This could be attributed to the fact that a slight increase in the state of stresses might result in yielding of thickened tailings pockets of small shear strength.

The effect of embankment height on the vertical strain associated with the upper limit of the 90% confidence level, ε_{95}, is presented in Figure 4.11.b. Generally, a small increase in this vertical strain was encountered for embankment heights less than 4m where the behavior of the embankments was mainly elastic except for some thickened fine tailings pockets very close to the embankment face. This was followed by a sharp increase in the vertical strain for embankment heights greater than 4m as a result of yielding of most of thickened tailings pockets within the embankment.

While the analysis results for S_u equal to 0.35 kPa, 0.40 kPa and 0.50 kPa were similar, the results for S_u equal to 0.25 kPa indicated a dramatic increase in ε_{95} for embankment heights between 1.50 m and 2.25 m. The modest increase in shear stresses resulting from the increase in embankment height was sufficient to initiate yielding of fine tailings pockets located close or at the embankment face and those near the embankment base. Beyond this threshold (2.25 m), no further significant yielding occurred until an embankment height of 3.75 m was reached, where the induced stresses were high enough to trigger yielding in most of the fine tailings pockets within the embankment body. This was manifested in an abrupt increase in ε_{95}, as shown in Figure 4.11.b. No parametric relationship, as the case of the third degree polynomials for probability of failure curves, could be obtained to curvefit the variation of ε_{95} with embankment height. To assess the value of ε_{95} for any embankment height, the author suggests that Equation 4.1 together Figure 4.12 can be used to assess probability of failure of this embankment. This probability of failure, in turn, can be used to assess the value of ε_{95} using Figure 4.13.

4.6.4. Assessment of a Critical Probability of Failure

As shown above, the engineering behavior of co-depositional embankments was found to be highly sensitive to different embankment characteristics. In addition, the stability analyses carried out in this study indicated that insignificant displacements were sometimes associated with factors of safety less than unity. This could be attributed to the shallow nature of shear failure encountered in these embankments that might result in localized failure without the overall stability of these embankments being drastically affected. As a result, there was a need to identify a critical failure probability, above which overall non-repairable damage occurs, in terms of excessive vertical displacements at the crest of co-depositional embankments.

The critical failure probability was determined by studying the variation in ε_{95} with the change in probability of failure for embankments of side slope 4.4:1, as shown in

Figure 4.13. A critical probability of failure of 34% was identified, where an abrupt increase in ε_{95} occurred. For design purposes, it was proposed that 50% of the critical probability of failure, or 17%, would be adopted as an allowable failure probability of co-depositional tailing embankments. This was assessed based on the analogy between the curve shown in Figure 4.13 and stress-strain curves for strain hardening materials and following the same argument used to identify secant elastic modulus, E_{50}, at 50% of failure stress. The proposed allowable probability of failure was found to be associated with a value of 0.28% for vertical strains associated with the upper limit of the 90% confidence level, ε_{95}. The allowable failure probability can be applied to Figure 4.8, together with the value of undrained shear strength of thickened tailings obtained from the thickening process, to obtain stable embankments with only 5% chance that vertical displacements at the embankment crest will exceed a value of 0.28% of the embankment height just after construction. It should be noted that different values of the allowable failure probability, other than 17%, could be obtained from Figure 4.13. However, the selection of these values is believed to be project and site specific and requires a through investigation of the failure consequences of co-depositional embankments.

4.7. CONCLUSIONS

The use of co-depositional thickened tailings - sand embankments has emerged as a possible technique for the disposal of fine tailings obtained from several mining activities, such as the oil sands industry. The main purpose of this study was to investigate the stability of co-depositional embankments with ratio of thickened tailings to sand equal to 1:10 in a geostatistical analysis framework. This was carried out by utilizing geostatistical theories to obtain several realizations of these embankments, where pockets of thickened fine tailings are randomly distributed in a mass of medium dense sand. These realizations were implemented in the FLAC software to assess the behavior of this disposal system in terms of factor of safety against shear failure and associated vertical deformations. The effects of different embankment characteristics,

such as height, slope angles, and shear strength of thickened tailings, were assessed to quantify their implications on engineering design.

Probability of failure of co-depositional embankments was found to decrease with increasing undrained shear strength of thickened tailings following an exponential relationship. A critical threshold of 0.23 kPa was identified for the undrained shear strength, for the cases considered in this chapter, below which it is unlikely to obtain stable co-depositional embankments.

The probability of failure was found to decrease with smaller slope angles of co-depositional embankments following a quadratic relationship when plotted on a semi-log scale. Similarly, the vertical strain associated with the upper limit of the 90% confidence level, ε_{95}, was found to decrease with smaller slope angles, but the rate of such decrease was more rapid following an exponential relationship. A critical threshold of 20 degrees was identified above which it is unlikely to obtain stable co-depositional embankments.

The variation of probability of failure of co-depositional embankments of side slopes 4.4:1 with changes in embankment heights was found to follow a third degree polynomial on a semi-log scale. This variation was found to be sensitive to geometrical effects of thickened tailings pockets and state of stress in the embankment body. A design methodology was proposed to assess the probability of failure and the associated ε_{95} for any embankment height with side slope 4.4:1.

A critical probability of failure of 34% was found to be correlated to irreparable damage, in terms of excessive vertical deformations, to the overall stability of co-depositional embankments. An allowable probability of failure of 17%, associated with 50% of the critical value, was proposed for use in engineering design. This allowable failure probability can be used to obtain stable embankments with only 5% chance that vertical displacements at the embankment crest will exceed a value of 0.28% of the embankment height just after construction. It should be noted, however, that different

allowable failure probability for co-depositional embankments could be developed from other performance criteria, such as liquefaction-related stability.

More attention should be given to other factors that may affect the performance of this disposal system, such as thickened tailings – sand ratio, shear strength of sand and the uncertainty in undrained shear strength of thickened tailings. It should be emphasized that a major challenge for the applicability of this disposal system is the success of the thickening process in accelerating the consolidation process and obtaining thickened fine tailings with considerable shear strength. In addition, the author suggests that the results obtained in this study be verified using full-scale field tests.

4.8. REFERENCES

Carrier, W. D. III, Scott, J. D., Shaw, W. H., and Maurice, M. B. Reclamation of Athabasca oil sand sludge. Geotechnical Practice for Waste Disposal '87, Proceedings of a Specialty Conference sponsored by the Geotechnical Division of ASCE, Ann Arbor, MI, USA. Geotechnical Special Publication. No. 13. pp. 377-391.

Deutsch, C. V. 2002. Geostatistical reservoir modeling. Oxford University press.

Deutsch, C. V. and Journel A. G. 1998. GSLIB geostatistical software library. Oxford University Press.

Dixon, D. A., Gray, M. N., and Thomas, A., W. 1984. Study of the compaction properties of potential clay-sand buffer mixtures for use in nuclear fuel waste disposal. Engineering Geology, 21 (3-4): 247-255

Hutcheson, H. 2000. Depositional and geotechnical characteristics of mineral sands thickened/paste tailings. Transportation and Deposition of Thickened/Paste Tailings Learning Seminar. Edmonton, Alberta, Canada.

Itasca Consulting Group Inc. 2000. FLAC 4.0: fast lagrangian analysis of continua. Minneapolis, Minnesota, USA.

Minns, A. 1988. Review of tailings disposal practices in North America and Australia. Hydraulic Fill Structures, Proceedings of a Specialty Conference sponsored by the Geotechnical Division of ASCE, Fort Collins, CO, USA. Geotechnical Special Publication. No. 21. pp. 52-68

Poulos, S. J., Robinsky, E. I., Keller-Thomas, O. 1985. Liquefaction resistance of thickened tailings. Journal of the Geotechnical Engineering Division, ASCE, 111 (GT12): 1380-1394.

Scott, J. D. and Cymerman, G. J. 1984. Prediction of viable tailings disposal methods. Sedimentation Consolidation Models: Predictions and Validation, Proceedings of a Symposium held in conjunction with the ASCE Convention, San Francisco, CA, USA, pp. 522-544

Townsend, F. C., McVay, M. C., Boolmquist, D. G., and McClimans, S. A. 1989. Clay waste pond reclamation by sand/clay mix or capping. Journal of the Geotechnical Engineering Division, ASCE, 115 (GT11): 1647-1666.

Table 4.1. A summary of material properties used in the analysis

Material property	Rock mass	Sand	Fine tailings				
Unit weight (kN/m3)	20	18			18		
Elastic modulus (kPa)	42,000	50,000	300	240	210	180	150
Poisson's ratio	0.20	0.30			0.49		
Friction angle (degree)	46	34			0.0		
Dilation angle (degree)	11	0.0			0.0		
Undrained shear strength / cohesion (kPa)	13,000	0.0	0.50	0.40	0.35	0.30	0.25

Table 4.2. A summary of different combinations of design parameters considered in this study

Case	Side Slope	Height (m)	S_u^* (kPa)	Case	Side Slope	Height (m)	S_u^* (kPa)
1	2:01	3.0	0.50	20	5.2:1	3.0	0.30
2	2:01	1.5	0.50	21	5.2:1	3.0	0.25
3	2.4:1	3.0	0.50	22	4.4:1	4.5	0.50
4	2.4:1	1.5	0.50	23	4.4:1	4.5	0.40
5	3.2:1	3.0	0.50	24	4.4:1	4.5	0.35
6	3.2:1	1.5	0.50	25	4.4:1	4.5	0.25
7	4.4:1	3.0	0.50	26	4.4:1	3.75	0.50
8	4.4:1	1.5	0.50	27	4.4:1	3.75	0.40
9	2.4:1	3.0	0.40	28	4.4:1	3.75	0.35
10	3.2:1	3.0	0.40	29	4.4:1	3.75	0.25
11	3.2:1	3.0	0.35	30	4.4:1	4.05	0.50
12	4.4:1	3.0	0.40	31	4.4:1	4.05	0.40
13	4.4:1	3.0	0.35	32	4.4:1	4.05	0.35
14	4.4:1	3.0	0.30	33	4.4:1	4.05	0.25
15	4.4:1	3.0	0.25	34	4.4:1	2.25	0.50
16	4.4:1	1.5	0.40	35	4.4:1	2.25	0.40
17	4.4:1	1.5	0.35	36	4.4:1	2.25	0.35
18	4.4:1	1.5	0.25	37	4.4:1	2.25	0.25
19	5.2:1	3.0	0.40				

* S_u is the undrained shear strength of fine tailings

Table 4.3. A summary of the factor of safety statistics

Case	Mean F.S.	COV (F.S.)	P_F (%)	Maximum Vertical Strain (%)	Mean Vertical Strain (%)	ε_{95} (%)
1	0.84	0.15	91.40	269.00	49.33	178.33
2	0.94	0.18	63.09	480.67	48.02	276.30
3	0.98	0.14	54.02	117.33	4.57	16.78
4	1.11	0.15	25.64	153.33	7.41	24.35
5	1.26	0.13	6.82	38.00	0.24	5.34
6	1.38	0.13	3.32	0.19	0.03	0.06
7	1.69	0.11	0.01	0.09	0.06	0.07
8	1.82	0.11	0.02	0.05	0.03	0.04
9	0.88	0.16	78.74	284.00	9.42	40.55
10	1.13	0.16	27.04	76.00	0.80	10.74
11	1.06	0.17	40.27	116.00	1.48	16.53
12	1.49	0.13	0.24	0.10	0.06	0.08
13	1.38	0.15	2.44	0.10	0.07	0.09
14	1.25	0.17	20.06	2.83	0.08	0.39
15	1.10	0.19	34.56	7.91	0.16	1.12
16	1.64	0.13	1.25	0.06	0.03	0.05
17	1.52	0.14	2.92	0.07	0.04	0.05
18	1.23	0.20	33.13	0.09	0.04	0.06
19	1.69	0.12	0.01	0.11	0.06	0.08
20	1.42	0.16	2.76	0.12	0.07	0.09
21	1.25	0.18	21.82	5.04	0.10	0.71
22	1.27	0.13	5.12	0.23	0.13	0.16
23	1.11	0.17	33.37	9.95	0.18	1.39
24	1.02	0.19	51.11	37.11	0.29	5.20
25	0.80	0.23	82.58	316.22	8.02	49.36
26	1.64	0.11	0.06	0.11	0.07	0.09

27	1.45	0.14	0.43	0.13	0.08	0.10
28	1.33	0.15	3.13	0.13	0.08	0.10
29	1.06	0.19	43.15	10.57	0.16	1.58
30	1.62	0.11	0.09	0.13	0.08	0.10
31	1.44	0.14	1.17	0.15	0.09	0.11
32	1.32	0.15	5.84	0.17	0.09	0.12
33	1.05	0.20	44.46	18.57	0.19	2.60
34	1.73	0.12	0.07	0.08	0.05	0.06
35	1.54	0.14	1.11	0.09	0.05	0.07
36	1.43	0.16	3.53	0.10	0.05	0.07
37	1.14	0.19	26.97	7.91	0.10	1.12
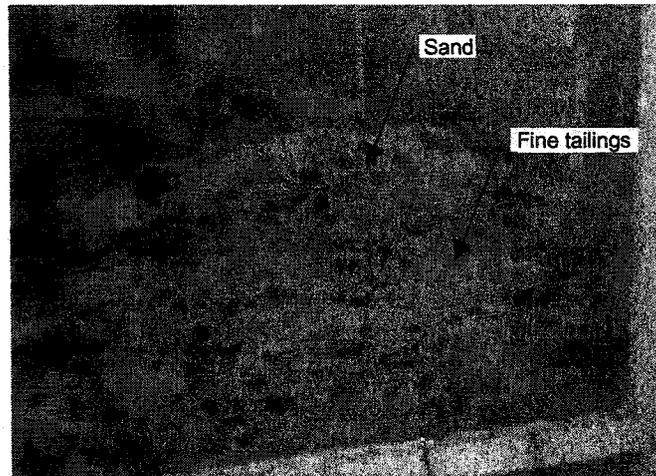
Figure 4.1. Fine tailings – sand mixture in laboratory model of co-depositional fine tailings embankments (modified from Hutcheson 2000)
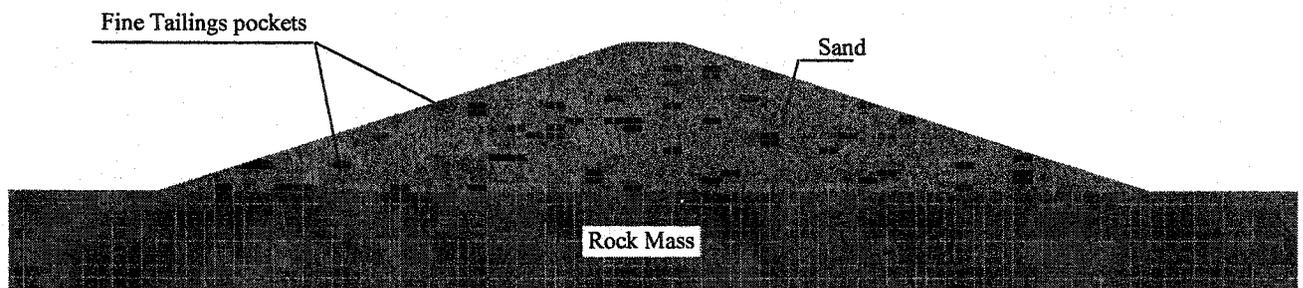
Figure 4.2. Schematic diagram showing the spatial distribution of fine tailings pockets within sand mass overlying a strong rock mass.

- 113 -
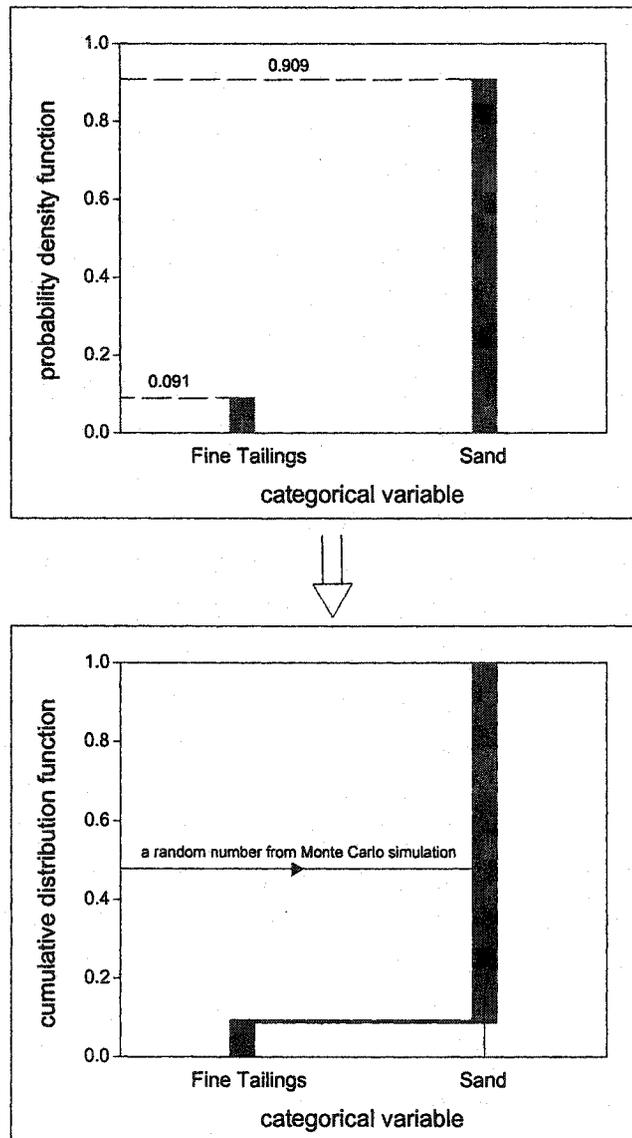
Figure 4.3. Assessment of lithological unit at a certain location in space using Monte Carlo simulation.
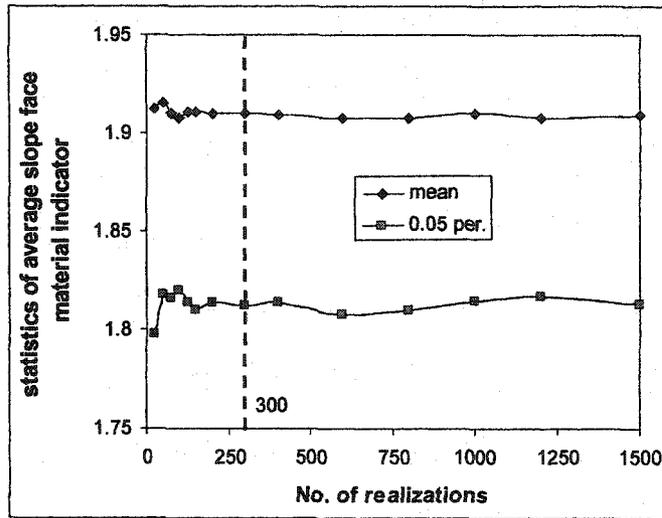
Figure 4.4. Sensitivity analysis to assess the number of realization for geostatistical analysis of co-depositional embankments.

Figure 4.5. Mode of shear failure in mixed fine tailing embankments

- 115 -
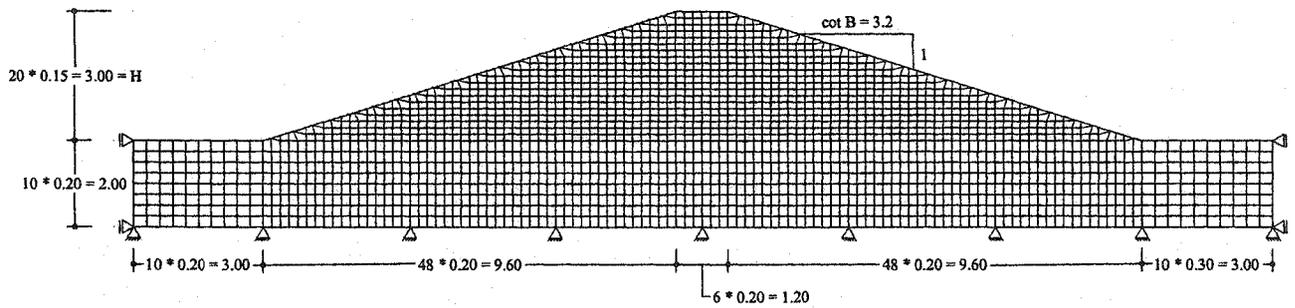
Figure 4.6. Typical mesh used in the numerical analysis for co-depositional tailings embankment of 3 m height and 3.2:1 side slopes
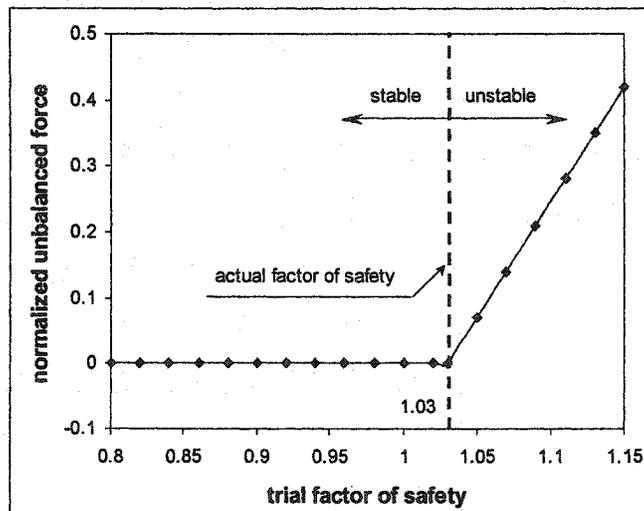
Figure 4.7. Assessment of the critical factor of safety associated with a sharp increase in unbalanced force (modified from Dawson et al. 1999).

- 116 -
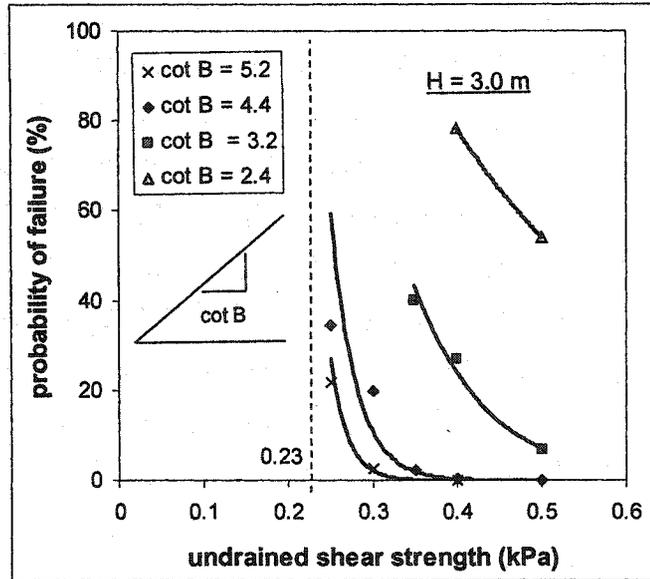
(a)
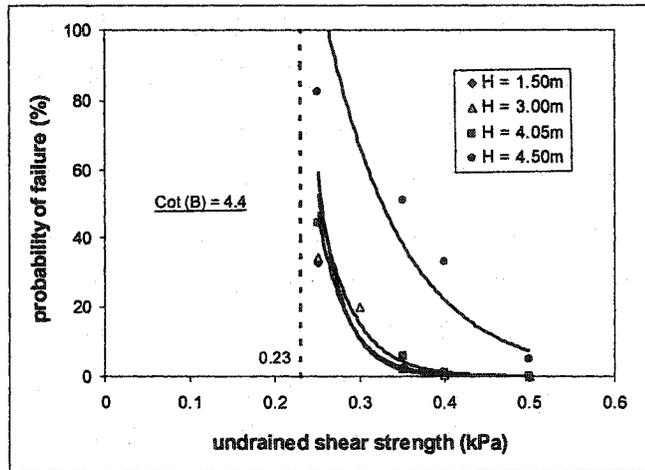
(b)

Figure 4.8. Effect of undrained shear strength of fine tailings on the probability of failure of co-depositional embankments. a) for different slope angles; and b) for different embankment heights.

- 117 -
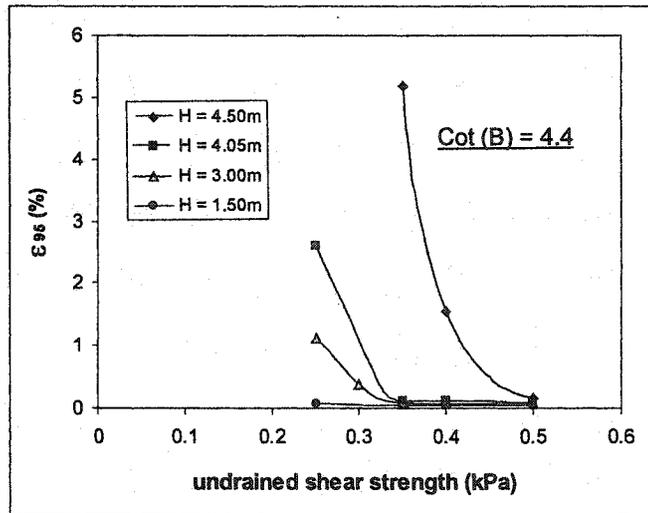
Figure 4.9. Effect of undrained shear strength of fine tailings on vertical strain associated with the upper limit of the 90% confidence level.
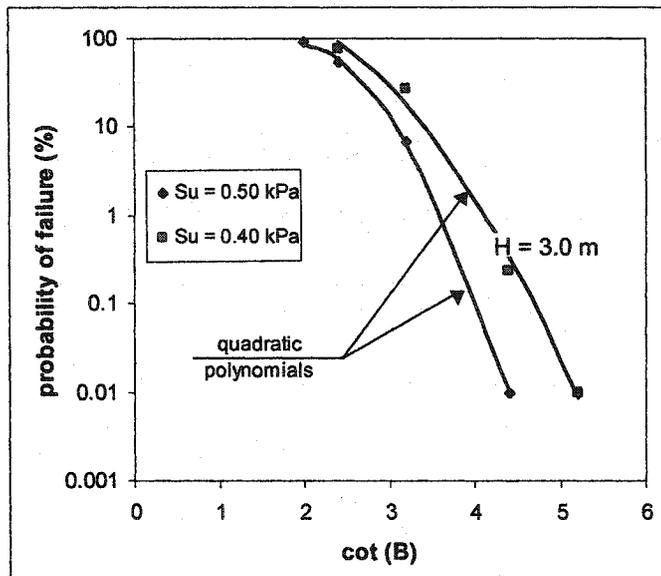
(a)
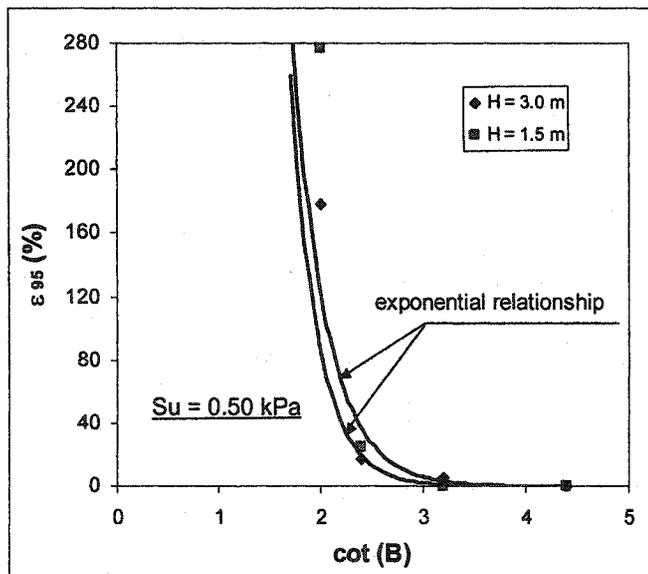
(b)

Figure 4.10. Effect of side slope angle. a) on the probability of failure; and b) on vertical strain associated with the upper limit of the 90% confidence level.
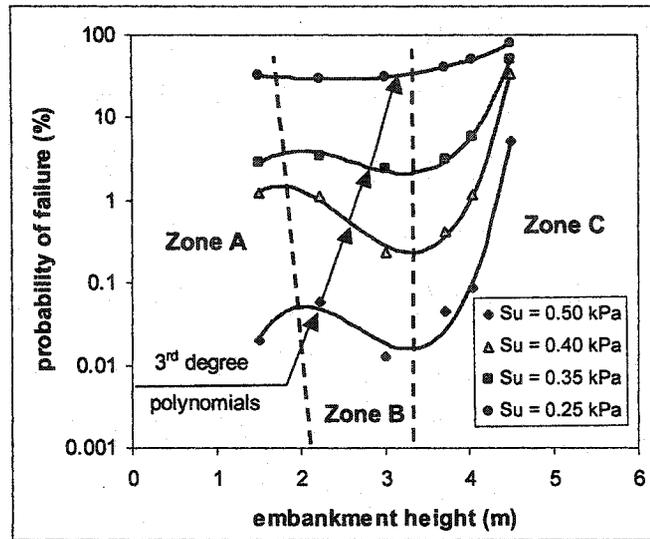
(a)
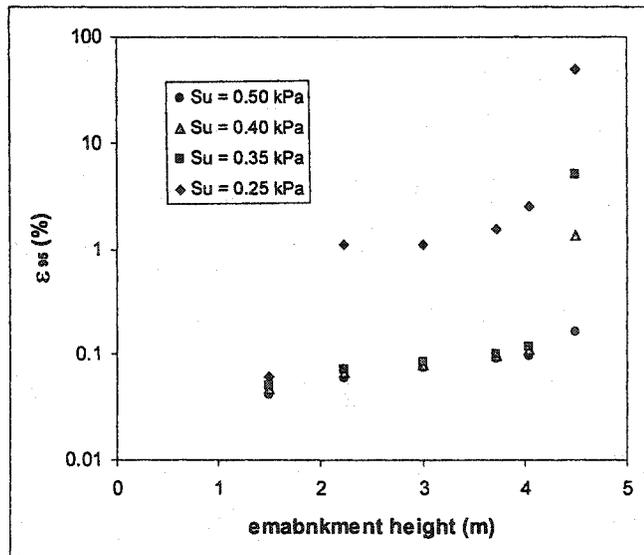
(b)

Figure 4.11. Effect of change in embankment height. a) on probability of failure; and b) on vertical strain associated with the upper limit of the 90% confidence level.
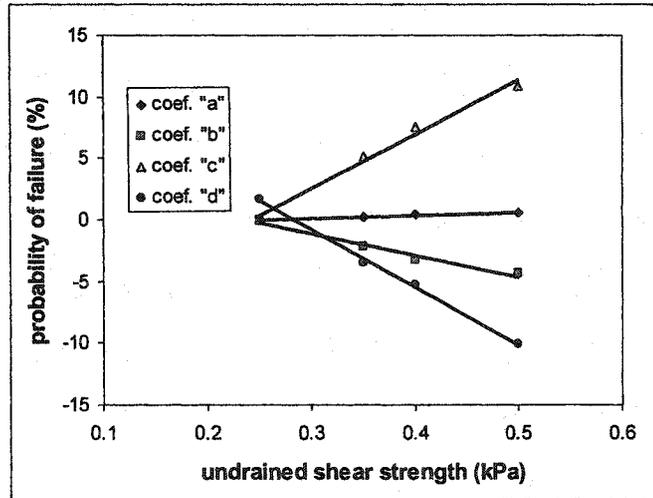
Figure 4.12. Coefficients of third degree polynomials used to curvefit the variation in probability of failure with change in embankment height.
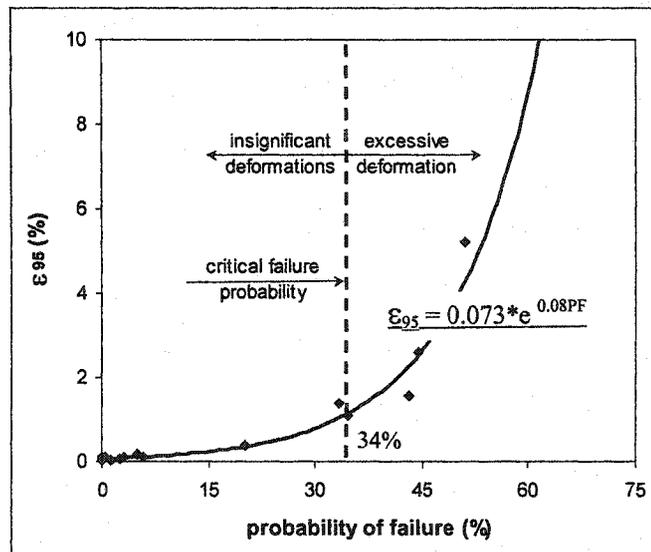
Figure 4.13. Determination of critical probability of failure.

CHAPTER 5

PLANE STRAIN BEHAVIOR OF SPATIALLY VARIABLE SAND MEDIA

5.1. INTRODUCTION

Safety measures in geotechnical design are usually expressed in terms of factors of safety, which can be defined as the ratio between failure and applied stresses. These safety factors are usually assessed in a deterministic framework implementing single-valued soil parameters. However, unavoidable degrees of uncertainty are involved in geotechnical design, which questions the applicability of these deterministic techniques. This uncertainty can be attributed to the following:

1. Uncertainties in loading conditions;
2. Inherent spatial variability of soil properties;
3. Uncertainty associated with selection of an appropriate analytical model;
4. Testing and measurements errors; and
5. Human errors.

Testing and measurements errors can be minimized by appropriate quality control and proper selection of test equipment, while human errors can be mitigated by design quality control and third party design review (Becker 1996). The impact of the first three sources of uncertainty on engineering design can be reasonably quantified by performing probabilistic analyses. Among these three sources of uncertainty, inherent spatial variability is likely to have the greatest impact on geotechnical design. Such variability can be defined as the variation of soil properties from one point to another in space due to difference in deposition environment and loading history. This variation may result in

A version of this chapter has been submitted for publication in the Geotechnique

- 122 -

various degrees of uncertainty associated with the selection of design parameters for classical deterministic analyses.

Due to the stochastic nature of the problem, several studies have been carried out to assess the effect of spatial variability of soil properties on different geotechnical field problems in a probabilistic design framework. These studies have covered various areas, such as liquefaction assessment (Popescu et al. 1998 and 1996; and Fenton and Vanmarcke 1991), seepage flow (Griffiths and Fenton 1993), retaining wall (Duncan 2000), and foundation settlement (Paice et al. 1994; Zeiton and Baker 1992; and Baecher and Ingra 1981).

The main focus of this chapter is to quantify the effect of different elements of soil spatial variability on the macro (overall) behavior of sand under plane strain conditions. This was carried out using deterministic numerical analysis implementing stochastic input soil parameters, where soil friction angle and elastic modulus were considered as random variables and were generated across the analysis domain. An attempt was made to obtain a risk-based characteristic elastic modulus that can be used in deterministic analyses while continuing to honor detailed ground heterogeneity. The results obtained in this chapter were applied to a shallow foundation problem to examine their applicability to geotechnical field problems, as outlined in Chapter 6.

5.2.   PROPOSED ANALYSIS METHODOLOGY

Most geotechnical analyses are deterministic in the sense that after having obtained detailed geological information from site investigation, engineering judgment is applied to assign average soil properties to each distinct soil layer. However, soil properties are rarely, if ever, uniform across any analysis domain as they tend to exhibit some form of spatial variation producing various degrees of uncertainty in the selection

- 123 -

of design parameters. In this study, a methodology was developed to incorporate spatial variability of soil properties in engineering design through the following steps:

1. Assessment of different elements of soil spatial variability;
2. Generation of random soil properties across the analysis domain; and
3. Deterministic elasto-plastic numerical analysis implementing stochastic input soil parameters, such as friction angle and elastic modulus.

A detailed discussion of this methodology is provided in the following sections.

5.3. ASSESSMENT OF DIFFERENT ELEMENTS OF SOIL SPATIAL VARIABILITY

The effect of spatial variability of sand properties on its engineering behavior was quantified by considering friction angle and elastic modulus as random variables, which were then implemented into stochastic numerical analyses. To proceed with stochastic analyses, the main geostatistical characteristics of these random variables have to be assessed. These characteristics can be summarized as follows:

1. Mean, coefficient of variation (COV), and probability distribution;
2. Spatial correlation structure model, which is an analytical expression to depict the variation of soil properties from one point to another in space;
3. Limit of spatial continuity, beyond which no or little correlation between soil properties exists; and
4. Volume variance relations, which help assess the reduction in the variance of field data (point statistics) upon averaging over a certain volume of interest.

In this chapter, the friction angle of sand was considered as the main random variable and was generated across the analysis domain, as shown in Figure 5.1. Soil elastic modulus was treated as a secondary random variable and was obtained by multiplying the tangent of friction angle by a constant ratio of 74. This ratio was selected

- 124 -

to maintain assumed mean values for the friction angle and elastic modulus of 34 degree and 50 MPa, respectively, which are typical values cited in geotechnical literature for medium dense sand. It should be emphasized that the friction angle of sand and its elastic modulus are not perfectly correlated everywhere across analyses domains, as assumed in this study. Nevertheless, this assumption was chosen to overcome the lack of statistical information about elastic modulus in the geotechnical engineering literature.

While the mean values of friction angle and elastic modulus were held constant, the coefficient of variation (COV) of the sand friction angle, which is the ratio between the standard deviation and the mean, was varied between 0.10 and 0.15. This range of COV is in agreement with typical values cited in previous geotechnical statistical studies, such as Lumb (1966), Schultze (1975), and Phoon and Kulhawy (1999). Different probability distribution models, used in geotechnical literature to curvefit field data of sand friction angle, were implemented to examine their effect on the outcomes of stochastic analyses. Examples of these probability distribution models, such as normal, lognormal and standardized beta distributions with g_1 and g_2 equal to 0.127 and –0.715, respectively (Lumb 1970), are shown in Figure 5.2.

The spatial correlation structure was quantified using the variogram (Deutsch 2002). The variogram is a measure of dis-similarity between soil properties at two points in space separated by a distance h. Variograms are usually characterized by their analytical models and limit of spatial continuity, as discussed in Chapter 2. Two variogram models were used, spherical and exponential models, to assess the effect of variogram model on the macro (overall) behavior of spatially variable soil mass. The spatial range, a, (Deutsch 2002) was adopted in this study as a measure of the limit of spatial continuity. Values of 20, 10, 5, and 2 for the normalized horizontal range, R_h/H, were used in this study to examine the effect of spatial range on the engineering behavior of random soil media. The normalized horizontal range was defined as the ratio between the horizontal spatial range, R_h, and the height of the soil block, H, as shown in Figure 5.1. The ratio between horizontal and vertical ranges is typically in the range of 10:1 to

100:1 for fluvial and eolian deposits (Deutsch 2002). As a result, this ratio was kept constant at a value of 20 for all cases considered in this study. Volume-variance relationships were not implemented in the current study as a result of using sufficiently small elements in the numerical analysis mesh, which would result in insignificant reduction in the variance of point statistics. A summary of different geostatistical characteristics implemented in this chapter is presented in Table 5.1.

5.4. GENERATION OF RANDOM VARIABLES ACROSS THE ANALYSIS DOMAIN

The GSLIB geostatistical software library (Deutsch and Journel 1998) was utilized to generate several realizations of the spatially variable friction angle, as shown in Figure 5.1. This was accomplished by using the Sequential Gaussian Simulation (SGS) technique (Deutsch 2002) to assess the value of the friction angle at the center of each element in the numerical analysis mesh. According to the SGS technique, the value of the simulated random variable was considered as the summation of the krigged estimate of the random variable and a residual value in the form:

$$Zs(u) = Z^*(u) + R(u) \tag{5.1}$$

where: $Zs(u)$ is the simulated value of the random variable Z at location u;

$Z^*(u)$ is the krigged estimate of the random variable Z at location u; and

$R(u)$ is a residual value.

The krigged estimate is an interpolated value of the random variable that depends on the characteristics of the spatial correlation structure, such as the model type and limit of spatial continuity. The residual value $R(u)$ is a normally distributed random variable of zero mean and a variance equal to the krigging variance (Deutsch 2002). Monte Carlo simulation was used to obtain several values of the random variable $R(u)$ and

- 126 -

consequently several realizations of the random variable, the friction angle, can be generated across the analysis domain.

It should be noted that the friction angle of each element in the numerical analysis mesh was assumed constant and equal to the value generated at the element center. Whereas, the elastic modulus of each element was assessed by multiplying the tangent of the friction angle by a constant value of 74, as discussed in the previous section.

A key factor for performing reliable stochastic analysis is a proper selection of the number of realizations. A detailed discussion of the assessment of number of realizations used in this study is provided in the next section.

5.5.   ASSESSMENT OF NUMBER OF REALIZATIONS

The number of realizations necessary for any statistical analysis is a function of the desired precision of the analysis, the greater the number of realizations the more precise the results are. In addition, extreme values statistics, i.e. values at the tails of the probability distribution function, may require a large number of realizations to be quantified with reasonable accuracy. On the other hand, increasing the number of realizations beyond a certain limit can be regarded as a time consuming process with very little improvement in numerical accuracy. To assess the required number of realizations in this study, a sensitivity analysis was carried out, as shown in Figure 5.3. For each realization, the arithmetic average (mean) of the friction angle of sand across the analysis domain was obtained. By repeating this process for several realizations a histogram of these averages was obtained, and the 0.05 percentile was determined as a measure of extreme values statistic. The 0.05 percentile is the value of the arithmetic average above which 95% of the histogram data occur, as shown in Figure 5.4. The optimum number of realizations was chosen to be 2000 as it was the number of realizations beyond which there was insignificant change in the value of the 0.05 percentile, as shown in Figure 5.3.

- 127 -

5.6. DETERMINISTIC NUMERICAL ANALYSIS IMPLEMENTING STOCHASTIC INPUT SOIL PARAMETERS

The effect of inherent spatial variability of soil properties on the engineering behavior of sand under plane strain conditions was assessed numerically. The FLAC software (Itasca Consulting Group Inc. 2000) was used to perform a series of deterministic numerical analyses with stochastic input soil parameters. The program adopts an explicit lagrangian finite difference scheme to simulate the engineering behavior of geotechnical materials. A typical mesh used in the analysis is shown in Figure 5.1, where a rectangular block of sand (10 elements wide by 20 elements high) was subjected to a bi-axial state of stress. Horizontal and vertical displacements were fixed along the bottom boundary of the model. Soil was assumed to exhibit elastic perfectly plastic constitutive behavior, for simplicity, implementing Mohr-Coulomb failure criterion. The effect of soil weight was ignored, i.e. weightless soil mass, and Poisson's ratio was assumed constant everywhere across the analysis domain at a value of 0.30. The angle of internal friction and soil elastic modulus were treated as spatially random variables as discussed in earlier sections. Different geostatistical characteristics of these random variables were employed in the numerical model to quantify their influence on the macro behavior of the sand mass. The confining stress was held constant at 50 kPa for all cases considered in this study, while the normalized deviator stress $(\Delta\sigma/\Delta\sigma_F)$ was increased gradually up to a value equal to 0.95. The normalized deviator stress was defined as the ratio between the applied deviator stress $(\Delta\sigma)$ and its value at failure $(\Delta\sigma_F)$. The deviator stress at failure was considered as the value of the deviator stress required to cause shear failure in a homogeneous sand mass with soil properties equal to the mean values of the random variables. It should be realized that normalized deviator stress equal to 0.95 was considered high enough to represent a spatially variable sand mass approaching failure yet to avoid any artificial scatter in the analyses results due to possible numerical instability associated with $(\Delta\sigma/\Delta\sigma_F)$ very close to unity.

- 128 -

5.7. ANALYSIS RESULTS

The main output variable in this study was the average vertical displacement of the sand mass under different state of stresses. The statistics of this variable were used to quantify the effect of different elements of soil spatial variability on:

1. The probability of failure of the sand mass; and
2. The selection of a risk-based characteristic elastic modulus, which can be used in deterministic analyses while continuing to honor detailed ground heterogeneity.

Detailed discussion of the analyses results is provided in the following sections.

5.8. EFFECT OF DIFFERENT ELEMENTS OF SOIL SPATIAL VARIABILITY ON FAILURE PROBABILITY

The probability of failure was defined in this study as the probability that the average vertical displacements at the top of the sand mass would exceed the average vertical displacements at failure. The vertical displacement at failure was obtained from a deterministic analysis using mean values of random variables as input soil properties and a deviator stress sufficient to cause shear failure in the sand mass ($\Delta\sigma_F$).

The effect of probability distribution type on the probability of failure of a spatially variable sand mass is shown in Figure 5.5 for $R_h/H = 10$, COV = 0.15, and exponential correlation structure. The figure presents a cross plot between the probability of failure and the normalized deviator stress ($\Delta\sigma/\Delta\sigma_F$) for different probability distributions types, such as normal, lognormal and beta distributions. The beta distribution was found to produce a relatively lower probability of failure, compared with normal and lognormal distributions, up to a normalized deviator stress of 0.76. Beyond this threshold, the beta distribution was found to produce the highest probability of failure. This could be attributed to the difference in shape between different cumulative

- 129 -

distribution function (CDF) curves, as shown in Figure 5.2. Both the normal and lognormal distributions produced relatively higher frequencies of the critical values of the random variable close to the left tail of the CDF curves. This would result in an increase in the likelihood of generating looser soil pockets susceptible to yielding under relatively small deviator stresses. On the other hand, the normal and lognormal produced relatively higher frequencies of the values of the random variable close to the right tail of the CDF curves thus increasing the probability of occurrence of rigid soil pockets within the soil mass. The presence of these rigid pockets might have contributed to the small probability of failure associated with high deviator stresses, as shown in Figure 5.5.

The coefficient of variation (COV) of the friction angle was found to have a profound effect on the probability of failure, as shown in Figure 5.6 for normal probability distribution, $R_h/H = 10$, and exponential correlation structure. As expected, the higher the COV, the more likely the soil will fail at a certain applied deviator stress. This could be attributed to the fact that increased coefficient of variation would result in more scatter in the simulated values of the random variables and consequently possible generation of looser soil pockets. It is believed that these loose pockets yielded upon increasing applied deviator stress resulting in higher failure probabilities.

The effect of spatial correlation structure (variogram) model on the probability of failure of the sand mass was quantified, as shown Figure 5.7 for normal probability distribution, $R_h/H = 10$, and COV = 0.15. It was found that spherical variograms produced slightly higher probabilities of failure compared with exponential variograms up to a normalized deviator stress of 0.68. Beyond this threshold, higher probabilities of failure were found to be associated with exponential variograms. This transition in soil response was considered to be a result of the difference in shape between variogram models and its implications on the outcome of stochastic analyses.

The effect of the normalized spatial range (R_h/H) on the probability of failure is presented in Figure 5.8. It was found that the probability of failure increased with higher

values of normalized horizontal range up to a normalized deviator stress ($\Delta\sigma/\Delta\sigma_F$) equal to 0.67. Beyond this threshold, probability of failure tended to increase with smaller values of normalized spatial range. This could be attributed to the fact that increasing the spatial range would result in a more gradual spatial variation of soil properties and consequently the possibility of generating continuous loose pockets, which would yield under small applied deviator stresses. Upon reaching ($\Delta\sigma/\Delta\sigma_F$) equal to 0.67, most of these loose pockets yielded leaving continuous pockets of relatively stiffer sand. These stiffer zones resulted in a slow increase in the failure probability with higher values of applied deviator stress. On the other hand, implementing smaller spatial ranges, such as $R_h/H = 2$, in stochastic analysis would result in the generation of discontinuous pockets of loose sand surrounded by stiffer zones, resulting in stress transfer from the looser to the stiffer pockets. This stress transfer mechanism would likely result in smaller yielded zones and consequently smaller probability of failure up to ($\Delta\sigma/\Delta\sigma_F$) equal to 0.67. Beyond this threshold, deviator stresses were likely high enough to trigger yielding in the loose soil pockets and the surrounding slightly stiffer zones resulting in a rapid increase in failure probability with the increase in applied deviator stresses.

To the author's knowledge, there have been few attempts to specify a target probability of failure for different geotechnical applications. Most of these attempts were related to slope stability problems, such as El-Ramly (2001) who proposed a target failure probability of 1% to 2% for earth slopes based on extensive probabilistic analysis of several case histories in Canada and Hong Kong. In addition, Becker (1996) proposed a target annual failure probability of 0.01 to 0.1% for foundation design. By selecting a target failure probability of 1% for spatially variable soil media under plane strain conditions, a safe practical range for applied deviator stresses can be obtained, as shown in Figure 5.6. The upper limits of this safe range were found to be associated with normalized deviator stresses of 0.60 and 0.65 for coefficients of variation of 0.15 and 0.10, respectively. Deviator stresses greater than these limits could be considered beyond the safe practical range of applied stresses in geotechnical applications.

It is worth noting that these limits were assessed for normalized spatial range, R_h/H, of 10, which was expected to produce the most critical ground conditions. This could be attributed to the fact that increasing spatial range would result in gradual spatial change in soil properties and consequently the generation of larger pockets of loose soil, which might affect the overall stability of soil mass. Accordingly, it would be anticipated that using R_h/H of 20 would produce more critical design conditions. However, the difference between the 2 cases was small, for normalized deviator stresses smaller than 0.65 as seen in Figure 5.8, that it was neglected for all practical purposes. In addition, the use of R_h/H of 10 was selected for comparison with the results obtained in Chapter 6.

Implementing the practical safe range of stress application to the results presented in Figure 5.5 to Figure 5.8, the following conclusions could be obtained:

1. The probability of failure of spatially variable sand media under plane strain conditions is independent of the spatial correlation structure model;

2. Curvefitting field data with beta distribution would result in smaller predicted probability of failure compared to normal and lognormal distributions;

3. The probability of failure of spatially variable sand media is highly sensitive to the coefficient of variation of soil properties; and

4. Increasing the range of spatial correlation between soil properties would result in an increased failure probability.

5.9. EFFECT OF SOIL SPATIAL VARIABILITY ON DIFFERENT ESTIMATES OF CHARACTERISTIC ELASTIC MODULUS OF SAND

Risk can be defined as a measure of the probability and severity of an adverse effect to health, property, or the environment (the Canadian Standards Association 1991). Accordingly, assessing risk level involves answering three main questions: "What can go wrong?", "How likely is it?", and "What are the consequences?". Robertson (1998) classified engineering projects qualitatively, based on their risk level, into 3 categories:

1. Low risk projects with few hazards, low probability of occurring of these hazards, and limited consequences;

2. Medium risk projects with moderate hazards, low/high probability of occurring of these hazards, and severe/limited consequences; and

3. High risk projects with many hazards, high probability of occurring of these hazards, and severe consequences.

An attempt was made in this study to obtain a risk-based characteristic elastic modulus, which could be used in deterministic geotechnical analyses while continuing to honor detailed ground variability. Not only would the value of this characteristic modulus depend on soil geostatistical characteristics, but also on the risk level of the project. For example, the characteristic modulus for high risk projects would be smaller than that of low risk projects even though they were derived from soil with the same geostatistical characteristics. The assessment of this characteristic modulus was accomplished by determining an equivalent elastic modulus, E, of a homogenous sand mass that would reproduce the same average vertical strain of the spatially variable block, as shown in Figure 5.9. Applying this methodology to several realizations of the soil mass, a histogram of the normalized equivalent elastic modulus (E/E_o) was obtained, as shown in Figure 5.10. This normalized modulus was assessed as the ratio between the equivalent elastic modulus (E) and the mean elastic modulus of sand (E_o) used in the current study. Depending on the desired risk level, different characteristic values of the normalized equivalent elastic modulus could be obtained, such as:

1. The mean normalized equivalent elastic modulus, which was regarded by the author as a suitable characteristic value for low risk projects;

2. The values associated with a linear loss function, as discussed in Chapter 2. These functions are mathematical expressions used to quantify the impact of making mistakes in selecting design parameters. Loss functions are employed in the Bayesian decision analysis (Benjamin and Cornell 1970, and Deutsch 2002), together with random variables histograms, to obtain optimal estimates of soil design parameters associated with minimum expected monetary loss of engineering projects. Ratios of

- 133 -

2.5:1 and 5:1 between the loss functions parameters "a" and "b", shown in Figure 2.19, were proposed to be associated with medium risk and high risk projects, respectively. It should be realized, however, that the selection of these ratios is primarily subjective and project dependent, as no generic design criterion for the selection of loss functions parameters (a and b) has been developed in risk-related engineering literature; and

3. The values associated with the lower/upper limits of the 90% confidence level, as discussed in Chapter 2. Using these estimates imply that there will be only a 5% chance that the actual deformation will be greater/smaller than the value predicted using these estimates. These limits were considered by the author to be suitable estimates for extremely high risk projects where consequences of failure can be catastrophic.

The influence of different elements of soil spatial variability on these characteristic values of soil elastic modulus is discussed in the following sections.

It is worth noting that Eurocode 7 has suggested the use of the lower limit of the 90% confidence level as a characteristic elastic modulus for use in limit state design (Orr 2000). It should be realized that this characteristic value should be obtained from histograms of mean elastic modulus over an averaging volume governing the occurrence of limit state rather than histograms obtained from field or laboratory testing of limited soil volumes (point statistics). The determination of this governing volume, however, is practically difficult, which imposes a considerable uncertainty in the value of this characteristic value and questions its applicability in geotechnical design.

5.9.1. Effect of Spatial Variability on Characteristic Elastic Modulus for Low Risk Projects

The effect of different elements of spatial variability of sand properties on the mean equivalent elastic modulus, as a proposed characteristic value for low risk projects,

is shown in Figure 5.11 to Figure 5.14. It was concluded from these figures that different geostatistical characteristics of soil properties have insignificant impact on the mean equivalent elastic modulus within the safe practical limit of stress application, i.e. for normalized deviator stresses smaller than 0.60. As a result, it was suggested that the mean normalized equivalent elastic modulus could be considered constant for all practical application at a value of 0.97. It is worth noting that this value is smaller than unity due to possible presence of looser pockets within the soil mass resulting in developing plastic zones, which can not be accounted for using classical deterministic analyses. Nevertheless, the difference between the proposed value (0.97) and 1.0 is small enough to consider mean elastic modulus as a suitable characteristic estimate for low risk projects.

5.9.2. Effect of Spatial Variability on Characteristic Elastic Modulus for Medium and High Risk Projects

In a fashion similar to the previous section, the effect of different elements of sand spatial variability on risk-based estimates of characteristic elastic modulus for medium and high risk projects is shown in Figure 5.15 to Figure 5.18.Within the practical limits of stress applications, i.e. for normalized deviator stresses smaller than 0.60, the following conclusions were obtained:

1. The probability distribution type and variogram model have an insignificant effect on the characteristic elastic modulus estimates for medium and high risk projects as well as on those associated with the upper and lower limits of the 90% confidence level, as shown in Figure 5.15 and Figure 5.16;

2. The coefficient of variation (COV) has a considerable impact on different estimates of risk-based characteristic elastic modulus. The impact of changing COV becomes more pronounced for estimates closer to the tail of probability distribution, as the case for the upper and lower limits of the 90% confidence level, as presented Figure 5.17. As discussed earlier, this can be attributed to the fact that higher values of COV might be associated with more scatter of field data and possible presence of loose soil pockets; and

- 135 -

3. Spatial range is likely to have an insignificant influence on different estimates of characteristic elastic modulus, as shown in Figure 5.18, since the differences between these estimates for R_h/H ranging between 2 and 10 was found to be smaller than 5% for all the cases considered in this study.

Based on the above findings, it can be reasonably assumed that different risk-based estimates of characteristic elastic modulus of sand are constants for a fixed value of COV regardless of the values of other geostatistical characteristics. Recommended values of these estimates for use in engineering design are summarized in Table 5.2.

5.10. CONCLUSIONS

The main objective of this chapter was to quantify the effect of different elements of soil spatial variability, such as probability distribution, coefficient of variation, spatial correlation structure models, and limit of spatial correlation, on the macro behavior of sand under plane strain conditions. This was carried out using numerical analysis techniques with stochastic input soil properties. Soil friction angle and elastic modulus were treated as random variables and implemented in the numerical analysis software "FLAC". In addition, an attempt was made to obtain risk-based characteristic elastic modulus for use in deterministic geotechnical analyses while continuing to honor detailed ground variability.

The effect of different elements of soil spatially variability on the failure probability of sand masses under plane strain conditions was investigated. Deviator stresses associated with a failure probability of 1% were considered as upper limits for a safe practical range of deviator stress application. These limits were found to be 0.60 and 0.65 for coefficient of variations of 0.15 and 0.10, respectively. Spatial correlation structure models were found to have insignificant influence on the probability of failure within the practical safe range of stress application. Whereas, probability of failure was

- 136 -

found to increase with higher values of coefficient of variation, and with larger limits of spatial correlation (spatial range).

Different risk-based estimates for characteristic elastic modulus of sand were introduced, such as mean values, estimates associated with linear loss functions, and upper and lower limits of the 90% confidence level. Coefficient of variation was found to have the greatest effect on these estimates within the safe practical range of stress application, compared to other geostatistical characteristics. Using mean values in deterministic geotechnical analyses was considered to be on the non-conservative side especially for medium and high risk projects, where there is a need to develop more rational characteristic soil parameters. Recommended values of different risk-based estimates of characteristic elastic modulus were provided for use in practical applications.

More attention should be given to assess the sensitivity of the outcomes of this study to geostatistical configurations not considered in this study, such as:
1. Different ratios between horizontal and vertical limits of spatial continuity; and
2. Treatment of sand friction angle and elastic modulus as two correlated primary random variables.

The results obtained in this chapter were applied to a shallow foundation problem in Chapter 6 to examine their applicability to geotechnical field problems with relatively similar stress path. The emphasis was to investigate whether the risk-based estimates of characteristic elastic modulus are of universal nature; or problem dependent that may be affected by changes in boundary conditions and stress path.

5.11. REFERENCES

Baecher G. B., and Ingra, T. S. 1981. Stochastic FEM in settlement predictions. Journal of the Geotechnical Engineering Division, ASCE, 107 (GT4): 449-463.

Becker, D. E. 1996. Eighteenth Canadian Geotechnical Colloquium: Limit state design for foundations. Part 1. An overview of the foundation design process. Canadian Geotechnical Journal, 33 (6): 956-983

Benjamin, J. R. and Cornell, C. A. 1970. Probability, statistics, and decision for civil engineers. McGraw-Hill Book Company, New York.

Deutsch, C. V. 2002. Geostatistical reservoir modeling. Oxford University press.

Deutsch, C. V. and Journel A. G. 1998. GSLIB geostatistical software library. Oxford University press.

Duncan, J. M. 2000. Factors of safety and reliability in geotechnical engineering. Journal of the Geotechnical and Geoenvironmental Engineering Division, ASCE, 126 (GT4): 307-316.

El-Ramly, H. 2001. Probabilistic and quantitative risk analysis for earth slopes. Ph.D. thesis, University of Alberta, Edmonton, Alberta, Canada.

Fenton, G. A., and Vanmarcke, E. H. 1991. Spatial variation in liquefaction risk assessment. Proceeding of the geotechnical Engineering Congress, Boulder, Colorado, USA. Geotechnical Special Publications, No. 27, Vol.1, pp. 594-607.

Griffiths, D.V., and Fenton, A. 1993. Seepage beneath water retaining structures founded on spatially random soil. Geotechnique, 43 (4): 577-587.

Itasca Consulting Group Inc. 2000. FLAC: fast lagrangian analysis of continua. Minneapolis, Minnesota, USA.

Lumb, P. 1966. Safety factors and the probability distribution of soil strength. Canadian Geotechnical Journal, 3 (2): 74-97.

Lumb, P. 1970. Safety factors and the probability distribution of soil strength. Canadian Geotechnical Journal, 7 (3): 225-242.

Orr, T. L. L. 2000. Selection of characteristic values and partial factors in geotechnical design to Eurocode 7. Computer and Geotechnics, 26: 263-279.

Paice, G. M., Griffiths, D. V., and Fenton, G. A. 1994. Influence of spatially random soil stiffness on foundation settlement. Proceeding of the Conference on Vertical and Horizontal Deformation of Foundations and Embankments, Part 1 (of 2), College Station, Texas, USA, pp. 628-639.

Phoon, K., and Kulhawy, F. H. 1999. Characterization of geotechnical variability. Canadian Geotechnical Journal, 36 (4): 612-624.

Popescu, R., Prevost, J. H., and Deodatis, G. 1996. Influence of spatial variability of soil properties on seismically induced liquefaction. Proceeding of the 1996 Conference on Uncertainty in the Geologic Environment, Uncertainty 96, Part 2 (of 2), Madison, WI, USA, pp. 1098-1112.

Popescu, R., Prevost, J. H., and Deodatis, G. 1998. Characteristic percentile of soil strength for dynamic analysis. Proceeding of the 1998 Conference on Geotechnical Earthquake Engineering and Soil Dynamics III, Part 2 (of 2), Seattle, WA, USA, pp. 1461-1471.

Schultze, E. 1975. Some aspects concerning the application of statistics and probability to foundation structures. Proceeding of the 2nd International Conference on Applications of statistics and probability in soil and structure Engineering, Aachen, Germany, pp. 457-494.

Vanmarcke, E. 1977. Probabilistic modeling of soil profiles. Journal of the Geotechnical Engineering Division, ASCE, 103 (GT11): 1227-1245.

Zeitoun, D. G. and Baker, R. 1992. A stochastic approach for settlement predictions of shallow foundations. Geotechnique, 42 (4): 617-629.

Table 5.1. Description of different geostatistical characteristics applied in this study

Case	Probability distribution type	COV	Variogram model	Normalized spatial range (R_h/H)
Case 1	Normal	0.15	Spherical	20
Case 2	Normal	0.15	Exponential	20
Case 3	Normal	0.15	Spherical	10
Case 4	Normal	0.15	Exponential	10
Case 5	Normal	0.10	Exponential	10
Case 6	Normal	0.15	Exponential	5
Case 7	Normal	0.15	Exponential	2
Case 8	Log-normal	0.15	Exponential	10
Case 9	Beta	0.15	Exponential	10

Table 5.2. Recommended values for risk-based estimates of characteristics elastic modulus of sand under plane strain conditions.

Estimate	Mean	Medium risk	High risk	L_{90}*	U_{90}**
COV = 0.10	0.97	0.93	0.89	0.81	1.15
COV = 0.15	0.97	0.90	0.87	0.75	1.17

* L_{90} is the lower limit of the 90 % confidence level
** U_{90} is the upper limit of the 90 % confidence level

- 140 -
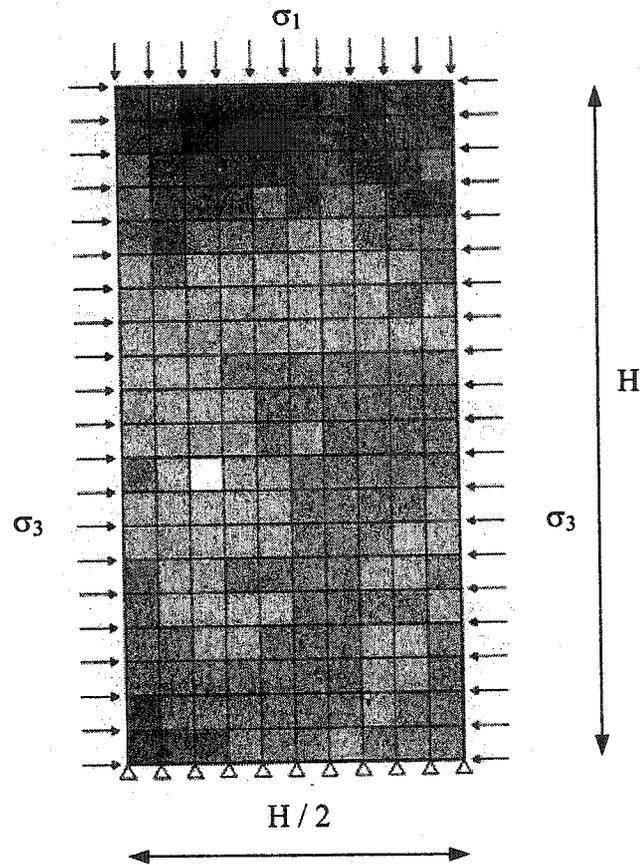
Figure 5.1. Spatial variation of sand friction angle across the numerical analysis mesh (darker zones indicate higher friction angles)

- 141 -
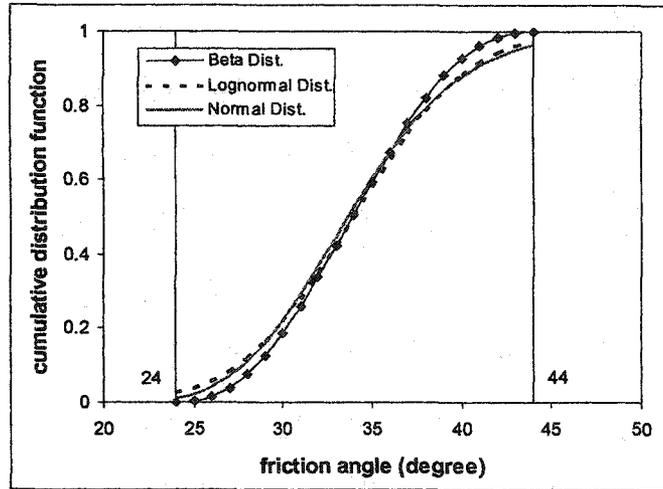
Figure 5.2. Cumulative distribution functions for different probability distribution models used in this study.
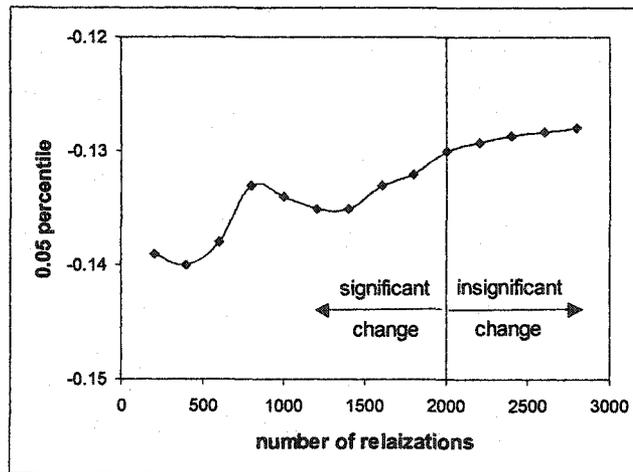
Figure 5.3. A sensitivity analysis to assess the required number of realizations for stochastic analysis.

- 142 -
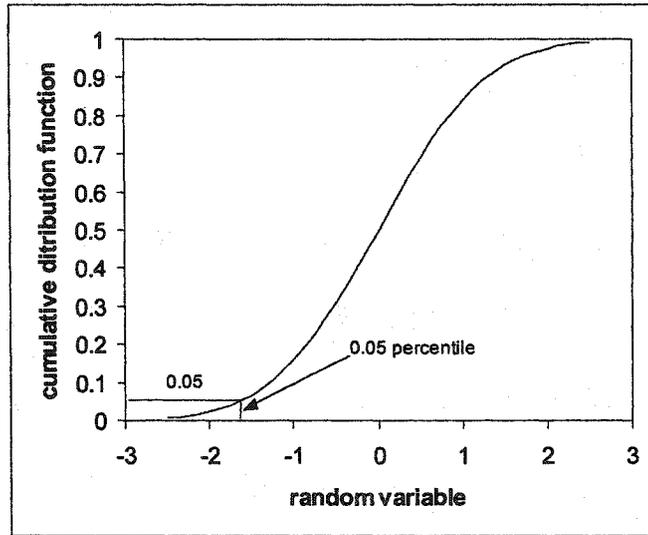
Figure 5.4. A schematic diagram illustrating the determination of the 0.05 percentile.
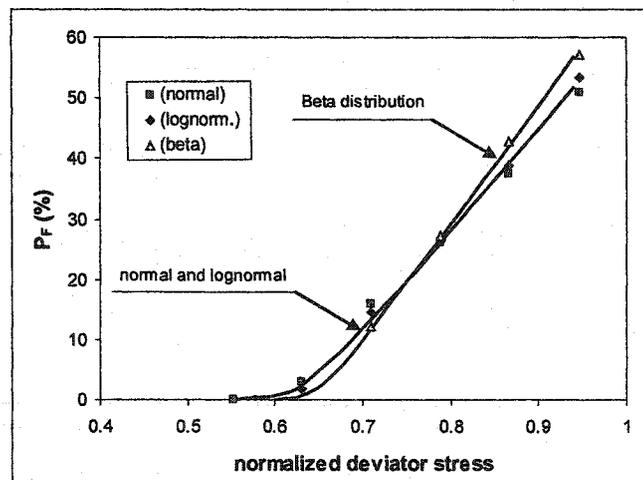
Figure 5.5. Effect of probability distribution type on the probability of failure of spatially variable sand mass. (exponential variogram model, $R_h/H = 10$, and COV = 0.15).
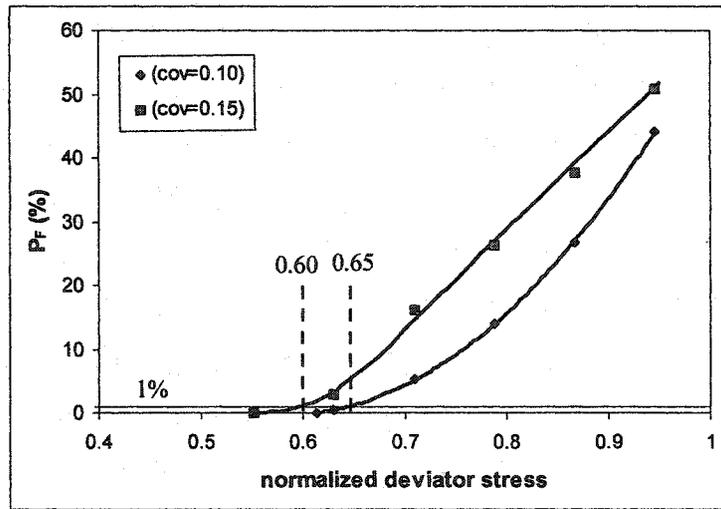
Figure 5.6. Effect of coefficient of variation of the friction angle on the probability of failure of the sand mass. (exponential variogram model, R_h/H = 10, and normal distribution)
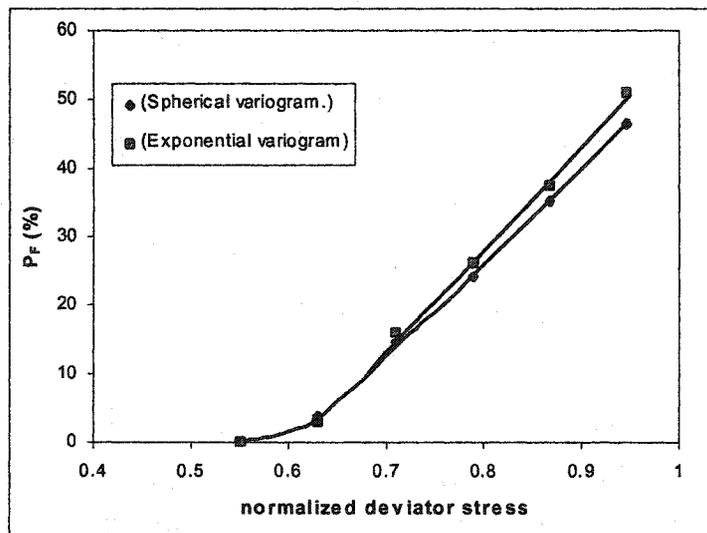
Figure 5.7. Effect of spatial correlation structure (variogram) model on the probability of failure of the sand mass. (R_h/H = 10, COV = 0.15, and normal distribution)

- 144 -
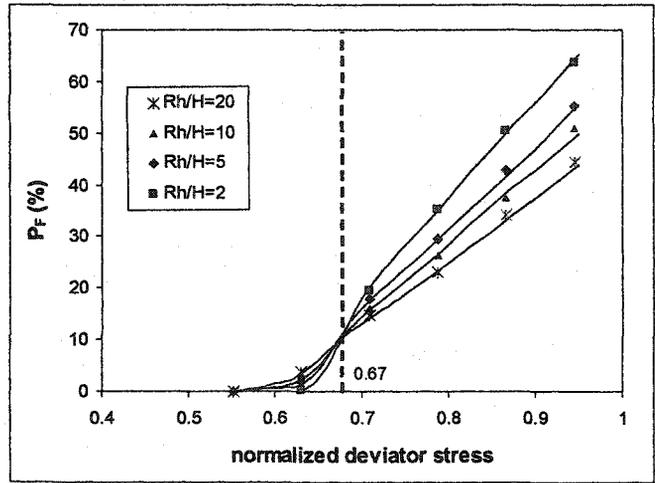
Figure 5.8. Effect of spatial range on the probability of failure of the sand mass. (COV = 0.15).
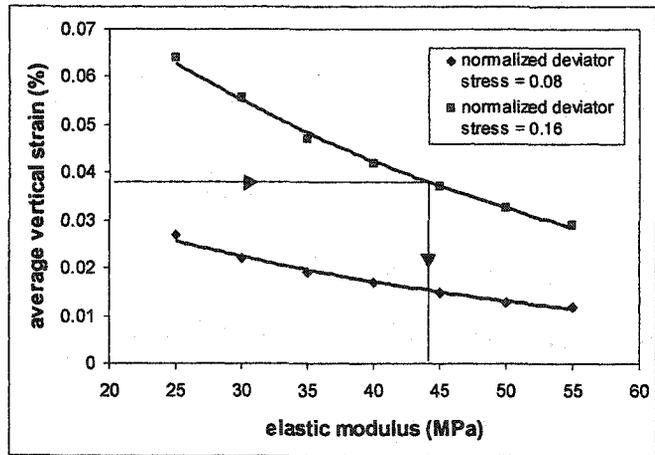
Figure 5.9. Schematic diagram showing the determination of equivalent elastic modulus
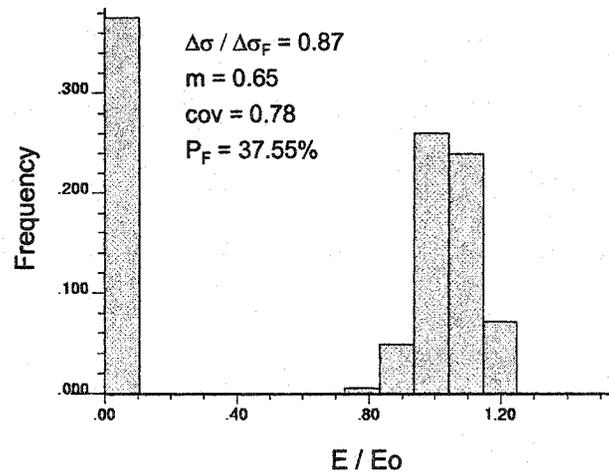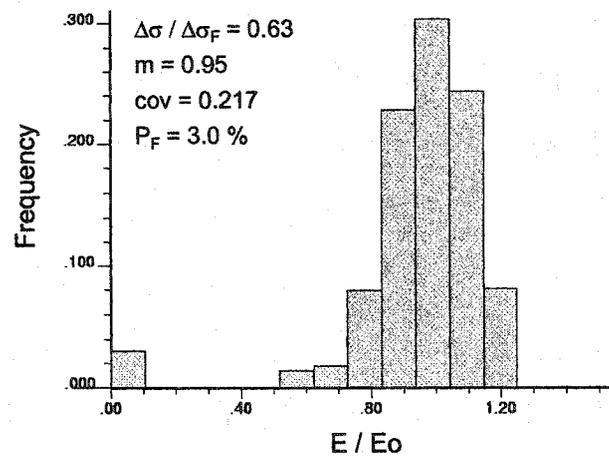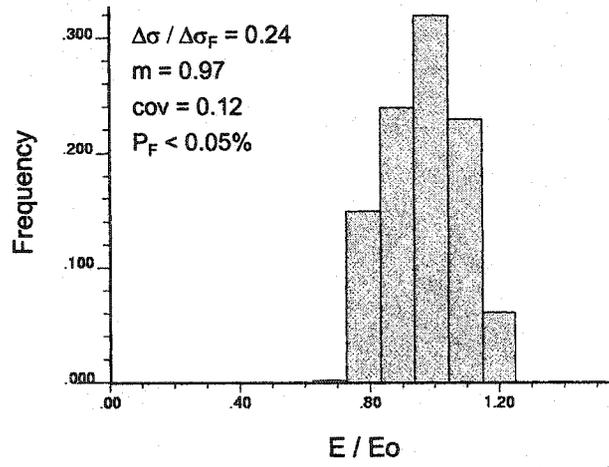
Figure 5.10. Histograms of normalized equivalent elastic modulus under different values of normalized deviator stress ($\Delta\sigma/\Delta\sigma_F$).
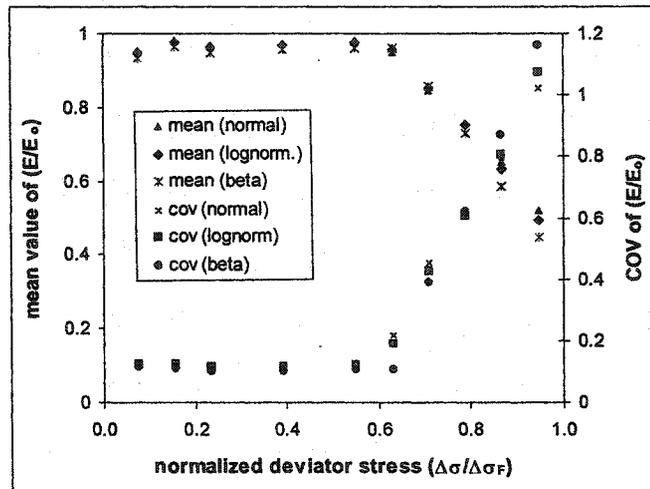
Figure 5.11. Effect of different types of probability distributions on the mean value of the equivalent elastic modulus and its coefficient of variation. (exponential variogram model, $R_h/H = 10$, $COV = 0.15$).
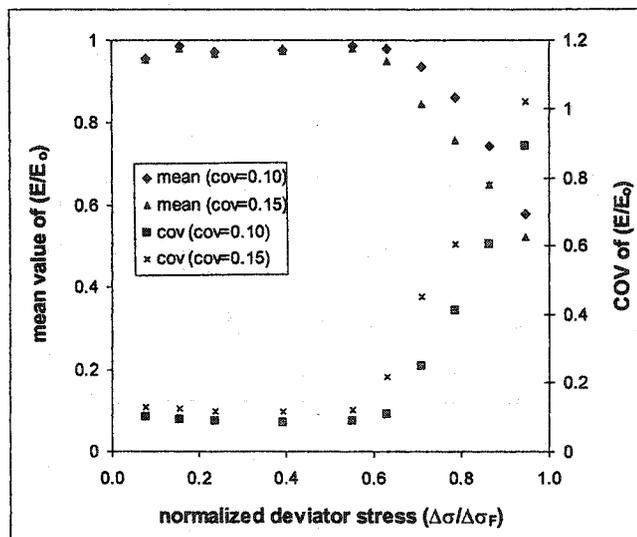
Figure 5.12. Effect of coefficient of variation of sand friction angle on the mean equivalent elastic modulus and its coefficient of variation. (Exponential variogram model, $R_h/H = 10$).

- 147 -
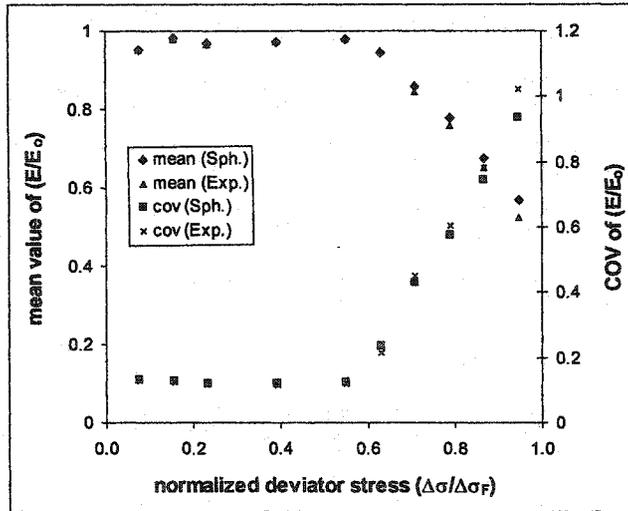
Figure 5.13. Effect of spatial correlation structure model on the mean equivalent elastic modulus and its coefficient of variation. (R_h/H = 10, COV = 0.15).
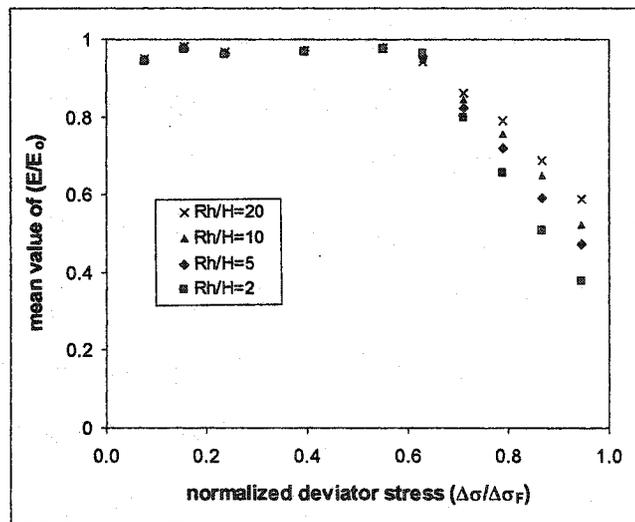
Figure 5.14. Effect of spatial range on the mean equivalent elastic modulus and its coefficient of variation. (COV = 0.15).

- 148 -
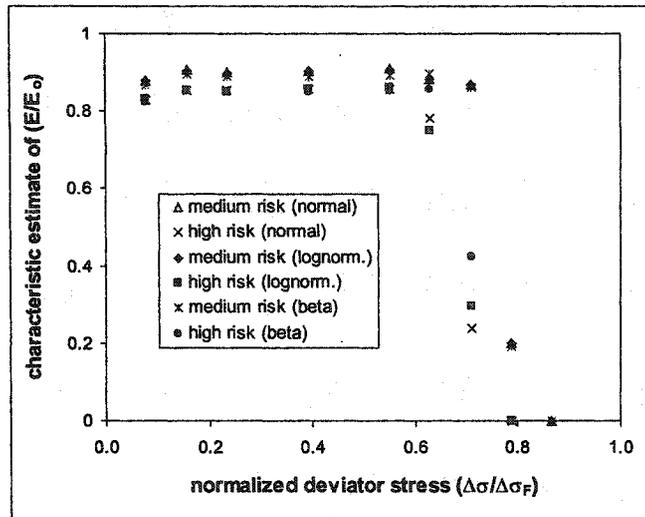
(a)
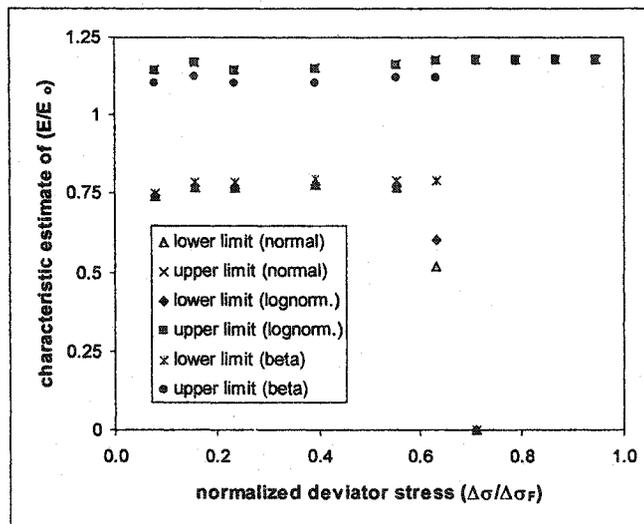
(b)

Figure 5.15. Effect of probability distribution type on different risk-based estimates of normalized characteristic elastic modulus (E/E_o). a) medium and high risk estimates based on linear loss functions; and b) estimates associated with the upper and lower limits of the 90% confidence level. (exponential variogram model, $R_h/H = 10$, COV = 0.15).

- 149 -
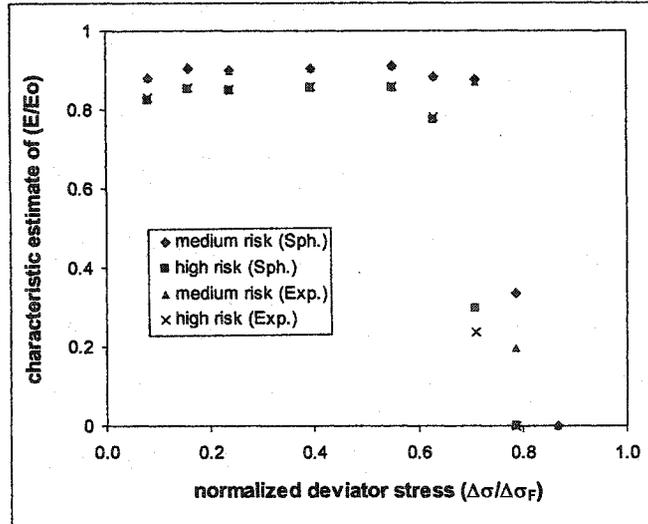
(a)
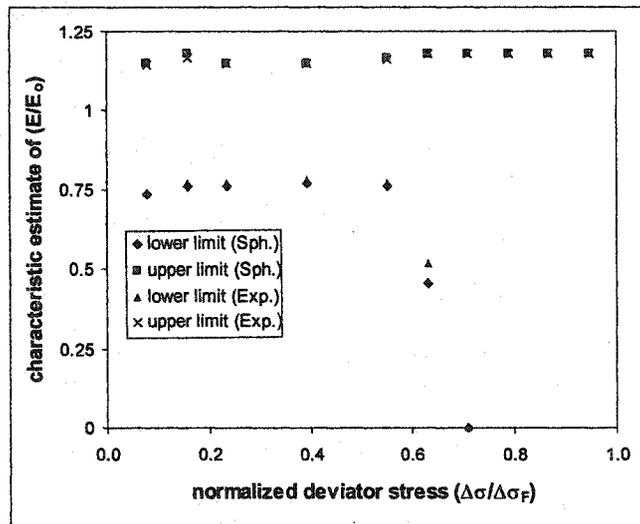
(b)

Figure 5.16. Effect of spatial correlation structure model on different risk-based estimates of normalized characteristic elastic modulus (E/E_o). a) medium and high risk estimates based on linear loss functions; and b) estimates associated with the upper and lower limits of the 90% confidence level. $(R_h/H = 10$, and $COV = 0.15)$.

- 150 -
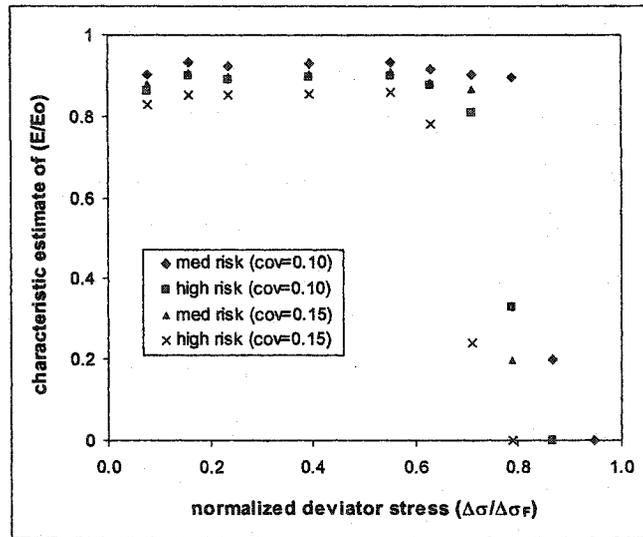
(a)
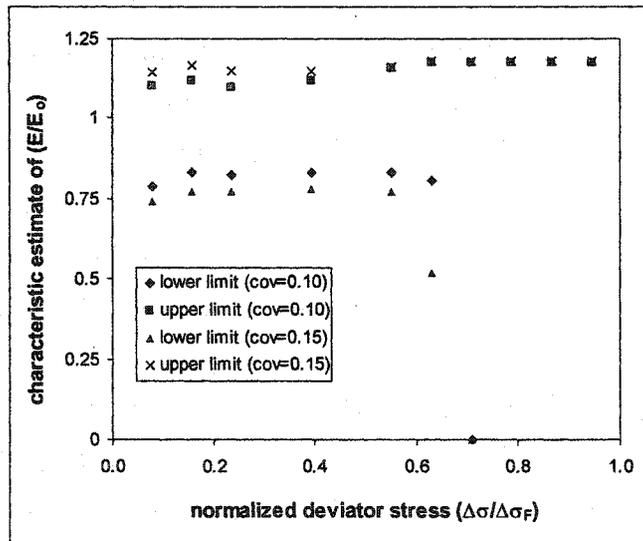
(b)

Figure 5.17. Effect of coefficient of variation (COV) on different risk-based estimates of normalized characteristic elastic modulus (E/E_o). a) medium and high risk estimates based on linear loss functions; and b) estimates associated with the upper and lower limits of the 90% confidence level. $(R_h/H = 10)$.

- 151 -
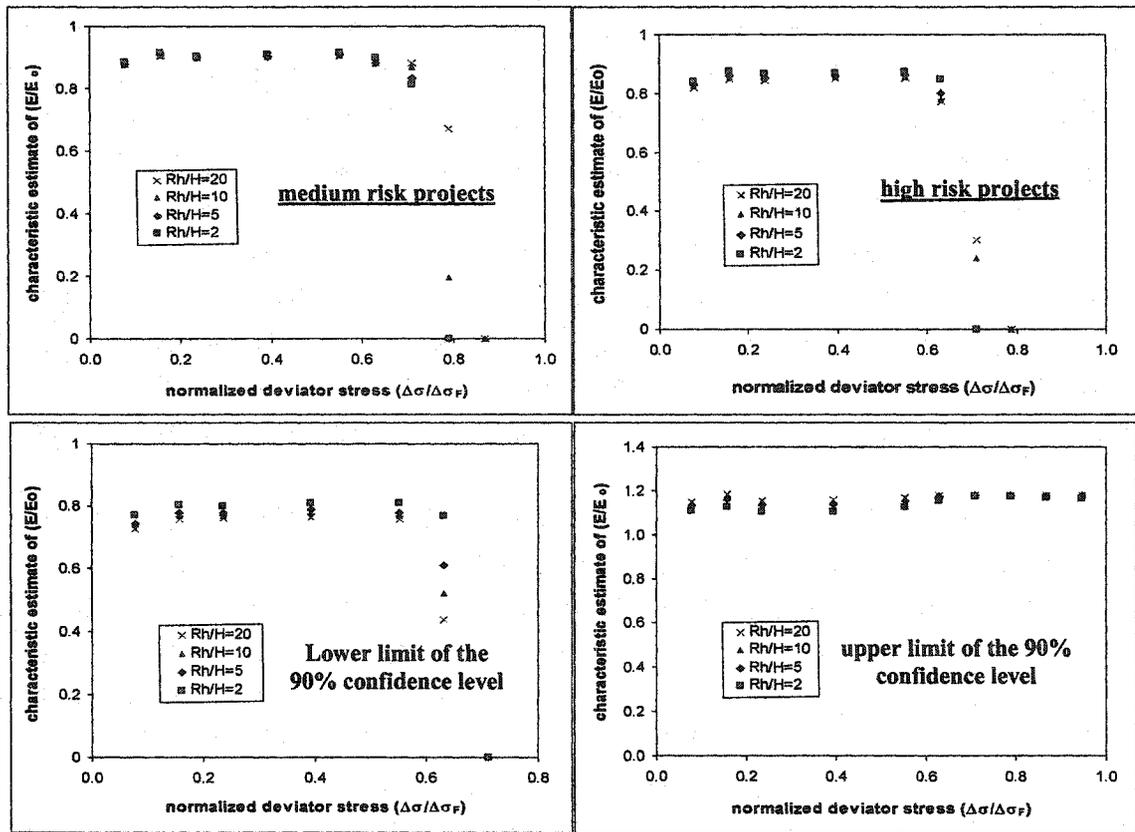
Figure 5.18. Effect of spatial range on different risk-based estimates of normalized characteristic elastic modulus (E/E₀). (COV=0.15).

CHAPTER 6

BEHAVIOR OF SHALLOW FOUNDATION ON SPATIALLY VARIABLE SOILS

6.1. INTRODUCTION

Factors of safety have been the conventional safety measures used in foundation design. Recently, strength and load factors have emerged as safety measures in foundation design within the limit state design framework. These safety measures are usually assessed in a deterministic fashion, which depends on engineering judgment to account for the inherent uncertainty associated with foundation design. This uncertainty can be attributed to several factors, such as:

1. Uncertainties in loading conditions;
2. Inherent spatial variability of soil properties;
3. Uncertainty associated with selection of an appropriate analytical model;
4. Testing and measurements errors; and
5. Human errors.

As discussed in Chapter 5, spatial variability of soil properties could be considered as a main source of uncertainty due to the difficulty associated with selecting representative parameters to implement in engineering design. This variability can be defined as the variation of soil properties from one point to another in space due to variation in deposition environment and loading history.

Several attempts have been made to assess the effect of spatial variability of soil properties on foundation design in a probabilistic design framework. This started with the

---

A version of this chapter has been submitted for publication in the Geotechnique

early work of Wu and Kraft (1967), and Resendiz and Herrera (1969). These studies were fairly primitive in the sense that some geostatistical characteristics of soil, such as the spatial correlation between soil properties, were not properly considered and that all soil properties were assumed to follow normal probability distributions. The modern approach to deal with uncertainty in foundation design started in the early 1980s with the introduction of different versions of the stochastic finite element, such as Baecher and Ingra (1981) and Zeitoun and Baker (1992). This approach has not gained much popularity among geotechnical practitioners due to the numerous limitations of the stochastic finite element method, as discussed in Chapter 2. Recently, deterministic numerical analysis with stochastic input soil parameters has been proven to be the most rigorous approach for stochastic analyses of different geotechnical field problems. This approach was applied to a shallow foundation problem by Paice et al. (1994) to investigate the effect of spatial variability of soil elastic modulus on foundation design.

Proper stochastic analysis of foundation problems, while being amenable to engineering design, can be regarded as a relatively sophisticated technique especially for engineers with a limited statistical background. There has been a need to develop risk-based soil parameters that can be used in simplified deterministic analyses, while continuing to honor detailed ground variability. In Chapter 5, an attempt was made to investigate the possibility of obtaining risk-based estimates for elastic modulus of sand under plane strain conditions. Stochastic input soil parameters were implemented in deterministic numerical analyses to examine the effect of different elements of soil inherent spatial variability on these estimates. Characteristic values of these estimates were provided for use in engineering design.

The main purpose of this chapter is to assess the effect of different elements of soil spatial variability on shallow foundation behavior in the form of a strip footing resting on a spatially variable sand medium. Mechanical properties of sand, such as friction angle and elastic modulus, were treated as random variables, and were implemented stochastically in deterministic numerical analyses using the FLAC software

(Itasca Consulting Group Inc. 2000). Attempts were made to estimate the safety level of the current state of practice in foundation design, and to obtain risk-based estimates for sand elastic modulus. These estimates were compared with those obtained in Chapter 5 to examine their applicability to geotechnical field problems. The sensitivity of these estimates to initial state of stress in subsurface soils was assessed together with its implications on shallow foundation design.

6.2.   PROPOSED ANALYSIS METHODOLOGY

Soils are one of the most spatially variable engineering materials. This usually results in an unavoidable degree of uncertainty in engineering design. However, most of the current foundation designs are deterministic in nature, where average soil properties are assigned to each distinct layer. Such analyses can not account for the presence of loose pockets and scatter in field data and their spatial correlation. To overcome these limitations, a design methodology was developed to incorporate spatial variability of soil properties in foundation design through the following steps:

1. Assessment of different elements of soil spatial variability;

2. Generation of random soil properties across the analysis domain; and

3. Deterministic elasto-plastic numerical analysis implementing stochastic input soil parameters, such as friction angle and elastic modulus.

A detailed discussion of this design methodology is provided in the following sections.

6.3.   ASSESSMENT OF DIFFERENT ELEMENTS OF SOIL SPATIAL VARIABILITY

The effect of spatial variability of sand properties on the engineering behavior of shallow foundation was quantified by considering friction angle and elastic modulus as

- 155 -

random variables, which were then implemented into stochastic numerical analyses. To proceed with stochastic analyses, the main geostatistical characteristics of these random variables have to be assessed, as discussed in Chapter 5, such as:

1. The mean, coefficient of variation (COV), and probability distribution;
2. Spatial correlation structure model, such as exponential and spherical models;
3. Limit of spatial continuity, expressed in terms of normalized horizontal spatial range as discussed in Chapter 5; and
4. Volume variance relationships.

Different geostatistical characteristics implemented in the current study were assessed in a fashion similar to Chapter 5. A summary of these characteristics is provided in Table 6.1.

6.4. GENERATION OF RANDOM VARIABLES ACROSS THE ANALYSIS DOMAIN

The GSLIB geostatistical software library (Deutsch and Journel 1998) was utilized to generate several realizations of the spatially variable friction angle across the foundation soil for different geostatistical characteristics, as shown in Figure 6.1. This was accomplished by using the Sequential Gaussian Simulation (SGS) technique (Deutsch 2002) to determine the value of the friction angle at the center of each element in the numerical analysis mesh. A simplified description of the SGS technique was provided in Chapter 5. The friction angle of each element in the numerical analysis mesh was assumed constant and equal to the value generated at the element center. Whereas, the elastic modulus was assessed by multiplying the tangent of the friction angle by a constant value of 74 to maintain assumed mean values for the friction angle and elastic modulus of 34 degree and 50 MPa, respectively.

A key factor for obtaining acceptable accuracy of stochastic analysis is a proper selection of the number of realizations. A detailed discussion of the assessment of number of realizations used in this study is provided in the next sections.

6.5.   ASSESSMENT OF NUMBER OF REALIZATIONS

The number of realizations necessary for any statistical analysis is a function of the desired precision of the analysis, and the type of statistics being considered, as discussed in Chapter 5. To assess the required number of realizations, a sensitivity analysis was carried out as shown in Figure 6.2. For each realization, the arithmetic average (mean) of the friction angle of sand across the foundation soil was assessed. By repeating this process for all realizations, a histogram of these averages was obtained and the 0.05 percentile was determined as a measure of extreme values statistic. The 0.05 percentile is the value of the arithmetic average above which 95% of the histogram data occur, as discussed in earlier chapters. The optimum number of realizations was found to be 800 as it was the number of realizations beyond which there was insignificant change in the value of the 0.05 percentile, as shown in Figure 6.2.

6.6.   IMPLEMENTATION OF STOCHASTIC INPUT SOIL PARAMETERS INTO DETERMINISTIC NUMERICAL ANALYSIS

The FLAC software (Itasca Consulting Group Inc. 2000) was used to perform a series of deterministic numerical analyses with stochastic input soil parameters to assess the effect of soil spatial variability on the behavior of shallow foundation under plane strain conditions. The program adopts an explicit lagrangian finite difference scheme to simulate the engineering behavior of geotechnical materials. A typical mesh used in the analyses is shown in Figure 6.1, where a strip footing rests on a sand mass with spatially variable friction angle and elastic modulus. The foundation depth was assumed to be 2 m below ground surface and the influence of this embedment was expressed in terms of a

- 157 -

uniform surcharge, equal to soil unit weight multiplied by the foundation depth, applied at the top of the numerical analysis mesh. Footing load was simulated as a uniform vertical stress applied at the top of the mesh, and affecting an area equal to the footing contact area, 3 m². This load was expressed in terms of normalized contact pressure (q/q_F) which was defined as the ratio between the applied footing stress, q, and its value at failure, q_F. The failure footing stress was assessed as the uniform contact pressure required to trigger general shear failure in a uniform sand mass with material properties equal to the mean values of the random variables used in the stochastic analyses. Soil was assumed to exhibit elastic perfectly plastic constitutive behavior, for simplicity, implementing Mohr-Coulomb failure criterion. The variability in soil unit weight, dilation angle and Poisson's ratio was considered to have a minor impact on the behavior of shallow foundations. As a result, these parameters were assumed constant everywhere across the analysis domain at values of 20 kN/m³, zero degrees, and 0.30, respectively. Angle of internal friction and elastic modulus were treated as spatially random variables as discussed in the previous section. Different geostatistical characteristics of these random variables were employed in the numerical model to quantify their influence on the macro behavior of the foundation soil. The depth of the soil mass, 6 m, was selected to ensure an average confining stress of 50 kPa at the center of the sand layer, so that the results of this study could be compared with the outcomes of Chapter 5.

6.7. ANALYSIS RESULTS

The main output parameter considered in this study was the average footing vertical displacement under different footing loads. The statistics of this variable were used to quantify the effect of different elements of soil spatial variability on:

1. The probability of failure of the foundation soil; and
2. The selection of a risk-based characteristic elastic modulus, which can be used in deterministic analyses while continuing to honor detailed ground variability.

Detailed discussion of the analyses results is provided in the following sections.

6.8. EFFECT OF DIFFERENT ELEMENTS OF SOIL SPATIAL VARIABILITY ON FAILURE PROBABILITY

The probability of failure was defined as the probability that footing average vertical displacements would exceed the average vertical displacement at failure. The average displacement at failure was assessed as the value associated with a deterministic analysis using mean soil parameters as the input properties, and a footing pressure enough to trigger shear failure in the foundation soil. The sensitivity of this failure probability to different geostatistical characteristics of the sand friction angle is discussed below.

The effect of probability distribution type on failure probability is shown in Figure 6.3. Beta distribution produced a relatively lower probability of failure, compared with both normal and lognormal distributions, up to a normalized footing pressure of 0.6. Beyond this threshold, beta distribution was found to produce the highest probability of failure. This could be attributed to the difference in shape between different cumulative distribution function (CDF) curves and its implications on stochastic simulation, as discussed in Chapter 5. It is worth noting that the effect of probability distribution type was more pronounced for higher values of applied footing pressure. This could be attributed to the influence of probability distribution tails on the generation of looser sand pockets and the formation of plastic zones, compared with small footing pressures where soil behavior was dominantly elastic.

The COV of the sand friction angle had a considerable influence on probability of failure, as illustrated in Figure 6.4. Higher values of COV resulted in an increased probability of failure and in a rapid variation in the probability of failure with the change in applied footing pressures. This could be attributed to the fact that increased coefficient

of variation would produce larger scatter in the simulated values of the random variables and consequently possible generation of looser pockets within the soil mass. These loose pockets would likely yield under small footing pressures resulting in a rapid increase in failure probability with the change in footing pressure.

The effect of spatial correlation structure (variogram) model on the probability of failure of the sand mass was quantified, as shown in Figure 6.5 for a value of R_h/H of 10 and COV of 0.15. These geostatistical characteristics were anticipated to produce the highest ground variability, and consequently a higher sensitivity of the stochastic analyses outcomes to variogram model. It was concluded from Figure 6.5 that both variogram models produced relatively similar values of failure probability up to a normalized footing pressure of about 0.50. Beyond this threshold, exponential variograms was found to produce slightly higher probabilities of failure.

The effect of the normalized spatial range of soil properties, R_h/H, on the probability of failure is presented in Figure 6.6. Increased values of normalized spatial range were found to be associated with higher probability of failure up to a normalized footing pressure of about 0.47. Beyond this threshold, a rapid increase in failure probability with higher applied footing pressures was observed for smaller values of normalized spatial range. This could be attributed to the fact that increasing the spatial range would result in a more gradual spatial variation of soil properties and consequently the possibility of generating continuous pockets of loose pockets, which would likely yield under small applied footing pressures. Upon reaching normalized footing pressure equal to 0.47, most of these loose pockets would have likely yielded leaving continuous pockets of relatively stiffer sand, which might have contributed to the slow increase in the failure probability with the change in footing pressure. On the other hand, implementing smaller spatial ranges, such as $R_h/H = 2$, in stochastic analysis would result in the generation of discontinuous pockets of loose sand surrounded by stiffer zones, which might result in stress transfer from the looser to the stiffer pockets. This stress transfer mechanism would likely result in a smaller yielded zones and consequently

- 160 -

smaller probability of failure under small applied footing pressures. Whereas, normalized footing pressures higher than 0.47 were likely high enough to trigger yielding in the loose soil pockets and the surrounding slightly stiffer zones resulting in a rapid increase in failure probability.

The failure probability curves were used to obtain a safe practical range for applied footing pressure, as shown in Figure 6.4, based on a desired allowable probability of failure for strip footings. In a fashion similar to Chapter 5, normalized footing pressures of 0.42 and 0.47 were assessed as upper limits for this range to fulfill a target failure probability of 1%, for coefficients of variation of 0.15 and 0.10, respectively. It is worth noting that these limits bracket the design soil resistance (ΦR_n) recommended by Becker (1996) for use in shallow foundation design according to the limit state design method. This design value was found equal to 0.455 upon the use of a resistance factor (Φ) of 0.50 and nominal resistance (R_n) equal to the failure footing pressure obtained using mean soil parameters divided by a factor of 1.1 (Becker 1996).

Revisiting Figure 6.3 to Figure 6.6 implementing the safe practical range for applied footing pressure, the following conclusions could be obtained:

1. Beta distribution produces significantly smaller failure probability than normal and lognormal distribution. The difference between the failure probabilities associated with normal and lognormal distribution is negligible; and

2. The probability of failure is insensitive to the spatial correlation structure model.

6.9. EFFECT OF SOIL SPATIAL VARIABILITY ON DIFFERENT ESTIMATES OF CHARACTERISTIC ELASTIC MODULUS OF SAND

An attempt was made in this study to obtain a risk-based characteristic elastic modulus, E, which can be used in deterministic analyses while continuing to honor detailed ground variability. The assessment of this characteristic modulus was

accomplished by determining an equivalent elastic modulus, E, of a homogenous sand mass that would reproduce the same average vertical displacement of a footing resting on a spatially variable medium, as shown in Figure 6.7. Applying this methodology to several realizations of a random soil medium below a strip footing, a histogram of normalized equivalent elastic modulus (E/E_o) was obtained, as shown in Figure 6.8. The normalized equivalent elastic modulus, E/E_o, was assessed as the ratio between the equivalent elastic modulus, E, and the mean elastic modulus, E_o, used in the stochastic analyses. As expected, increasing footing pressure resulted in a decrease in the mean value of (E/E_o) and an increase in its coefficient of variation (COV), as shown in Figure 6.8. This could be attributed to an increase in the likelihood of developing plastic zones, and consequently zero equivalent elastic modulus, in the soil mass upon the application of higher footing pressures. It is worth noting that the value of the equivalent elastic modulus was set to zero for cases where average vertical displacement exceeded the average footing displacement at failure.

In Chapter 5, different estimates for this characteristic elastic modulus were proposed based on the desired risk level. These estimates can be summarized as follows:

1. The mean normalized equivalent elastic modulus, which was regarded as a suitable estimate for low risk projects;

2. The values associated with a linear loss function, a technique to quantify making an error in estimating design parameters (Deutsch 2002). Ratios of 2.5 and 5 between the consequences of over-estimating and under-estimating design parameters were assumed in this study to be associated with medium risk and high risk projects, respectively, as discussed in Chapter 5; and

3. The values associated with the lower and upper limits of the 90% confidence level. These limits were considered as suitable estimates for extremely high risk projects where consequences of failure could be catastrophic.

The effect of different elements of soil spatial variability on the above estimates is discussed in the following sections.

6.9.1. Effect of Spatial Variability on Characteristic Elastic Modulus for Low Risk Projects

The effect of different elements of spatial variability of sand friction angle on the mean equivalent elastic modulus, as a proposed characteristic value for low risk project, was quantified, as shown in Figure 6.9 to Figure 6.12. Within the safe practical range of applied footing pressure, i.e. for normalized footing pressure smaller than 0.42, the following conclusions were obtained:

1. The coefficients of variation, spatial correlation structure (variogram) model, and the spatial range have insignificant influence on the mean equivalent elastic modulus; and

2. The most conservative estimate of the mean equivalent elastic modulus is likely to be associated with beta distribution, while the least conservative estimate is likely to be associated with normal distribution.

Referring to Figures 6.9 to 6.12, it can be reasonably assumed, for practical purposes, that estimates of mean normalized equivalent elastic modulus can be regarded constants within the safe practical limits of applied footing pressures. These estimates were found to be 0.97, 0.945, 0.92 for normal, lognormal, and beta distributions, respectively. It is worth noting that these values are smaller than unity due to possible presence of looser pockets within the soil mass. These pockets are susceptible to yielding under relatively small applied footing pressures, which can not be accounted for using classical deterministic analyses. This implies that using mean soil parameters in deterministic shallow foundation analyses may result in a design on the unsafe (non-conservative) side by a value up to 8%, which is beyond the zone of excellent prediction of geotechnical performance proposed by Morgenstern (2001).

6.9.2. Effect of Spatial Variability on Characteristic Elastic Modulus for Medium and High Risk Projects

The effect of spatial variability of sand friction angle on different risk-based estimates of characteristic elastic modulus was quantified in a fashion similar to the previous section. Within the practical limits of stress applications, i.e. for normalized deviator stresses smaller than 0.42, the following conclusions were obtained:

1. The probability distribution type has an insignificant effect of the characteristic elastic modulus estimates for medium and high risk projects. However, the effect is more pronounced for the estimates associated with the upper and lower limits of the 90% confidence level, as shown in Figure 6.13;

2. The variogram model has a minor influence on the characteristic elastic modulus estimates for medium and high risk projects as well as those associated with the upper and lower limits of the 90% confidence level, as presented Figure 6.14;

3. The coefficient of variation (COV) has a considerable impact on different estimates of risk-based characteristic elastic modulus. The impact of changing COV becomes more prominent for estimates closer to the tail of probability distribution, as the case for the upper and lower limits of the 90% confidence level, as illustrated Figure 6.15; and

4. Spatial range is likely to have a significant effect on elastic modulus estimates closer to probability distribution tail, as the case for the upper and lower limits associated with the 90% confidence level shown in Figure 6.16. As expected, such effect is smaller for COV of 0.10 compared with COV of 0.15.

Based on the results of the above analyses, design charts for different risk based estimates of the equivalent elastic modulus of sand were developed as shown in Figure 6.17. However, in the absence of enough data to reliably assess different elements of soil spatial variability, relatively conservative estimates, associated with the worst conditions in Figure 6.17, can be used in shallow foundation design. A summary of these estimates is provided in Table 6.2.

6.10. COMPARISON WITH IDEAL PLANE STRAIN CONDITIONS

The results obtained in Chapter 5 for ideal plane strain conditions were compared with those obtained in this chapter to investigate their applicability to geotechnical field problems with relatively similar stress paths. The vertical and horizontal stresses at the center of the foundation soil below the footing were considered as principal stresses. The minor principal stress was taken equal to the horizontal at rest earth pressure, while the major principal stress was assessed as the summation of the total vertical overburden pressure and the average footing stress. The average footing stress was determined using the simplified 1 horizontal to 2 vertical stress distribution method. A comparison between the results of the two chapters is provided in Figure 6.18 for normalized horizontal ranges, R_h/H, of 10 and 2, respectively. The mean normalized equivalent elastic modulus (E/E_o) were similar in both studies, while considerable differences were found between the coefficients of variation resulting in different values of other risk-based estimates of characteristic elastic modulus. These differences in the coefficients of variation could be attributed to the different boundary conditions associated with the footing problem as a result of having a horizontal confining pressure varying with depth, and a vertical load affecting a small part of the surface of the soil mass. In addition, soil elements within the Prandtl passive zone were likely to be subjected to unloading conditions rather than the uniform loading conditions affecting all soil elements in the ideal plane strain case. This different stress path may have contributed to the difference in the values of the coefficients of variation obtained from both cases.

This implies that the effect of soil spatial variability on the engineering behavior of soils is problem dependent and that each geotechnical field problem requires a separate study in order to assess such effect.

- 165 -

6.11. EFFECT OF CONFINING PRESSURE ON DIFFERENT ESTIMATES OF EQUIVALENT ELASTIC MODULUS

The results presented in the previous sections were obtained for a spatially variable foundation soil of 6 m height, where the average confining stress was 50 kPa. To investigate the sensitivity of characteristic elastic modulus estimates to change in confining stress, the above analyses were repeated for soil heights of 3 m and 9 m, where the average confining stresses were 25 kPa and 75 kPa, respectively. Confining stresses between 25 kPa and 75 kPa were considered to cover the typical range of in-situ horizontal stresses for shallow foundation problems. The ratio between the soil height, H, and the width of the strip footing was held constant at a value of 2 for all cases together with geostatistical characteristics similar to those used in previous sections. The effect of changing confining stress on the mean equivalent elastic modulus, its coefficient of variation, and probability of failure is shown in Figure 6.19. Changing confining stress was found to have a minor influence on the mean equivalent elastic modulus and the coefficient of variation, and consequently all characteristic elastic modulus estimates, up to a normalized footing pressure of 0.40. This can be attributed to the domination of elastic behavior for this stress range where soil elastic modulus was assumed constant in the used constitutive model. Beyond a normalized confining pressure of 0.40, soil spatial variability was found to have a larger impact on soil masses subjected to smaller average confining stresses. This was manifested in smaller mean equivalent elastic modulus and higher coefficient of variation, primarily the result of plastic zones development in looser pockets of sand. These zones occur more readily for lower state of stresses, where a small increase in shear stress may trigger a plastic state of stresses. Plastic zones are more difficult to develop at higher state of stresses, where a considerable shear stress is required to trigger failure. In a similar fashion, it was concluded from Figure 6.19 that spatial variability of soil properties had a significant impact on the probability of failure at smaller state of stresses.

The variation of the upper limit of the safe practical range of applied footing pressure with the change in average confining (horizontal in-situ) stress is shown in Figure 6.20, for a COV of 0.15. This upper limit was found to increase with higher average horizontal stresses. However, the rate of such increase seemed to decrease for larger values of average confining stresses. It is worth noting that for an average confining stress of 25 kPa and a COV equal to 0.15, a normalized footing pressure of 0.37 was assessed as an upper limit for the safe practical range of applied footing pressure, as shown in Figure 6.20.

This value is about 18% smaller than the design soil resistance proposed by Becker (1996) for use in limit state design of shallow foundation, as discussed earlier. This implies that depending solely on deterministic limit state design may result in inconsistent safety levels of shallow foundation depending on initial in-situ state of stresses.

6.12. CONCLUSIONS

The main purpose of this study was to quantify the effect of different elements of soil inherent spatial variability on the behavior of a shallow foundation under plane strain conditions. This was carried out through numerical simulation of a strip footing resting on spatially variable sand medium using the FLAC software. Stochastic input soil parameters, such as friction angle and elastic modulus, were generated using the GSLIB software and implemented in the numerical analysis scheme. An attempt was made to obtain a risk-based characteristic elastic modulus, which can be used in simplified deterministic analyses while continuing to honor detailed ground variability.

The effect of different elements of soil spatially variability on the failure probability of the strip footing was assessed. Footing pressures associated with a failure probability of 1% were considered as upper limits for a safe practical range of stress

application. These limits were found to be 0.42 and 0.47 for normalized horizontal spatial range of 10, and for coefficient of variations of 0.15 and 0.10, respectively. These limits are in a reasonable agreement with the design soil resistance recommended by Becker (1996) for use in shallow foundation design according to the limit state design method. Probability distribution functions and spatial correlation structure models were found to have insignificant influence on the failure probability within the safe practical ranges of stress application compared to coefficient of variation and limit of spatial correlation structure.

Different risk-based estimates for characteristic elastic modulus of sand were introduced, such as mean values, estimates associated with linear loss functions, and upper and lower limits of the 90% confidence level. Coefficient of variation and spatial range were found to have the greatest effect on these estimates. Using mean values in deterministic analyses was considered to be on the non-conservative side especially for medium and high risk projects, where there is a need to develop more reliable characteristic soil parameters. Design charts for risk-based estimates of characteristic elastic modulus of sand were provided for use in practical applications.

The results obtained in Chapter 5 for spatially variable sand media under ideal plane strain conditions were compared with those of the current study to examine their applicability to geotechnical field problems with relatively similar stress path. Considerable differences were noted especially for the coefficients of variation of equivalent elastic modulus and the associated risk-based estimates of sand characteristic elastic modulus. This implies that the effect of soil spatial variability on engineering behavior of soils is problem dependent and that each geotechnical field problem must be studied separately in order to assess such effect.

Changing in-situ state of stresses in spatially variable sand media beneath a strip footing was found to have a minor impact on different risk-based estimates of soil elastic modulus within the safe practical range of applied footing pressure. However, this range

is likely to be affected by the average state of stresses in the ground. The upper limit of the practical range of stress application is likely to increase with higher mean normal stress in the soil mass. In addition, depending solely on deterministic limit state design was found to produce inconsistent safety level of shallow foundation design depending on in-situ state of stresses.

6.13. REFERENCES

Baecher G. B., and Ingra, T. S. 1981. Stochastic FEM in settlement predictions. Journal of the Geotechnical Engineering Division, ASCE, 107 (GT4): 449-463.

Becker, D. E. 1996. Eighteenth Canadian Geotechnical Colloquium: Limit state design for foundations. Part 2. Development for the National Building Code of Canada. Canadian Geotechnical Journal, 33 (6): 984-1007.

Deutsch, C. V. 2002. Geostatistical reservoir modeling. Oxford University Press.

Deutsch, C. V. and Journel A. G. 1998. GSLIB geostatistical software library. Oxford University Press.

El-Ramly, H. 2001. Probabilistic and quantitative risk analysis for earth slopes. Ph.D. thesis, University of Alberta, Edmonton, Alberta, Canada.

Fenton, G. A., and Vanmarcke, E. H. 1991. Spatial variation in liquefaction risk assessment. Proceeding of the geotechnical Engineering Congress, Boulder, Colorado, USA. Geotechnical Special Publications, No. 27, Vol.1, pp. 594-607.

Griffiths, D.V., and Fenton, A. 1993. Seepage beneath water retaining structures founded on spatially random soil. Geotechnique, 43 (4): 577-587.

Itasca Consulting Group Inc. 2000. FLAC: fast lagrangian analysis of continua. Minneapolis, Minnesota, USA.

Lumb, P. 1966. . Safety factors and the probability distribution of soil strength. Canadian Geotechnical Journal, 3 (2): 74-97.

Lumb, P. 1970. . Safety factors and the probability distribution of soil strength. Canadian Geotechnical Journal, 7 (3): 225-242.

Paice, G. M., Griffiths, D. V., and Fenton, G. A. 1994. Influence of spatially random soil stiffness on foundation settlement. Proceeding of the Conference on Vertical and Horizontal Deformation of Foundations and Embankments, Part 1 (of 2), College Station, Texas, USA, pp. 628-639.

Phoon, K., and Kulhawy, F. H. 1999. Characterization of geotechnical variability. Canadian Geotechnical Journal, 36 (4): 612-624.

Popescu, R., Prevost, J. H., and Deodatis, G. 1996. Influence of spatial variability of soil properties on seismically induced liquefaction. Proceeding of the 1996 Conference on Uncertainty in the Geologic Environment, Uncertainty 96, Part 2 (of 2), Madison, WI, USA, pp. 1098-1112.

Popescu, R., Prevost, J. H., and Deodatis, G. 1998. Characteristic percentile of soil strength for dynamic analysis. Proceeding of the 1998 Conference on Geotechnical Earthquake Engineering and Soil Dynamics III, Part 2 (of 2), Seattle, WA, USA, pp. 1461-1471.

Resendiz, D. and Herrera, I. 1969. A probabilistic formulation of settlement control design. Proceeding of the 6th International Conference on Soil Mechanics and Foundation Engineering, Mexico City, Mexico, pp. 217-225.

Schultze, E. 1975. Some aspects concerning the application of statistics and probability to foundation structures. Proceeding of the 2nd International Conference on Applications of statistics and probability in soil and structure Engineering, Aachen, Germany, pp. 457-494.

Wu, T. H., and Kraft, L. M. 1967. The probability of foundation safety. Journal of Soil Mechanics and Foundation Division, ASCE, 93 (SM5): 213-231.

Zeitoun, D. G. and Baker, R. 1992. A stochastic approach for settlement predictions of shallow foundations. Geotechnique, 42 (4): 617-629.

Table 6.1. Description of different geostatistical characteristics applied in this study.

Case	Probability distribution type	COV	Variogram model	Normalized spatial range (R_h/H)
Case 1	Normal	0.15	Spherical	10
Case 2	Normal	0.15	Exponential	10
Case 3	Normal	0.10	Exponential	10
Case 4	Normal	0.15	Exponential	5
Case 5	Normal	0.15	Exponential	2
Case 6	Log-normal	0.15	Exponential	10
Case 7	Beta	0.15	Exponential	10
Case 8	Normal	0.10	Exponential	5
Case 9	Normal	0.10	Exponential	2

Table 6.2. Relatively conservative estimates for risk-based equivalent elastic modulus of sand under plane strain conditions in the absence of enough data to reliably assess different elements of soil spatial variability.

Estimate	Mean	Medium risk	High risk	L_{90}*	U_{90}**
COV = 0.10	0.92	0.87	0.78	0.63	1.24
COV = 0.15	0.92	0.79	0.65	0.40	1.40

*L_{90} is the lower limit of the 90% confidence level.

** U_{90} is the upper limit of the 90% confidence level.
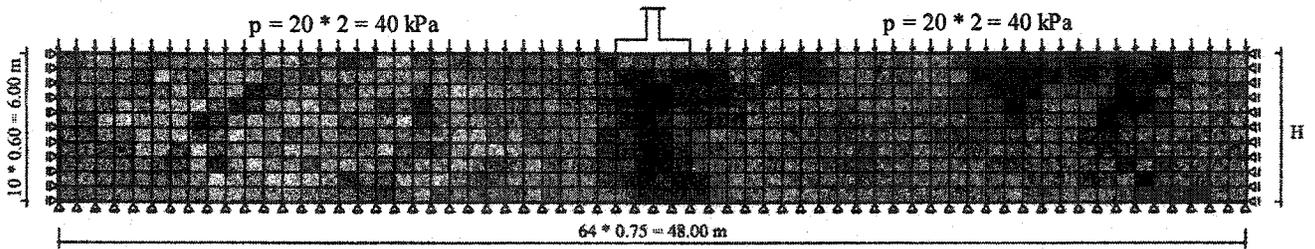
Figure 6.1. Spatial variation of sand friction angle across the numerical analysis mesh (darker zones indicate higher friction angles).
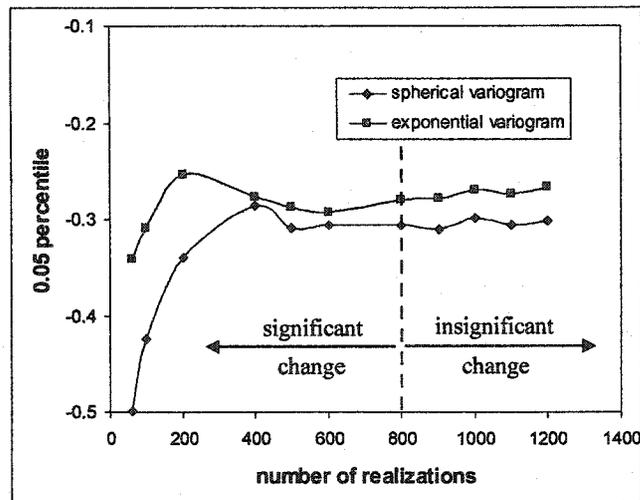
Figure 6.2. A sensitivity analysis to assess the required number of realizations for different spatial correlation structure models ($R_h/H = 10$).
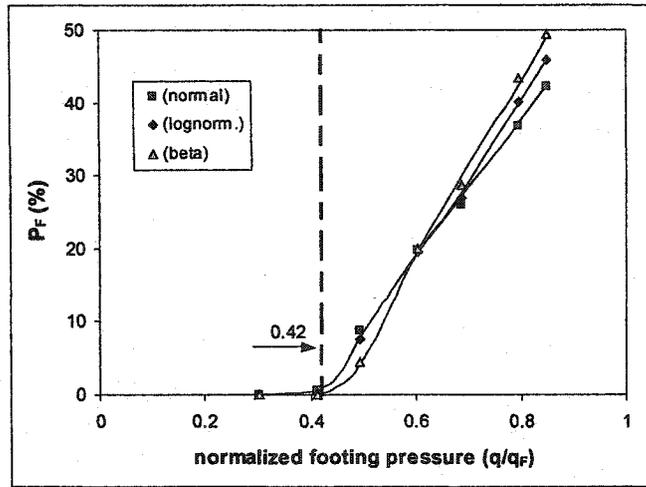
Figure 6.3. Effect of probability distribution type on the probability of failure of the sand mass. (exponential variogram model, $R_h/H = 10$, and COV = 0.15).
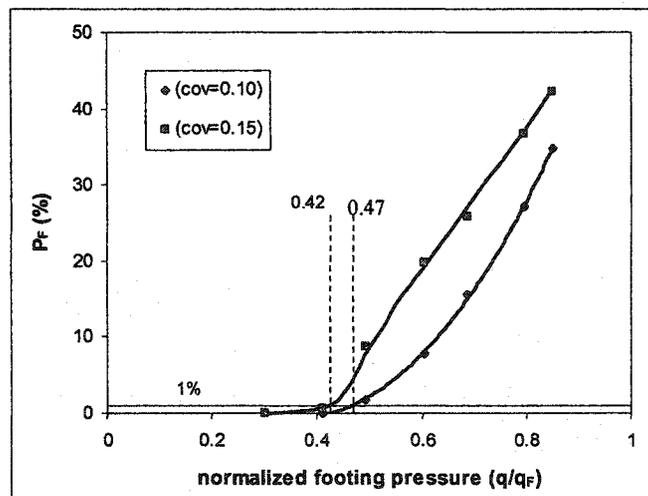
Figure 6.4. Effect of coefficient of variation (COV) of the friction angle on the probability of failure of the sand mass. (exponential variogram model, $R_h/H = 10$, and normal distribution).

- 173 -
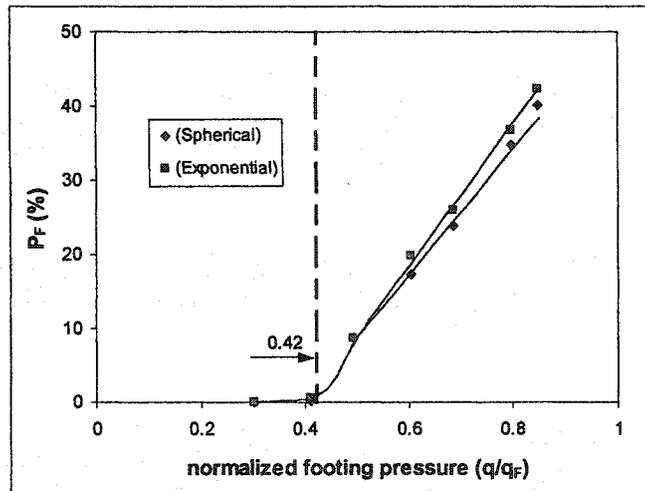
Figure 6.5. Effect of spatial correlation structure (variogram) model on the probability of failure of the sand mass. ($R_h/H = 10$, COV = 0.15, and normal distribution).
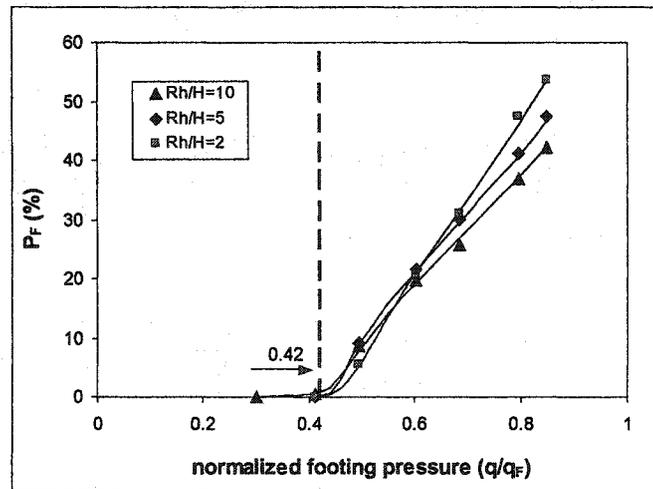
Figure 6.6. Effect of spatial range on the probability of failure of the sand mass. (exponential variogram model, COV = 0.15, and normal distribution).

- 174 -
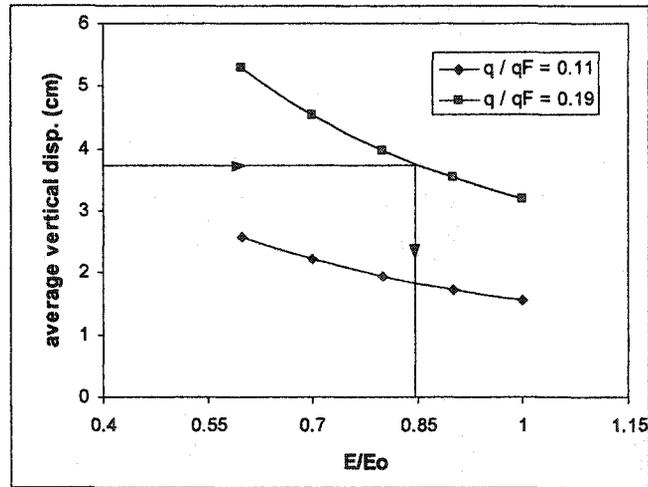
Figure 6.7. Schematic diagram showing the determination of equivalent elastic modulus.
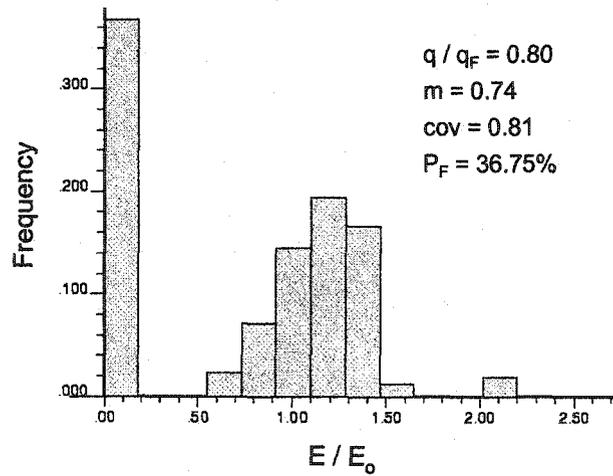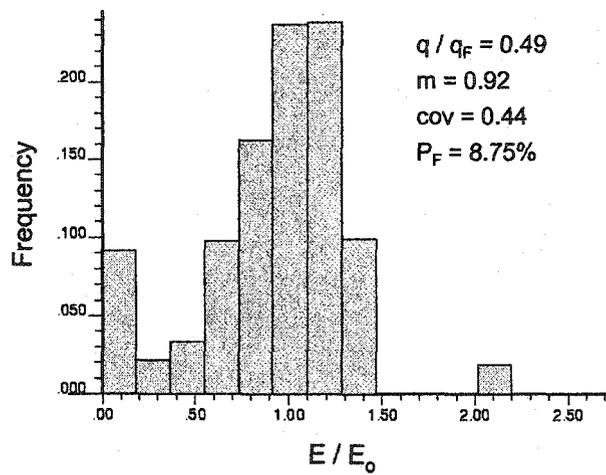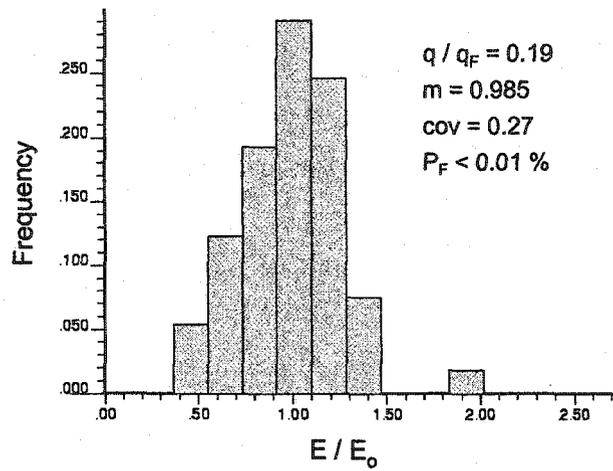
Figure 6.8. Histograms of normalized elastic modulus under different values of normalized footing pressure (q/q_F).
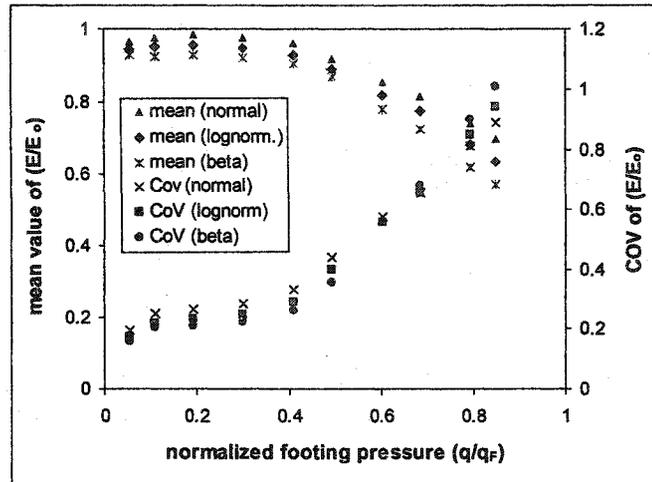
Figure 6.9. Effect of different types of probability distributions on the mean value of the equivalent elastic modulus and its coefficient of variation. (Exponential variogram model, $R_h/H = 10$, COV = 0.15).
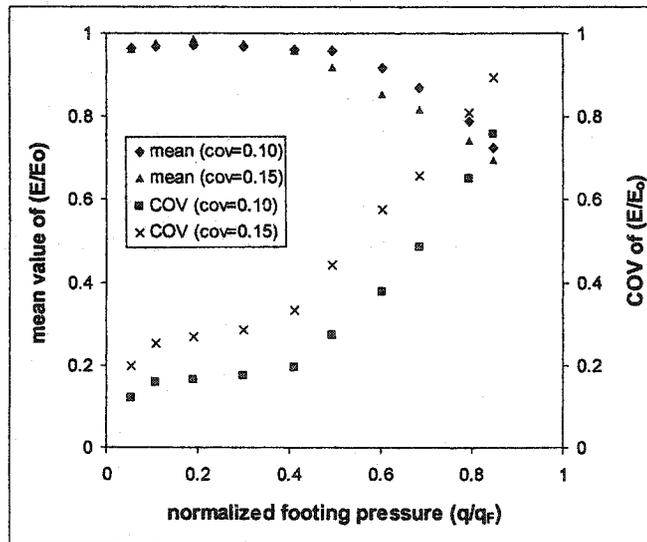
Figure 6.10. Effect of coefficient of variation of sand friction angle on the mean equivalent elastic modulus and its coefficient of variation. (Exponential variogram model, $R_h/H = 10$).

- 177 -
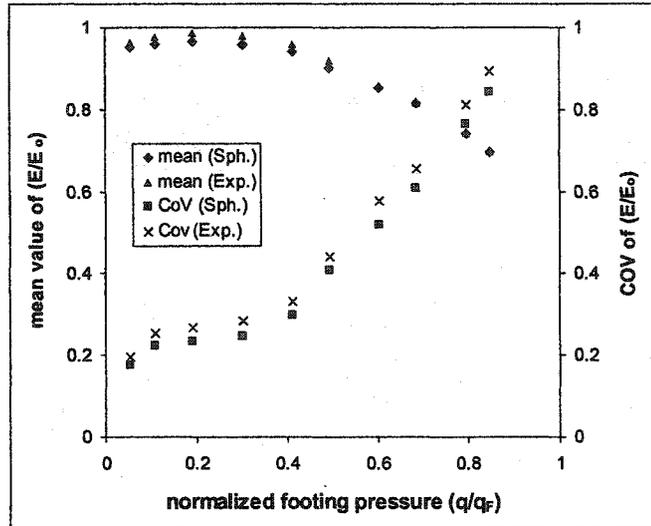
Figure 6.11. Effect of spatial correlation structure model on the mean equivalent elastic modulus and its coefficient of variation. ($R_h/H = 10$, COV = 0.15).
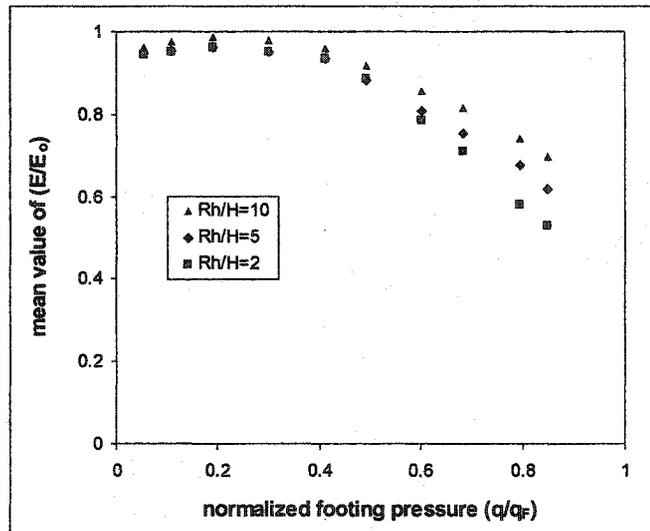
Figure 6.12. Effect of spatial range on the mean equivalent elastic modulus (COV = 0.15).

- 178 -
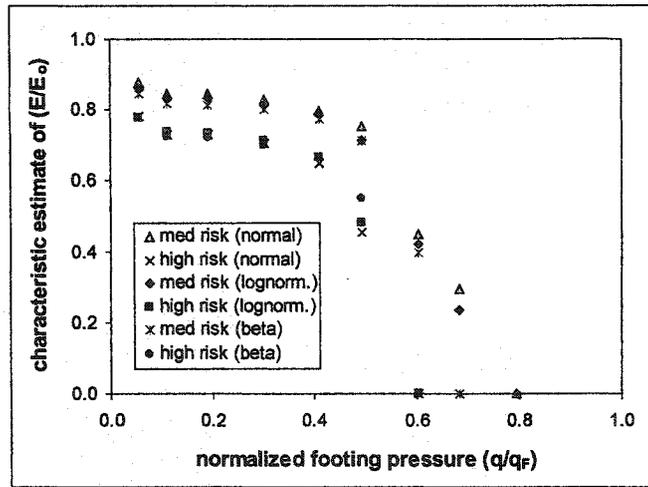
(a)
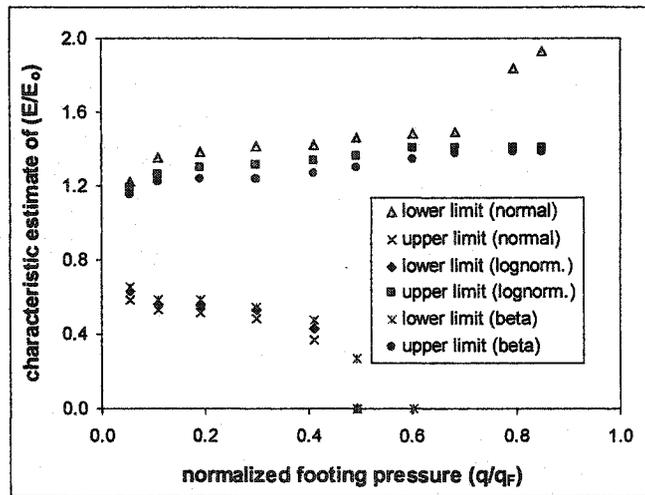
(b)

Figure 6.13. Effect of probability distribution type on different risk-based estimates of normalized characteristic elastic modulus (E/E_o). a) medium and high risk estimates based on linear loss functions; and b) estimates associated with the upper and lower limits of the 90% confidence level. (exponential variogram model, $R_h/H = 10$, COV = 0.15).

- 179 -
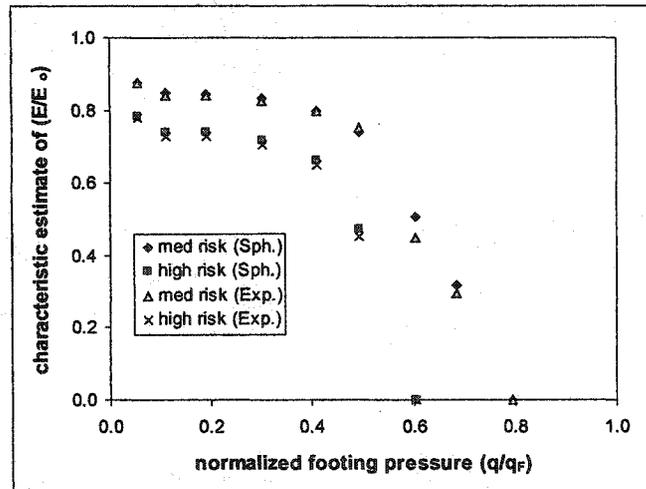
(a)
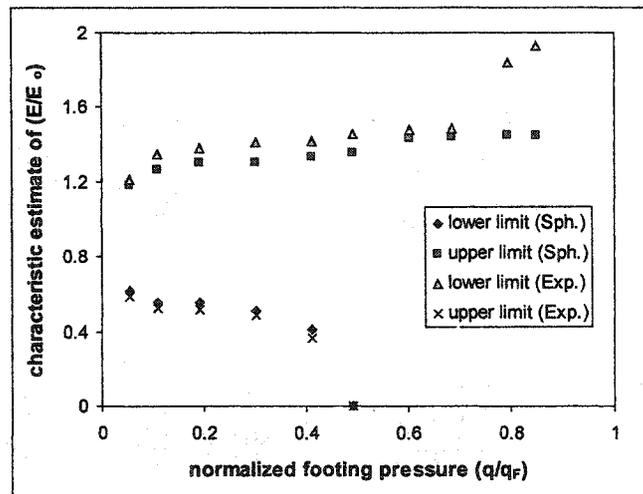
(b)

Figure 6.14. Effect of spatial correlation structure model on different risk-based estimates of normalized characteristic elastic modulus (E/E_o). a) medium and high risk estimates based on linear loss functions; and b) estimates associated with the upper and lower limits of the 90% confidence level. ($R_h/H = 10$, and COV = 0.15).

- 180 -
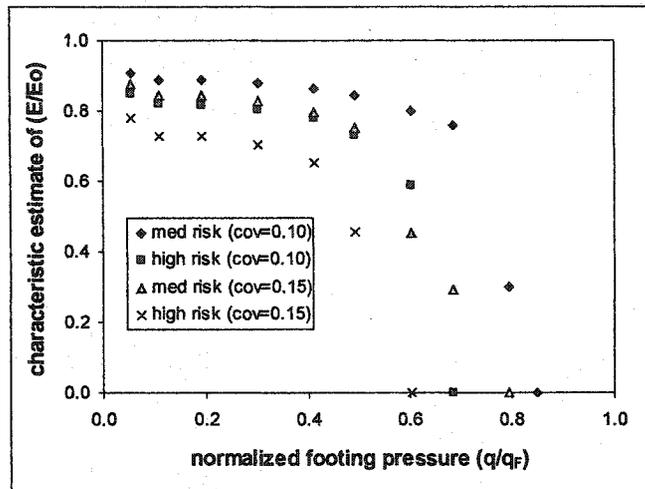
(a)
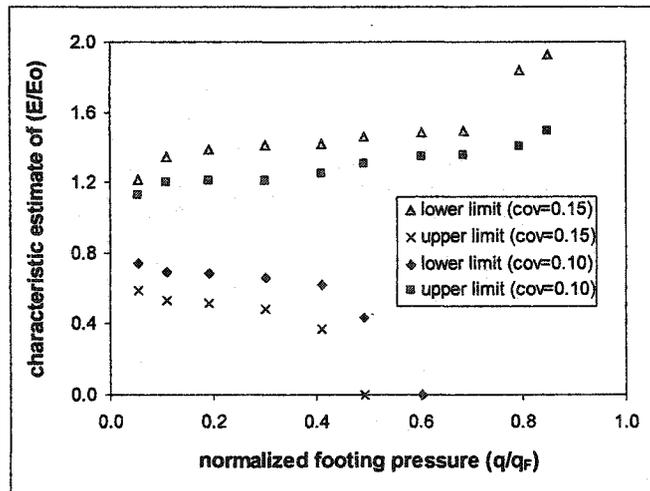
(b)

Figure 6.15. Effect of coefficient of variation (COV) on different risk-based estimates of normalized characteristic elastic modulus (E/E$_o$). a) medium and high risk estimates based on linear loss functions; and b) estimates associated with the upper and lower limits of the 90% confidence level. (R$_h$/H = 10).

- 181 -
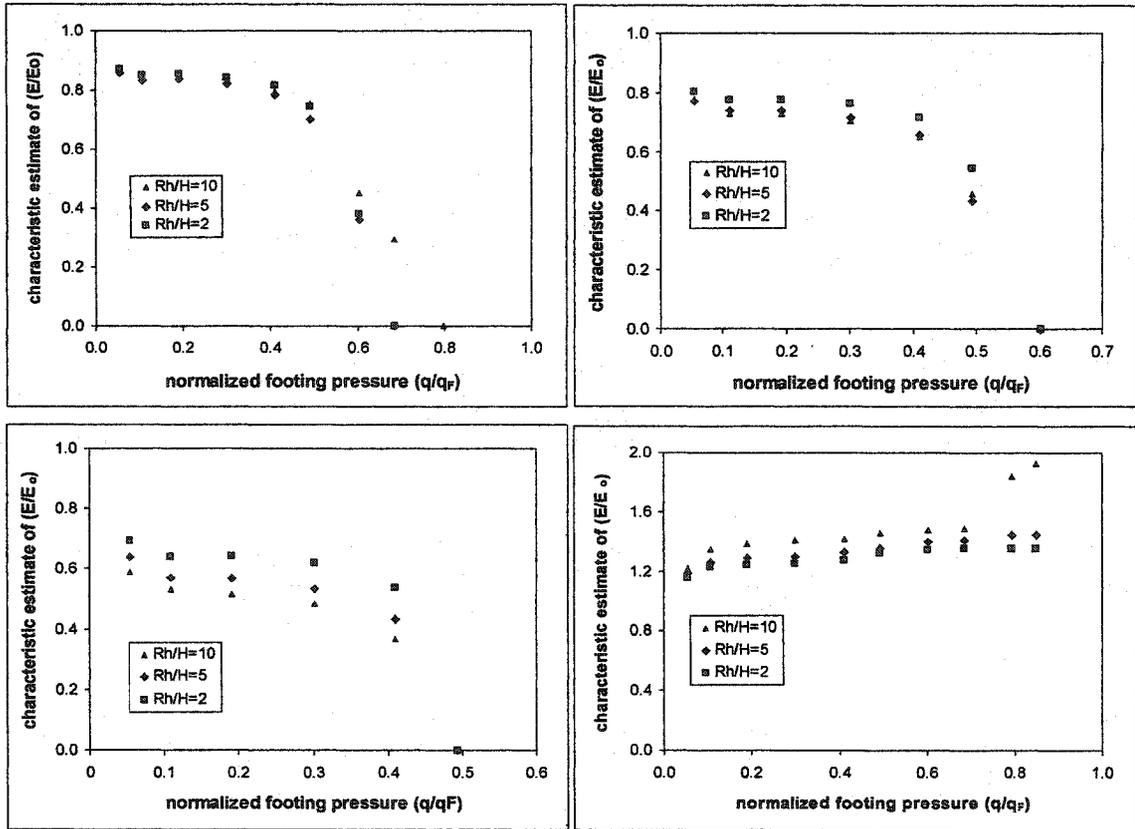
Figure 6.16. Effect of spatial range on different risk-based estimates of normalized characteristic elastic modulus (E/E_o). (COV=0.15).
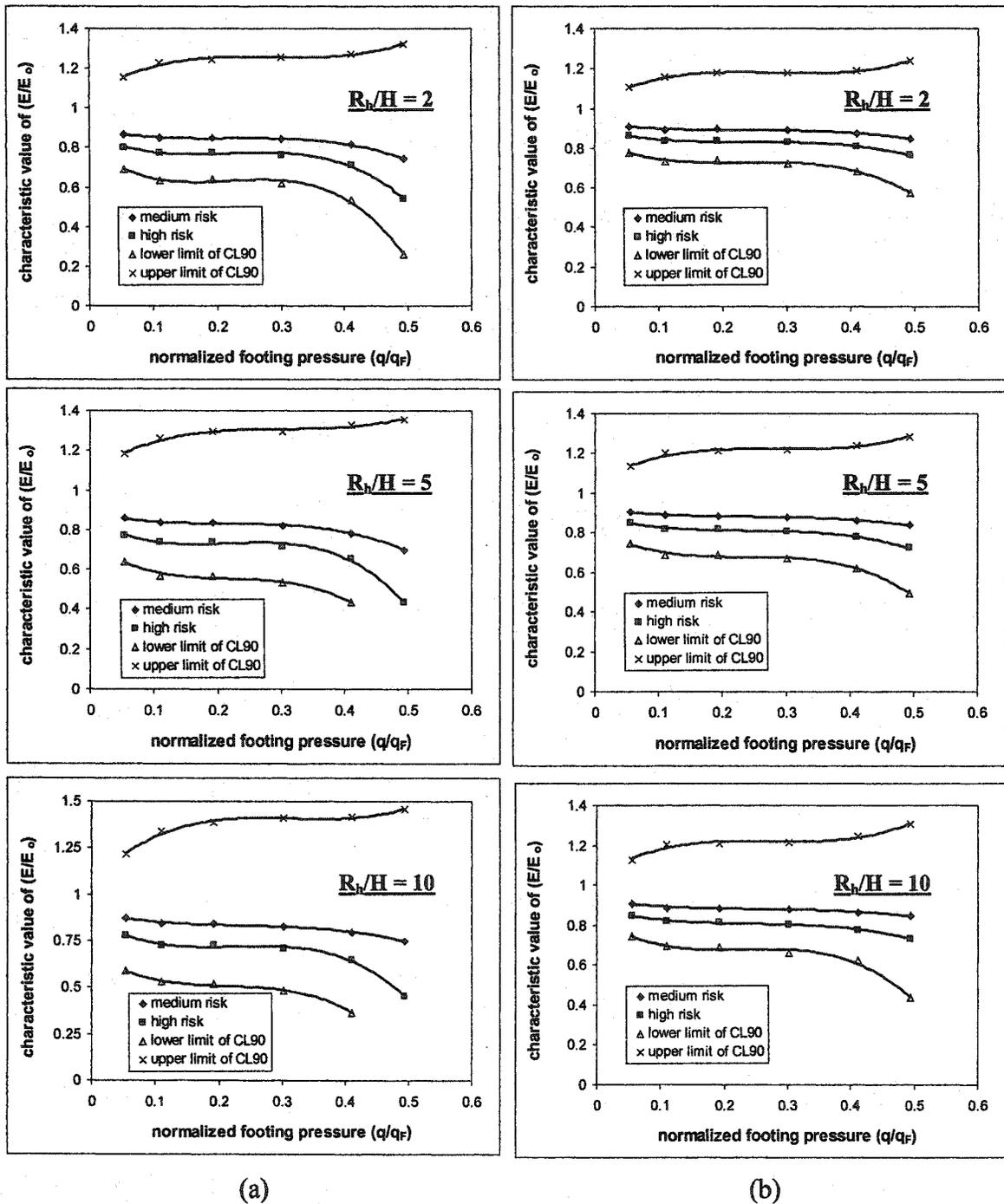
Figure 6.17. Design charts for different risk-based estimates of characteristic elastic modulus. a) COV = 0.10; b) COV = 0.15. (CL90 is the 90% confidence level)

- 183 -
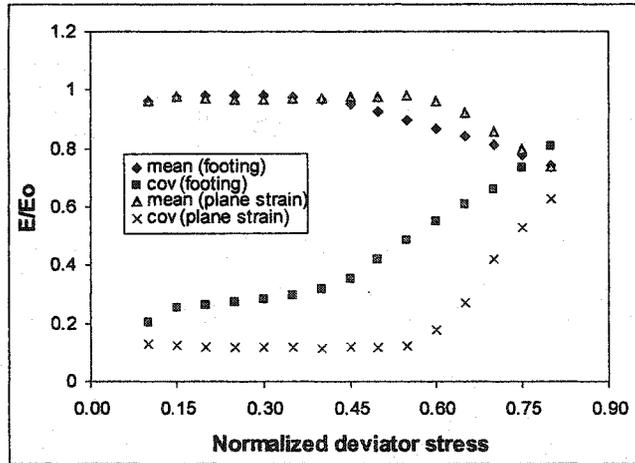
(a)
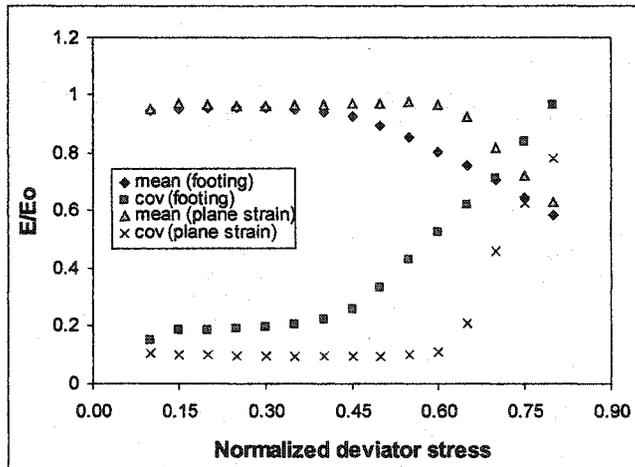
(b)

Figure 6.18. Comparison between the results of ideal plane strain conditions and the results of the current study. a) $R_h/H = 10$; and b) $R_h/H = 2$.

- 184 -
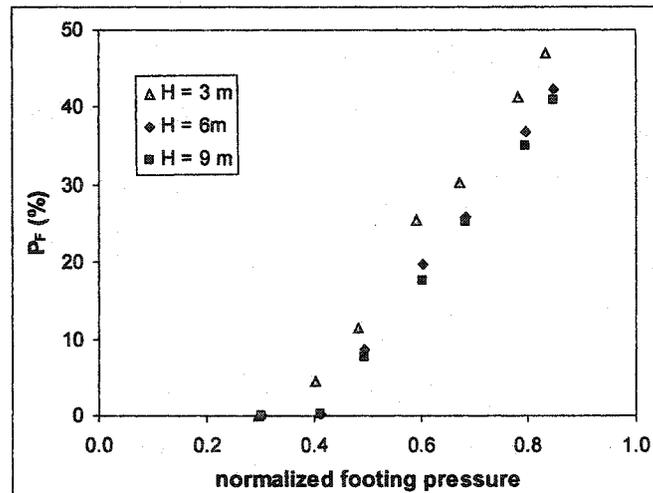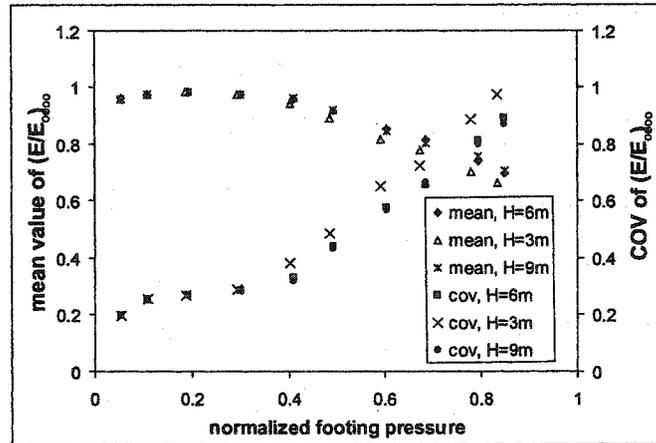
Figure 6.19. Effect of changing confining pressure on mean equivalent elastic modulus, its coefficient of variation, and probability of failure.
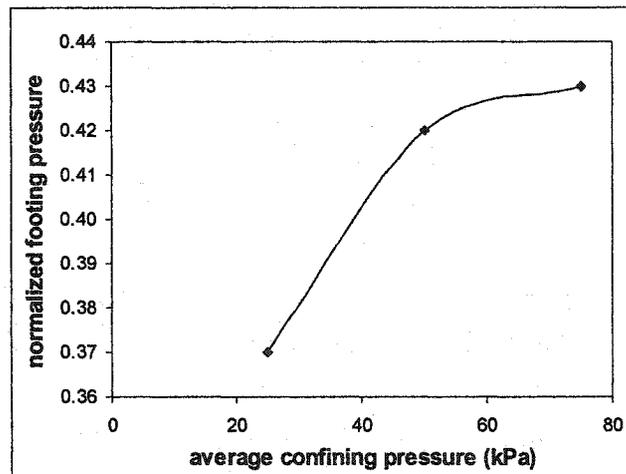
Figure 6.20. Variation of normalized footing pressure associated with the upper limit of the safe practical range of applied footing with change in average confining pressure.

CHAPTER 7

SIMPLIFIED GEOSTATISTICAL ANALYSIS OF EARTHQUAKE INDUCED GROUND RESPONSE AT THE WILDLIFE SITE

7.1 INTRODUCTION

Seismically induced liquefaction can be defined as the loss of shear strength and degradation in soil stiffness due to earthquake-induced pore pressure development, up to the value of the total geostatic stresses. Surface evidence of liquefaction can be in the form of ground settlement, lateral spread, sand boils, or extension cracks and may cause damage to overlying structures. Almost all natural soils are highly variable in their properties and are rarely homogeneous. Soil heterogeneity can be classified into two main categories. Lithological heterogeneity, which can be manifested in the form of thin soft/stiff layers embedded in a stiffer/softer media or the inclusion of pockets of different lithology within a more uniform soil mass. The second source of heterogeneity can be attributed to inherent soil variability, which is the spatial variation of soil properties from one point to another in space due to different deposition and loading history. Soil variability can have a profound effect on its behavior under earthquake loading, as discussed by Fenton and Vanmarcke (1991), and Popescu et al. (1998). Quantitative treatment of this variability with respect to liquefaction assessment is important for geotechnical design, as classical deterministic techniques can not account for the scatter of field data and their spatial correlation. Well-documented case histories offer an opportunity to explore options of quantifying the influence of soil heterogeneity on liquefaction assessment. One such case history, the Wildlife Site, Imperial valley, California, USA, provides an excellent source for such studies as it was subjected to several earthquakes throughout the late twentieth century. In addition, the site was instrumented by the US Geological Survey (USGS) and subsequently recorded a unique

set of ground responses during the 1987 Elmore Ranch and Superstition Hill earthquakes.

Several studies have been carried out to investigate the ground response at the Wildlife site during the Superstition Hill earthquake, where various evidences of liquefaction were observed across the site. One of the early attempts to analyse the pore pressure response in the ground at the site was carried out by Dobry et al. (1989). A nonlinear one-dimensional finite element program was used in the analysis and reasonable agreement was found between predicted and measured pore pressures. A limitation of the analysis was the use of a one-dimensional model, which could not capture the interaction and stress transfer between different soil columns. Baziar et al. (1992) analysed the observed lateral spread behavior, implementing Newmark's sliding block method of analysis. It was assumed that failure would occur only in the top sandy silt and silt layers and that the sliding block could only move towards the free face. The high sensitivity of predicted displacements to presumed failure mechanisms illustrated the uncertainties associated with the proposed methodology. Moreover, the assumption of a vertical free face may have dramatically influenced the predicted behavior.

Gu et al. (1994) studied the ground response at the site with emphasis on the delayed development of pore pressure recorded by the piezometers after the strong motion had seized. That delayed response was attributed to stress redistribution within the ground and the onset of static liquefaction following the period of strong ground motion. The stress redistribution was analysed using a static finite element model implementing a simplified undrained boundary surface model and hyperbolic strain softening relationship. In addition, an elastic model was adopted to simulate the ground response during the re-consolidation stage. The main shortcoming of the analysis was the assumption that soil had been brought to the collapse surface everywhere across the site by the earthquake. Moreover, the author believes that the delayed pore pressure development could be attributed to other factors, such as heterogeneous ground conditions leading to increased pore pressures within loose zones some distance from the piezometer locations.

Zeghal and Elgamal (1994) carried out a simplified analysis of the ground behavior using acceleration and pore water pressure records during the 1987 Elmore Ranch and Superstition Hill earthquakes. Shear strain was assumed constant within the top 7.5 m of the ground, while linear interpolation was used to determine the shear stress at the location of piezometer readings. The estimated shear stress and strain histories together with pore pressure measurements were used to investigate the mechanisms of non-linear hysteretic soil response and pore pressure buildup. The major drawback of the analysis was the approximation associated with the assumption of constant shear strain across the ground. As well, the linear interpolation of shear stress does not agree with the fact that a different soil type exists in the top 2.5 m of the ground.

Recently, Beaty and Byrne (1998) re-investigated the ground response at the Wildlife site using a simplified elastoplastic constitutive model. The model was implemented into a one-dimensional finite difference analysis using the FLAC software (Itasca Consulting Group 1993), where the recorded downhole motion in the North-South direction was applied at the base of the model. The analysis showed reasonable agreement between the predicted and recorded seismic response prior to liquefaction and the time of liquefaction onset was accurately forecasted. Predicted post-liquefaction behavior, however, was found to be substantially different from field records.

To the author's knowledge, the only attempt to incorporate spatial variability of soil properties at the site in a probabilistic analysis framework was the pioneer study by Fenton and Vanmarcke (1991). Stochastic modeling of soil properties, such as permeability, porosity, modulus of elasticity, Poisson's ratio and friction angle, was carried out using Monte Carlo simulation techniques. Different realizations of soil properties were implemented in one-dimensional finite element analyses with earthquake excitation applied at the base of the model. The effect of the limit of spatial correlation between soil properties on ground response was discussed together with the influence of connectivity of liquefied zones. In addition, a critical threshold of the area ratio of potentially liquefiable zones was suggested to be associated with high risk of liquefaction

occurrence. A limitation of the study was the assumption of a homogeneous soil profile. As well, the influence of the spatial correlation structure model on ground response was not accounted for.

In this chapter, a simplified geostatistical approach was adopted to assess the effect of lithological heterogeneity and spatial variability of soil properties on earthquake-induced ground response at the Wildlife site. Cone penetration test (CPT) results, applying the soil behavior type index (I_c), were used to identify different lithologies, for which statistical properties and spatial correlation characteristics were estimated. The Cyclic Stress Ratio – Cyclic Resistance Ratio (CSR-CRR) approach (Robertson and Wride 1998) was employed stochastically to estimate the liquefaction susceptibility of the ground. This was accomplished by implementing Monte Carlo simulation techniques to obtain several realizations of CPT data across the wildlife site. On the other hand, the earthquake loading was assessed deterministically using simplified techniques that correlated the CSR to earthquake magnitude and maximum surface acceleration. It should be noted that earthquake loading could be treated as a random variable, yet it was estimated in a deterministic fashion in this chapter as the Wildlife site has experienced several earthquakes with known magnitude and surface accelerations. In addition, different procedures were used to assess the level of liquefaction damage, such as total damage potential and settlement criterion. A primary focus of these assessments was to ascertain whether methods could be developed for estimating representative soil parameters that can be used in simplified deterministic liquefaction analyses, while continuing to honor the detailed ground heterogeneity.

7.2 BACKGROUND ON THE WILDLIFE SITE

The Wildlife site is located on the west side of the Alamo River, Imperial valley, California, USA. Several earthquakes, of magnitude ranging from 5 to 7, have shaken the site during the twentieth century, as shown in Table 7.1. The site showed signs of

liquefaction during the 1950 and 1981 Westmoreland earthquakes, and as a result was investigated and instrumented by the USGS to record ground response during future earthquakes, as shown in Figure 7.1. The geology at the site was described by Bennett et al. (1984) based on the results of several laboratory and field tests. The top 12 meters consist of a surface layer of interbedded sandy silt, silt and clayey silt to a depth of 2.50 m; followed by a loose sandy silt to silty sand up to a depth of 6.80 m; underlain by medium to stiff clayey silt to silty clay. The ground water table was found to be at depth of 1.20 meters below ground surface. Site instrumentation, as described by O'Rourke and Hamada (1992), consisted of two accelerometers, one at the ground surface and the other at a depth of 7.50 m. In addition, six piezometers were installed to monitor pore pressure response together with an inclinometer and several survey points to capture expected lateral spread. The ground responses during the 1987 Superstition Hill and Elmore Ranch earthquakes were captured by the field instrumentation. These records showed an increase in pore water pressure up to the value of the total geostatic pressure in response to the Superstition Hill earthquake. In addition, a maximum of 232 mm lateral spread of the ground, obtained from survey points, was measured together with development of surface cracks and sand boils, as shown in Figure 7.2.

7.3 CHARACTERIZATION OF GROUND HETEROGENEITY

Characterization of ground heterogeneity at the wildlife site was carried out through three main stages:
1. Standardization and filtration of CPT data;
2. Quantification of geostatistical characteristics of standardized CPT data; and
3. Stochastic simulation of the standardized data.

Details of these stages are discussed in the following sections.

7.3.1. Standardizing Cone Penetration Test Data

The results from 11 cone penetration tests were used to characterize both the lithological and inherent property variability at the Wildlife site. The CPT data were used to identify different ground lithologies using the soil behavior type index, I_c, (Robertson 1990), which was obtained through the relation:

$$I_c = \sqrt{(3.47-Q)^2 + (\log F + 1.22)^2} \tag{7-1}$$

where: Q and F are the normalized CPT tip resistance and sleeve friction, respectively, which can be determined through:

$$Q = \frac{q_c - \sigma_v}{\sigma_v'} \text{ and } F = \frac{f_s}{q_c - \sigma_v};$$

q_c is CPT tip resistance;

f_s is CPT sleeve friction resistance; and

σ_v and σ_v' are the total and effective vertical overburden pressure at the location of CPT reading, respectively.

The soil behavior type index, I_c, can be used to classify soils according to their behavior type, as shown in Table 7.2. By applying this concept to different CPT data recorded at the Wildlife site, a detailed East-West longitudinal ground profile was obtained, as shown in Figure 7.3. Four cohesionless soil layers below ground water table (GWT), L_1, L_2, L_3 and L_4, were identified from the calculated values of I_c, and implementing the soil classification system presented in Table 7.2. These layers, denoted by soil behavior types 5 and 6, were regarded as potentially liquefiable zones. Each of these layers was considered as a statistically homogeneous domain, where cone tip resistance, q_c, was treated as a random variable. It should be noted that zones associated with $I_c > 2.6$, denoted by soil behavior type 2-4 in Figure 7.3, were assumed to be non-liquefiable layers (Robertson and Wride 1998).

Data filtration is an important process to maintain statistical consistency within CPT data as it is possible that the soil being tested includes anomalies in the form of very thin lenses of clay or sand, or pockets of gravel (Campanella et al. 1987). In this study, the filtration process was carried out by excluding such inhomogeneities, which were manifested in the form of spikes in CPT data at certain depths, following the procedure proposed by Harder and Van Bloh (1988). Each soil layer was divided into sublayers of 0.30 m thickness, for which the mean and variance, m and σ^2, of cone tip resistance data were determined. Outliers were identified as values of q_c that lie outside a range of $m \pm 2\sigma$; and were excluded from the data set for each of the potentially liquefiable layers. In addition, upper and lower limits of $m \pm \sigma$ were proposed for the remaining data so that cone tip resistance can not be greater than $m + \sigma$ or smaller than $m - \sigma$.

A necessary condition for the variogram modeling technique used in this study, as outlined in the next section, is stationarity, which implies that statistical properties of random variables, such as mean and variance, do not depend on location in space. It can be expected, however, that CPT data will exhibit vertical trends due to their sensitivity to changes in effective confining pressure. In order to use cone tip resistance, q_c, as a random variable and meet the stationarity condition, any possible vertical trend in q_c should be removed (detrended). To achieve this, filtered data from all CPT soundings were utilized to identify deterministic linear vertical trends in q_c within each of the four potentially liquefiable layers using regression analysis. Then, these trends were removed, as illustrated in Figure 7.4, producing the detrended data for each of these layers through the relation:

$$q = q_c - q_o(z) \tag{7-2}$$

where q is the detrended cone tip resistance and $q_o(z)$ is a deterministic vertical trend.

It should be realized that the linear variation of vertical trends with depth is a simplifying assumption for practical application as such variation can take other forms especially for sandy soils. This assumption, however, has been used in several geostatistical studies in geotechnical engineering literature, such as Campanella et al. (1987) and Popescu et al. (1998). In addition, the uncertainty associated with the assessment of these vertical trends may have a significant influence on the site response under earthquake loading. However, this uncertainty decreases with increasing field data, as the case for CPT data, and quantifying its effect is beyond the scope of this study and needs to be considered in future stochastic liquefaction studies.

7.3.2. Geostatistical Characteristics of Detrended CPT Data

To proceed with stochastic analyses, geostatistical characteristics of different random variables, such as mean, variance, probability distribution and correlation structure, must be determined. A summary of the geostatistical characteristics of detrended cone data for layers L_1 to L_4 is presented in Table 7.3. The mean values were found to be around zero, as expected, whereas the standard deviations ranged from 849 kPa to 1570 kPa. The probability distributions were in close agreement with normal distributions as concluded from the Q-Q plots (Deutsch 2002), as shown in Figure 7.5. These Q-Q plots are comparisons between quantiles, which correspond to certain percentiles of the random variable, obtained from probability distributions of field data and those of a reference distribution, such as the normal distribution in this case study. If the cross plot between the two sets of quantiles results in points close to a 45 degree line, this indicates a similar shape and variance of both distributions.

Soil properties do not usually vary randomly in space; rather such variation is gradual and follows a pattern that can be quantified using what is called spatial correlation structure. This structure can be expressed in terms of the variogram or the covariance function. The variogram is a measure of dis-similarity between two points in space separated by a distance h, whereas the covariance is a measure of similarity

- 194 -

between these points. In this chapter, variogram functions were adopted as measures of quantifying spatial correlation between detrended CPT data, and were determined through the relation:

$$2\gamma(h) = Var[Z(u+h) - Z(u)]$$ (7-3)

where: $2\gamma(h)$ is the variogram value at a separation distance h;

Z (u) is the value of the random variable, q, at location u;

Z (u+h) is the value of the random variable, q, at distance h from Z (u); and

Var [] is the variance operator.

Variograms are usually characterized by their model types and spatial ranges (Deutsch 2002). The variogram model is a parametric relationship used to curvefit the experimental variograms obtained from analysis of field data. Examples of these variogram models, such as spherical, exponential and Gaussian models, are shown in Figure 2.6 in Chapter 2. These models help determine the variogram at any separation distance and in different directions. In addition, they can incorporate other geological information such as direction of maximum continuity and maintain numerical stability of stochastic simulation (Deutsch 2002). Variogram range is a measure of the limit of spatial continuity of soil properties and can be defined as the separation distance at which the variogram reaches the sill (variance).

The GSLIB Geostatistical Software Library (Deutsch and Journel 1998) was used to obtain the variogram characteristics in both vertical and horizontal directions for each of the four layers, L_1 to L_4, as shown in Table 7.3. This was carried out by using the GSLIB software to assess the value of the normal score variogram at several separation distances, as shown in Figure 7.6 for detrended CPT data in the vertical direction. The normal score variogram is the variogram obtained from transforming detrended CPT data into a reference standard normal distribution of zero mean and unit variance (Deutsch and Journel 1998). Then, an iteration process was followed to obtain a theoretical variogram

model that curvefit the variogram of transformed field data together with its spatial range, as shown in Figure 7.6. It should be noted that variogram characteristics obtained from analysis of CPT data are, generally, sensitive to deposition conditions, loading history and variation in fine content. This can explain the variation in variogram characteristics from one layer to another, as seen in Figure 7.6.

One limiting boundary condition required to use GSLIB to obtain variogram characteristics is that each of the potentially liquefiable layers has to be rectangular in shape, as it is an extremely complicated process to obtain variogram characteristics using non-orthogonal coordinates system. Consequently, a coordinate transformation process was carried out for each potentially liquefiable layer, as shown in Figure 7.7, following the procedure of Deutsch (2002). Another objective of this transformation process was to retain spatial continuity between field data, as non-transformed section may result in under-estimated variogram ranges in the horizontal direction. This can be explained from Figure 7.7 where variogram value can not be assessed at a separation distance equal to AB^*, as points A and B^* exist in 2 different layers, which implies that the variogram range can not be greater than the separation distance AC. On the other hand, variogram values can be assessed at any separation distance in the horizontal direction in the transformed section, as seen in Figure 7.7. It should be realized, however, that this transformation process might result in some inherent uncertainty in variogram characteristics and consequently affects the results of stochastic liquefaction analyses. Quantification of this uncertainty is beyond the scope of this simplified study.

For the Wildlife site, insufficient data was available to reliably assess the horizontal anisotropy in variograms characteristics for different layers. As a result, it was assumed that the variograms would exhibit isotropic behavior in the horizontal direction, i.e. variogram characteristics did not depend on the azimuth in the horizontal direction. Furthermore, it was assumed that the horizontal variogram had the same model type as the vertical one, but with a larger range, as suggested by Deutsch (2002).

7.3.3. Stochastic Simulation Of Detrended CPT Data

To quantify the effect of soil spatial variability on liquefaction susceptibility, several realizations of the detrended CPT data were obtained for each of the potentially liquefiable layers, L_1 through L_4. This was carried out implementing Monte Carlo simulation using the @Risk software (Palisade Corporation 1996), where each outcome of the simulation process was regarded as a representative (average) value of cone tip resistance for the layer under consideration. The number of realizations, about 10000, was obtained through specifying an acceptable tolerance, around 0.50%, between the input distribution and the distribution of the sampled values of the detrended data obtained from the @Risk software.

It should be emphasized that the variance used in Monte Carlo simulation, for each of the four layers, was not the point variance shown in Table 7.3. Rather, it was the variance of the spatial average of CPT data over selected averaging volumes. These spatial averages typically have a narrower probability distribution function than point statistics (Vanmarcke 1977) and consequently a smaller variance, as shown in Figure 7.8. The variance of these spatial averages can be correlated to the point (field) variance using a variance reduction factor (Vanmarcke 1984) through the following relationship:

$$\sigma_\Gamma = \Gamma_v \times \sigma \qquad\qquad (7\text{-}4)$$

where: σ is the standard deviation of field data (square root of point variance);

σ_Γ is the standard deviation of the spatial average of data over volume v; and

Γ_v is the square root of the variance reduction factor.

The variance reduction factor depends on the averaging volume, type of correlation structure, and the limit of spatial correlation between field data. Several analytical expressions for the variance reduction factor have been developed in geotechnical engineering literature. A summary of these expressions is provided in

- 197 -

Equations 2-8 and 2-10 in Chapter 2. It should be noted that the lateral extent of a liquefied zones required to cause damage to overlying structures is usually small compared to the spatial range of horizontal variograms. For example, a sand boil of 1 m diameter may cause a significant damage to overlying structure. Averaging CPT data over this small volume, compared with horizontal spatial range, which is typically in the range of tens of meters, will result in a variance reduction factor very close to 1 and consequently has a negligible influence on the outcome of Monte Carlo simulation. As a result, it was assumed that the variance reduction factor would be affected only by the size of the averaging volume in vertical direction, i.e. layer thickness. It is worth noting that the thickness of the four potentially liquefiable layers, L_1 to L_4 were not uniform across the site. As a result, an average thickness for each layer was obtained by dividing the volume contained between the upper and lower boundaries by the area covered by the layer. These average thicknesses were used to develop the variance reduction factors shown in Table 7.4.

The average thickness of layers L_1 and L_4 were divided into 3 and 2 horizontal sublayers, respectively, to avoid having high variance reduction factors, which might affect the shape of the scaled probability distribution of CPT data, of standard deviation equal to σ_Γ, as discussed by Deutsch (2002). It is worth noting that a minimum value of 0.70 for the variance reduction factor was recommended by Deutsch (2002) for use in stochastic analyses. Comparing this minimum value with the values used in this chapter, resulted in differences of about 5%, which was considered insignificant by the author. However, the author believes that there is a need to quantify the effect of selecting a specific averaging volume on the outcome of geostatistical liquefaction analysis in any future study. In addition, the average thickness of layer L_3 was larger than the spatial range, a, of its spherical variogram, where the variance reduction factor developed in Chapter 2 can not be applied. As a result, this layer, in turn, was divided into two sublayers. It should be emphasized that the outcomes of applying Monte Carlo simulation to different sublayers of any potentially liquefiable layer were not independent due to the vertical correlation between field data in these sublayers. The effect of such correlation

- 198 -

was accounted for through implementing a correlation coefficient into the Monte Carlo simulation algorithm in the @Risk Software (Palisade Corporation 1996). As a result, the values of cone tip resistance sampled in every realization, for different sublayers, preserved the value of the correlation coefficient. This value was taken equal to the correlation coefficient between the spatial averages of CPT tip resistance data over a vertical distance equal to the thickness of each sublayer, as proposed by Vanmarcke (1984) and illustrated in Equation 2-11 in Chapter2.

7.4   STOCHASTIC ANALYSIS OF LIQUEFACTION SUSCEPTIBILITY

Stochastic analyses of liquefaction susceptibility of the ground at the Wildlife site were performed by applying different realizations of re-trended cone tip resistance data into a deterministic empirical approach. The re-trended data were obtained by adding back the deterministic vertical trends to different realizations of the de-trended CPT tip resistance data obtained from Monte Carlo simulations. The CPT-based empirical approach of Robertson and Wride (1998) was used in the analysis, where the factor of safety against liquefaction could be obtained through:

$$F.S = \frac{CRR}{CSR} \qquad (7\text{-}5)$$

where: CRR and CSR are the cyclic resistance ratio and the cyclic stress ratio, respectively.

The cyclic stress ratio (CSR), the average normalized cyclic shear stress developed in the ground during the earthquake, was determined using the simplified approach of Seed and Idriss (1971) that relates CSR to earthquake magnitude and maximum surface acceleration through:

$$CSR = \frac{\tau_{av}}{\sigma_v'} = 0.65 \cdot \left(\frac{a_{max}}{g}\right) \cdot \left(\frac{\sigma_v}{\sigma_v'}\right) \cdot r_d \qquad (7\text{-}6)$$

where: a_{max} is the maximum acceleration at the ground surface;

g is the acceleration of gravity;

r_d is a stress reduction factor that depends on embedment depth; and

σ_v and σ_v' are total and effective vertical overburden pressures, respectively.

The cyclic resistance ratio (CRR) could be regarded as the average normalized shear stress required to cause cyclic liquefaction in the ground, and was determined as proposed by Seed and Idriss (1971):

$$CRR = \frac{\tau_{cr}}{\sigma_v'} = (CRR)_{7.5} \cdot MSF \qquad (7\text{-}7)$$

where: $(CRR)_{7.5}$ is the cyclic resistance ratio for an earthquake of magnitude 7.5 and MSF is the magnitude scaling factor.

The cyclic resistance ratio of clean sand for an earthquake of magnitude 7.5 was determined using the empirical correlation proposed by Robertson and Wride (1998):

$$(CRR)_{7.5} = 0.833 \cdot \left(\frac{(q_{c1N})_{cs}}{1000}\right) + 0.05 \qquad , (q_{c1N})_{cs} \leq 50 \qquad (7\text{-}8\text{-}a)$$

$$(CRR)_{7.5} = 93 \cdot \left(\frac{(q_{c1N})_{cs}}{1000}\right)^3 + 0.08 \qquad , 50 \leq (q_{c1N})_{cs} \leq 160 \qquad (7\text{-}8\text{-}b)$$

The term $(q_{c1N})_{cs}$ is the equivalent clean sand normalized cone tip resistance that accounts for the effect of grain characteristics, such as the presence of fines, which

- 200 -

might result in higher liquefaction resistance due to development of minor cohesion. This equivalent resistance can be assessed through:

$$(q_{c1N})_{cs} = K_c \cdot q_{c1N} \qquad (7\text{-}9)$$

where: K_c is a correction factor that depends on grain characteristics and q_{c1N} is the normalized cone tip resistance.

K_c and q_{c1N} were determined using the following relationships proposed by Robertson and Wride (1998):

$$K_c = -0.403\, I_c^4 + 5.581\, I_c^3 - 21.63\, I_c^2 + 33.75\, I_c - 17.88 \qquad (7\text{-}10)$$

$$q_{c1N} = \frac{q_c}{\sigma_v'} \cdot \sqrt{\frac{\sigma_v'}{P_a}} \qquad (7\text{-}11)$$

where: I_c is the soil behavior type index, as presented in Equation 7-1; and

P_a is the atmospheric pressure.

Several studies have been carried out to assess reasonable values for earthquake magnitude scaling factors (Seed and Idriss 1971, Ambrayses 1988, and Idriss 1995). Following the recommendation of the NCEER 1996 (Youd et al. 2001), Idriss's modified scaling factor was adopted in this study in the form of:

$$MSF = \frac{10^{2.24}}{M^{2.56}} \qquad (7\text{-}12)$$

where: M is the Richter magnitude of the earthquake.

- 201 -

The above relations were used to assess the ground response during the 1987 Superstition Hill earthquake, M = 6.6, where the maximum surface acceleration recorded was approximately 0.21g. Stochastic assessment of the factor of safety against liquefaction was carried out for each of the four layers using 10,000 realizations of re-trended CPT data. The results of these analyses, as shown in Figure 7.9, indicated that the mean factors of safety for layers L_1 to L_4 were 0.75, 1.18, 1.12, and 1.56, respectively. The coefficients of variation were assessed to be 0.14, 0.29, 0.26, and 0.20. Whereas, the probabilities of failure (factor of safety less than unity), P_F, were found to be 98.8, 32.9, 37.5 and 3.2%, respectively.

Similar analyses were conducted for other earthquakes, which had occurred at the site, such as the 1987 Elmore Ranch (M=6.2, a_{max}=0.13g); the 1981 Westmorland (M=5.6, a_{max}=0.22g); and the 1979 earthquake (M=6.6, a_{max}=0.115g). It should be noted that the maximum surface accelerations for both the 1981 and 1979 earthquakes were not recorded at the site. These surface accelerations were estimated through empirical relations that correlated maximum ground acceleration to earthquake magnitude and epicentral distances (Krinitzsky et al. 1988). A summary of the analysis results for these earthquakes is shown in Table 7.5.

Liquefaction occurred during the 1981 Westmoreland earthquake, in spite of the fact that the mean factors of safety for all layers at the site were larger than one. This implies that the use of mean values in a liquefaction analysis could be on the unsafe (non-conservative) side as a result of ignoring the scatter in field data and the spatial correlation between soil properties. Consequently, more meaningful representative values have to be identified to assess liquefaction susceptibility. Moreover, it is worth noting that liquefaction occurred at a failure probability of 37.7% for the shallowest layer compared to significantly smaller values, less than 8%, for deeper layers. This emphasizes the importance of embedment depth of liquefiable layers on liquefaction occurrence and suggests that depending on the factor of safety solely may not be an accurate measure of liquefaction potential. Conversely, liquefaction did not occur during

- 202 -

the 1979 Earthquake where the probability of failure of the shallowest layer was 2.5%. This implied that a critical probability of failure, ranging between 2.5 and 37.7%, could be identified for shallow layers above which liquefaction is likely to occur in sites of similar subsurface conditions. Studying additional case histories can help narrow the wide range of this critical threshold.

To account for the thickness and embedment depth of potentially liquefiable layers and their implications on liquefaction potential, an estimate of equivalent (representative) probability of failure was developed in this study in the form of:

$$P = \sum_{i=1}^{n} P_{Fi} \cdot \frac{T_i / Z_i}{\sum T_i / Z_i}$$
(7-13)

where: P is the equivalent failure probability of the site;

P_{Fi} and is the probability of failure of layer i;

T_i and is the average thickness of layer i; and

Z_i is the vertical distance from ground surface to the center of layer i.

The above equation was used to estimate the equivalent failure probability under the effect of the Superstition Hill, Elmore Ranch, Westmoreland, and 1979 earthquakes, and was found to be 49, 1.2, 15.36, and 1.17%, respectively. This implied that an equivalent failure probability range of 1.2% to 15% could be identified as a critical threshold above which liquefaction would likely to occur. This relatively wide range can be verified and refined through the analysis of more case histories.

It is worth noting that the empirical formulae used in this section involve some degree of inherent uncertainty. This is more significant for the CRR formula, where various degrees of engineering judgment were implemented in the assessment of different points used to develop the CRR formula (Equations 7-8). Quantifying such uncertainty was considered as a very complicated process beyond the scope of the current study.

7.5 DAMAGE CRITERIA OF LIQUEFACTION

A major concern in liquefaction analysis is the impact of liquefaction occurrence in subsurface layers on overlying structures, i.e. liquefaction-induced damage. Due to the complexity of the problem, few attempts have been made to quantify liquefaction-induced surface damage.

Iwasaki et al. (1978) proposed a damage criterion, based on several liquefaction case histories in Japan, where surface damage was assumed to be inversely proportional to subsurface depth of liquefiable layers. A total liquefaction damage potential, P_L, was introduced through:

$$P_L = \int_0^{20} D(z)dz \qquad , 0 \leq P_L \leq 20 \qquad (7\text{-}14)$$

where: $D(z) = (1 - F.S) \cdot (10 - 0.5z)$;

        F.S is the factor of safety against liquefaction; and

        z is the embedment depth in meters.

It should be noted that for negative values of $D(z)$ in Equation 7-14, $D(z)$ should be set equal to zero. A value of P_L less than 5 was found to be associated with minimal liquefaction damage to surface structures.

Another damage criterion was suggested by Ishihara and Yoshimine (1992) where liquefaction-induced damage was correlated to surface settlement. It was suggested that significant surface damage was usually associated with a ground settlement of 10 cm or more. Dobry (1994) proposed a relatively similar measure of liquefaction damage based on different types of ground displacements required to cause repairable or irreparable damage in overlying foundation upon earthquake loading, as listed in Table 7.6. This

- 204 -

Reproduced with permission of the copyright owner. Further reproduction prohibited without permission.

7.5 DAMAGE CRITERIA OF LIQUEFACTION

A major concern in liquefaction analysis is the impact of liquefaction occurrence in subsurface layers on overlying structures, i.e. liquefaction-induced damage. Due to the complexity of the problem, few attempts have been made to quantify liquefaction-induced surface damage.

Iwasaki et al. (1978) proposed a damage criterion, based on several liquefaction case histories in Japan, where surface damage was assumed to be inversely proportional to subsurface depth of liquefiable layers. A total liquefaction damage potential, P_L, was introduced through:

$$P_L = \int_0^{20} D(z)dz \qquad , 0 \leq P_L \leq 20 \qquad (7\text{-}14)$$

where: $D(z) = (1 - F.S) \cdot (10 - 0.5z)$;

    F.S is the factor of safety against liquefaction; and

    z is the embedment depth in meters.

It should be noted that for negative values of $D(z)$ in Equation 7-14, $D(z)$ should be set equal to zero. A value of P_L less than 5 was found to be associated with minimal liquefaction damage to surface structures.

Another damage criterion was suggested by Ishihara and Yoshimine (1992) where liquefaction-induced damage was correlated to surface settlement. It was suggested that significant surface damage was usually associated with a ground settlement of 10 cm or more. Dobry (1994) proposed a relatively similar measure of liquefaction damage based on different types of ground displacements required to cause repairable or irreparable damage in overlying foundation upon earthquake loading, as listed in Table 7.6. This

Reproduced with permission of the copyright owner. Further reproduction prohibited without permission.

work was in agreement with that of Ishihara and Yoshimine (1992) in selecting 10 cm ground settlement as a lower limit for significant surface damage.

For the 1987 Superstition Hill earthquake, Iwasaki's damage criterion was applied to the 10,000 realizations of re-trended CPT data, used in the previous section, and the total damage potential index, P_L, was determined at each CPT location. The results were used to generate contours of the probability that P_L will be larger than 5 ($P_L > 5$), a threshold of P_L associated with significant surface damage, as shown in Figure 7.10. For this chapter, it was assumed that sand boils and ground cracks identified zones of surface damage. The locations of these manifestation of liquefaction damage are shown in Figure 7.10, where sand boils are represented by hatched zones, indicating that surface damage is likely to occur only if the probability of ($P_L > 5$) is larger than a critical threshold of about 1.2%.

In order to apply the damage criterion of Ishihara and Yoshimine (1992), ground settlements at the site under the effect of Superstition Hill earthquake were estimated using the empirical approach proposed by Ishihara (1993). In this approach, earthquake-induced volumetric strain is correlated to the factor of safety against liquefaction and relative density as shown in Figure 7.11. The relative densities of different soil layers were expressed in terms of normalized cone tip resistance, q_{c1}, where:

$$q_{c1} = \frac{q_c}{\sqrt{\sigma_v' / P_a}} \qquad (7\text{-}15)$$

The above 10,000 realizations of re-trended CPT data were implemented into Ishihara's approach and the associated settlements were determined resulting in a settlement histogram at each location of the CPT soundings. It was found that the value of mean settlements across the site ranged from 4.4 cm to 13.3 cm, whereas the coefficients of variation ranged from 0.18 to 0.86. A summary of the main characteristics of the ground settlement histograms is provided in Appendix 7-A. The settlement

- 205 -

analysis results were used to compute the probability of occurrence of liquefaction-induced settlement greater than 10 cm, a value considered to be associated with significant surface damage (Ishihara and Yoshimine 1992). Contours of the probability of settlements greater than 10 cm were generated across the Wildlife site, as illustrated in Figure 7.12. It can be concluded from this figure that zones of surface damage are likely to be bounded by a 12% probability of occurrence of settlement larger than 10 cm.

Contours of computed mean settlements and those associated with the upper and lower limits of the 90% level of confidence for the Superstition Hill earthquake (1987) are shown in Figure 7.13. The 90% confidence level provides useful design guidelines as it implies that there is only a 10% chance of having ground settlements outside the range predicted using its upper and lower limits. In other words, there is a 5% chance of having settlements either larger than the upper limit or smaller than the lower limit. As expected, the use of mean values could be on the non-conservative side as shown in Figure 7.13, where the settlements associated with the upper limit of the 90% confidence level may be as high as 2.5 times the mean settlements. This can be attributed to the presence of loose pockets resulting in low factors of safety and higher settlements, which can not be accounted for using classical deterministic analyses.

The above settlement analysis was repeated for other earthquakes occurred at the Wildlife site. Detailed results of these analyses are presented in Appendix 7-A. For both the 1979 and the Elmore Ranch earthquakes, where no sign of liquefaction was recorded at the site, the analyses showed that there was insignificant probability, less than 0.01%, of occurrence of surface settlements larger than 10 cm. This implies that liquefaction is likely to occur if there is a chance of having a vertical settlement larger than 10 cm somewhere across potentially liquefiable sites. It should be realized, however, that these results were obtained using Ishihara's method for the assessment of liquefaction-induced settlement and should not be generalized for other cases where different methods are used for the assessment of ground settlement.

It is worth noting that the effect of non-uniformity in the thickness of different potentially liquefiable layers on the stochastic settlement analysis at each CPT sounding location was taken into consideration through re-scaling of the outcome of Monte Carlo simulation. The re-scaling process was carried out by transforming the outcome of Monte Carlo simulation from its original distribution to a reference distribution with the same type and mean value but with a modified variance, σ_{mod}. This variance depends on layer thickness at each CPT location according to:

$$\sigma_{mod} = (\sigma)_\Gamma \cdot C_R \qquad (7\text{-}16)$$

where: σ_{mod} is the modified variance at each CPT location; and

C_R is a correction factor

The correction factor, C_R, was determined through:

$$C_R = \frac{\Gamma_{vi}}{\Gamma_v} \qquad (7\text{-}17)$$

where: Γ_{vi}^2 is the variance reduction factor at each CPT location, as shown in Figure 7.14.

7.6 REPRESENTATIVE PARAMETERS FOR DETERMINISTIC ANALYSES

The above methodology, while being amenable to engineering design, could be regarded as a relatively sophisticated process for engineers with limited statistical background. Moreover, relying on mean values may provide a non-conservative estimate of liquefaction potential as discussed in the previous sections. To overcome these issues, an attempt was made to ascertain whether more representative soil parameters could be determined that honor the detailed ground heterogeneity and could be used more reliably in simplified deterministic analyses.

As discussed in the previous section, liquefaction is unlikely to occur if there is an insignificant, less than 0.01%, probability of having settlement of 10 cm everywhere across the site, as the case for the Elmore Ranch and the 1979 earthquakes. As a result, it was suggested that a characteristic percentile of cone tip resistance that could be used for liquefaction prediction would likely be correlated with 10 cm settlement. In other words, such a characteristic percentile would not predict any settlement greater than 10 cm anywhere across potentially liquefiable sites when used in deterministic analysis under the effect of earthquakes that do not trigger liquefaction. Using this percentile was considered to provide a more rational basis for the assessment of liquefaction potential.

To obtain this deterministic percentile, contours of probability of occurrence of liquefaction-induced settlement greater than 10 cm (P_{10}) under the effect of the 1981 Westmoreland earthquake were generated, as shown in Figure 7.15. It was found that the surface area covered by P_{10} greater than zero represented 89% of the effective statistical area of the site. The effective statistical area, A_1, can be defined as the rectangular surface area determined by the minimum and maximum horizontal coordinates of all the CPT soundings taking the CPT sounding 7cp as the origin of coordinates, as shown in Figure 7.16. In other words, this area extends from 7cp as far north as the sounding 6ct and as far east as the sounding 1cg. Then, a series of deterministic settlement analyses was carried out using different percentiles of CPT tip resistance data. The characteristic percentile was assessed as that would reproduce an area ratio of 0.89 for a 10 cm settlement, i.e. the area covered by a ground settlement greater than 10 cm represented 0.89 of the effective statistical area, A_1. This procedure is shown in Figure 7.17 where the characteristic percentile was found to be 0.085, i.e. 8.5% of CPT tip resistance data were found to be smaller than the characteristic q_c. It should be noted that the above procedure was not applied to other earthquakes recorded at the wildlife site, as these earthquakes resulted in P_{10} either negligible or more than zero everywhere across the site.

In a similar fashion, attempts were made to obtain a representative cone tip resistance value that can be used in a deterministic analysis to predict liquefaction-

- 208 -

induced ground settlement associated with the upper limit of the 90% confidence level. In other words, upon using this representative value in a simplified deterministic analysis, liquefaction-induced settlement can be predicted with only 5% chance that actual settlements would exceed the predicted values. To obtain this percentile, the volume change associated with the upper limit of the 90% confidence interval of ground settlement, ΔV_{90}, was determined across the statistical effective area, A_1, and was found to be 105 m^3 for the 1987 Superstition Hill earthquake. Then, a series of deterministic settlement analyses was carried out using different percentiles of cone tip resistance data. The characteristic percentile was assessed as the percentile that would reproduce ΔV_{90}, i.e. would result in a volumetric change equal to 105 m^3. This procedure is shown in Figure 7.18 where the characteristic percentile was found to be 0.29. Similar analyses were applied to the 1987 Elmore Ranch, 1981 Westmoreland earthquake, and the 1979 earthquake, where the characteristic percentiles were found to be 0.18, 0.20, and 0.17, respectively. These analyses showed that no unique percentile of cone tip resistance could reproduce ΔV_{90}, for the different earthquake considered in this chapter. Rather, these percentiles were found to be dependent on the shear stresses generated in the ground upon earthquake loading, and on whether or not the site would liquefy under the effect of these stresses. From the results obtained, however, it could be postulated that these percentiles range between 0.20 and 0.29 when liquefaction would be expected to occur; and range between 0.17 and 0.18 otherwise. The use of these percentiles can account for the presence of looser pockets in the ground, which are likely to have a great influence on the liquefaction potential of the site.

7.7 ASSESSMENT OF THE DEGREE OF VARIABILITY OF POTENTIALLY LIQUEFIABLE SITES

The results obtained from the previous section are valid for sites with similar subsurface conditions and geostatistical characteristics. However, they can be used as relatively conservative measures for potentially liquefiable sites of smaller variability. As

- 209 -

a result, an empirical estimate was developed in this chapter as a qualitative measure to compare the degree variability of potentially liquefiable sites. This estimate was expressed in terms of the Overall Variability Factor, OVF, which is the weighted mean of the Local Variability Factor, LVF, calculated at the location of each CPT sounding. The weights used in the calculation of OVF were assessed based on the area of influence (tributary area) of each CPT sounding, as shown in Figure 7.19, while the LVF was estimated through:

$$LVF = \sum_{i=1}^{n} \frac{(COV)_i \cdot (D_F)_i \cdot (T_N)_i}{(R_\Gamma)_i} \qquad (7\text{-}18)$$

where: $(COV)_i$ is the coefficient of variation of layer i in percentage;

$(D_F)_i$ is the depth factor that varies linearly from a value of 1 at ground surface to 0 at a depth of 20m;

$(T_N)_i$ is the normalized thickness of layer i with respect to a nominal thickness of 20m; and

$(R_\Gamma)_i$ is a factor that depends on the type of correlation structure and the spatial range.

The factor R_Γ was obtained through regression analysis of the relation between the square root of the variance reduction factor (Γ) and the ratio between the average layer thickness and the spatial range (T_{av}/a), as shown in Figure 7.20 for exponential variograms. The results of the regression analysis can be expressed in the form:

$$R_\Gamma = 1 - 0.25 \left(\frac{T_{av}}{a/3}\right) , \qquad \text{for spherical variograms} \qquad (7\text{-}19\text{-}a)$$

$$R_\Gamma = 1 - 0.15 \left(\frac{T_{av}}{a/3}\right) + 0.015 \left(\frac{T_{av}}{a/3}\right)^2 , \text{ for exponential variograms} \qquad (7\text{-}19\text{-}b)$$

- 210 -

The value of OVF was found to be 5.49 for the Wildlife site. Sites with greater values of OVF will be expected to exhibit higher variability than that considered in this chapter.

7.8 CONCLUSIONS

The effect of ground heterogeneity on earthquake-induced ground response at the Wildlife Site was investigated in this chapter. This was carried out through assessment of different ground lithologies and applying geostatistical principles to estimate elements of soil spatial variability using the results of 11 cone penetration tests conducted at the site covering an area of about 800 m^2. The CPT results were used stochastically, using Monte Carlo simulation techniques, to estimate the factor of safety against liquefaction and to examine the applicability of different damage criteria, such as total liquefaction damage (P_L) and liquefaction-induced surface settlement.

The use of mean values in CPT liquefaction analysis was found to be on the unsafe (non-conservative) side. This was indicated by the analysis of ground response during the Westmoreland earthquake, where mean factors of safety were greater than one for different potentially liquefiable layers at the site even though liquefaction was observed. This could be attributed to the fact that using mean values in liquefaction assessment can not capture the presence of looser pockets within the soil mass, which are likely to affect site response upon earthquake loading. Moreover, it was found that depending on safety factors solely might not be an accurate measure of liquefaction susceptibility, as it does not necessarily capture the effect of embedment depth of potentially liquefiable layers. As a result, an equivalent failure probability was proposed to take into consideration the effect of embedment depth and thickness of these layers on liquefaction assessment. An equivalent failure probability of 1.2% to 15% was assessed as a critical threshold above which liquefaction would likely occur.

It was found that surface damage zones are likely to be associated with a 1.2% probability, or higher, that total liquefaction damage, P_L, would exceed 5. In a similar fashion, these zones were found to be correlated with a 12% probability, or higher, that liquefaction-induced settlement would be greater than 10 cm. In addition, settlement profiles associated with the upper and lower limits of the 90% confidence interval were introduced to account for the effect of ground variability on liquefaction settlement analyses. Using this interval in engineering design provides risk-based estimates of expected settlement at potentially liquefiable sites with a chance of only 5% that the actual settlement will be greater/smaller than the upper/lower limit.

Equivalent representative soil parameters were obtained for use in simplified deterministic analysis in order to assess liquefaction susceptibility and maximum ground settlement. It was concluded that liquefaction is unlikely to occur if no settlement greater than 10 cm was predicted anywhere across potentially liquefiable sites upon the use of a percentile of q_c equal to 0.085 in deterministic settlement analyses. The 0.085 percentile can be defined as the value of cone tip resistance below which 8.5% of q_c data occur. More efforts are needed to obtain characteristic percentiles for liquefaction-induced settlement prediction as these percentiles were found to be dependent on the shear stress generated in the ground during earthquake excitation. However, a range of characteristic percentiles between 0.17 and 0.29 was obtained in this chapter based on the upper limit of the 90% confidence interval. In other words, using this range in a simplified deterministic analysis implies that there will be only a 5% chance that the actual ground settlements will be greater than the predicted values.

It should be emphasized that the results obtained in this chapter are valid for sites with similar subsurface conditions and geostatistical characteristics and need to be verified and refined by analyzing more case histories and earthquake excitations. However, they can be used as relatively conservative measures for sites of smaller variability. To compare the degree of variability of different potentially liquefiable sites, an empirical factor, the Overall Variability Factor (OVF), was developed in this chapter.

- 212 -

The higher the value of OVF, the greater the ground variability expected at the site. In addition, it should be realized that the outcomes of this chapter were obtained using specific analysis techniques, such the CSR-CRR for liquefaction assessment, Iwasaki's method for quantification of liquefaction damage and Ishihara's method for estimation of liquefaction-induced surface damage. Each of these analysis techniques has its own inherent uncertainty that might affect the outcome of geostatistical liquefaction analyses. The assessment of such uncertainty was considered beyond the scope of this simplified study. As a result, the outcome of this chapter should not be extended to other case histories where different analysis methods are used.

It is worth noting that more efforts are needed to quantify the effect of other sources of uncertainty, which were not considered in this study, on the outcome of stochastic analyses of liquefaction case histories. These uncertainties can be summarized as follows:

1. Uncertainty resulting from spatial variation of CPT sleeve friction;
2. Uncertainty associated with selecting vertical trends of field data to fulfill stationarity requirement;
3. Uncertainty in selecting upper and lower boundaries of potentially liquefiable layers;
4. Uncertainty in estimating variogram characteristics due to the coordinates transformation process and selecting a theoretical model that bestfits field data variogram; and
5. Inherent uncertainty in the equations used in the assessment of liquefaction susceptibility and liquefaction-induced damage and settlement, such as the CSR-CRR approach, Iwasaki's damage criterion, and Ishihara's settlement curves.

Additional attention should be given to the site investigation process to provide sufficient field data to reliably assess different elements of soil spatial variability. Finally, there is a need to develop a generic decision making process for different geotechnical field problems depending on the risk level associated with these problems.

7.9 REFERENCES

Ambraseys, N. N. 1988. Engineering seismology. Earthquake Engineering and Structural Dynamics, 17: 1-105.

Baziar, M., Dobry, R and Alemi, M. 1992. Evaluation of lateral ground deformation using sliding block model. *In* Proceedings of the 10th world conference on earthquake engineering, Madrid, Spain, Vol. 3, pp. 1401-1406

Beaty, M. and Byrne, P. 1998. An effective stress model for predicting liquefaction behavior of sand. *In* Geotechnical Earthquake Engineering and Soil Dynamics III. Geotechnical Special Publication No.75, Vol. 1, pp. 766-777.

Bennett, M. J., Mclaughlin, P. V., Sarmiento, J. S., and Youd, T. L. 1984. Geotechnical investigation of liquefaction sites, Imperial valley, California. Open-file Report 84-252, U.S. Geological Survey, Washington D.C.

Campanella, R. G., Wickremesinghe, D. S. and Robertson, P. K. 1987. Statistical treatment of cone penetration test data. Reliability and Risk Analysis in Civil Engineering. *In* Proceedings of ICAPS 5, the 5th International Conference on Applications of Statistics and Probability in Soil and Structural Engineering, Vancouver, B.C., Canada, pp. 1011-1019.

Deutsch, C. V. 2002. Geostatistical reservoir modeling. Oxford University Press, Oxford, New York

Deutsch, C. V. and Journel A. G. 1998. GSLIB geostatistical software library. Oxford University Press, Oxford, New York

Dobry, R. 1994. Foundation deformation due to earthquakes. *In* Proceedings of the Conference on Vertical and Horizontal Deformations of Foundations and Embankment, College Station, Texas, USA. Geotechnical Special Publications No. 40, Vol. 2, pp. 1846-1863.

Dobry, R., Elgamal, A., Baziar, M., and Vucetic, M. 1989. Pore pressure and acceleration response of Wildlife site during the 1987 earthquake. *In* Proceedings of the 2nd U.S-Japan Workshop on Liquefaction, Large Deformation and Effect on buried Pipelines, Niagara Falls, NY, USA, pp. 145-160.

Fenton, G. A. and Vanmarcke, E. H. (1991). Spatial variation in liquefaction risk assessment. *In* Proceedings of the Geotechnical Engineering Congress, Boulder, Colorado, USA. Geotechnical Special Publications No. 27, Vol. 1, pp. 594-607.

Gu, W. H., Morgenstern, N. R. and Robertson, P. K. 1994. Postearthquake deformation analysis of Wildlife site. Journal of the Geotechnical Engineering Division, ASCE, 120 GT(2): 274-289.

Harder, H. and Von Bloh, G. 1988. Determination of representative CPT-parameters. *In* Penetration testing in the UK, Thomas Telford, London, pp.237-240

Ishihara, K. 1993. Liquefaction and flow failure during earthquakes. The 33rd Rankin Lecture. Geotechnique, 43 (3): 351-415.

Ishihara, K. and Yoshimine, M. 1992. Evaluation of settlements in sand deposits following liquefaction during earthquakes. Soils and Foundations, 32 (1): 178-188.

Itasca Consulting Group. 1993. FLAC Fast Lagrangian Analysis of Continua. Program Software Version 3.22, Minneapolis, Minnesota.

Iwasaki, T., Tatsuoka, F., Tokida, F., and Yasuda, S. 1978. A practical method for assessing soil liquefaction potential based on case studies at various sites in Japan. *In* Proceedings of the Second Conference on Microzonation, San Francisco, CA, USA, Vol. 2, pp. 885-896.

Krinitzsky, E. L., Chang, F. K., and Nuttli, O. W. 1988. Magnitude-related earthquake ground motions. Bulletin of the Association of Engineering Geologists, 25 (4): 399-423.

O'Rourke, T. and Hamada M. 1992. *In* Case studies of liquefaction and lifeline performance during past earthquakes, Vol. 2, United States Case Studies. Technical Report NCEER-92-0002

Palisade Corporation. 1996. @Risk: Risk analysis and simulation add-in for Microsoft Excel or Lotus 1-2-3. Palisade Corporation, NY, USA.

Popescu, R., Prevost, J. H., and Deodatis, G. 1998. Characteristic percentile of soil strength for dynamic analysis. *In* Proceedings of the 1998 Conference on Geotechnical Earthquake Engineering and Soil Dynamics III, Vol. 2, Seattle, WA, USA, pp. 1461-1471.

Robertson, P. K. 1990. Soil classification using the cone penetration test. Canadian Geotechnical Journal, 27 (1): 151-158.

Robertson, P. K. and Wride, C. E. 1998. Evaluating cyclic liquefaction potential using the cone penetration test. Canadian Geotechnical Journal, 35 (3): 442-459

Seed, H. B. and Idriss, I. M. 1971. Simplified procedure for evaluating soil liquefaction potential. Journal of Soil Mechanics and Foundation Division, ASCE, 97 (SM9): 1249-1273

Vanmarcke, E. 1977. Probabilistic modeling of soil profiles. Journal of the Geotechnical Engineering Division, ASCE, 103 GT(11): 1227-1245.

Vanmarcke, E. H. 1984. Random fields, analysis and synthesis. MIT Press, Cambridge, MA.

Youd, T. L., Idriss, I. M., Andrus, R. D., Arango, I., Castro, G., Christian, J. T., Dobry, R., Finn, W. D. L., Harder Jr., L. F., Hynes, M. E., Ishihara, K., Koester, J. P., Liao S. S. C., Marcuson III, W. F., Martin, G. R., Mitchell, J. K., Moriwaki, Y., Power, M. S., Robertson, P. K., Seed, R. B. and Stokoe II, K. H. 2001. Liquefaction resistance of soils: Summary Report from the 1996 NCEER and 1998 NCEER/NSF Workshops on Evaluation of Liquefaction Resistance of Soils. Journal of the Geotechnical Engineering Division, ASCE, 127 GT(10): 817-833.

Zeghal, M. and Elgamal, A. 1994. Analysis of site liquefaction using Earthquake records. Journal of the Geotechnical Engineering Division, ASCE, 120 GT(6): 996-1017.

Liquefaction Induced Ground Settlement At Different CPT Locations

Table A.1: Statistical characteristics of liquefaction-induced ground settlement at the Wildlife Site:

Profile	Superstition Hill Earthquake (1987)					Elmore Ranch Earthquake (1987)				
	m (cm)	σ (cm)	P_{10} (%)	S_5 (cm)	S_{95} (cm)	m (cm)	σ (cm)	P_{10} (%)	S_5 (cm)	S_{95} (cm)
1cg	7.835	2.188	16.96	4.600	11.700	0.702	0.579	< 0.01	0.01	1.750
1cp	9.153	2.298	32.42	5.400	12.988	0.797	0.630	< 0.01	0.010	1.920
3cp	13.262	2.489	90.55	9.028	17.158	1.084	0.730	< 0.01	0.070	2.420
3cg	7.610	1.628	6.56	4.812	10.040	0.701	0.602	< 0.01	0.004	1.850
2cg	7.758	4.099	26.71	3.000	15.644	0.565	0.489	< 0.01	0.005	1.530
4cg	6.039	2.615	11.09	2.751	10.930	0.469	0.414	< 0.01	0.004	1.290
6cg	10.385	1.979	59.25	6.949	13.340	0.889	0.669	< 0.01	0.031	2.100
5cg	6.900	2.772	18.39	3.382	12.150	0.553	0.480	< 0.01	0.005	1.510
6ct	7.055	4.429	27.28	0.662	14.720	0.402	0.357	< 0.01	0.006	1.100
7cg	6.369	5.362	25.91	0.183	16.690	0.222	0.338	< 0.01	0.000	1.130
7cp	4.454	3.826	13.52	0.113	11.983	0.181	0.281	< 0.01	0.000	0.960
Profile	Westmoreland Earthquake (1981)					1979 Earthquake				
	m (cm)	σ (cm)	P_{10} (%)	S_5 (cm)	S_{95} (cm)	m (cm)	σ (cm)	P_{10} (%)	S_5 (cm)	S_{95} (cm)
1cg	7.835	2.188	16.96	4.600	11.700	0.702	0.579	< 0.01	0.01	1.750
1cp	9.153	2.298	32.42	5.400	12.988	0.797	0.630	< 0.01	0.010	1.920
3cp	13.262	2.489	90.55	9.028	17.158	1.084	0.730	< 0.01	0.070	2.420
3cg	7.610	1.628	6.56	4.812	10.040	0.701	0.602	< 0.01	0.004	1.850
2cg	7.758	4.099	26.71	3.000	15.644	0.565	0.489	< 0.01	0.005	1.530
4cg	6.039	2.615	11.09	2.751	10.930	0.469	0.414	< 0.01	0.004	1.290
6cg	10.385	1.979	59.25	6.949	13.340	0.889	0.669	< 0.01	0.031	2.100
5cg	6.900	2.772	18.39	3.382	12.150	0.553	0.480	< 0.01	0.005	1.510
6ct	7.055	4.429	27.28	0.662	14.720	0.402	0.357	< 0.01	0.006	1.100
7cg	6.369	5.362	25.91	0.183	16.690	0.222	0.338	< 0.01	0.000	1.130
7cp	4.454	3.826	13.52	0.113	11.983	0.181	0.281	< 0.01	0.000	0.960

Table 7.1. List of major earthquakes in the Imperial Valley in the twentieth century (modified from O'Rourke and Hamada 1992)

Date	Richter Magnitude	Recorded maximum surface acceleration	Occurrence of liquefaction
April 1906	6.00	N/A	No
June 1915	6.30	N/A	No
May 1917	5.50	N/A	No
January 1927	5.80	N/A	No
May 1940	6.40	N/A	Yes
May 1940	5.50	N/A	No
October 1979	6.60	N/A	No
April 1981 (Westmoland earthquake)	5.6	N/A	Yes
November 1987 (Elmore Ranch earthquake)	6.2	0.13 g	No
November 1987 (Superstition Hill earthquake)	6.6	0.21 g	Yes

Table 7.2. Classification of soil using the soil behavior type index, I_c. (modified from Robertson and Wride 1998):

I_c	Soil Behavior Type	Description
< 1.31	7	Gravelly sand to dense sand
1.31 – 2.05	6	Clean sand to silty sand
2.05 – 2.60	5	Silty sand to sandy silt
2.60 – 2.95	4	Clayey silt to silty clay
2.95 – 3.60	3	Silty clay to clay
> 3.60	2	Organic soils

Table 7.3. Statistical properties of detrended cone tip resistance data for different potentially liquefiable layers at the Wildlife site.

Layer	Mean (kPa)	Standard dev. (kPa)	Variogram characteristics			
			Model*	Nugget effect**	Vertical Range (m)	Horizontal Range (m)
L1	-0.128	849.501	exponential	0.05	0.55	10.00
L2	-0.134	1567.03	spherical	0.05	1.40	22.00
L3	0.036	1258.86	spherical	0.05	1.45	22.00
L4	0.219	1333.85	exponential	0.05	0.75	13.60

* in both horizontal and vertical directions

** nugget effect is the random portion of the variogram model (Deutsch 2002)

Table 7.4. Variance reduction factors for different potentially liquefiable layers at the Wildlife site.

Layer	L_1	L_2	L_3	L_4
Averaging thickness (m)	1.17	1.19	2.04	1.02
Variance reduction factor	0.551	0.605	0.666	0.667

Table 7.5. Statistical characteristics of factors of safety against liquefaction for different earthquakes at the Wildlife site.

Earthquake	F.S	Layer			
		L_1	L_2	L_3	L_4
Superstition Hill (1987)	mean	0.749	1.179	1.12	1.556
	COV	0.138	0.285	0.258	0.197
	P_F (%)*	98.79	32.85	37.53	3.16
Elmore Ranch (1987)	mean	1.419	2.214	2.116	2.95
	COV	0.138	0.285	0.258	0.197
	P_F (%)*	1.35	1.89	1.36	< 0.01
Westmoreland (1981)	mean	1.042	1.64	1.56	2.165
	COV	0.138	0.285	0.258	0.197
	P_F (%)*	37.65	7.82	7.46	0.34
1979 Earthquake	mean	1.365	2.346	2.182	2.836
	COV	0.138	0.285	0.258	0.197
	P_F (%)*	2.54	0.57	0.88	< 0.01

Table 7.6. Approximate ground displacements (in cm) required to cause repairable and irreparable damage (modified from Dobry 1994).

Type of deformation	Foundation type	Displacement required to cause	
		Repairable damage	Irreparable damage
Shear	Poorly reinforced	0.10	> 0.30
	Well reinforced	> 0.30	....
Extension	Poorly reinforced	< 0.05	> 0.30
	Well reinforced	> 0.10	....
Compression	Poorly reinforced	< 0.30	> 0.50
	Well reinforced	> 0.50	....
Compression with vertical	Poorly reinforced	< 0.20	> 0.20
	Well reinforced	< 0.30	> 0.30
Vertical	Poorly reinforced	< 0.05	> 0.20
	Well reinforced	< 0.10	> 0.30
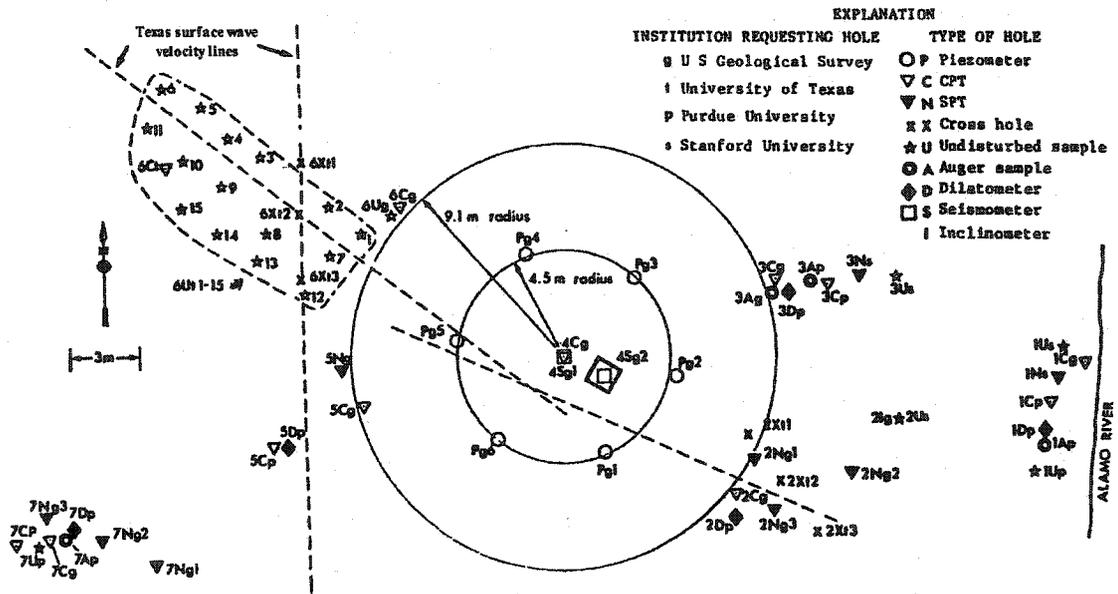
Figure 7.1. Layout of locations of CPT data and boreholes at Wildlife Site. (modified from Bennett et al. 1984)
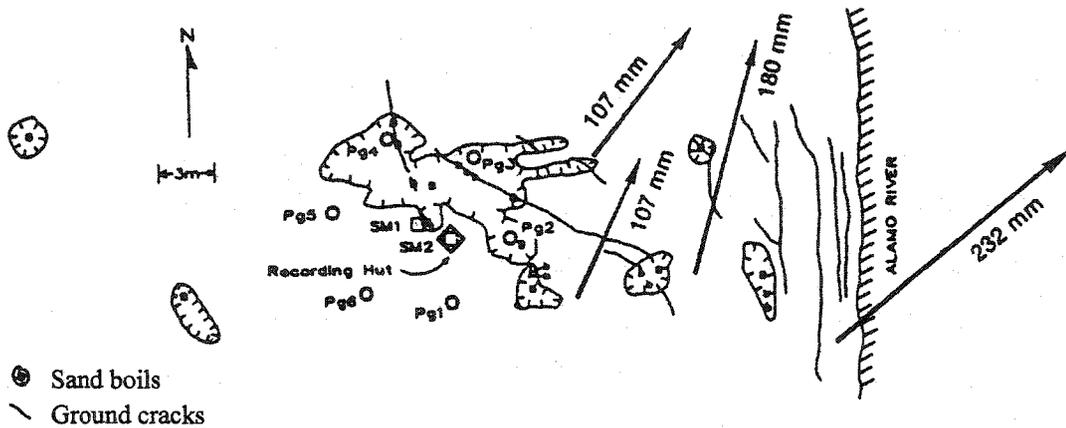
Figure 7.2. Field records of lateral spreads, sand boils and ground cracks at Wildlife Site during the Superstition Hill earthquake. (modified from O'Rourke and Hamada 1992)

- 222 -
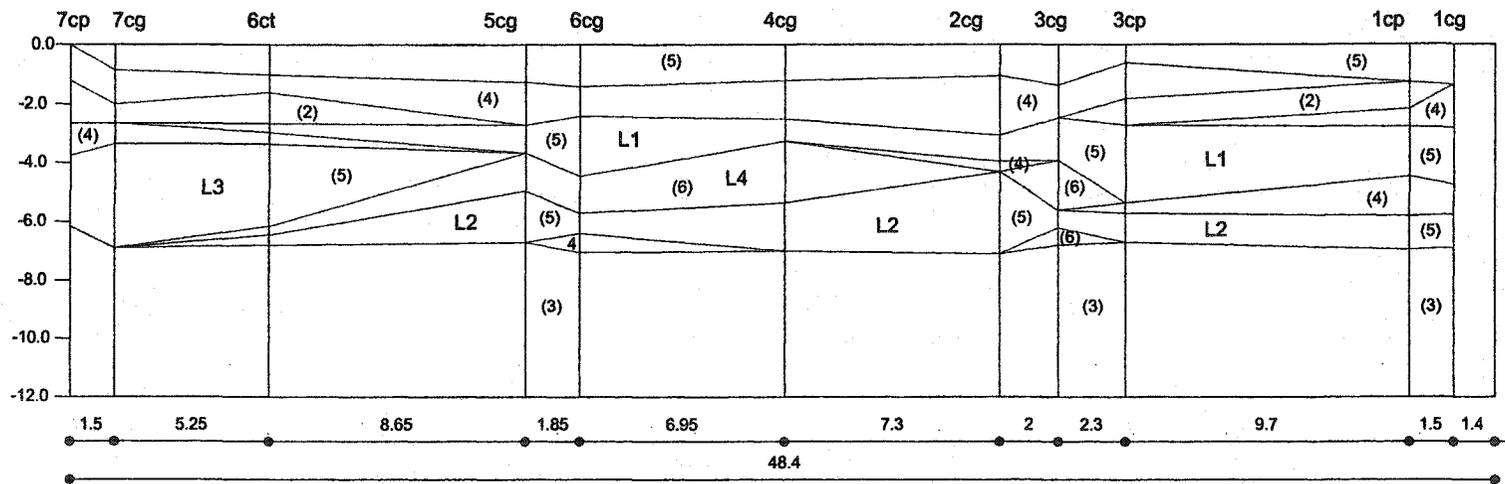
Figure 7.3. An East-West view showing the Lithological distribution across the Wildlife site. (Position of cone wells are shown in Figure 7.1; numbers between brackets represent soil behavior type based on soil behavior type index, I_c; dimensions are in meters)
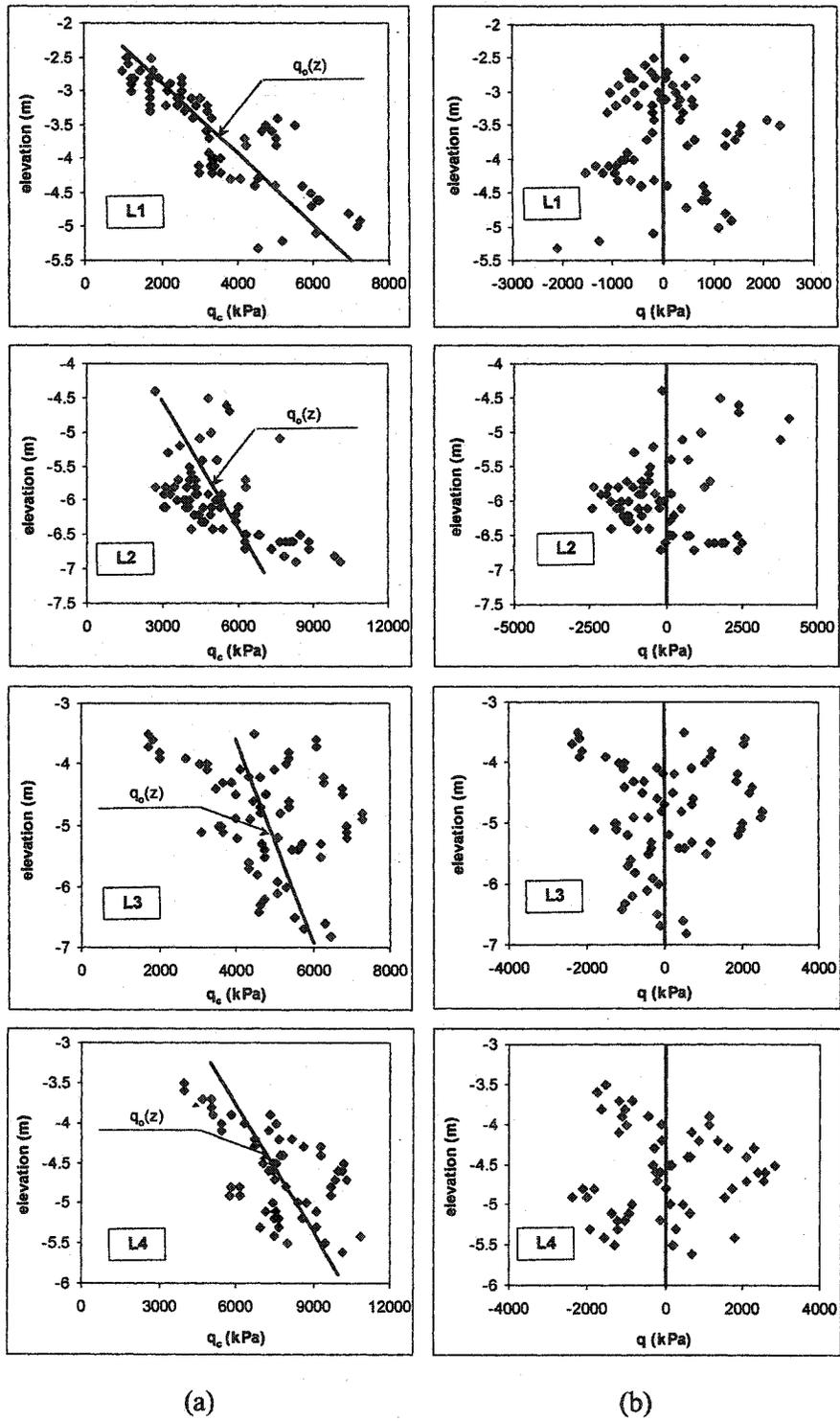
Figure 7.4. Detrending of CPT data. a) identifying linear vertical trends; and b) detrended data.
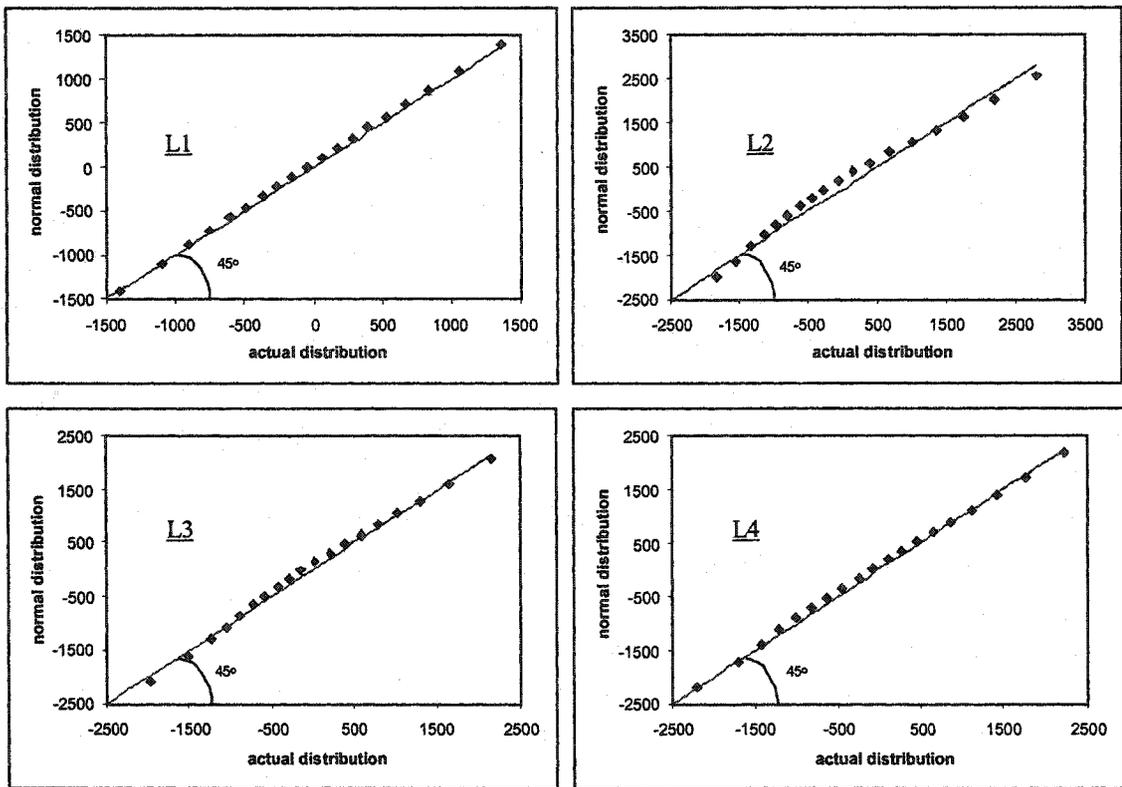
Figure 7.5. Q-Q plots comparing actual and normal distribution for de-trended cone tip resistance data.
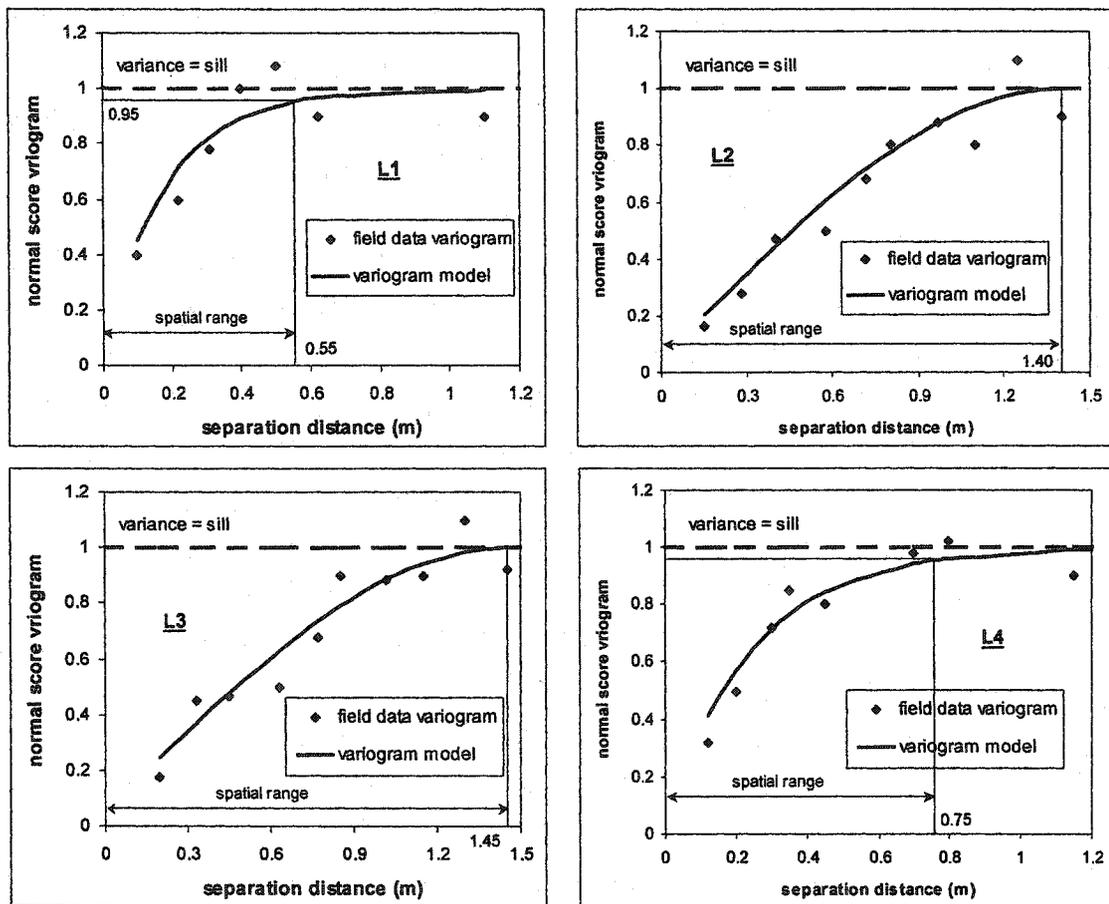
Figure 7.6. Assessment of vertical variogram characteristics for standardized detrended CPT data using the GSLIB software.

Original layer profile   Transformed layer profile
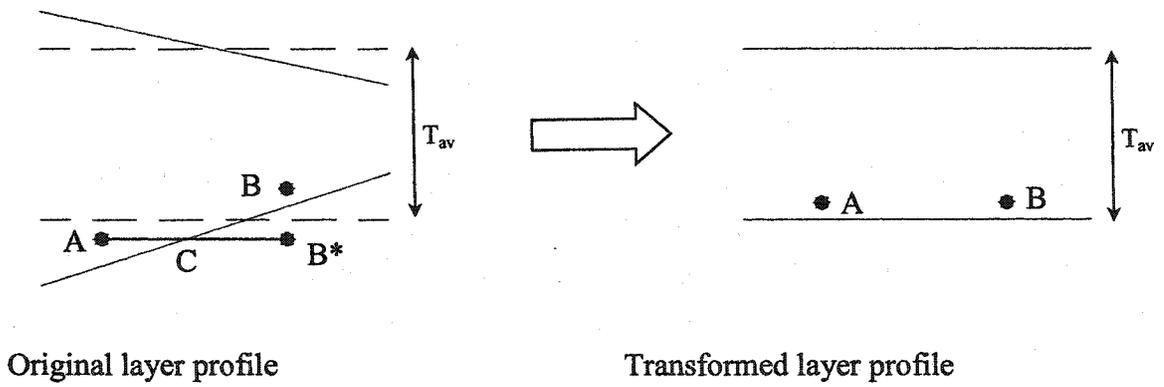
Figure 7.7. Coordinates transformation process of potentially liquefiable layers.
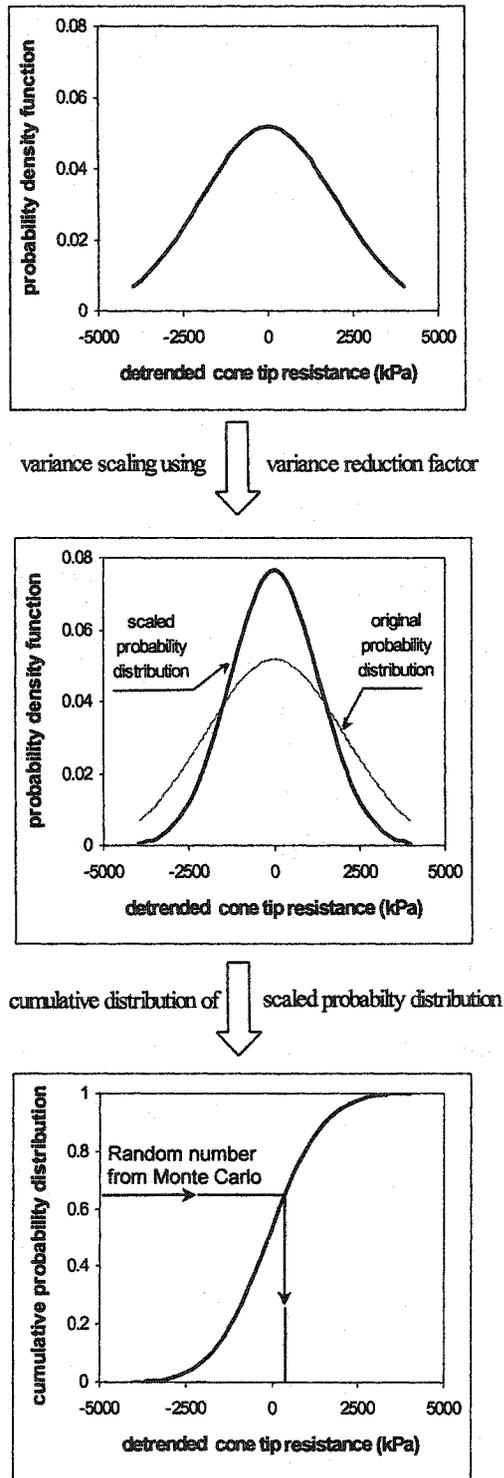
Figure 7.8. Scaling of probability distribution of detrended CPT data using the variance reduction factor and its effect on Monte Carlo simulation.

- 228 -
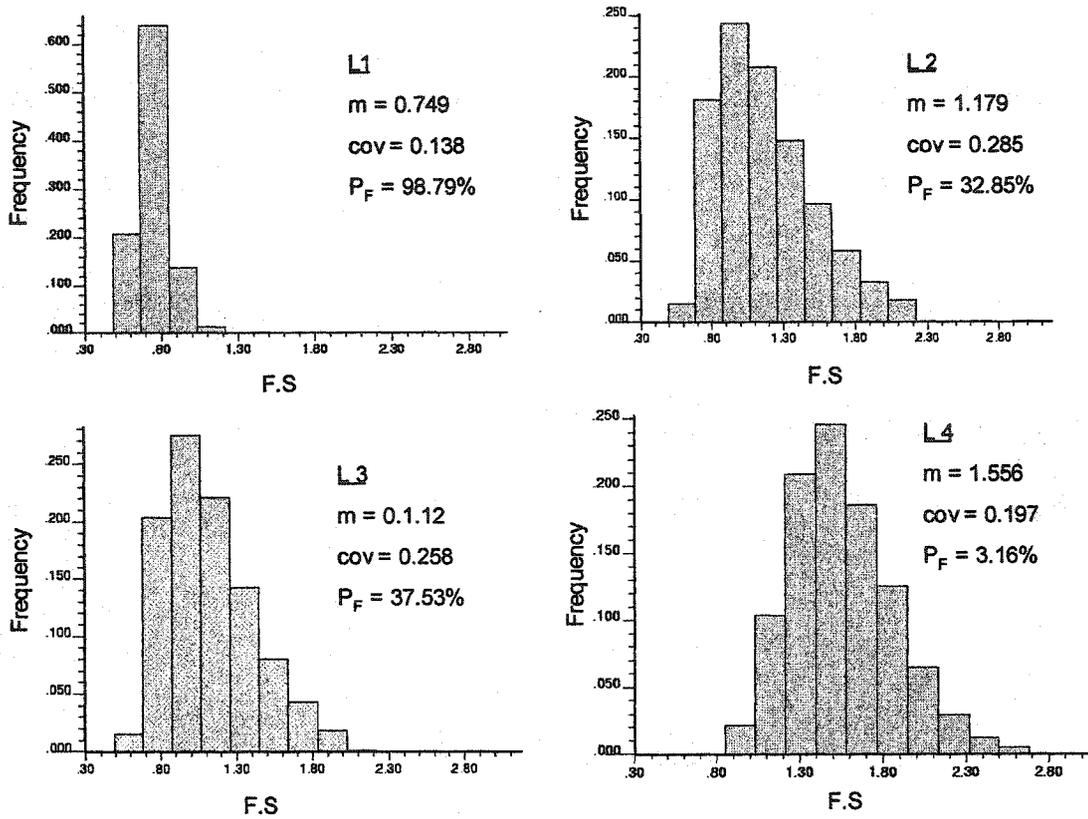
Figure 7.9. Factors of safety against liquefaction for different potentially liquefiable layers at the Wildlife site during the 1987 Superstition Hill earthquake.
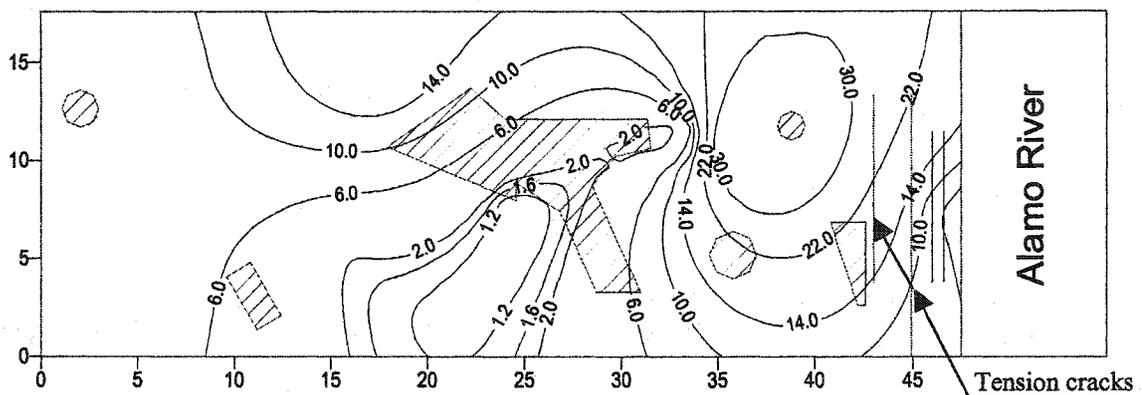
Figure 7.10. A site plan showing contours of probability of occurrence of total liquefaction damage potential (P_L) greater than 5 for the Superstition Hill earthquake (hatched zones indicate observed sand boils at the site). Dimensions are in meters.

- 229 -
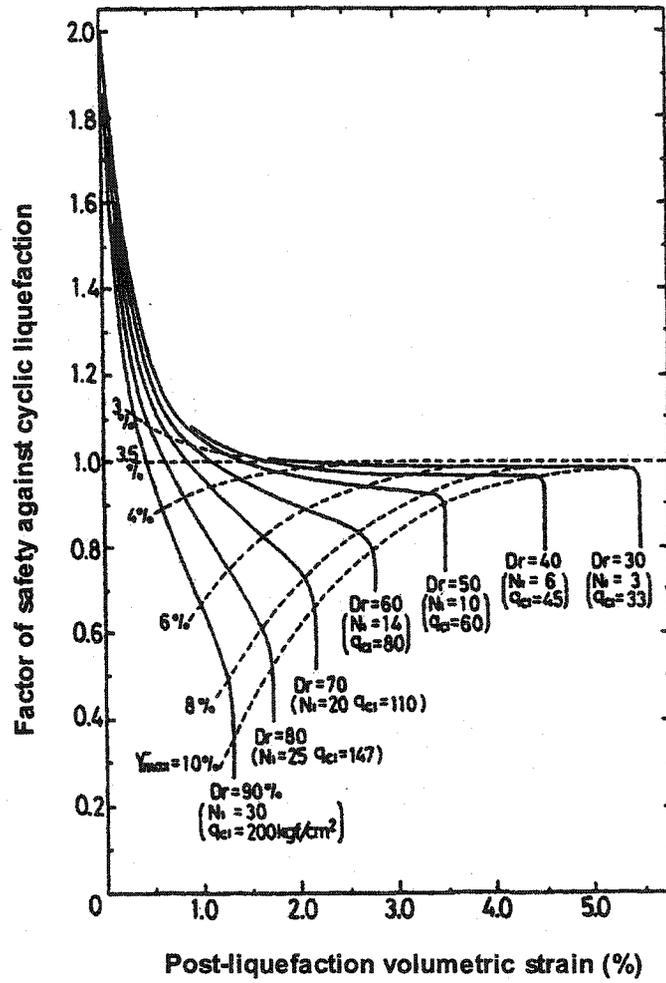
Figure 7.11. Post-liquefaction volumetric strain as a function of factor of safety and relative density. (modified from Ishihara 1993)

- 230 -
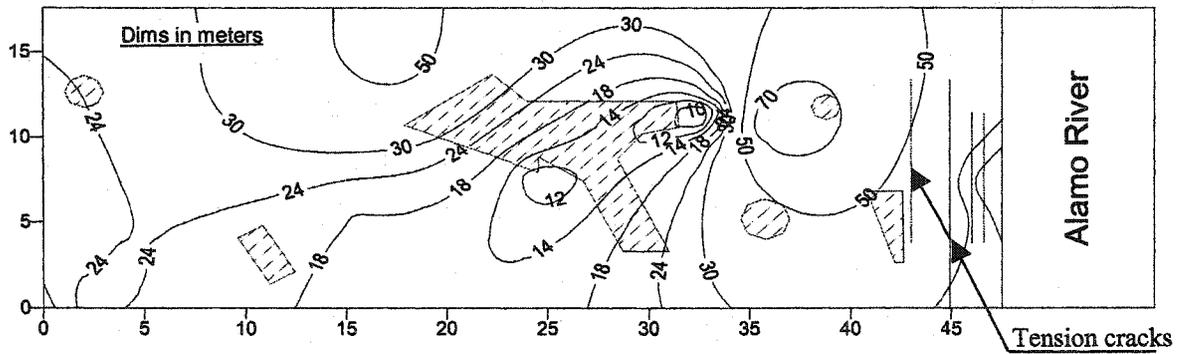
Figure 7.12. A site plan showing contours of probability of liquefaction induced settlements greater than 10cm for the Superstition Hill earthquake. (hatched zones indicate observed sand boils at the site)
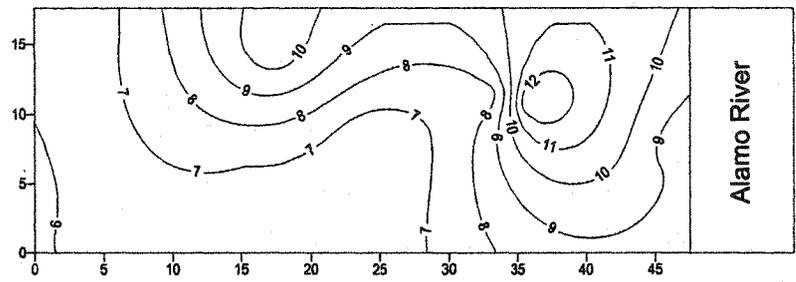
(a)
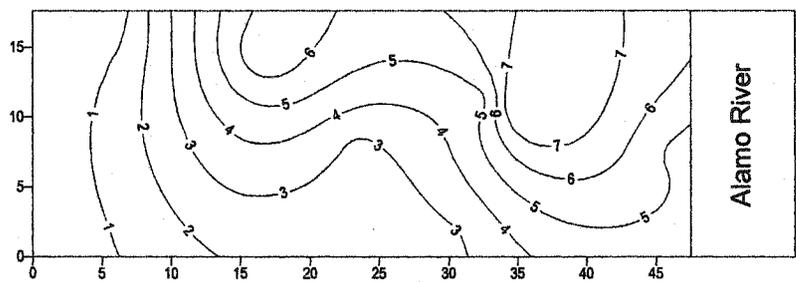
(b)
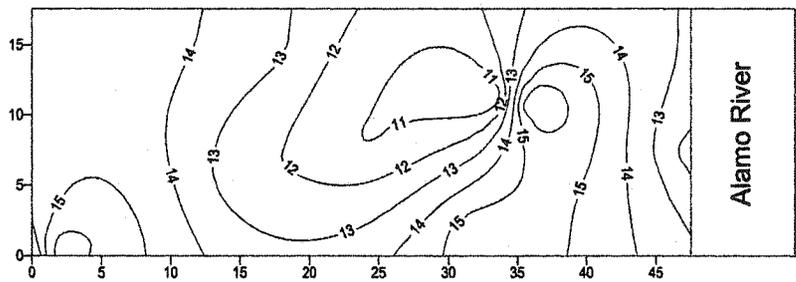
(c)

Figure 7.13. A site plan showing contours of computed settlements (in cm) across the Wildlife Site under the effect of the Superstition Hill earthquake. a) mean settlement; b) lower limit of 90% confidence interval; and c) upper limit of 90% confidence interval.
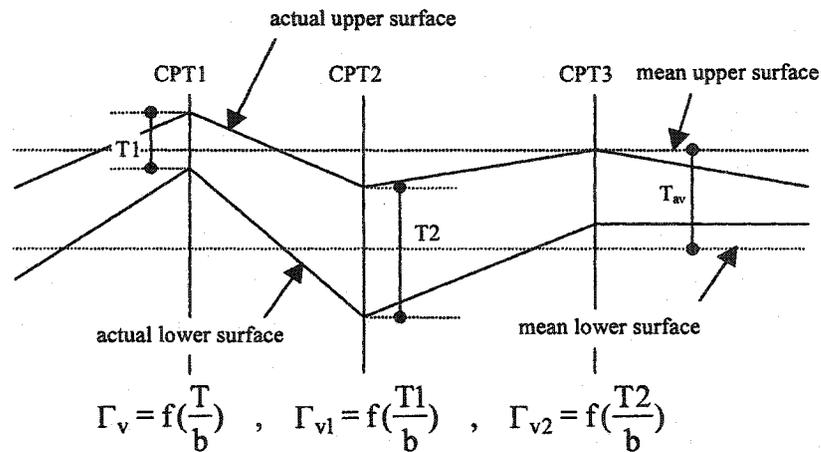
Figure 7.14. Modified variance reduction factor at each CPT sounding location.
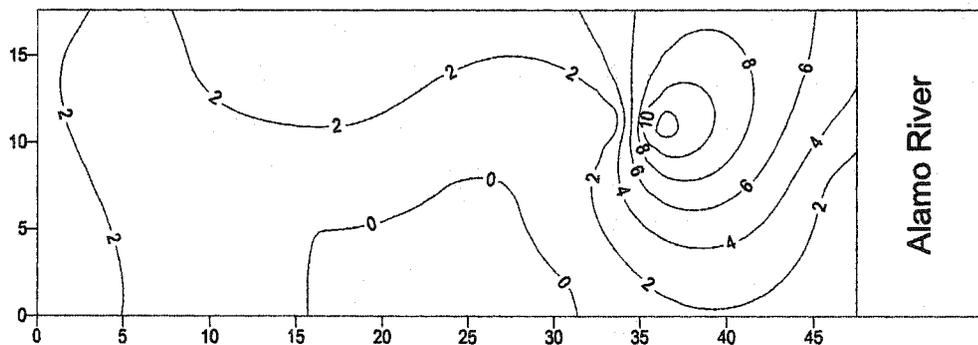
Figure 7.15. A site plan showing contours of probability of liquefaction induced settlements greater than 10cm for the 1981 Westmoreland earthquake.
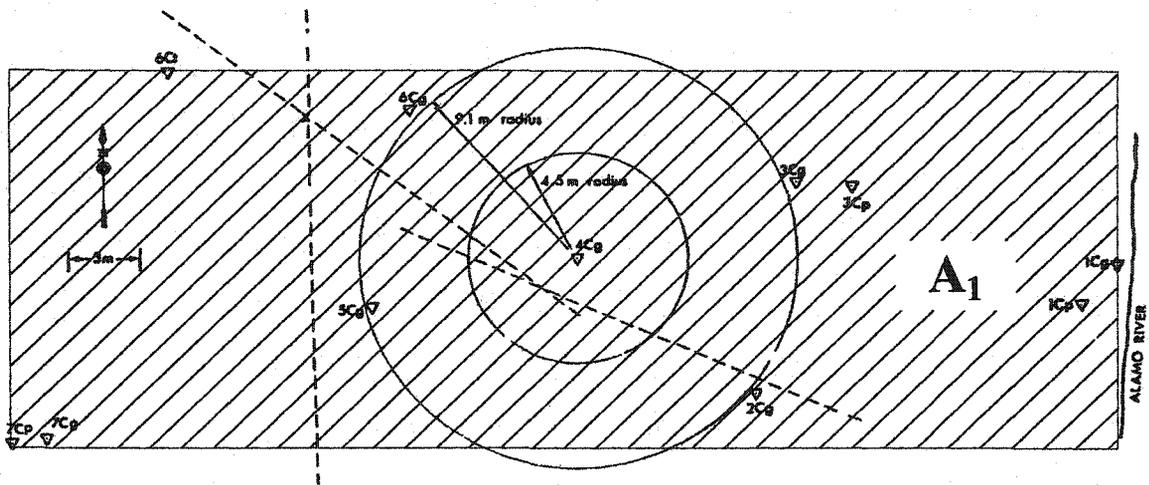
Figure 7.16. A site plan showing the effective statistical area (A_1).
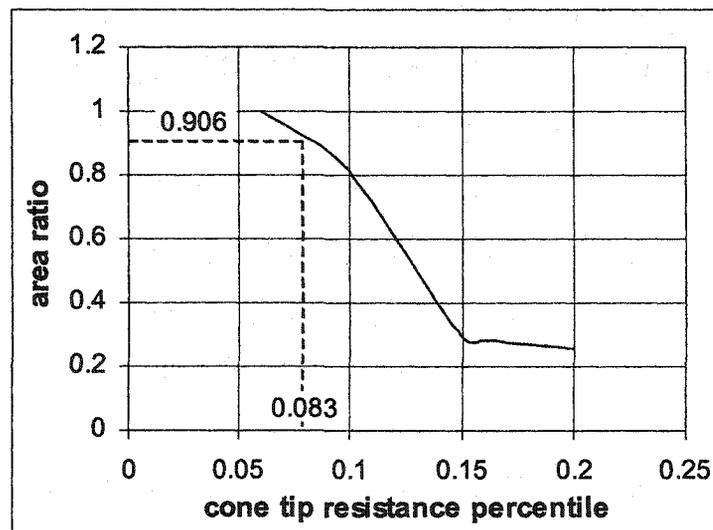
Figure 7.17. Determination of characteristic percentile of cone tip resistance associated with liquefaction assessment of the Wildlife site.

- 234 -
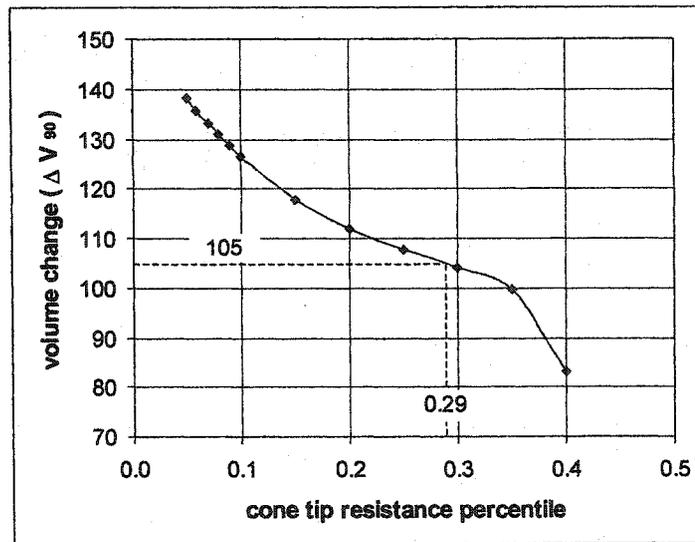
Figure 7.18. Determination of characteristic percentile of cone tip resistance associated with liquefaction induced settlement of the Wildlife site under the effect of the 1987 Superstition Hill earthquake.
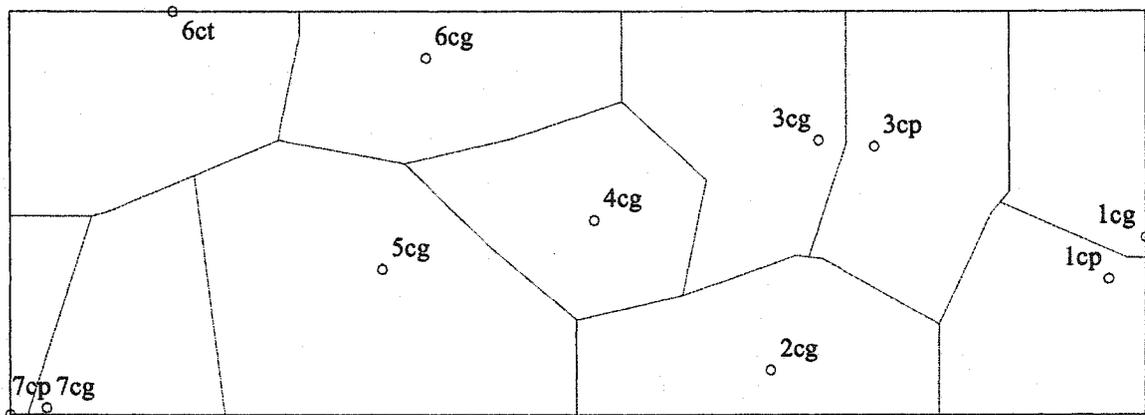
Figure 7.19. A site plan of the effective statistical area at the Wildlife showing the influence (tributary) area of each CPT sounding used to calculate the Overall Variability Factor (OVF).
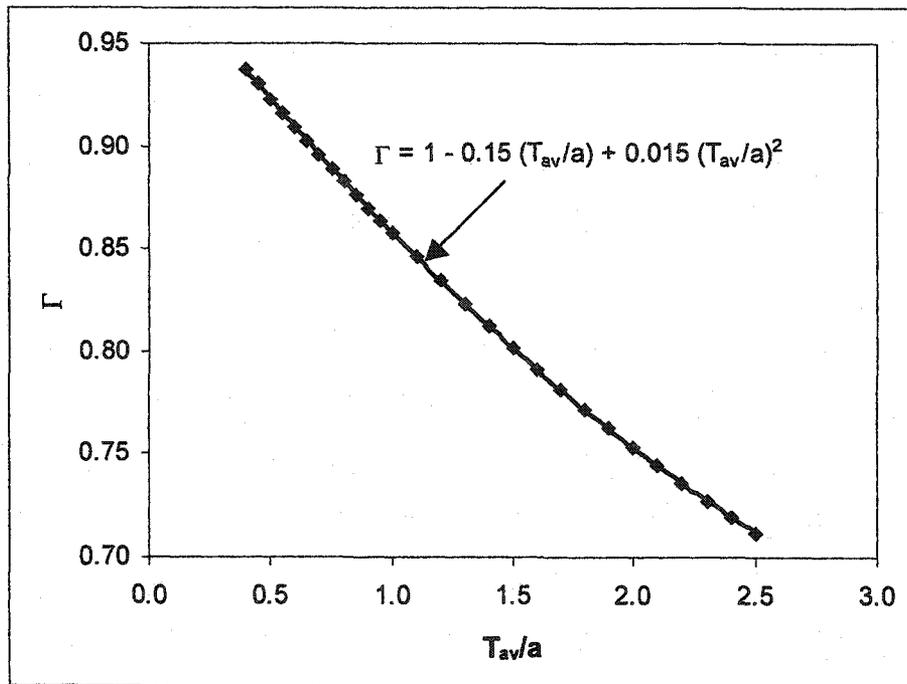
Figure 7.20. Regression analysis to obtain the factor R_Γ for exponential variograms.

CHAPTER 8

GEOSTATISTICAL ANALYSIS OF LIQUEFACTION INDUCED GROUND RESPONSE AT THE TREASURE ISLAND

8.1 INTRODUCTION

Most soils are heterogeneous in nature either due to the presence of different lithologies or as a result of their inherent spatial variability. This heterogeneity can have a profound effect on ground response under earthquake loading, as discussed by Fenton and Vanmarcke (1991) and Popescu et al (1998). Quantitative treatment of this variability with respect to liquefaction assessment is important, as classical deterministic techniques can not account for the scatter of field data and their spatial correlation. Well-documented case histories provide an opportunity to explore options of quantifying the effect of soil heterogeneity on liquefaction-induced ground response. A good example of this type of case histories is the Treasure Island site, California, where different signs of liquefaction, such as sand boils, lateral spreads, and surface settlements, were recorded at the site during the 1989 Loma Prieta earthquake.

Several studies have been carried out to investigate ground response at the Treasure Island site during the 1989 Loma Prieta earthquake. Bennett (1998) documented different liquefaction evidences, such as sand boils and surface settlement, encountered at the site after the earthquake. The most comprehensive study of the site was that by Power et al. (1998), where different liquefaction features recorded at the site, such as ground settlement, lateral spread, and sand boils, were thoroughly discussed and analysed. Different empirical approaches where used in the analysis, such as that by Seed and Idriss (1971) to assess liquefaction susceptibility, and that by Tokimatsu and Seed (1987) for

---

A version of this chapter will be submitted for publication in the Canadian Geotechnical Journal.

estimating liquefaction-induced ground settlement.

Recently, Andrus and Stokoe (2000) conducted a study to evaluate the performance of the improved areas at the Treasure Island site. The study followed the simplified scheme proposed by Seed and Idriss (1971) using different in-situ tests such as Cone Penetration Test (CPT), Standard Penetration Test (SPT), and Seismic Analysis of Surface Waves (SASW). On the other hand, Luna and Frost (2000) implemented the total liquefaction damage potential, P_L, (Iwasaki 1978) and simplified methods to predict liquefaction-induced settlement (Tokimatsu and Seed 1987) into a GIS environment. Consequently, the spatial distributions of P_L, as a measure of liquefaction-induced surface damage, and surface settlement were obtained across the site.

To the author's knowledge, no attempt has been made to quantify the effect of spatial variability of soil properties at the Treasure Island site on its seismic-induced ground response in a probabilistic analysis framework. In this chapter, a geostatistical approach was adopted to assess the effect of lithological heterogeneity and spatial variability of soil properties on the ground response during the 1989 Loma Prieta earthquake. Cone Penetration Test (CPT) results were used to identify different ground lithologies implementing the soil behavior type index, I_c, (Robertson 1990). Different geostatistical characteristics, such as mean, variance, and spatial correlation structures, were estimated for each of these lithologies. The cyclic stress ratio – cyclic resistance ratio (CSR-CRR) approach (Robertson and Wride 1998) was employed stochastically to estimate the liquefaction susceptibility of the ground, expressed in terms of the factor of safety against cyclic liquefaction. This was carried out by implementing Monte Carlo simulation techniques to obtain several realizations of CPT data, which were used to estimate the value of CRR. On the other hand, the earthquake loading was assessed deterministically using simplified techniques that correlated the CSR to earthquake magnitude and maximum surface acceleration recorded at the site. In addition, different procedures were used to assess the level of liquefaction damage, such as total damage potential (P_L) and settlement criteria. Finally, the characteristic cone tip resistance values

- 238 -

developed in Chapter 7 from the analysis of the Wildlife site, California, were applied to examine their applicability to the Treasure Island site. These representative values were thought to be suitable for use in simplified deterministic analyses, while continuing to honor detailed ground heterogeneity.

8.2 BACKGROUND ON THE TREASURE ISLAND SITE

The Treasure Island is a manmade island that was constructed in the 1930's by hydraulically placing sand fill behind a perimeter rock dyke in San Francisco bay, California. The sand fill ranged from clean sand to silty sand with occasional clayey zones, and was obtained from borrow pits in San Francisco Bay. The geology at the site was described by Power et al. (1984) based on the results of extensive field investigation program. The uppermost layer consists of silty sand and shoal sand to a depth of 10 to 16 m, followed by a stratum of bay mud consisting of soft to stiff silty clay underlain by older bay sediments of very stiff silty clay and dense sand. The ground water table (GWT) at the site was affected by tidal fluctuation, but it was believed that the GWT was at a depth of 3m during the Loma Prieta earthquake (Power et al. 1998). Site instrumentation consisted of two accelerometers, one at ground surface and the other on the bedrock on the neighboring Yerba Buena Island. In addition, several survey points were installed to capture ground settlement and lateral spreads.

The ground responses during the 1989 Loma Prieta earthquake, Richter magnitude of 7, were captured by the field instrumentation. A peak surface acceleration of 0.16g was recorded at the site compared with a value of 0.06g recorded at the bedrock of Yerba Buena Island. Numerous ground cracks, generally as wide as 10 cm, were encountered along the perimeter of the island together with lateral spreads up to 25 cm. Surface settlements were found to be in the range of 5 to 15 cm with the greater values associated with zones of thicker sand fill. It is worth noting that no significant damage

was recorded in several areas where ground improvements, such as compaction piles and vibroflotation, had been implemented before the earthquake.

8.3 CHARACTERIZATION OF GROUND HETEROGENEITY

Characterization of ground heterogeneity at the site for the Southwestern and Northeastern sections, indicated by the hatched zones in Figure 8.1, was carried out through three main stages. In the first stage, standardization and filtration procedures were implemented to CPT data. In the second stage, geostatistical characteristics of the standardized data were obtained. Finally, stochastic simulation of the standardized data was performed in the third stage. Details of these stages are discussed in the following sections.

8.3.1. Standardizing Cone Penetration Test Data

The results of several cone penetration tests soundings, shown in Figure 8.1, were used to characterize both lithological heterogeneity and inherent spatial variability of soil properties at the Treasure Island site. CPT data were used to identify different ground lithologies, expressed in terms of soil behavior type, using the soil behavior type index, I_c, (Robertson 1990). Detailed ground profiles along the perimeter dyke of the Southwestern and Northeastern sections are shown in Figure 8.2. Five cohesionless soil layers below GWT, L_{1A}, L_{2A}, L_{3A}, L_{4A} and L_{5A}, were considered as potentially liquefiable zones for the Southwestern section. These layers were denoted by soil behavior types 5, 6 and 7, as illustrated in Figure 8.2. Similarly, four layers, L_{1B}, L_{2B}, L_{3B}, and L_{4B}, were identified as potentially liquefiable zones for the Northeastern section. Each of these layers was treated as a statistically homogeneous domain, where cone tip resistance, q_c, was treated as a random variable. It should be emphasized that cohesive soils associated with $I_c > 2.6$, denoted by soil behavior types 2,3, and 4, were assumed to be non-liquefiable layers (Robertson and Wride 1998).

Data filtration is an important process where outliers are identified and excluded from field data to maintain statistical consistency. Outliers can be manifested in the form of spikes in CPT profiles at certain depths, which can be attributed to presence of pieces of gravel at the cone tip. These spikes should not be considered representative of soil characteristics underneath the cone tip. In this chapter, data filtration was carried out following the procedure presented in Chapter 7 for the analysis of the Wildlife site.

A necessary condition for stochastic analyses is stationarity, which implies that the mean and variance of random variables do not depend on location in space. It can be expected, however, that cone tip resistance data will exhibit vertical trends due to their sensitivity to changes in effective confining pressure. In order to use cone tip resistance, q_c, as a random variable and meet the stationarity condition, any possible vertical trend in q_c should be removed (detrended). To achieve this, filtered data from all CPT soundings were utilized to identify deterministic linear vertical trends in q_c within each of the potentially liquefiable layers using linear regression analysis. Then, these trends were removed, as illustrated in Figure 8.3 for layer L_{2A}, producing detrended cone tip resistance data through the relation:

$$q = q_c - q_o(z) \tag{8-1}$$

where q is the detrended cone tip resistance and $q_o(z)$ is a deterministic vertical trend.

8.3.2. Geostatistical Properties of Detrended CPT Data

To proceed with stochastic analyses, geostatistical characteristics of different random variables, such as mean, variance, probability distribution and correlation structure, have to be determined. A summary of geostatistical characteristics of detrended cone tip resistance data for different potentially liquefiable layers is presented in Table 8.1. The mean values were found to be around zero, as expected, whereas the standard deviations ranged from 627 kPa to 4299 kPa. The probability distributions were in close

- 241 -

agreement with normal distributions for layers L_{1A}, L_{2A}, L_{3A}, L_{4A}, L_{5A}, and L_{4B}. This was assessed using Q-Q plots (Deutsch 2002), as shown in Figure 8.4 and Figure 8.5. These Q-Q plots are comparisons between quantiles, which correspond to certain percentiles of the random variable, obtained from probability distribution of field data and those of a reference distribution, such as the normal distribution in this case. If the cross plot between the two sets of quantiles results in points close to a 45 degree line, this indicates a similar shape and variance of both distributions. On the other hand, the Chi square test (Benjamin and Cornell 1970) was used to assess probability distributions for layers L_{1B}, L_{2B}, and L_{3B}, which were in poor agreement with normal distribution, as deduced from Figure 8.5. These layers were found to follow beta distributions with 95, 90, and 85 levels of significance, respectively (Benjamin and Cornell 1970).

Soil properties do not vary randomly in space; rather such variation is gradual and follows a pattern that can be quantified using what is called spatial correlation structure. In this chapter, variogram functions (Deutsch 2002) were adopted as measures of quantifying spatial correlation between detrended CPT data. The GSLIB Geostatistical Software Library (Deutsch and Journel 1998) was used to obtain the variogram characteristics, such as the model and spatial range, in the vertical direction for each of the potentially liquefiable layers, as shown in Table 8.1.

One limiting boundary condition required to use GSLIB to obtain variogram characteristics is that each of the layers considered has to be rectangular in shape. Consequently, a coordinate transformation process was carried out producing transformed sections of different potentially liquefiable layers following the procedure presented in Chapter 7. These transformed sections retain spatial continuity between field data and are amenable to analysis within GSLIB.

It is worth noting that insufficient data was available to reliably assess the variogram characteristics in the horizontal direction. As a result, it was assumed that the horizontal variogram had the same model type as the vertical one, but with a larger range

as suggested by Deutsch (2002). A ratio of 17 between horizontal and vertical ranges was assumed for the Treasure Island site, similar to the value obtained from the analysis of the Wildlife site in Chapter 7.

8.3.3. Stochastic Simulation of Detrended CPT Data

To quantify the effect of soil spatial variability, several realizations of detrended CPT data were obtained for each of the potentially liquefiable layers. This was carried out by implementing Monte Carlo simulation using the @Risk software (Palisade Corporation 1996). The number of realizations used in the analysis, about 10,000, was assessed by specifying an acceptable tolerance of 0.50% between the input distributions and the distributions of the sampled valued obtained from Monte Carlo simulation.

It should be noted that the variance used in the simulation process was not the point variance shown in Table 8.1. Rather, it was the variance of the spatial average of CPT data over certain averaging volumes. These spatial averages typically have narrower probability distributions than field data (point statistics) and consequently smaller variances (Vanmarcke 1977). The variance of these spatial averages can be correlated to the point variance using a variance reduction factor (Vanmarcke 1984) through:

$$(\sigma)_{\Gamma} = \Gamma_v \times \sigma \qquad (8\text{-}2)$$

where: σ is the standard deviation of field data (point statistics);

σ_{Γ} is the standard deviation of the spatial average of data over volume v; and

Γ_v is the square root of the variance reduction factor.

The variance reduction factor depends on the averaging volume, type of correlation structure, and the limit of spatial correlation between field data. Analytical expressions for the variance reduction commonly used in practice are summarized in

Chapter 2. It was assumed in this chapter that the variance reduction factor would be affected only by the size of the averaging volume in the vertical direction, i.e. layer thickness, as discussed in Chapter 7. It is worth noting that the thicknesses of different potentially liquefiable layers were not uniform across the Treasure Island site. As a result, an average thickness was obtained for each layer, which was employed to obtain the variance reduction factors presented in Table 8.2. These average thicknesses were divided into horizontal sublayers, as shown in Table 8.2, to maintain a minimum value of 0.70 for the variance reduction factor to ensure high accuracy upon applying Equation 8-2, as recommended by Deutsch (2002). It should be emphasized that the outcomes of applying Monte Carlo simulation to these sublayers were not independent due to the vertical correlation between the data in these sublayers. This correlation was accounted for through implementing a correlation coefficient between the spatial averages of CPT data over these sublayers into the simulation process, as discussed in Chapter 7.

8.4 STOCHASTIC ANALYSIS OF LIQUEFACTION SUSCEPTIBILITY

Stochastic analysis of liquefaction susceptibility of the ground at the Treasure Island site was performed by applying a deterministic empirical approach to different realizations of retrended cone tip resistance data, as illustrated in Chapter 7. The CPT-based empirical approach of Robertson and Wride (1998) was used in the analysis to correlate the cyclic resistance ratio, CRR, to the retrended CPT data. The retrended data were obtained by adding back the deterministic vertical trends to different realizations of detrended CPT tip resistance obtained from Monte Carlo simulations. On the other hand, the cyclic stress ratio, CSR, was assessed deterministically from earthquake magnitude and maximum recorded surface acceleration using the simplified approach of Seed and Idriss (1971). The CSR was assessed in a deterministic fashion as recording the maximum surface acceleration at the Treasure Island site implied a very little uncertainty associated with the application of Seed and Idriss empirical correlation. Consequently, the factor of safety against cyclic liquefaction was obtained stochastically through:

$$F.S = \frac{CRR}{CSR} \qquad (8\text{-}3)$$

Due to the stochastic nature of the CRR, applying the above relation resulted in histograms of the factors of safety for each of the potentially liquefiable layers, as shown in Figure 8.6 and Figure 8.7. A summary of the statistical characteristics of the factor of safety against cyclic liquefaction is presented in Table 8.3. The mean factors of safety were found to range between 1.02 and 4.37 for the Southwestern section, and between 0.99 and 1.37 for the Northeastern section. The coefficients of variation, COV, were assessed to range between 0.11 and 0.60 for the Southwestern section, and between 0.06 and 0.13 for the Northeastern section. The probabilities of failure (factor of safety less than unity) were found to range between 2.7% and 46.8% for the Southwestern section, and between 0.58% and 57.9% for the Northeastern section.

It is worth noting that the mean factors of safety against cyclic liquefaction were greater than unity for all of the potentially liquefiable layers at the Southwestern section, which exhibited different signs of liquefaction during the Loma Prieta earthquake. This implies that using mean values in liquefaction analyses can be on the unsafe (non-conservative) side as a result of ignoring the scatter in field data and their spatial correlation.

Embedment depths and thickness of potentially liquefiable layers play an important role in assessing their liquefaction potential. For example, two layers with same failure probability may have different impacts on the overall (macro) liquefaction potential if there is considerable difference in their thicknesses. Similarly, the influence of two potentially liquefiable layers with same failure probability on the overall liquefaction potential would be different if one layer is at 2 m deep and the other is 8 m deep below ground surface.

As a result, an estimate of equivalent failure probability was developed in Chapter 7 to take into consideration the effect of the thickness and embedment depth of different layers in the form:

$$P = P_{Fi} \cdot \frac{T_i / Z_i}{\sum T_i / Z_i} \qquad (8\text{-}4)$$

where: P is the equivalent failure probability of the site;

P_{Fi} is the failure probability of layer i;

T_i and is the average thickness of layer i; and

z_i is the vertical distance from ground surface to the center of layer i.

The equivalent failure probabilities for the Southwestern and Northeastern sections, where different signs of liquefaction were recorded during the Loma Prieta earthquake, were found to be 18.6% and 11.9% respectively. This is in agreement with the findings of Chapter 7, which identified a critical threshold range of 1.2% to 15% for the equivalent failure probability above which liquefaction is likely to occur. Based on these two case histories, the critical threshold for the equivalent failure probability appears to lie in the range 1.2% to 11.9%, but continued analysis of case histories is required to refine the selection of this value.

8.5 DAMAGE CRITERIA OF LIQUEFACTION

A major concern in liquefaction analysis is the impact of liquefaction occurrence in subsurface layers on overlying structures. Due to the complexity of the problem, few attempts have been made to quantify liquefaction induced surface damage. In this chapter, two damage criteria were adopted, Iwasaki et al. (1978) and Ishihara and Yoshimini (1992). Details of these two criteria are summarized in Chapter 7.

Iwasaki's damage criterion was applied to the 10,000 realizations of retrended CPT data, used in the previous section, and the total damage potential index, P_L, was determined at each CPT location. The results were then used to generate contours of the probability that P_L would exceed 5, a threshold associated with significant surface damage, as shown in Figure 8.8. The location of the sand boils encountered at the site after the earthquake, represented by the hatched zones in Figure 8.8, indicated that zones of surface damage were likely to be correlated with probability of ($P_L > 5$) greater than a threshold of 0.1%. This may be considered as a refinement of the 1.2% threshold suggested in Chapter 7 based on the study of the Wildlife site, California. Alternatively, this may question the validity of the P_L approach as a universal measure of quantifying liquefaction-induced damage. This can be attributed to the lack of physical meaning and the different assumptions associated with the approach, such as the linear variation of D (z) with depth.

Ishihara and Yoshimine (1992) proposed another damage criterion where liquefaction induced damage was correlated to surface settlement. It was suggested that significant surface damage was usually associated with a ground settlement of 10 cm or more. In order to apply this damage criterion, ground settlements were estimated under the effect of the Loma Prieta earthquake using Ishihara's empirical approach (1993). The 10,000 realizations of retrended CPT data were implemented in the analysis resulting in a settlement histogram at each CPT sounding. The mean settlements were found to range from 7.75 cm to 12.88 cm for the Southwestern section, and from 7.25 cm to 24.74 cm for the Northeastern section. The coefficients of variation were assessed to range from 0.36 to 0.54 for the Southwestern section, and from 0.24 to 0.46 for the Northeastern section. The settlement analysis results were used to compute the probability of occurrence of liquefaction-induced settlement greater than 10 cm, a value considered to be associated with significant surface damage. Contours of these probabilities are presented in Figure 8.9. This figure verified the findings of Chapter 7, where zones of surface damage were suggested to be correlated with a 12% probability, or more, of occurrence of settlement larger than 10 cm.

It is worth noting that the effect of non-uniformity of thickness of different layers on the variance reduction factors was accounted for by re-scaling of the outcome of Monte Carlo simulation at each CPT sounding location. The re-scaling process was carried out by transforming the outcome of Monte Carlo simulation from its original distribution to a reference distribution with the same type and mean value but with a modified variance that depends on layer thickness at each CPT sounding location, as discussed in Chapter 7.

8.6 STOCHASTIC ASSESSMENT OF LIQUEFACTION-INDUCED SETTLEMENT

Another important concern in liquefaction analysis is the ability to reliably predict liquefaction-induced settlement. The results of the stochastic settlement analysis, mentioned in the above section, were used to generate contours of the mean settlements across the site, as shown in Figure 8.10 and Figure 8.11. In addition, the readings of several settlement points at the site during the Loma Prieta earthquake were located on the contour lines as indicated by the hatched squares in Figure 8.10 and Figure 8.11. The recorded settlements were found to be greater than the computed mean values at some settlement points. This implies that the use of mean values in liquefaction-induced settlement analysis may be on the unsafe side, which can be attributed to possible presence of loose pockets resulting in low factors of safety and higher settlements. Alternatively, settlements associated with the upper and lower limits of the 90% confidence level were determined as risk-based estimates of liquefaction-induced settlement, as proposed in Chapter 7. Using these estimates in settlement assessment implies that there is only a 5% chance of having actual settlement either greater than the upper limit or smaller than the lower limit. Contours of settlements associated with the 90% confidence level were generated across both the Southwestern and Northeastern sections, as shown in Figure 8.10 and Figure 8.11, indicating that the use of these estimates embraced the recorded field settlements. Nevertheless, the wide range of

predicted settlements obtained from these estimates seems to be over-conservative and need to be verified and refined through the analyses of more case histories.

In addition, settlements associated with the upper and lower limits of the 80% confidence level were assessed as a less conservative risk-based estimates of liquefaction-induced settlements. Contours of these settlements, shown in Figure 8.10 and Figure 8.11, validated the applicability of these estimates to the Treasure Island site. However, this needs to be verified through applying these estimates to other potentially liquefiable sites.

8.7 USE OF REPRESENTATIVE DETERMINISTIC CPT PERCENTILES

The above methodology, while being amenable to engineering design, could be regarded as a relatively sophisticated process for engineers with limited statistical background. Moreover, relying on mean values may provide a non-conservative estimate of liquefaction potential as discussed in the previous sections. To overcome these issues, an attempt was made in Chapter 7 to ascertain whether more representative soil parameters could be determined that honor detailed ground heterogeneity and can be used more reliably in a simplified deterministic analysis. A characteristic percentile for liquefaction assessment purposes was found to be associated with the 0.085 percentile of q_c, i.e. the value of q_c below which 8.5 % of the q_c data occurred. It was suggested that using such percentile in a deterministic settlement analysis would not predict settlements greater than 10 cm anywhere across potentially liquefiable sites if the earthquake loading did not trigger liquefaction.

Following the above procedure, liquefaction-induced ground settlement was estimated at each CPT sounding location resulting in the contour maps shown in Figure 8.12. As seen from this figure, the computed settlements were greater than 10 cm everywhere across both sections of the Treasure Island site. This implied that both the

Southwestern and Northeastern sections of the Treasure Island site would liquefy under the effect of the Loma Prieta earthquake, which is in agreement with the actual case.

In a similar fashion, a characteristic percentile of cone tip resistance percentile was obtained in Chapter 7 to predict liquefaction-induced surface settlement associated with the upper limit of the 90% confidence interval. In other word, using this percentile in a simplified deterministic analysis will provide an estimate of surface settlement with a 5% chance that the actual settlement will exceed this estimate. The value of this percentile was found to range from 0.20 to 0.29 for cases where liquefaction would likely to occur. Upon using these percentiles for the Treasure Island site, contours of surface settlements were obtained, as shown in Figure 8.13 and Figure 8.14. Comparing these figures with Figure 8.10 and Figure 8.11 indicated that settlements obtained using these percentiles were in good agreement with those associated with the upper limit of the 90% confidence interval.

Alternatively, Robertson et al. (2000) proposed the use of mean values minus the standard deviation in liquefaction analyses as a risk-based estimate for CPT data. Upon applying this estimate in deterministic settlement analysis, contours of surface settlements were obtained, as shown in Figure 8.15. Comparing this figure with Figure 8.10 and Figure 8.11 indicated a reasonable agreement. However, the settlements predicted using this estimate were slightly outside the range associated the 90% confidence level. This might imply that the estimate of Robertson et al. (2000) is slightly on the over-conservative side and that the estimates proposed in this study are more refined explicit risk-based estimates for CPT data. It is worth noting that the above results validated the applicability of the representative CPT percentiles derived from the analysis of the Wildlife site in spite of the fact that both sections of the Treasure Island site showed different overall variabilities. These variabilities were assessed using an Overall Variability Factor (OVF), developed in Chapter 7 as a qualitative measure to compare the variability of potentially liquefiable sites. Sites with higher overall variability were expected to produce higher values of OVF.

- 250 -

The values of OVF were found to be 10.15 and 3.75 for the Southwestern and the Northeastern sections, respectively, compared with a value of 5.49 for the Wildlife site. This implies that the applicability of the characteristic CPT percentiles, developed in Chapter 7, is likely to be insensitive to the overall variability of CPT data recorded at potentially liquefiable sites. This could be attributed to the fact that all elements of soil spatial variability were taken into consideration while assessing the value of such estimates. In other words, it can be said that these estimates are normalized with respect to different elements of soil spatial variability. However, this needs to be investigated through the analysis of more liquefaction case histories.

8.8 CONCLUSIONS

The effect of ground heterogeneity on earthquake-induced ground response at the Southwestern and Northeastern part of the Treasure Island Site was investigated in this chapter. This was carried out through assessment of different ground lithologies and applying geostatistical principles to estimate elements of soil spatial variability using the results of several CPT soundings conducted at the site.

This chapter validated the applicability of the equivalent probability of failure concept, developed in Chapter 7, as a more rational technique to assess liquefaction potential. This technique takes into consideration the effect of embedment and thickness of liquefiable layers on their probability of failure. A critical threshold for equivalent failure probability, ranging between 1.2% and 12%, was identified for potentially liquefiable sites, above which liquefaction would likely occur.

For the conditions at the Treasure Island site, it was found that surface damage zones were likely to be associated with a 0.1% probability, or higher, that total liquefaction damage, P_L, will exceed 5. This value is not in agreement with the 1.2% probability threshold suggested in Chapter 7 from a previous analysis of the Wildlife

- 251 -

Site. The significant disparity between these values provides little insight into the damage approach. Alternatively, the wide range in threshold probability values may cast some doubt on the P_L approach as a universal measure of quantifying liquefaction-induced damage. Clearly, additional case histories must be analyzed to reach a formal conclusion regarding the P_L approach. On the other hand, this chapter validated the recommendation of Chapter 7 that surface damage zones were likely to be associated with a 12% probability, or higher, that liquefaction-induced settlement will be greater than 10 cm.

The use of mean value of CPT data in liquefaction analysis was found to be on the unsafe (non-conservative) side. This was indicated by the results of the settlement analysis at the site, where mean settlements were found to be smaller than the actual settlement recorded during the 1989 Loma Prieta earthquake. This could be attributed to possible presence of looser pockets within the soil mass, which results in smaller factors of safety against liquefaction and consequently larger settlements.

This chapter verified the applicability of the characteristic CPT percentiles developed in Chapter 7. These percentiles could be considered as risk-based estimates of characteristic cone tip resistance, which can be used in simplified deterministic analyses to predict liquefaction susceptibility and ground settlement, while continuing to honor detailed ground heterogeneity. Nevertheless, more efforts are needed to refine and verify these representative values through the analyses of more case histories.

8.9 REFERENCES

Andrus, R. D. and Stokoe, K. H. II. 2000. Liquefaction evaluation of densified sand at Treasure Island, California. National Geotechnical Experimentation Sites. Geotechnical Special publication No.93, pp. 264-278.

Benjamin, J. R. and Cornell, C. A. 1970. Probability, statistics, and decision for civil engineers. McGraw-Hill, New York, USA.

Bennett, M. J. 1998. Sand boils and settlement on Treasure Island after the earthquake. The Loma Prieta, California Earthquake of October 17, 1989 - Liquefaction, U.S. Geological Survey Professional Paper 1551-B, pp. 121-128.

Deutsch, C. V. 2002. Geostatistical reservoir modeling. Oxford University press.

Deutsch, C. V. and Journel, A. G. 1998. GSLIB geostatistical software library. Oxford University press.

Fenton, G. A. and Vanmarcke, E. H. (1991). Spatial variation in liquefaction risk assessment. Proceedings of the geotechnical Engineering Congress, Boulder, Colorado, USA. Geotechnical Special Publications, No. 27, Vol.1, pp. 594-607.

Ishihara, K. 1993. Liquefaction and flow failure during earthquakes. Geotechnique, 43 (3): 351-415.

Ishihara, K. and Yoshimine, M. 1992. Evaluation of settlements in sand deposits following liquefaction during earthquakes. Soils and Foundations, 32 (1): 178-188.

Iwasaki, T., Tatsuoka, F., Tokida, F., and Yasuda, S. 1978. A practical method for assessing soil liquefaction potential based on case studies at various sites in Japan. Proceedings of the Second Conference on Microzonation, San Francisco, CA, USA, Vol. (2), pp. 885-896.

Luna, R. and Frost, J. D. 2000. Treasure Island's spatial liquefaction evaluation. National Geotechnical Experimentation Sites. Geotechnical Special publication No.93, pp. 306-320.

Palisade Corporation. 1996. @Risk: Risk analysis and simulation add-in for Microsoft Excel or Lotus 1-2-3. Palisade Corporation, NY, USA.

Popescu, R., Prevost, J. H., and Deodatis, G. 1998. Characteristic percentile of soil strength for dynamic analysis. Proc. of the 1998 Conf. on Geotechnical Earthquake Eng. and Soil Dynamics III, Part 2 (of 2), Seattle, WA, USA, pp. 1461-1471.

Power, M.S., Egan, J. A., Shewbridge, S. E., Debecker, J., and Faris, J. R. 1998. Analysis of liquefaction induced damage on Treasure Island. The Loma Prieta, California Earthquake of October 17, 1989 - Liquefaction, U.S. Geological Survey Professional Paper 1551-B, pp. 87-119.

Robertson, P. K. 1990. Soil classification using the cone penetration test. Canadian Geotechnical Journal, 27 (1): 151-158.

Robertson, P. K. and Wride, C. E. 1998. Evaluating cyclic liquefaction potential using the cone penetration test. Canadian Geotechnical Journal, 35 (3): 442-459.

Robertson, P.K., (Fear) Wride, C.E., List B.R., Atukorala, U., Biggar, K.W., Byrne, P.M., Campanella, R.G., Cathro, D.C., Chan, D.H., Czajewski, K., Finn, W.D.L., Gu, W.H., Hammamji, Y., Hofmann, B.A., Howie, J.A., Hughes, J., Imrie, A.S., Konrad, J-M., Küpper, A., Law T., Lord, E.R.F., Monahan, P.A., Morgenstern, N.R., Phillips, R., Piché, R., Plewes, H.D., Scott, D., Sego, D.C., Sobkowicz, J., Stewart, R.A., Watts, B.D., Woeller, D.J., Youd, T.L., and Zavodn, Z. 2000. "The CANLEX project: summary and conclusions". Canadian Geotechnical Journal, 37 (3), 563-591Seed, H. B. and Idriss, I. M. 1971. Simplified procedure for evaluating soil liquefaction potential. Journal of the Soil Mechanics and Foundation Division, ASCE, 97, SM(9): 1249-1273.

Tokimatsu, K. and Seed, H. B. 1987. Evaluation of settlements in sands due to earthquake shaking. Journal of the Geotechnical Engineering Division, ASCE, 113, GT(8): 861-878.

Vanmarcke, E. 1977. Probabilistic modeling of soil profiles. Journal of the Geotechnical Engineering Division, ASCE, 103 GT(11): 1227-1245.

Vanmarcke, E. H. 1984. Random fields, analysis and synthesis. MIT Press, Cambridge, MA, USA.

Table 8.1. Geostatistical properties of detrended CPT tip resistance for different potentially liquefiable layers at the Treasure Island.

Layer	Mean (kPa)	Standard Deviation (kPa)	Variogram Characteristics		
			Model[*]	Vertical Range (m)	Horizontal Range (m)
L_{1A}	-0.53	4185	Exponential	2.20	37.00
L_{2A}	-0.05	645	Exponential	0.85	14.50
L_{3A}	0.35	4299	Exponential	0.85	14.50
L_{4A}	0.04	1360	Exponential	0.95	16.00
L_{5A}	0.08	985	Spherical	0.80	13.50
L_{1B}	-0.06	1229	Exponential	0.90	15.50
L_{2B}	-0.01	627	Exponential	1.50	25.50
L_{3B}	-0.25	1707	Exponential	0.90	15.50
L_{4B}	-0.04	744	Exponential	0.55	9.50

[*] for both horizontal and vertical directions

Table 8.2. Variance reduction factor for different potentially liquefiable layers at the Treasure Island site.

Layer	L_{1A}	L_{2A}	L_{3A}	L_{4A}	L_{5A}	L_{1B}	L_{2B}	L_{3B}	L_{4B}
Average thickness (m)	1.12	0.78	0.99	1.52	1.80	4.19	1.78	2.41	1.64
Number of horizontal segments	2	3	3	4	3	12	3	7	8
Variance reduction factor	0.79	0.75	0.70	0.70	0.70	0.70	0.70	0.71	0.71

Table 8.3. A summary of statistical characteristics of the factor of safety against cyclic liquefaction for different potentially liquefiable layers at the Treasure Island site.

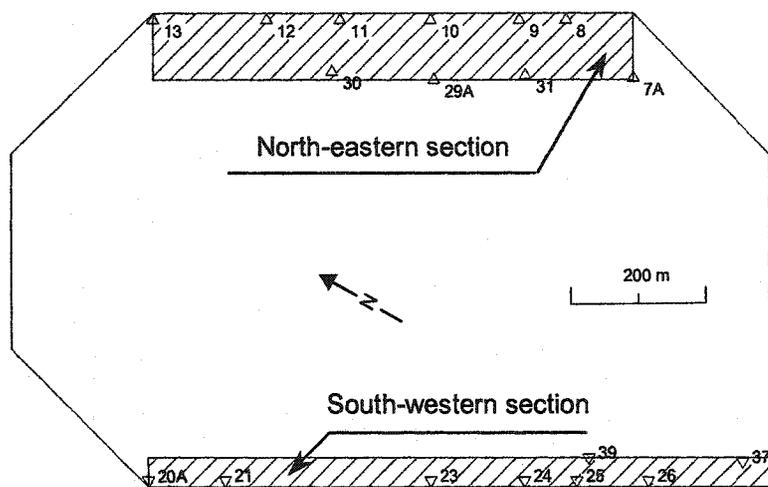| Layer	L_{1A}	L_{2A}	L_{3A}	L_{4A}	L_{5A}	L_{1B}	L_{2B}	L_{3B}	L_{4B}
Mean	2.57	1.02	4.37	1.35	1.07	1.26	0.99	1.37	1.06
Coefficient of variation	0.60	0.11	0.46	0.14	0.14	0.08	0.08	0.13	0.06
Probability of failure (%)	14.82	46.81	3.83	2.72	33.70	0.58	57.87	1.99	15.60

Figure 8.1. Layout of CPT data locations at the Treasure Island site.

(a)

(b)
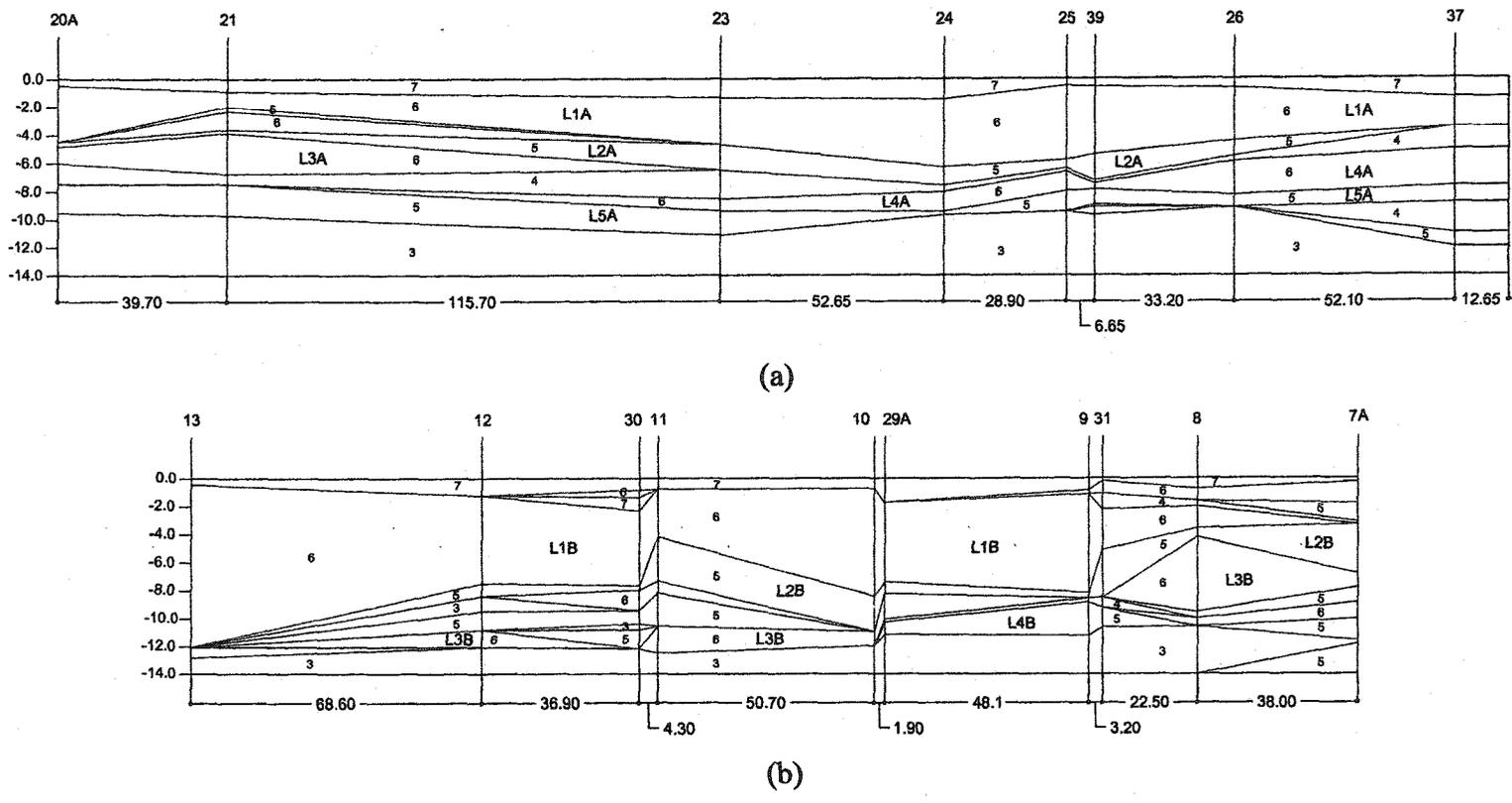
Figure 8.2. A longitudinal view showing the lithological distribution across the Treasure Island site. (a) South-western section; and (b) North-eastern section. (positions of CPT soundings are shown in Figure 1; and numbers represent soil behavior type based on soil behavior type index I_c)
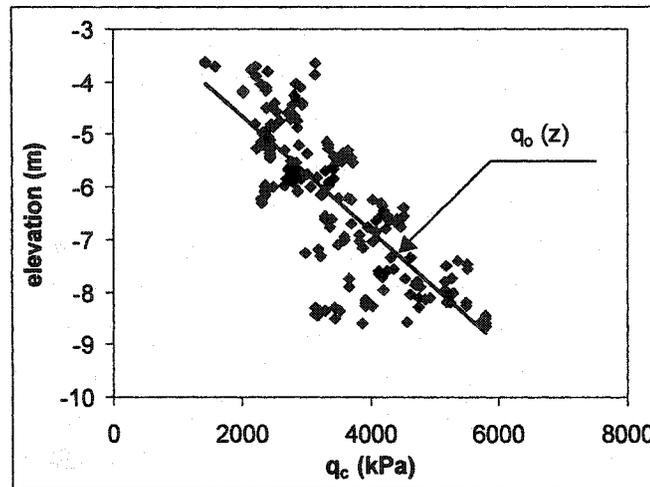
(a)
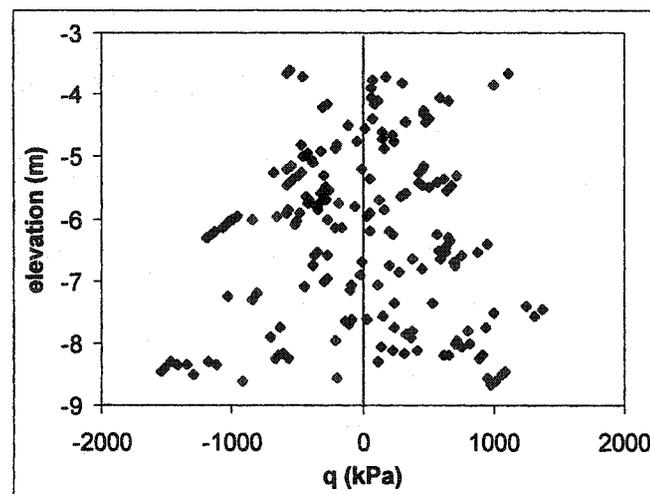
(b)

Figure 8.3. Detrending of cone tip resistance data for layer L2A. a) identifying linear vertical trend; and b) detrended data.
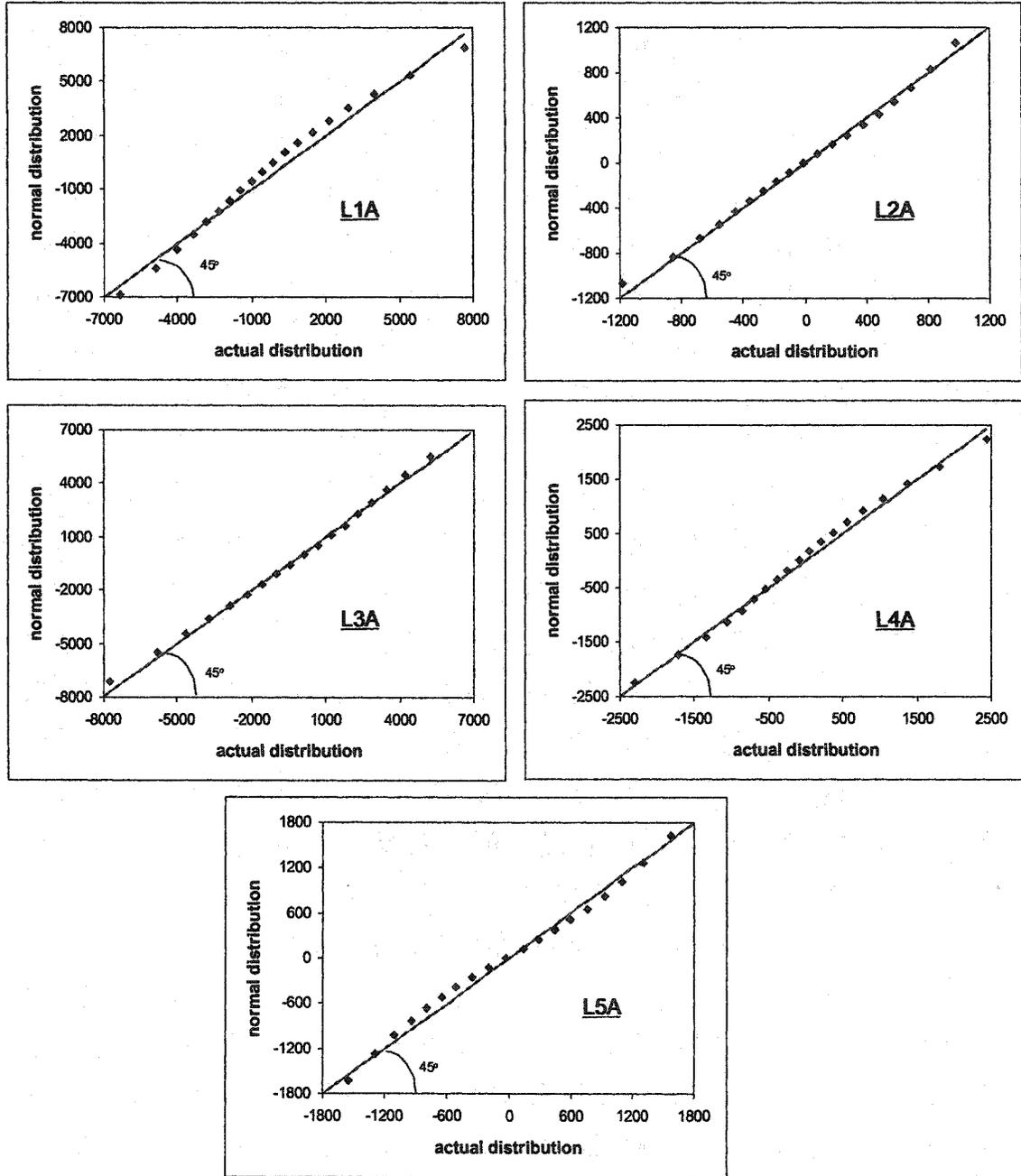
Figure 8.4. Assessment of the agreement between probability distributions of detrended CPT data and normal distribution using Q-Q plots for the Southwestern section of the Treasure Island site.
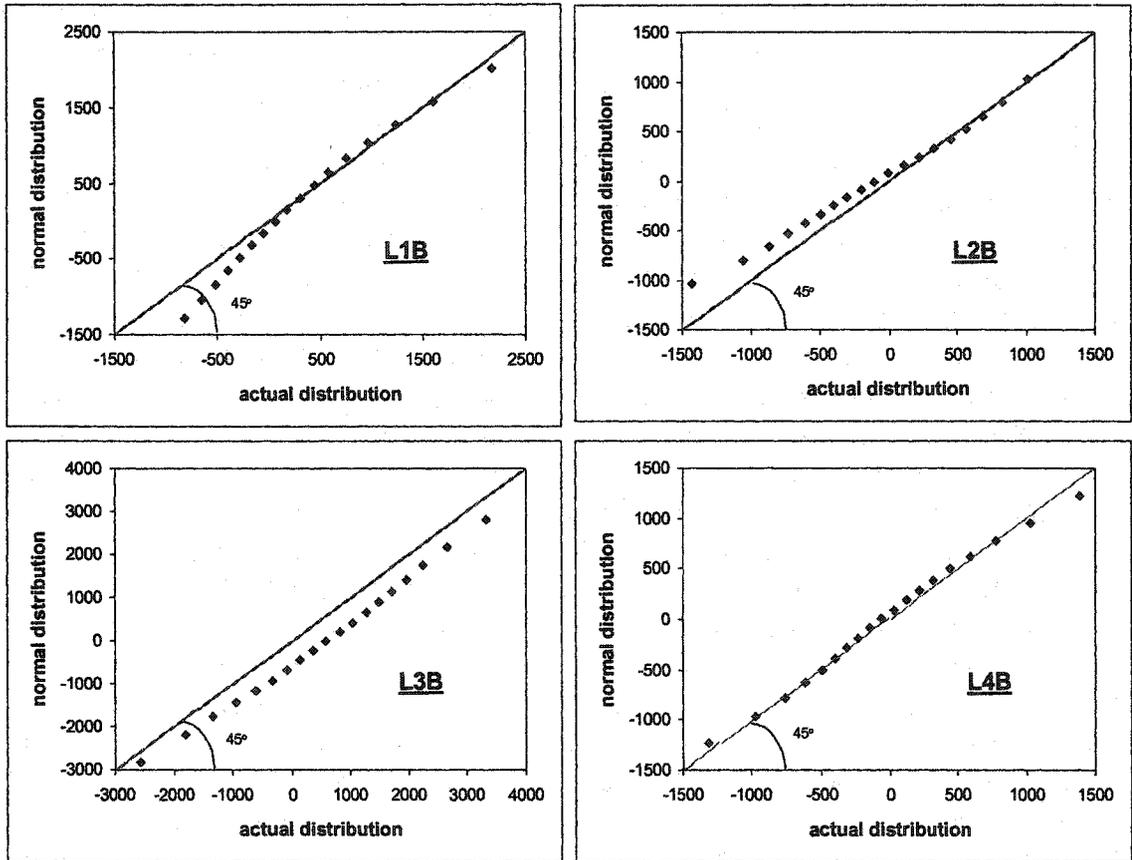
Figure 8.5. Assessment of the agreement between probability distributions of detrended CPT data and normal distribution using Q-Q plots for the Northeastern section of the Treasure Island site.
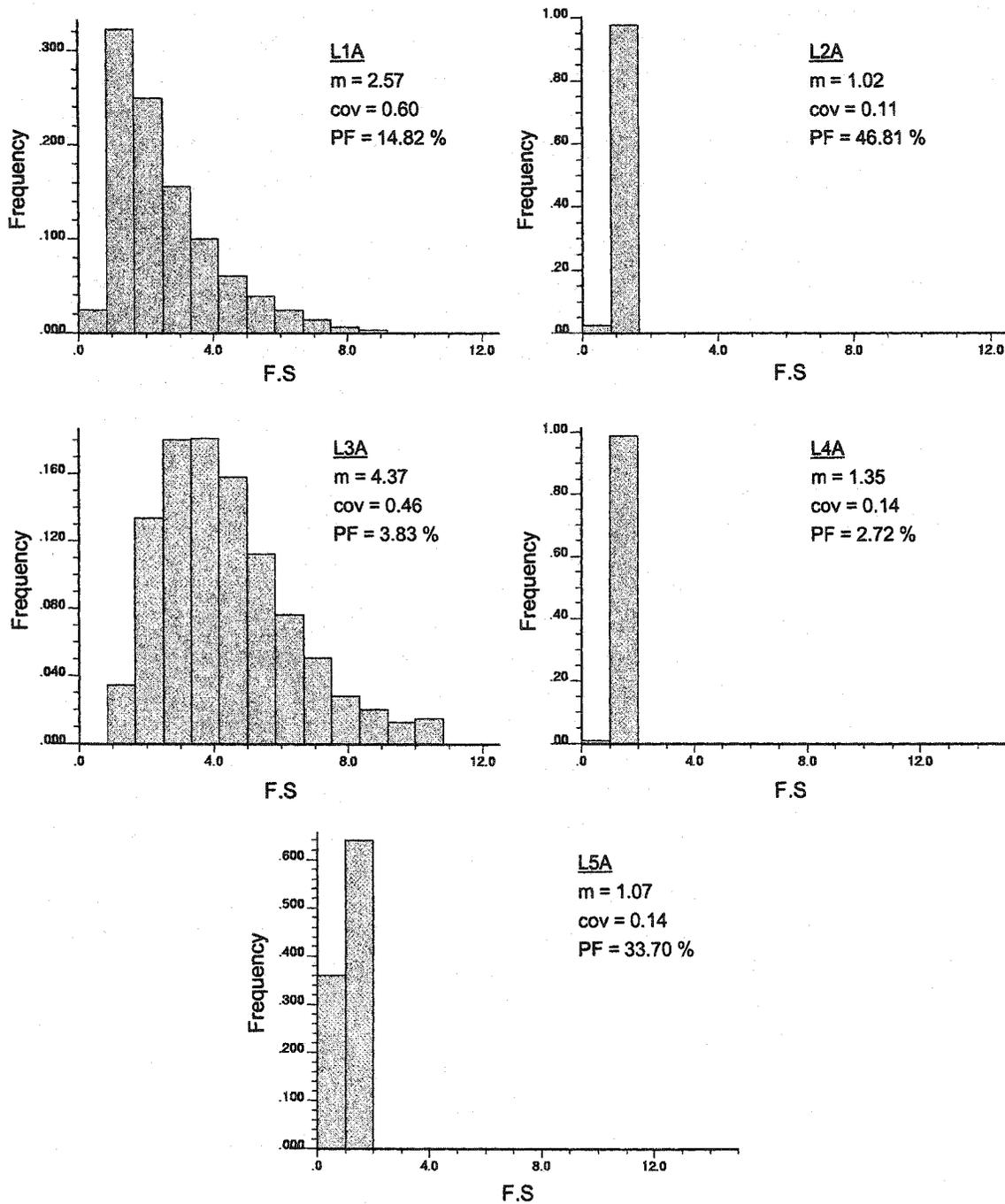
Figure 8.6. Histograms of factors of safety against cyclic liquefaction for the Southwestern section of the Treasure Island site.
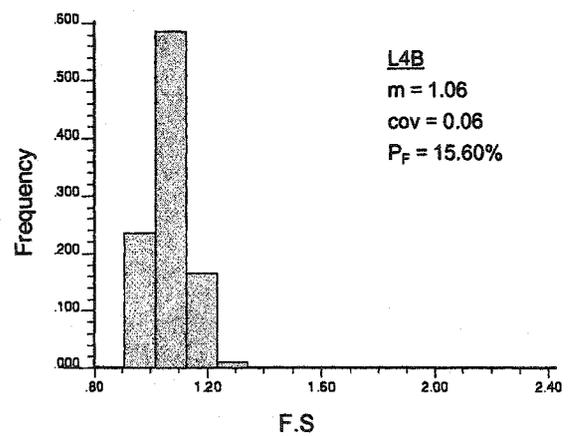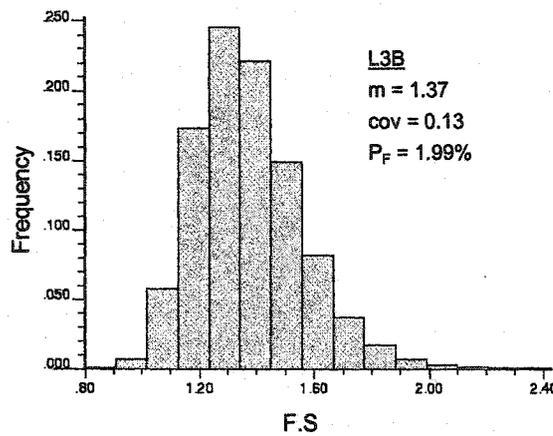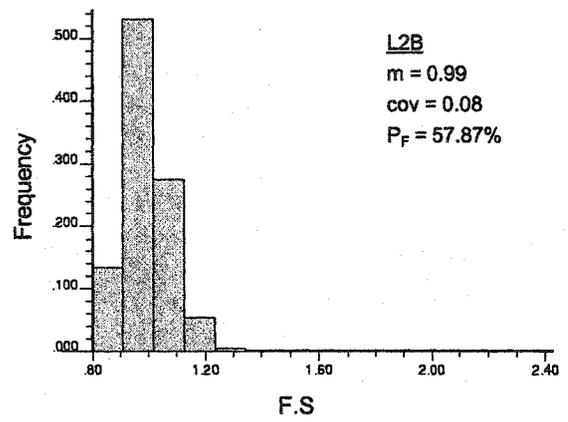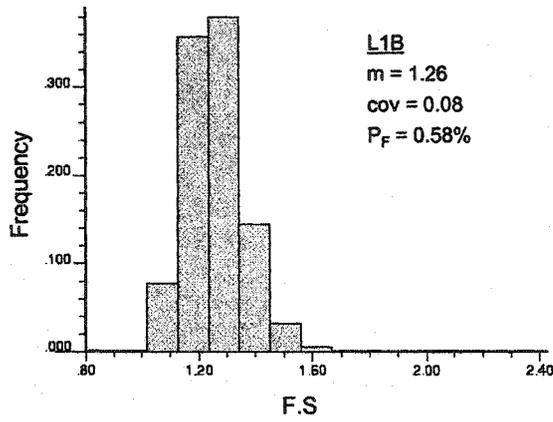
Figure 8.7. Histograms of factors of safety against cyclic liquefaction for the Northeastern section of the Treasure Island site.
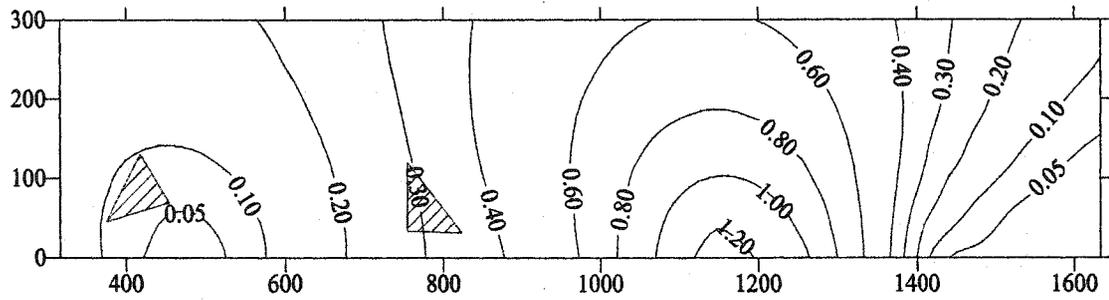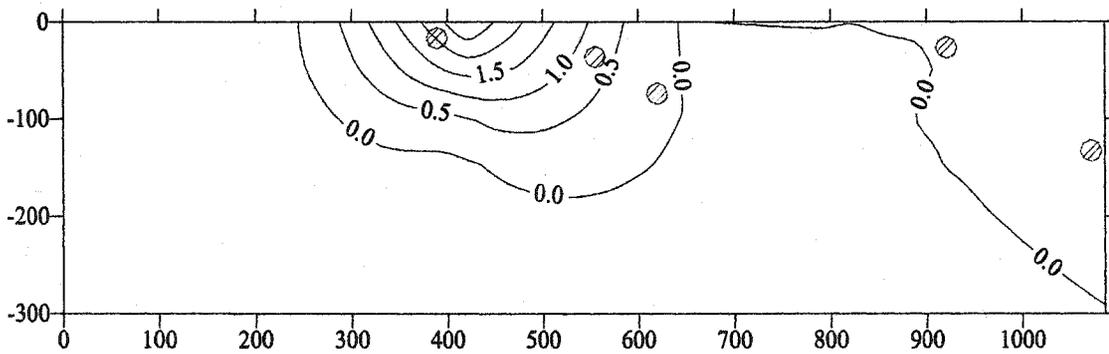
Figure 8.8. A site plan showing contours of probability of occurrence of total liquefaction damage potential (P_L) greater than 5 for the Loma Prieta earthquake (hatched zones indicate observed sand boils at the site). Dimensions are in meters. a) Southwestern section; and b) Northeastern section.

- 264 -
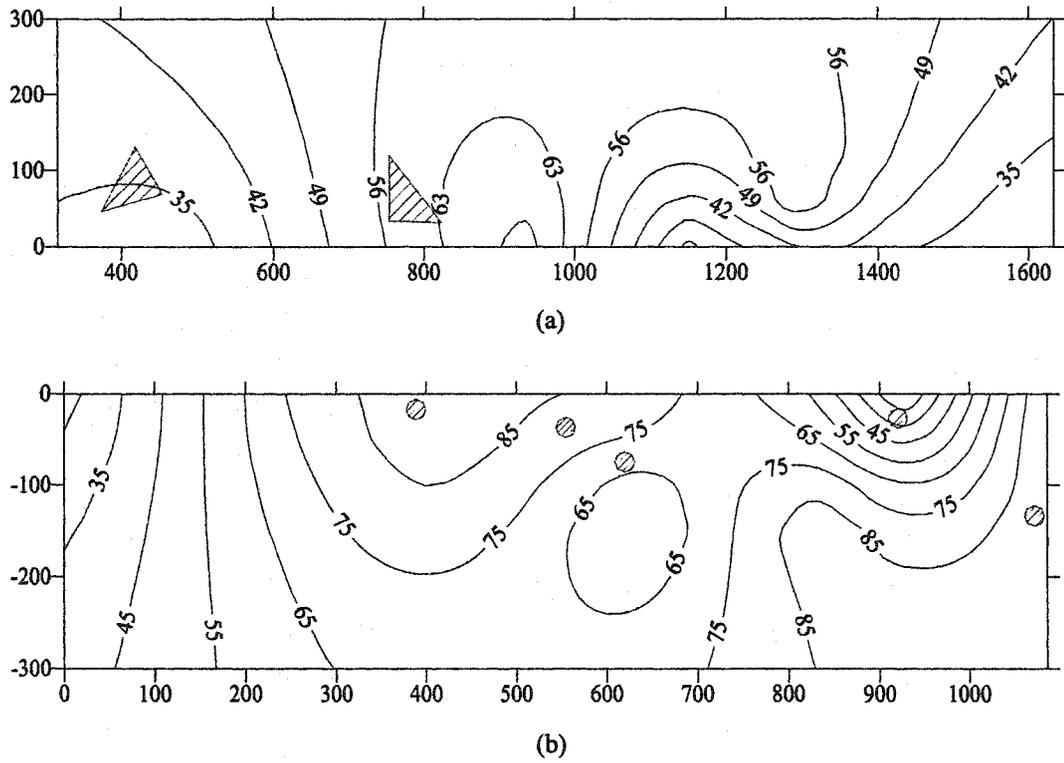
Figure 8.9. A site plan showing contours of probability of occurrence of liquefaction-induced settlement greater than 10 cm for the Loma Prieta earthquake (hatched zones indicate observed sand boils at the site). Dimensions are in meters. a) Southwestern section; and b) Northeastern section.
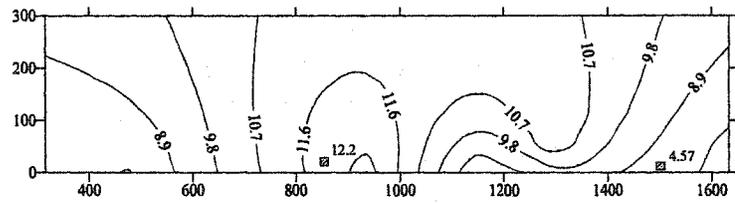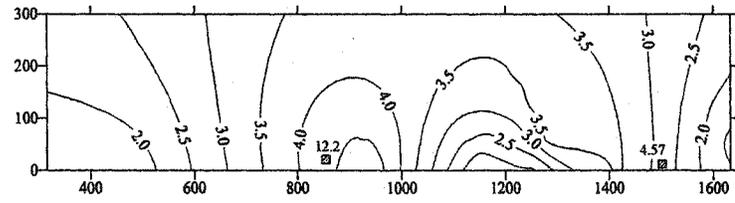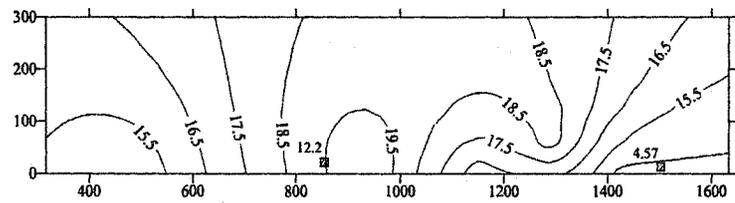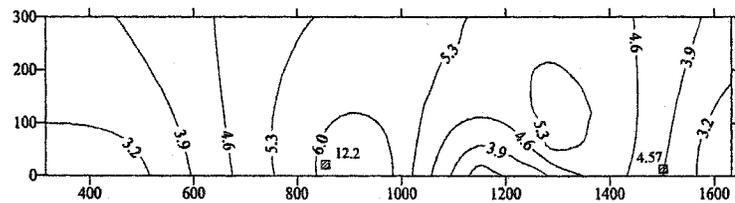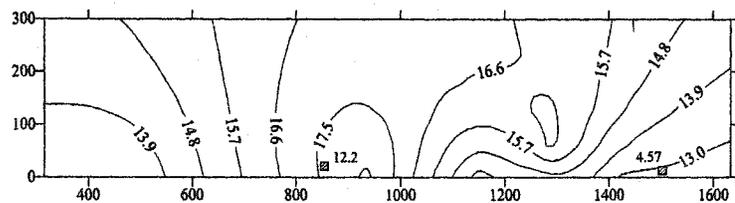
Figure 8.10. A site plan showing contours of computed settlements (in cm) across the Southwestern section of the Treasure Island site. a) mean settlement; b) lower limit of 90% confidence interval; c) upper limit of 90% confidence interval; d) lower limit of 80% confidence interval; and e) upper limit of 80% confidence interval.

- 266 -
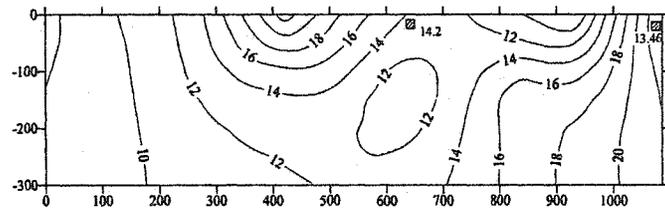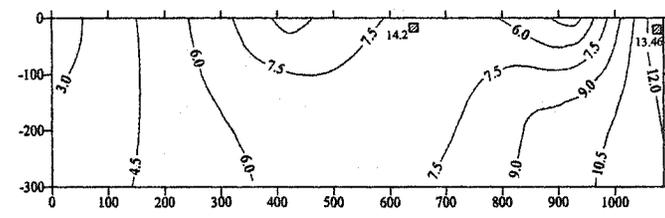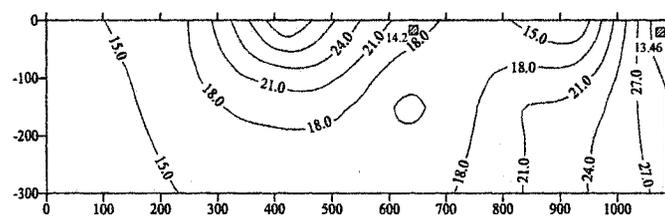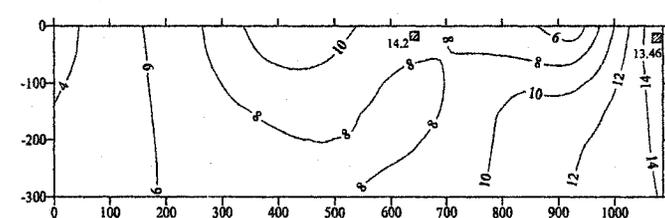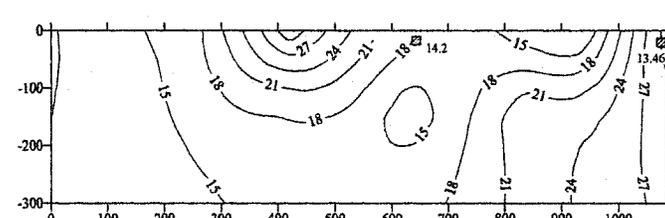
Figure 8.11. A site plan showing contours of computed settlements (in cm) across the Northeastern section of the Treasure Island site. a) mean settlement; b) lower limit of 90% confidence interval; c) upper limit of 90% confidence interval; d) lower limit of 80% confidence interval; and e) upper limit of 80% confidence interval.

- 267 -
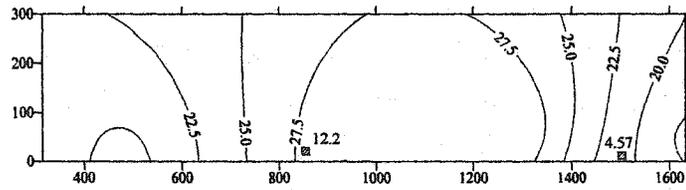
(a)
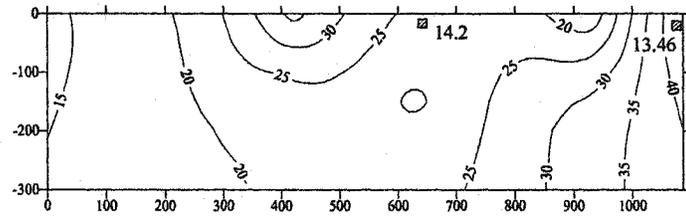
(b)

Figure 8.12. A site plan showing contours of computed settlements (in cm) across the Treasure Island site using the 0.085 percentile of the CPT tip resistance data. a) Southwestern section; and b) Northwestern section.
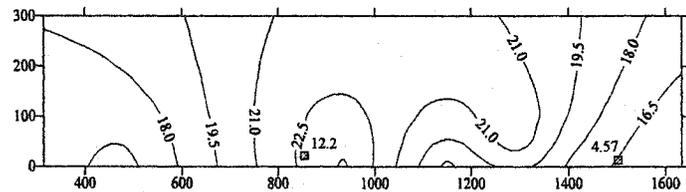
(a)
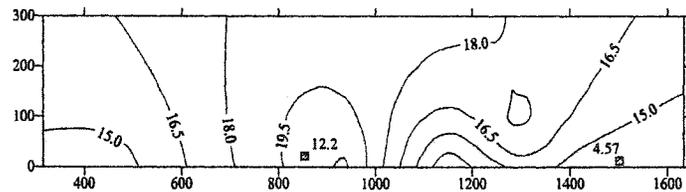
(b)

Figure 8.13. A site plan showing contours of computed settlements (in cm) across the Southwestern section of the Treasure Island site using characteristic CPT tip resistance percentiles. a) 0.20 percentile; and b) 0.29 percentile.
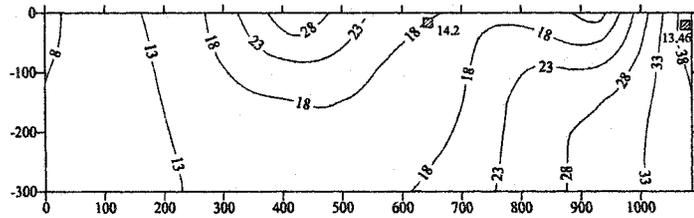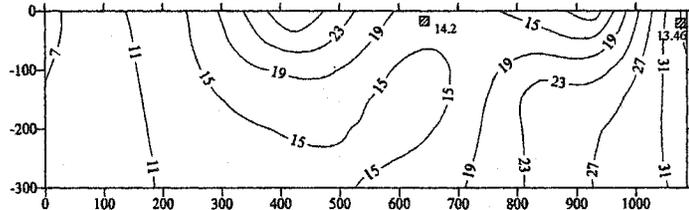
Figure 8.14. A site plan showing contours of computed settlements (in cm) across the Northeastern section of the Treasure Island site using characteristic CPT tip resistance percentiles. a) 0.20 percentile; and b) 0.29 percentile.
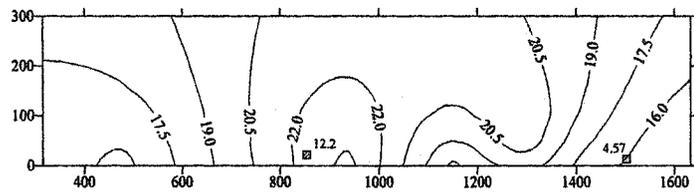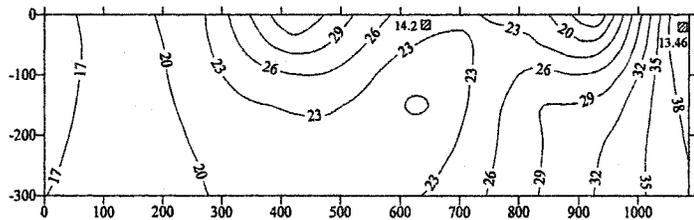
Figure 8.15. A site plan showing contours of computed settlements (in cm) using (m-σ) as a characteristic CPT tip resistance (Robertson et al. 2000). a) Southwestern section; and b) Northwestern section.

- 269 -

CHAPTER 9

GEOSTATISTICAL ANALYSIS OF LIQUEFACTION INDUCED GROUND RESPONSE AT THE MARINA DISTRICT

9.1. INTRODUCTION

Most soils are heterogeneous in nature either due to the presence of different lithologies or as a result of their inherent spatial variability. This heterogeneity can have a profound effect on ground response under earthquake loading, as discussed by Fenton and Vanmarcke (1991), Popescu et al (1998). Quantitative treatment of this variability is important, as classical deterministic analyses can not account for the scatter of field data and their spatial correlation, which may result in the presence of continuous pockets of looser sand highly susceptible to liquefaction. Well-documented case histories provide an opportunity to explore options of quantifying the effect of soil heterogeneity on liquefaction-induced ground response. A good example of this type of case histories is the Marina District site, California, where different signs of liquefaction, such as sand boils, lateral spreads, building destruction and surface settlements, were recorded at the site during the 1989 Loma Prieta earthquake.

Several studies have been carried out to investigate the ground response at the Marina District during the 1989 Loma Prieta earthquake making it one of the most comprehensively studied liquefaction case histories. Pease and O'rourke (1997) performed one-dimensional linear seismic response analysis of the Marina District using the SHAKE software. Bardet et al. (1992) compared the results of one-dimensional linear seismic response with two-dimensional and non-linear analyses and concluded that the maximum surface acceleration predicted using one-dimensional analysis could be on the

- 270 -

non-conservative side. Bardet and Kapuskar (1993) carried out an extensive survey of different forms of liquefaction-induced damage in the Marina District with emphasis on sand boils. O'rourke and Pease (1992) conducted a comprehensive assessment of liquefaction-induced deformations and their effect on lifeline performance. O'rourke and Pease (1997) carried out a study to develop a correlation between seismic hazards in terms of liquefaction induced settlement and lateral spread, and thickness of potentially liquefiable layers. Moreover, they developed contours of the settlements at the Marina District after the Loma Prieta earthquake from different surveys carried out by the city of San Francisco.

To the author's knowledge, the only attempt made to quantify the effect of spatial variability of soil properties at the Marina District on its seismic response was that of Rollins and McHood (1998). The mean plus/minus the standard deviation of the Standard Penetration Test results were implemented in Seed and Tokimatsu (1987) empirical settlement approach to obtain a risk-based range of expected settlement at the site. A reasonable agreement was obtained between the predicted and recorded settlements. However, this was not done in a probabilistic framework and as a result the effect of extreme value statistics was not accounted for. In addition, the spatial correlation between soil properties and its implications on expected settlement was not taken into consideration.

In this chapter, a geostatistical approach was adopted to assess the effect of lithological heterogeneity and spatial variability of soil properties on the ground response at the Marina District during the 1989 Loma Prieta earthquake. Cone Penetration Test results were used to identify different ground lithologies implementing the soil behavior type index, I_c, (Robertson 1990). Different geostatistical characteristics, such as mean, variance, and spatial correlation structures, were estimated for each of these lithologies. The cyclic stress ratio – cyclic resistance ratio (CSR-CRR) approach (Robertson and Wride 1998) was employed stochastically to estimate the liquefaction susceptibility of the ground, expressed in terms of the factor of safety against cyclic liquefaction. This was

carried out by implementing Monte Carlo simulation techniques to obtain several realizations of the CPT data, which were used to estimate the value of CRR. On the other hand, the earthquake loading was assessed deterministically using simplified techniques that correlated the CSR to the earthquake magnitude and the maximum surface acceleration recorded at the site. In addition, different procedures were used to assess the level of liquefaction damage, such as total damage potential (P_L) and settlement criteria. Finally, representative cone tip resistance values developed from the analysis of the Wildlife site in Chapter 7 were applied to examine their applicability to the Marina District. These representative values were thought to be suitable for use in simplified deterministic empirical liquefaction analyses, while continuing to honor detailed ground heterogeneity.

9.2. BACKGROUND ON THE MARINA DISTRICT

The Marina District is located on the north end of San Francisco at a distance of 107 km from the epicenter of the Loma Prieta earthquake. The geology at the site was described by many authors, such as Rollins and McHood (1998), based on the results of an extensive field investigation program. The upper most layer, which extends to a depth of 4 to 7 m below ground surface, can be divided into 3 distinct units, as shown in Figure 9.1, which are:

1. Natural ground associated with the original shoreline in 1857 (section C) consisting primarily of beach and sand bar deposits;

2. Land and barge tipped sand fill, which was backfilled in the site as a part of the construction of a seawall and an earthen mole between 1857 and 1912 (section B); and

3. Hydraulic fill, mostly sand with some zones of fine-grained soils, which was obtained from several borrow pits in San Francisco Bay and dumped in the lagoon enclosed by the seawall as a part of reclamation projects in preparation for the 1915 Panama Pacific International Exhibition (section A).

Different units of surface layers are underlain by soft to medium clay (Holocene bay mud) up to a depth of 11 to 14 m followed by dense cemented sand (hardpan) up to depth of 22 to 25 m. The hardpan is underlain by stiff clay (Pleistocene bay mud) up to a depth of 74 to 77 m followed by bedrock. The ground water table (GWT) was found at a depth of 2.4 m below the flat area immediately to the south of San Francisco Bay.

The Loma Prieta earthquake, Richter magnitude of 7, hit the Marina District in 1989 causing a devastating damage, where 10 people died and another 40 were injured along with the destruction of more than 40 houses. Different signs of liquefaction were recorded at the site during the earthquake in the form of buckling of sidewalks, tension cracks and more than 74 sand boils. Almost all of these damages were restricted to the hydraulic fill area (section A) except for the buckling of two side walks in section C. This buckling was likely a result of lateral spread of the liquefied section A rather than a manifestation of liquefaction of underlying potentially liquefiable layers in section C. However, the most severe structural damage occurred on the boundary between the hydraulic fill and other units as a result of considerable differential settlement. In addition, lateral spreads up to 30 cm and vertical settlements more than 12.5 cm were recorded in section A, compared with negligible lateral spreads and settlements less than 2.5 cm in section C. Based on these field observations and a site visit by Peter K. Robertson, it is believed that only section A of the Marina District liquefied during the Loma Prieta earthquake.

It should be noted that there were no records available of the ground acceleration at the Marina District during the Loma Prieta earthquake. However, several records of bedrock and surface acceleration were recorded at different locations in the vicinity of the Marina District. These records were used to obtain the design maximum surface acceleration used in the liquefaction analyses, as illustrated in the subsequent sections.

9.3. CHARACTERIZATION OF GROUND HETEROGENEITY

The area under investigation is bounded by Marina Boulevard, Francisco, Fillmore and Baker Streets in the north, south, east and west, respectively. Only the section underlain by hydraulic fill (section A) and that underlain by natural deposits (section C) were considered where a reasonable amount of CPT soundings were available, as shown in Figure 9.1. Characterization of ground heterogeneity at these two sections was carried out through three main stages. In the first stage, standardization and filtration procedures were implemented to the CPT data. In the second stage, geostatistical characteristics of the standardized data were obtained. Finally, stochastic simulation of the standardized data was performed in the third stage. Details of these stages are discussed in the following sections.

9.3.1. Standardizing Cone Penetration Test Data

The results of several cone penetration tests soundings, shown in Figure 9.1, were used to characterize both the lithological heterogeneity and the spatial variation of soil properties for sections A and C of the Marina District. These CPT sounding were conducted by the United States Geological Survey (USGS), denoted by M1 to M8, and by the University of Southern California, denoted by C1 to C4. The cone data were used to identify different ground lithologies using the soil behavior type index, I_c, which can be used to classify soils according to their behavior type (Robertson 1990). As a result, a detailed west-east ground profile was obtained, as shown in Figure 9.2, where four cohesionless soil layers below GWT, L_{1A}, L_{2A}, L_{3A} and L_{4A}, were considered as potentially liquefiable zones for section A. Similarly, four layers, L_{1B}, L_{2B}, L_{3B}, and L_{4B}, were identified as potentially liquefiable zones for section C. Each of these layers was treated as a statistically homogeneous domain, where the cone tip resistance, q_c, was treated as a random variable. On the other hand, cohesive soils associated with $I_c > 2.6$, denoted by soil behavior types 2, 3, and 4, were assumed to be non-liquefiable layers (Robertson and Wride 1998).

- 274 -

Data filtration is an important process where outliers are identified and excluded from field data to maintain statistical consistency (Campanella et al. 1987). Outliers can be manifested in the form of spikes in CPT profiles at certain depths, which can be attributed to presence of pieces of gravel at the cone tip. These spikes should not be considered representative of soil characteristics underneath the cone tip. Data filtration was carried out following the procedure presented in Chapter 7.

A necessary condition for stochastic analyses is stationarity, which implies that the mean and variance of random variables are constants along the analysis domain. It can be expected, however, that CPT data will exhibit vertical trends due to their sensitivity to changes in effective confining pressure. In order to use the tip resistance, q_c, as a random variable and meet the stationarity condition, any possible vertical trend in q_c should be removed (detrended). To achieve this, filtered data from all CPT soundings were utilized to identify deterministic linear vertical trends in q_c within each of the potentially liquefiable layers using linear regression analysis. Then, these trends were removed, as illustrated in Figure 9.3 for layer L_{2A}, producing the detrended data through the relation:

$$q = q_c - q_o(z) \qquad\qquad (9\text{-}1)$$

where q is the detrended cone tip resistance and $q_o(z)$ is the deterministic vertical trend.

9.3.2. Statistical Properties of Detrended CPT Data

To proceed with stochastic analyses, statistical characteristics of random variables, such as mean, variance, probability distribution and correlation structure, have to be determined. A summary of the statistical characteristics of detrended CPT tip

resistance for different potentially liquefiable layers is presented in Table 9.1. The mean values were found to be around zero, as expected, whereas the standard deviations ranged from 380 kPa to 4420 kPa. The probability distributions were in close agreement with normal distributions for all of the potentially liquefiable layers. This was assessed using Q-Q plots (Deutsch 2002), as shown in Figure 9.4 for layers L_{1A} and L_{1B}. These Q-Q plots are comparisons between quantiles that correspond to certain percentiles of the random variable obtained from the actual distribution of field data, and those of a reference distribution such as the normal distribution in this case. If the cross plot between the two sets of quantiles results in points close to a 45 degree line, this indicates a similar shape and variance of both distributions.

Soil properties do not vary randomly in space; rather such variation is gradual and follows a pattern that can be quantified using what is called spatial correlation structure. In this study, variogram functions (Deutsch 2002) were adopted as measures of quantifying spatial correlation between detrended CPT data. The GSLIB Geostatistical Software Library (Deutsch and Journel 1998) was used to obtain the variogram characteristics, such as the model and spatial range, in the vertical direction for each of the potentially liquefiable layers, as shown in Table 9.1. It should be noted that insufficient data was available to quantify the variogram characteristics of layers L_{3A}, L_{3B} and L_{4B}. As a result, it was assumed that layer L_{3A} had the same variogram characteristics as layer L_{2A} and layers L_{3B} and L_{4B} had variogram characteristics similar to layer L_{2B}.

One limiting boundary condition required to use GSLIB to obtain the variogram is that each of the layers considered has to be rectangular in shape. Consequently, a coordinate transformation process was carried out producing transformed rectangular profiles for the potentially liquefiable layers that retain their actual spatial continuity and are amenable to analysis within GSLIB. Details of this transformation process are presented in Chapter 7.

Reproduced with permission of the copyright owner. Further reproduction prohibited without permission.

It is worth noting that the available CPT data were not sufficient to reliably assess the variogram characteristics in the horizontal direction. As a result, it was assumed that the horizontal variogram had the same model type as the vertical one, but with a larger range as suggested by Deutsch (2002). A ratio of 17 between horizontal and vertical spatial ranges was assumed in this chapter, based on the analysis of the Wildlife site in Chapter 7.

9.3.3. Stochastic Simulation of Detrended CPT Data

To quantify the effect of soil spatial variability, several realizations of detrended CPT data were obtained for each of the potentially liquefiable. This was carried out implementing Monte Carlo simulation using the @Risk software (Palisade Corporation 1996). The number of realizations used in the analysis, about 10,000, was assessed through specifying an acceptable tolerance of 0.50% between the input distributions and the distributions of the sampled values obtained from Monte Carlo simulation.

It should be emphasized that the point variance of field data, shown in Table 9.1, was not used in the stochastic simulation as the variation of soil properties at a single point in space usually has a minor impact on soil macro behavior under earthquake loading. Rather, such behavior is influenced by averaged soil parameters over certain critical volumes of interest. As a result, the variance of the spatial average of CPT data over selected averaging volumes, shown in Table 9.2, were used in the stochastic simulation. These spatial averages typically have narrower probability distributions than point statistics (Vanmarcke 1977) and consequently smaller variances. The variance of these spatial averages can be correlated to the point variance using a variance reduction factor (Vanmarcke 1984) through the relationship:

$$(\sigma)_\Gamma = \Gamma_v \times \sigma \tag{9-2}$$

where: σ is the standard deviation of field data (point statistics);

σ_Γ is the standard deviation of the spatial average of data over volume v; and

Γ_v is the square root of the variance reduction factor.

The variance reduction factor depends on the averaging volume, type of correlation structure, and the limit of spatial correlation between field data. Several analytical expressions for the variance reduction factor have been developed in the geotechnical literature and are summarized in Chapter 2. It was assumed in this study that the variance reduction factor would be affected only by the size of the averaging volume in the vertical direction, i.e. layer thickness, as discussed in Chapter 7. It is worth noting that the thicknesses of potentially liquefiable layers were not uniform across the analysis domain. As a result, an average thickness was obtained for each layer, following the procedure of Chapter 7, which was employed to obtain the variance reduction factors presented in Table 9.2. These average thicknesses were divided into horizontal sublayers, as shown in Table 9.2, to maintain a minimum value of 0.70 for the variance reduction factor, which is recommended by Deutsch (2002) to ensure high accuracy upon applying Equation 9-2. It should be emphasized that the outcomes of applying Monte Carlo simulation to these sublayers were not independent due to the vertical correlation between the data in these sublayers. The effect of such correlation was accounted for through implementing a correlation coefficient between the spatial averages of the cone data over these sublayers into the simulation process, as illustrated in Chapter 7.

9.4.   STOCHASTIC ANALYSIS OF LIQUEFACTION SUSCEPTIBILITY

Stochastic analysis of liquefaction susceptibility of the ground at the Marina District was performed by applying a deterministic empirical approach to different realizations of the retrended cone tip resistance data. The CPT-based empirical approach of Robertson and Wride (1998) was used in the analysis to correlate the cyclic resistance ratio, CRR, to the retrended CPT data. The retrended data were obtained by adding back

- 278 -

the linear deterministic trends to the realizations of detrended CPT tip resistance obtained from Monte Carlo simulations. On the other hand, the cyclic stress ratio, CSR, was obtained deterministically from the earthquake magnitude and the maximum surface acceleration using the simplified approach of Seed and Idriss (1971). It should be realized that the CSR can be treated as random variable by considering the variation and uncertainty in earthquake magnitude and maximum surface acceleration. This was, however, beyond the scope of this study and can be addressed in future studies. The factor of safety against liquefaction was obtained stochastically through the relationship:

$$F.S = \frac{CRR}{CSR} \tag{9-3}$$

It should be noted that the maximum surface acceleration was not recorded at the Marina district. However, several bedrock accelerogram records were obtained at several locations in the vicinity of the Marina District, where the horizontal acceleration ranged between 0.05g and 0.11g, as shown in Table 9.3. The ground acceleration on bedrock at the Marina District was estimated as the weighted average of the maximum surface acceleration recorded at these locations, and was found to be around 0.065g. This value was in close agreement with the recorded acceleration on bedrock at the neighboring Yerba Buena Island, which was considered by Bardet et al. (1992) to be representative of the ground acceleration on bedrock at the Marina District. The weights used in the assessment of this average acceleration were considered to be inversely proportional to the distance between the location of the recorded acceleration and the Marina district. The estimated ground acceleration on bedrock together with the design charts of Idriss (1990) and Seed et al. (1994) were used to estimate a maximum surface acceleration of 0.17g at the Marina District. These design charts were developed to take into account the effect of local site conditions on the amplification of ground accelerations on bedrock.

Due to the stochastic nature of the CRR, applying Equation 9-3 resulted in histograms of the factors of safety for each of the potentially liquefiable layers, as shown

in Figure 9.5 for layers L_{1A} and L_{1B}. A summary of the statistical characteristics of the factor of safety against cyclic liquefaction is presented in Table 9.4. The mean factors of safety were found to range between 0.74 and 1.17 for section A, and between 1.03 and 14.26 section C. The coefficients of variation, COV, were assessed to range between 0.05 and 0.16 for section A, and between 0.14 and 0.53 for section C. The probabilities of failure (factor of safety less than unity) were found to range between 19.81% and 100% for section A, and between 0.01% and 46.92% for section C.

Embedment depths and thickness of potentially liquefiable layers play an important role in assessing their liquefaction potential. For example, two layers with same failure probability may have different impacts on the overall (macro) liquefaction potential if there is considerable difference in their thicknesses. Similarly, the influence of two potentially liquefiable layers with same failure probability on the overall liquefaction potential would be different if one layer is at 2 m deep and the other is 8 m deep below ground surface.

As a result, an estimate of equivalent failure probability was developed in Chapter 7 to take into consideration the effect of the thickness and embedment depth of different layers in the form:

$$P = \sum_{j=1}^{n} P_{Fi} \cdot \frac{T_i / Z_i}{\sum T_i / Z_i} \tag{9-4}$$

where: P is the equivalent failure probability of the site;

P_{Fi} is the probability of failure of layer i;

T_i and is the average thickness of layer i; and

z_i is the vertical distance from ground surface to the center of layer i.

- 280 -

The equivalent failure probability for Section A, where different signs of liquefaction were recorded during the Loma Prieta earthquake, was found to be 63.5%. This is in agreement with the findings of Chapter 8, which identified a critical threshold ranging between 1.2% and 11.9% for the equivalent failure probability above which liquefaction is likely to occur. For Section C where no sign of liquefaction was encountered, an equivalent failure probability of 6.5% was assessed. This implied that the critical threshold for the equivalent failure probability could be refined to a range of 6.5% to 11.9%, but continued analysis of liquefaction case histories is required to refine the selection of this value.

9.5. DAMAGE CRITERIA OF LIQUEFACTION

A major concern in liquefaction analysis is the impact of liquefaction occurrence in subsurface layers on overlying structures. Due to the complexity of the problem, few attempts have been made to quantify liquefaction-induced surface damage. Two damage criteria were applied in this chapter: Iwasaki et al. (1978) and Ishihara and Yoshimini (1992).

In a fashion similar to Chapter 8, Iwasaki's damage criterion was applied to the 10,000 realizations of CPT data, used in the previous section, and the total damage potential index, P_L, was determined at each CPT location. The results were then used to generate contours of the probability that P_L would exceed 5 ($P_L > 5$), a threshold associated with significant surface damage. These contours are shown in Figure 9.6 together with different manifestation of surface damage encountered at the site after the earthquake.

The results presented in Figure 9.6 implied that zones of surface damage were associated with a probability of ($P_L > 5$) equal to 0.5%, or more. This is not in a close agreement with the outcomes of the Treasure Island liquefaction analysis in Chapter 8,

- 281 -

where zones of surface damage were considered to be correlated with probability of $(P_L >$ 5) greater than a threshold of 0.1%. This inconsistency between the two sites may question the validity of the P_L approach as a universal measure of quantifying liquefaction-induced damage. This can be attributed to the empirical nature of P_L and the associated simplifying assumptions, such as the linear variation of D(z) with depth. Detailed investigation of the fundamental reasons for the inconsistencies in applying the P_L approach to different potentially liquefiable sites is beyond the scope of this study, which is limited to the application of this damage approach in a geostatistical framework.

Ishihara and Yoshimine (1992) proposed another damage criterion where liquefaction induced damage was correlated to surface settlement. It was suggested that significant surface damage was usually associated with a ground settlement of 10 cm or more. In order to apply this damage criterion, ground settlements were estimated under the effect of the Loma Prieta earthquake using Ishihara's empirical approach (Ishihara 1993). The 10,000 realizations of retrended CPT data were implemented in the analysis resulting in a settlement histogram at each CPT sounding. The mean settlements were found to range from 10.5 cm to 19.1 cm for section A, and from 1.4 cm to 3.8 cm for section C. The coefficients of variation were assessed to range from 0.05 to 0.28 for the section A, and from 0.71 to 1.21 for section C. The settlement analysis results were used to compute the probability of occurrence of liquefaction-induced settlement greater than 10 cm, a value considered to be associated with significant surface damage. Contours of these probabilities are presented in Figure 9.7.

The results presented in Figure 9.7 verified the outcomes of the geostatistical liquefaction analyses of the Wildlife and the Treasure Island sites in Chapters 7 and 8. It was concluded from the analyses of these two sites that zones of surface damage were correlated with a 12% probability, or more, of occurrence of settlement larger than 10 cm. In other words, if the probability that liquefaction induced settlement would exceed 10 cm is smaller than 12% everywhere across a potentially liquefiable site, it would be

anticipated that different manifestations of liquefaction surface damage, such as sand boils, would not occur at that site.

It should be realized that the variation of thickness of different potentially liquefiable layers from one point to another in space might have an impact on the outcome of geostatistical liquefaction analyses. This impact is more pronounced when the output (response) variable varies spatially, as the case for P_L and surface settlement. For the Marina District, this has been accounted for by re-scaling of the outcome of Monte Carlo simulation at each CPT sounding location. The re-scaling process was carried out by transforming the outcome of Monte Carlo simulation from its original distribution to a reference distribution with the same type and mean value but with a modified variance that depends on layer thickness at each CPT sounding location. Details of this transformation process are presented in Chapter 7.

9.6. STOCHASTIC ASSESSMENT OF LIQUEFACTION-INDUCED SETTLEMENT

Another important concern in liquefaction analysis is the ability to reliably predict liquefaction-induced settlement. The results of the stochastic settlement analysis using Ishihara's empirical approach were used to generate contours of the mean settlements across the site, as shown in Figure 9.8.a. In addition, the readings of several settlement points at the site during the Loma Prieta earthquake were located on the contour lines as indicated by the hatched squares in Figure 9.8. The recorded settlements were found to be greater than the computed mean values at few settlement points in section C. This implied that the use of mean values in liquefaction-induced settlement analysis could be on the unsafe (non-conservative) side. This can be attributed to the presence of loose pockets resulting in low factors of safety and higher settlements, which can not be accounted for using the classical deterministic analyses using mean values. Alternatively, it was suggested in Chapter 7 that settlements associated with the upper and lower limits

of the 90% confidence level could be considered as risk-based estimates of liquefaction-induced settlement. Using these estimates in settlement assessment implies that there is only a 5% chance of having actual settlement either higher than the upper limit or smaller than the lower limit. Contours of settlements associated with the lower and upper limits of the 90% confidence level were generated across the Marina District, as shown in Figure 9.8.b and Figure 9.8.c, respectively. It is worth noting that some settlement records showed smaller settlements than those associated with the lower limit of the 90% confidence level. However, the use of these estimates in Chapters 7 and 8 was found to provide a wide range of predicted settlement, which can be considered to be on the over-conservative side. This paradox can be attributed to the following:

1. The uncertainty in the maximum surface acceleration at the Marina District. It is the author's opinion that the computed acceleration was over-estimated and greater than the actual acceleration that hit the site during the Loma Prieta earthquake. This can be overcome through performing a comprehensive probabilistic analysis that takes into consideration the uncertainty in ground acceleration;

2. The number of CPT soundings could be considered insufficient to perform reliable probabilistic analysis of liquefaction-induced settlement;

3. The poor distribution of the CPT sounding across the site, where large zones of the potentially liquefiable layers were not covered by CPT soundings; and

4. The CPT soundings of the University of Southern California, C1 to C4, had cone tip resistance data at 0.30 m interval, which might not lead to a reliable quantification of some elements of soil spatial variability. This was manifested in assuming the model type and the spatial range of layers L3A, L3B and L4B.

9.7. USE OF REPRESENTATIVE DETERMINISTIC CPT PERCENTILES

The above methodology, while being amenable to engineering design, could be regarded as a relatively sophisticated process for engineers with limited statistical background. In addition, relying on mean values may provide a non-conservative

estimate of liquefaction potential as discussed in the previous sections. To overcome these issues, an attempt was made in Chapter 7 to ascertain whether or not more representative soil parameters could be determined that honor detailed ground heterogeneity and can be used more reliably in simplified deterministic analyses.

Based on the analysis of the Wildlife site in Chapter 7, the 0.085 percentile of q_c, i.e. the value of q_c below which 8.5 % of the q_c data occurred, was assessed as a characteristic cone tip resistance value for liquefaction assessment. Upon using this percentile in simplified deterministic liquefaction-induced settlement analysis, it can be decided whether or not potentially liquefiable sites were likely to liquefy. It was suggested that no settlement greater than 10 cm would be predicted anywhere across the site if the earthquake loading was not to trigger liquefaction. Following the above procedure, liquefaction- induced ground settlement was estimated at each CPT sounding, using the 0.085 percentile, resulting in the contour maps shown in Figure 9.9. As can be seen from this figure, the computed settlement was greater than 10 cm everywhere across Section A, while no settlement greater than 10 cm was predicted across section C. This implied that only Section A of the Marina District site would likely liquefy under the effect of the Loma Prieta earthquake, which is in agreement with the actual case.

In a similar fashion, an equivalent cone tip resistance percentile to predict liquefaction-induced surface settlement associated with the upper limit of the 90% confidence interval was developed in Chapter 7. Using this percentile in a simplified deterministic analysis will provide an estimate of surface settlement with a 5% chance that the actual settlement will exceed this estimate. The value of this percentile was found to range from 0.20 to 0.29 for cases where liquefaction would likely to occur, and 0.17 to 0.18 otherwise. Upon using these percentiles in the liquefaction settlement analyses of the Marina District, contours of surface settlements across the site were obtained, as shown in Figure 9.10. Comparing these figures with Figure 9.8 indicated that settlements obtained using these percentiles were in good agreements with those associated with the upper limit of the 90% confidence interval for Section A. This agreement validated the

applicability of these representative CPT percentiles in spite of the fact that Sections A and C showed different overall variabilities from that considered at the Wildlife site. These variabilities were assessed using the Overall Variability Factor (OVF), developed in Chapter 7 as a qualitative measure to compare the variability of potentially liquefiable sites. Sites with higher overall variability were expected to produce higher values of OVF. The OVF was considered as the weighted average of a Local Variability Factor (LVF) calculated at the location of each CPT sounding through the relationship:

$$LVF = \sum_{i=1}^{n} \frac{(COV)_i \cdot (D_F)_i \cdot (T_N)_i}{(R_\Gamma)_i}$$
(9-6)

where: $(COV)_i$ is the coefficient of variation of layer i in percentage;

$(D_F)_i$ is the depth factor that varies linearly from a value of 1 at ground surface to 0 at a depth of 20m;

$(T_N)_i$ is the normalized thickness of layer i with respect to a nominal thickness of 20m; and

$(R_\Gamma)_i$ is a factor that depends on the type of correlation structure and the spatial range.

The weights used in the calculation of OVF were assessed based on the area of influence of each CPT sounding at which LVF is determined. The values of OVF were found to be 4.18 and 7.17 for sections A and C, respectively, compared with a value of 5.49 for the Wildlife site. This implies that the applicability of the representative CPT percentiles developed in Chapter 7 is likely to be insensitive to the overall variability of CPT data recorded at potentially liquefiable sites. This can be attributed to the fact that all elements of soil spatial variability were taken into consideration while assessing the value of such estimates. In other words, it can be said that these estimates are normalized with

- 286 -

respect to different elements of soil spatial variability. However, this needs to be investigated through the analysis of more case histories.

On the other hand, the predicted settlement using these percentiles for Section C were found to be on the non-conservative side compared to those associated with the upper limit of the 90% confidence level. This questions the applicability of these percentiles for potentially liquefiable sites with OVF greater than that of the Wildlife site when liquefaction is not likely to occur. This could be attributed to the fact that the mean factors of safety for these sites and the characteristic percentiles of Chapter 7 are likely to fall within part A of Ishihara's chart, used for settlement prediction, as shown in Figure 9.11. Whereas, applying Monte Carlo simulation to sites with high OVF may result in sampling extreme values statistics falling in part B of Ishihara's chart where the predicted settlement is highly sensitive to the change in factors of safety. As a result, the settlements associated with the upper limit of the 90% confidence level may be greater settlements than those predicted using the characteristic percentiles.

Similarly, Robertson et al. (2000) proposed the use of mean values minus the standard deviation in liquefaction analyses as a risk-based estimate for CPT data. Upon applying this estimate in deterministic settlement analysis of the Marina District, contours of surface settlements were obtained, as shown in Figure 9.12. Comparing this figure with Figure 9.8 indicated a reasonable agreement between the predicted settlements and those of the upper limit of the 90% confidence level for Section A, and a non-conservative settlement estimate for Section C. This can be attributed to the same reasons that have affected the applicability of the characteristic percentiles of Chapter 7, as discussed in the previous paragraph. In addition, it is worth noting that Robertson's estimate did not take into consideration the effect of the spatial correlation structure on the proposed risk-based estimate, which might affect its applicability to sites with different spatial correlation characteristics.

9.8. CONCLUSIONS

The effect of ground heterogeneity on earthquake-induced ground response at the Marina District was investigated in this chapter. This was carried out through assessment of different ground lithologies and applying geostatistical principles to estimate elements of soil spatial variability using the results of several CPT soundings conducted at the site.

The findings of this chapter are in agreement with that of the Wildlife site in Chapter 7, where zones of liquefaction-induced surface damage were considered to be associated with a 1.2% probability, or higher, that total liquefaction damage (P_L) will exceed 5. However, it was found from the analysis of the Treasure Island in Chapter 8 that these zones are likely to be bounded with a critical threshold of 0.1% that P_L will exceed 5. The significant disparity between these values provides little insight into the damage approach. Alternatively, the wide range in threshold probability values may cast some doubt on the P_L approach as a universal measure of quantifying liquefaction-induced damage. Additional case histories must be analyzed to reach a formal conclusion regarding the P_L approach. On the other hand, this chapter validated the recommendation of Chapters 7 and 8 that surface damage zones were likely to be associated with a 12% probability, or higher, that liquefaction-induced settlement will be greater than 10 cm.

This chapter verified the applicability of the equivalent failure probability approach for liquefaction prediction. This approach was developed in Chapter 7 to account for the effect of thickness and embedment depth of potentially liquefiable layers on their failure probabilities and its implications on the site susceptibility to liquefaction. The outcomes of this chapter were used to refine the critical threshold of the equivalent failure probability to be in the range of 6.5% and 11.9%, rather than the 1.2% to 11.9% range obtained from the analysis of the Treasure Island in Chapter 8. Liquefaction occurrence is likely to be correlated to equivalent failure probabilities greater than such critical threshold. However, care should be taken while using this threshold due to the uncertainty associated with the maximum surface acceleration at the Marina District. This

- 288 -

uncertainty was manifested in recorded settlement outside the predicted range of settlement associated with the upper and lower limit of the 90% confidence level. This implies that such uncertainty is likely to have a profound effect on the methodology applied in this study. This can be overcome by performing comprehensive probabilistic analysis that takes into consideration the uncertainty in earthquake loading.

This chapter verified the applicability of the 0.085 percentile, developed in Chapter 7 as a characteristic cone tip resistance value that can be used in simplified deterministic analysis for the purpose of liquefaction prediction. Similarly, this chapter verified the applicability of the 0.20 and 0.29 percentiles as characteristic values for settlement prediction for potentially liquefiable sites when liquefaction is likely to occur. On the other hand, the applicability of the 0.17 and 0.18 percentiles, as representative values for sites where liquefaction is not likely to occur, was questioned in this chapter for sites of overall variability greater than that of the Wildlife site, California. However, more efforts are needed to refine and verify these representative values through the analyses of more case histories.

9.9.   REFERENCES

Bardet J. P. and Kapuskar, M. 1993. Liquefaction sand boils in San Francisco during the 1989 Loma Prieta earthquake. Journal of the Geotechnical Engineering Division, ASCE, 119, GT(3): 543-562.

Bardet J. P., Kapuskar, M., Martin, G. R., and Proubet, J. 1992. Site response analysis. The Loma Prieta, California, earthquake of October 17, 1989; Marina District; strong ground motion and ground failure. U. S. Geological Survey Professional Paper 1551-F, pp. 85-114.

Deutsch, C. V. 2002. Geostatistical reservoir modeling. Oxford University press.

Deutsch, C. V. and Journel, A. G. 1998. GSLIB geostatistical software library. Oxford University press.

Fenton, G. A. and Vanmarcke, E. H. (1991). Spatial variation in liquefaction risk assessment. Proceedings of the geotechnical Engineering Congress, Boulder, Colorado, USA. Geotechnical Special Publications, No. 27, Vol.1, pp. 594-607.

Idriss I. M. 1990. Response of soft sits during earthquakes. Proceedings of H. Bolton Seed Memorial Symposium, Vancouver, BC, Canada, Vol.2, pp. 273-289.

Ishihara, K. 1993. Liquefaction and flow failure during earthquakes. Geotechnique, 43 (3): 351-415.

Ishihara, K. and Yoshimine, M. 1992. Evaluation of settlements in sand deposits following liquefaction during earthquakes. Soils and Foundations, 32 (1): 178-188.

Iwasaki, T., Tatsuoka, F., Tokida, F., and Yasuda, S. 1978. A practical method for assessing soil liquefaction potential based on case studies at various sites in Japan. Proceedings of the Second Conference on Microzonation, San Francisco, CA, USA, Vol. (2), pp. 885-896.

O'rourke, T. D and Pease, J. W. 1992. Large ground deformations and their effects on lifeline facilities; 1989 Loma Prieta earthquake. Case studies of Liquefaction and Lifeline Performance during Past Earthquakes; Volume 2, United States case studies. Technical Report NCEER-92-0002, pp. 5-1 – 5-85

O'rourke, T. D and Pease, J. W. 1997. Mapping liquefiable layer thickness for seismic hazard assessment. Journal of the Geotechnical and Geoenvironmental Engineering Division, ASCE, 123 GT(1): 46-56.

Palisade Corporation. 1996. @Risk: Risk analysis and simulation add-in for Microsoft Excel or Lotus 1-2-3. Palisade Corporation, NY, USA.

Pease, J. W. and O'rourke, T. D. 1997. Seismic response of liquefaction sites. Journal of the Geotechnical and Geoenvironmental Engineering Division, ASCE, 123 GT (1): 37-45.

Popescu, R., Prevost, J. H., and Deodatis, G. 1998. Characteristic percentile of soil strength for dynamic analysis. Proc. of the 1998 Conf. on Geotechnical Earthquake Eng. and Soil Dynamics III, Part 2 (of 2), Seattle, WA, USA, pp. 1461-1471.

Robertson, P. K. 1990. Soil classification using the cone penetration test. Canadian Geotechnical Journal, 27 (1): 151-158.

Robertson, P. K. and Wride, C. E. 1998. Evaluating cyclic liquefaction potential using the cone penetration test. Canadian Geotechnical Journal, 35 (3): 442-459.

Robertson, P.K., (Fear) Wride, C.E., List B.R., Atukorala, U., Biggar, K.W., Byrne, P.M., Campanella, R.G., Cathro, D.C., Chan, D.H., Czajewski, K., Finn, W.D.L., Gu, W.H., Hammamji, Y., Hofmann, B.A., Howie, J.A., Hughes, J., Imrie, A.S., Konrad, J-M., Küpper, A., Law T., Lord, E.R.F., Monahan, P.A., Morgenstern, N.R., Phillips, R., Piché, R., Plewes, H.D., Scott, D., Sego, D.C., Sobkowicz, J., Stewart, R.A., Watts, B.D., Woeller, D.J., Youd, T.L., and Zavodn, Z. 2000. "The CANLEX project: summary and conclusions". Canadian Geotechnical Journal, 37 (3), 563-591Seed, H. B. and Idriss, I. M. 1971. Simplified procedure for evaluating soil liquefaction potential. Journal of the Soil Mechanics and Foundation Division, ASCE, 97, SM(9): 1249-1273.

Rollins, K. M. and McHood, M. D. 1998. Comparison of computed and measured liquefaction-induced settlements in the Marina District, San Francisco. The Loma Prieta, California, earthquake of October 17, 1989; Liquefaction. U. S. Geological Survey Professional Paper 1551-B, pp. 223-239.

Seed, H. B. and Idriss, I. M. 1971. Simplified procedure for evaluating soil liquefaction potential. Journal of Soil Mechanics and Foundation Division, ASCE, 97 (SM9): 1249-1273

Seed, R. B., Dickenson, S. E., and Mok, Chin Man. 1994. Site effects on strong shaking and seismic risk: recent developments and their impact on seismic design codes and practice. Proceedings of the Structures Congress '94, Atlanta, Georgia, USA. Vol.1, pp. 573-578.

Tokimatsu, K. and Seed, H. B. 1987. Evaluation of settlements in sands due to earthquake shaking. Journal of the Geotechnical Engineering Division, ASCE, 113, GT(8): 861-878.

Vamarcke, E. H. 1984. Random fields, analysis and synthesis. MIT Press, Cambridge, MA, USA.

Vanmarcke, E. 1977. Probabilistic modeling of soil profiles. Journal of the Geotechnical Engineering Division, ASCE, 103 GT(11): 1227-1245.

Table 9.1. Statistical properties of detrended CPT tip resistance for different layers

Layer	Mean (kPa)	Standard Deviation (kPa)	Variogram Characteristics		
			Model	Vertical Range (m)	Horizontal Range (kPa)
L_{1A}	0.038	862	Exponential	0.65	11.05
L_{2A}	0.004	444	Gaussian	0.80	13.6
L_{3A}	-0.23	380	Gaussian	0.80	13.6
L_{4A}	0.003	1466	Spherical	1.40	23.8
L_{1B}	-0.117	585	Exponential	0.75	12.75
L_{2B}	-0.065	4418	Exponential	2.15	36.55
L_{3B}	0.161	1938	Exponential	2.15	36.55
L_{4B}	0.049	668	Exponential	2.15	36.55

Table 9.2. Variance reduction factor for different potentially liquefiable layers at the Marina District

Layer	L_{1A}	L_{2A}	L_{3A}	L_{4A}	L_{1B}	L_{2B}	L_{3B}	L_{4B}
Average thickness (m)	0.92	1.77	0.59	1.63	0.45	1.80	0.85	0.58
Number of horizontal segments	4	3	1	2	2	3	1	1
Variance reduction factor	0.72	0.80	0.80	0.72	0.76	0.77	0.70	0.78

Table 9.3. A summary of recorded maximum accelerations on bedrock at different locations in the vicinity of the Marina District

Location	Distance from Marina District (km)	Maximum acceleration	
		Horizontal (g)	Vertical (g)
Rincon Hill	4.90	0.09	0.03
Pacific Heights	1.70	0.05	0.03
Telegraph Hill	2.70	0.08	0.03
Cliff House	6.70	0.11	0.08
Yerba Buena Island	7.00	0.06	0.03

Table 9.4. A summary of the statistical characteristics of the factor of safety against cyclic liquefaction for different potentially liquefiable layers

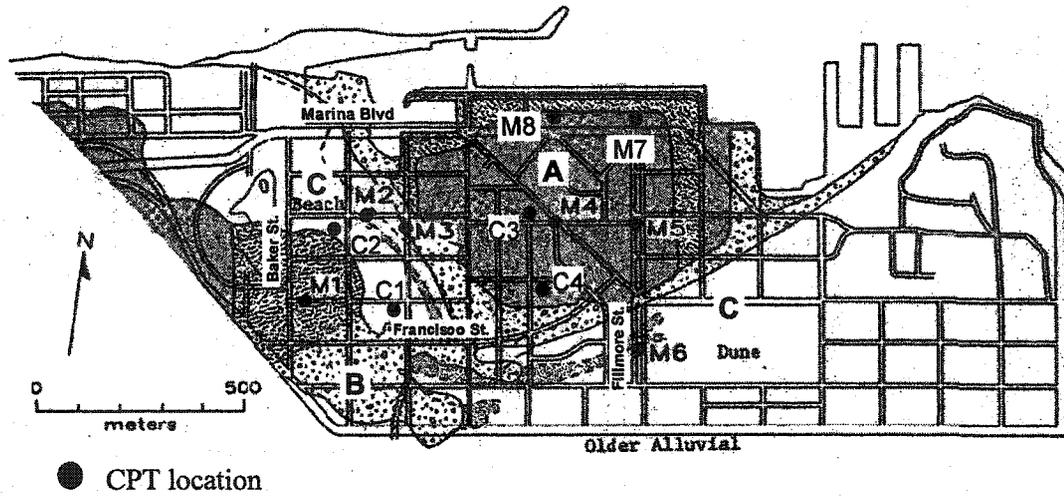| Layer	L_{1A}	L_{2A}	L_{3A}	L_{4A}	L_{1B}	L_{2B}	L_{3B}	L_{4B}
Mean	1.05	0.84	0.74	1.17	1.48	5.46	14.26	1.03
Coefficient of variation	0.09	0.06	0.05	0.16	0.14	0.53	0.22	0.16
Probability of failure (%)	33.95	99.86	100	19.81	1.13	5.20	<0.01	46.92

Figure 9.1. Layout of CPT data locations at the Marina District. (A: sections underlain by hydraulic fill, B: sections underlain by dumped fill, and C: sections underlain by natural ground). modified from Bennett (1990).
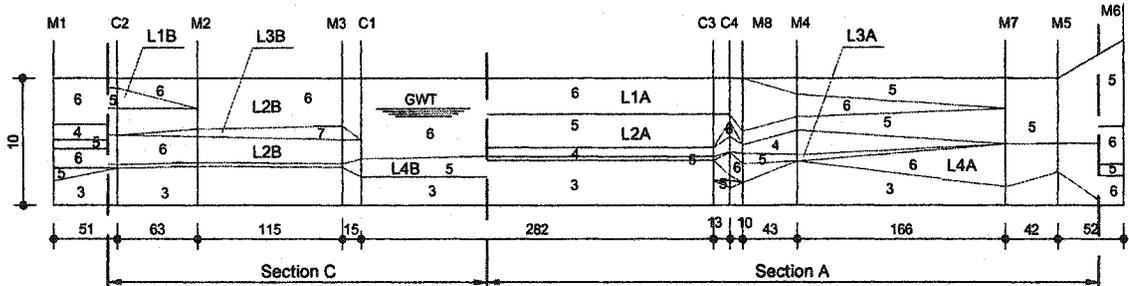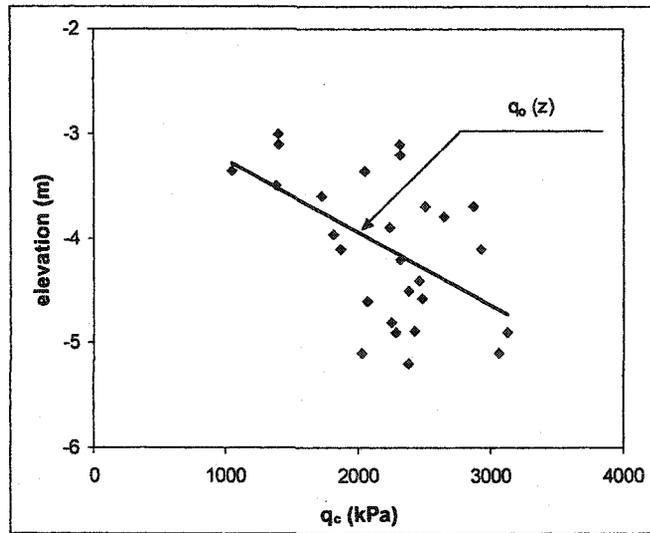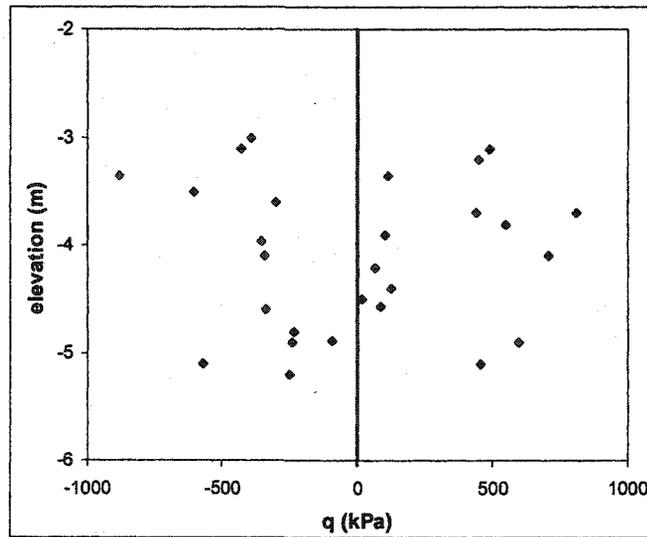

Figure 9.2. A longitudinal west-east view showing the lithological distribution across the Marina District (positions of CPT soundings are shown in Figure 1; numbers represent soil behavior type based on soil behavior type index Ic)
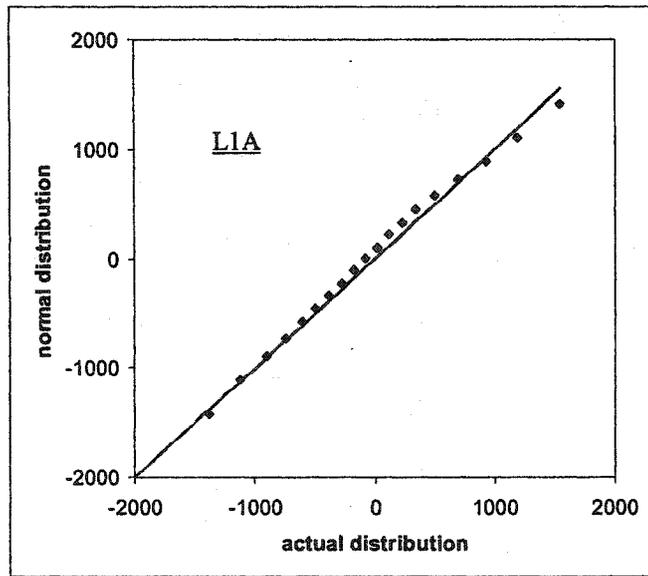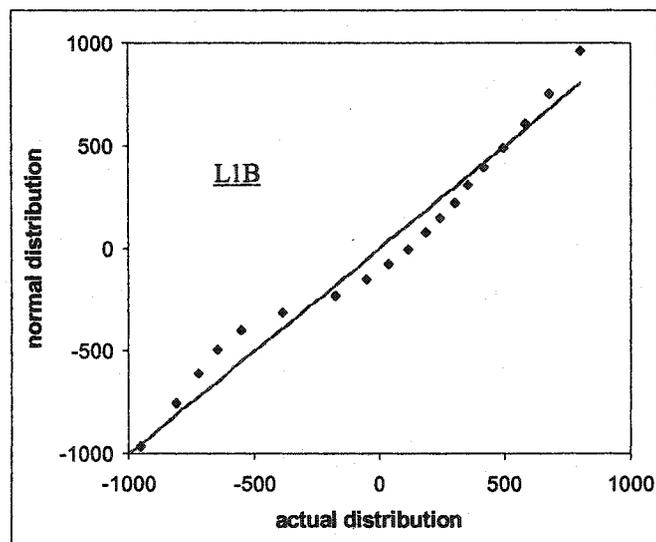
- 294 -

(a)

(b)

Figure 9.3. Detrending of cone data for layer L_{2A}. a) identifying linear vertical trend; and b) detrended data.

(a)

(b)

Figure 9.4. Close agreement between probability distributions of detrended CPT data and normal distribution using Q-Q plots for layers L_{1A} and L_{1B}
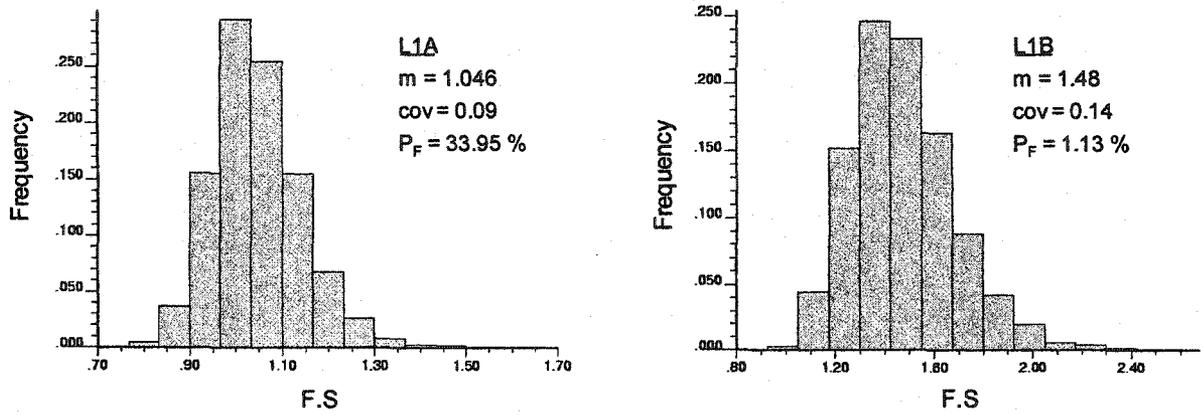
- 296 -

Figure 9.5. Histograms of the factor of safety against liquefaction for layer L_{1A} and L_{1B} at the Marina District.
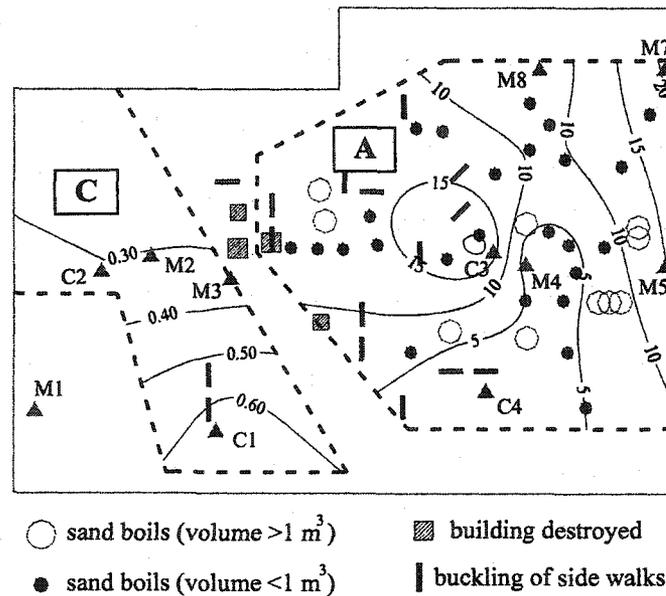

Figure 9.6. A site plan showing contours of probability (%) of occurrence of total liquefaction damage potential (P_L) greater than 5.
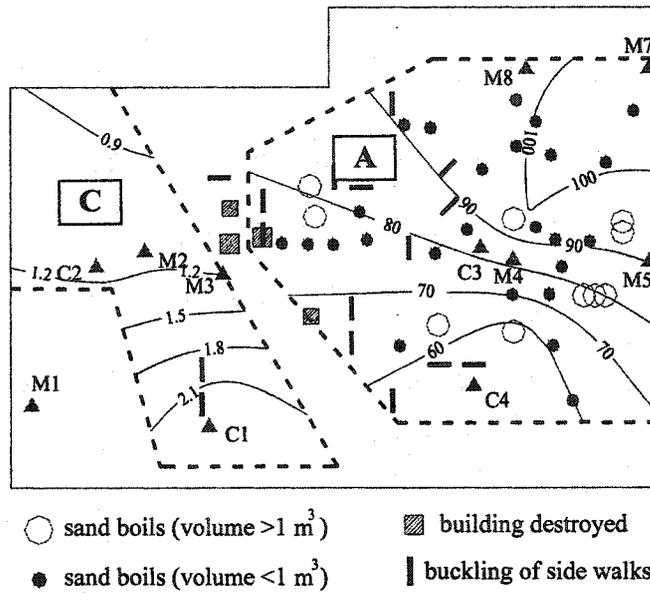
Figure 9.7. A site plan showing contours of probability (%) of occurrence of liquefaction-induced settlement greater than 10 cm.
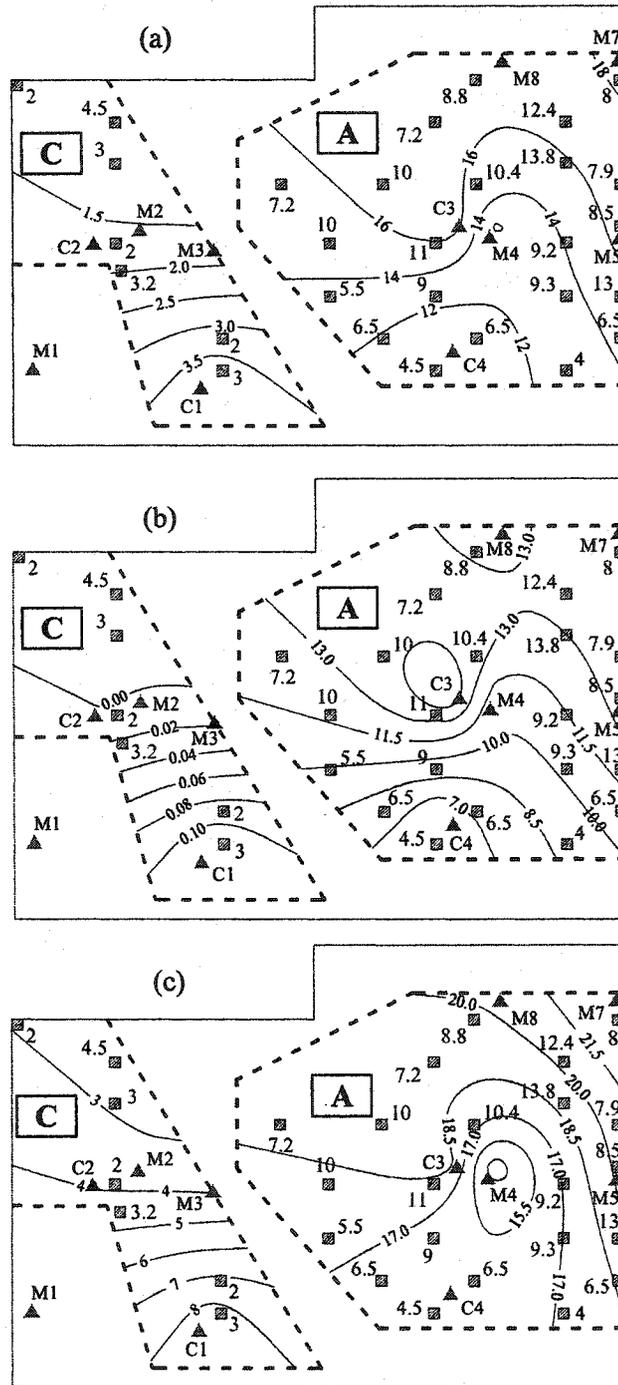
Figure 9.8. A site plan showing contours of computed settlements (in cm) across the Marina District under the effect of the Loma Prieta earthquake. a) mean settlement; b) lower limit of 90% confidence interval; and c) upper limit of 90% confidence interval.
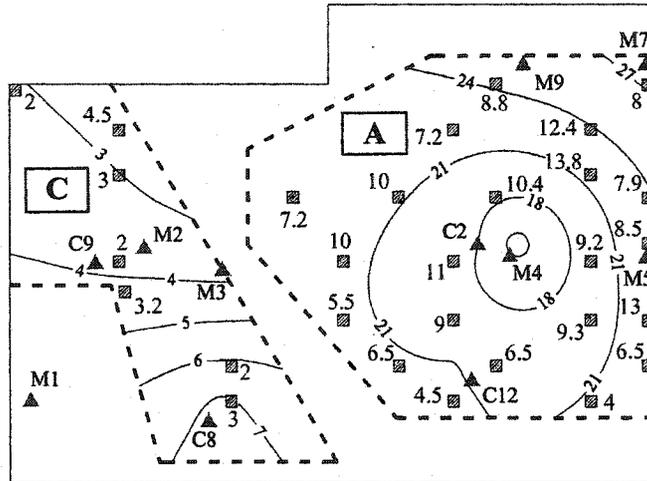
- 299 -

Figure 9.9. A site plan showing contours of computed settlements (in cm) across the Marina District using the 0.085 percentile of the CPT tip resistance data. (hatched squares represent measured settlements at the site in cm)

(a)
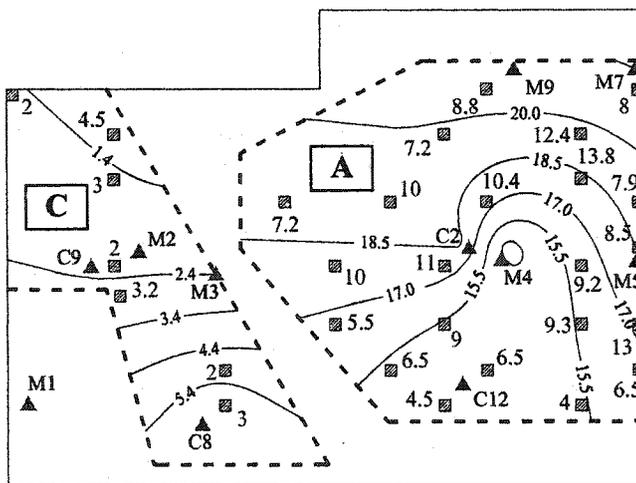
(b)

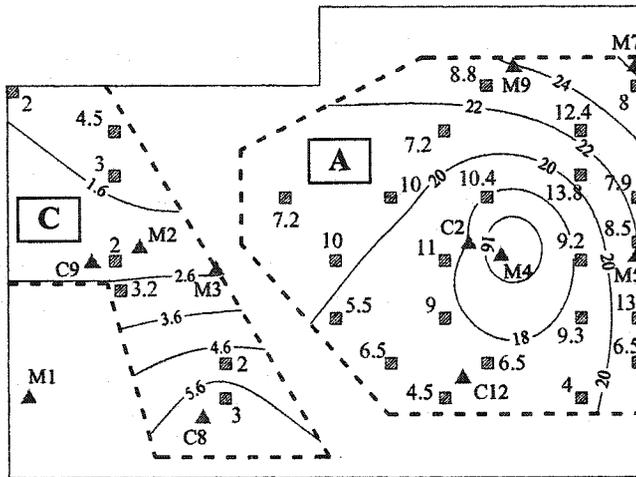Figure 9.10. A site plan showing contours of computed settlements (in cm) across the Marina District using representative CPT tip resistance percentiles. a) the upper limits for estimated settlements using the 0.20 and the 0.17 percentiles for sections A and C, respectively; and b) the upper limits for estimated settlements using the 0.20 and the 0.17 percentiles for sections A and C, respectively.

Figure 9.11. Post-liquefaction volumetric strain as a function of factor of safety (modified from Ishihara 1993).
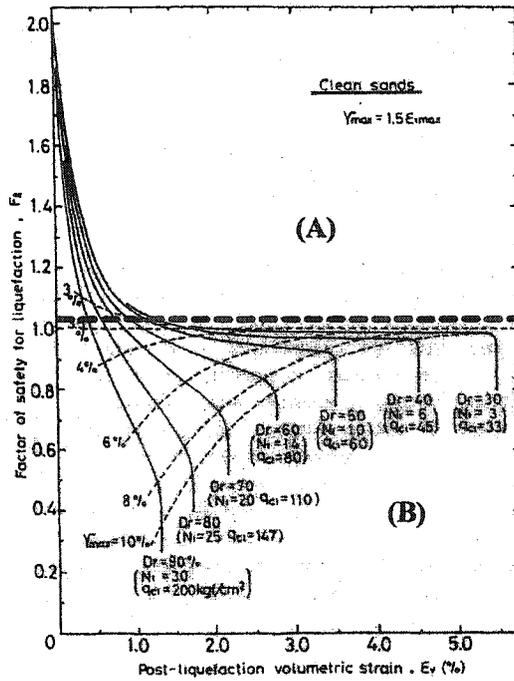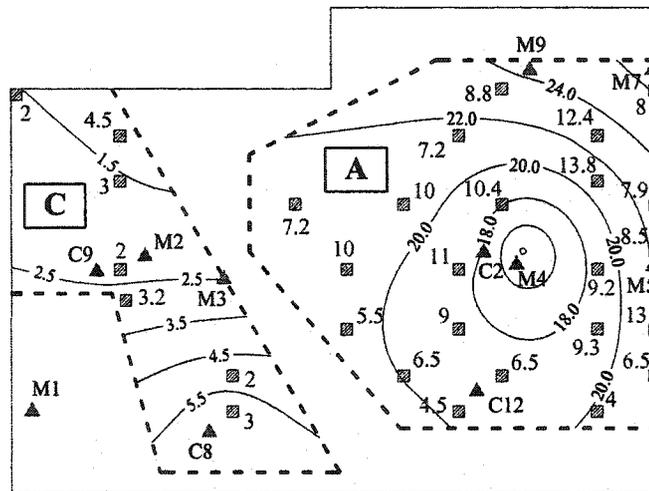

Figure 9.12. A site plan showing contours of computed settlements (in cm) using (m-σ) as a representative CPT tip resistance (Robertson 1995).

- 302 -

CHAPTER 10

SUMMARY, CONCLUSIONS AND RECOMMENDATIONS

10.1. SUMMARY OF THIS RESEARCH STUDY

Almost all natural soils are heterogeneous in nature. This heterogeneity can be classified into two main categories. Lithological heterogeneity, which can be manifested in the form of thin soft/stiff layers embedded in a stiffer/softer media or the inclusion of pockets of different lithology within a more uniform soil mass. The second source of heterogeneity can be attributed to inherent soil variability, which is the spatial variation of soil properties from one point to another in space due to different deposition conditions and loading history.

An attempt was made in this study to quantify the effect of different manifestations of ground heterogeneity on engineering behavior of soils, which included:

1. Assessment of the influence of intercalated clay seams on the macro (overall) behavior of sand media below strip footings, in terms of their strength and deformability. This was carried out in a numerical analysis framework using the FLAC software (Itasca Consulting Group Inc. 2000);

2. Developing a risk-based design methodology for co-depositional thickened fine tailings – sand embankments that takes into consideration the effect of spatial distribution of fine tailings pockets on the overall stability of these disposal systems. This was assessed numerically using the FLAC software, which employs the strength reduction technique (Dawson et al. 1999) to assess the stability of natural and man-made slopes;

3. Quantification of spatial variability of soil properties and its implications on soil behavior under static loading in the form of a strip footing resting on spatially variable sand media. This was carried out using the GSLIB software (Deutsch and

- 303 -

Journel 1998) to generate several realizations of stochastic soil properties, which were then implemented in deterministic numerical analyses using the FLAC software; and

4. Assessment of the impact of soil spatial variability on its behavior under dynamic loading, which was carried out by analyzing several liquefaction case histories in California, USA. This was accomplished by using the @Risk software (Palisade Corporation 1996) to generate several realizations of CPT data at these potentially liquefiable sites. These realizations were implemented in CPT-based empirical analyses techniques, such as Robertson and Wride (1998) and Ishihara (1993).

10.2. GENERAL CONCLUSIONS

Different analysis techniques, discussed in the previous section, were applied in this study resulting in several detailed conclusions, as presented in Chapters 3 to 9. A general summary of these conclusions is provided below.

Generally, the influence of different types of soil heterogeneity on engineering behavior of soil was found to be problem dependent. Quantitative assessment of this influence can be obtained by separate comprehensive analyses of each geotechnical field problem. In addition, using mean values of soil properties in deterministic geotechnical analyses can be on the unsafe (non-conservative) side as they can not account for the scatter of field data and their spatial correlation.

Neglecting lithological heterogeneity in geotechnical design, in terms of intercalated soft to medium clay seams at the center of bigger sand masses, can have a catastrophic impact on soil behavior under static loading. This was manifested in ultimate (failure) pressures of strip footings resting on these heterogeneous media being smaller than the allowable footing pressure of a uniform sand, obtained using a factor of safety equal to 3. An attempt was made to homogenize these heterogeneous media by

developing simplified equivalent (representative) soil parameters for use in engineering design. Design charts of these equivalent parameters are provided in Chapter 3.

Probability of failure of co-depositional fine tailings – sand embankments was found to be sensitive to several factors, such as undrained shear strength of fine tailings, side slope and height of these embankments. A minimum undrained shear strength of fine tailings equal to 0.23 kPa was identified below which it is unlikely to obtain stable embankments. In a similar fashion, a critical threshold of 20 degrees was identified for embankments side slopes above which it is unlikely to obtain stable co-depositional embankments. A critical probability of failure of 34% was identified to be correlated to irreparable damage to the overall stability of co-depositional embankments. An allowable probability of failure of 17% was proposed for use in engineering design, with only 5% chance that vertical displacements at the embankment crest will exceed a value of 0.28% of the embankment height immediately after construction.

Footing pressures associated with a failure probability of 1% for strip footings resting on spatially variable sand media were proposed as upper limits for safe ranges of stress application. Probability density functions and spatial correlation structure models were found to have insignificant influence on the probability of failure within these ranges compared to coefficient of variation and limit of spatial continuity. The values of these limits were found to increase with higher mean normal stress in the soil mass. Different risk-based estimates for characteristic elastic modulus of sand were introduced, such as mean values, estimates associated with linear loss functions, and upper and lower limits of the 90% confidence level. Design charts for these estimates are provided in Chapter 6 where they found to be highly sensitive to coefficient of variation and limit of spatial continuity.

Spatial variability of soil properties has a profound effect on liquefaction analyses. This variability was employed in geostatistical analyses to assess the probability of failure of potentially liquefiable sites. An equivalent failure probability was developed

- 305 -

in this study to take into consideration the effect of embedment depth and thickness of potentially liquefiable layers on ground liquefaction susceptibility. Liquefaction occurrence is likely to be associated with equivalent probability of failure above a critical threshold ranging between 1.2 and 12%. In addition, an empirical factor, the Overall Variability Factor (OVF), was developed to compare the degree of variability of different potentially liquefiable sites. The higher the value of OVF, the greater the ground variability expected at the site.

An attempt was made in this study to quantify liquefaction-induced surface damage in a probabilistic analysis framework. It was concluded that zones of surface damage were likely to be associated with a 12% probability, or higher, that liquefaction-induced settlement will be greater than 10 cm.

Risk-based characteristic CPT percentiles were obtained for use in simplified deterministic analysis to assess liquefaction susceptibility and ground settlement while continuing to honor detailed ground variability. It was found that liquefaction was unlikely to occur if no settlement greater than 10 cm was predicted anywhere across the site upon the use of a percentile of q_c equal to 0.085 in a deterministic analysis framework. More efforts are needed to obtain characteristic percentiles for liquefaction-induced settlement prediction as these percentiles were found to be dependent on the shear stress generated in the ground during earthquake excitation. However, a range of percentiles between 0.17 and 0.29 was obtained in this study based on the upper limit of the 90% confidence interval. In other words, using this range in simplified deterministic analyses implies that there will be only a 5% chance that actual ground settlements will be greater than the predicted values.

Uncertainty in maximum earthquake-induced ground acceleration can have a profound effect on geostatistical liquefaction analyses. In addition, using mean values of ground accelerations obtained form different design charts developed to take into account the effect of local site conditions on the amplification of ground accelerations may

- 306 -

provide misleading results. The effect of this uncertainty in ground acceleration can be overcome, however, by performing comprehensive probabilistic analysis that takes into consideration the uncertainty in earthquake loading.

10.3. RECOMMENDATIONS FOR FUTURE RESEARCH

This research study can be considered as a first step towards rational consideration of ground heterogeneity in geotechnical design. As a result, the outcomes of this study need to be verified and refined by comprehensive research studies in the different geotechnical applications considered in this thesis.

More efforts are needed to assess the sensitivity of the equivalent soil parameters developed for heterogeneous sand media with intercalated clay seams to other factors, such as:

1. The constitutive model employed in the numerical analyses;
2. Uncertainty in undrained shear strength of the clay seams; and
3. Footing geometry, in terms of different footing types such as rectangular and circular footings.

It is highly recommended that the risk-based design methodology developed in this study for co-depositional sand - fine tailings embankments be verified by field data obtained from a full scale test embankment. In addition, different measures should be explored to improve the maximum undrained shear strength of fine tailings obtained from the thickening process as it has a profound effect on the performance of these embankments. Attention should be given to construction to investigate whether a surface shell of cohesionless soil can be built to prevent shallow shear failures in these embankments. It is worth noting that this design methodology of co-depositional sand - fine tailings embankments should be extended to take into account some factors, which were not considered in the current study, such as:

- 307 -

1. Uncertainty in undrained shear strength of thickened tailings;

2. Effect of different sand/fine tailings ratios on stability analysis;

3. Thixotropy of fine tailings and its implications on displacement fields within the embankments;

4. Possible spatial correlation between fine tailings pockets within mixed fine tailings dams due to the used deposition technique; and

5. Sand shear strength and deformability on the performance of the mixed fine tailing dam.

Attention should be given to other sources of uncertainty associated with liquefaction assessment and their implications on the outcomes of geostatistical analyses. These uncertainties can be summarized as follows:

1. Model uncertainty, which can be manifested in uncertainty in maximum ground surface acceleration, magnitude scaling factor, and the curves used for the assessment of the cyclic resistance ration (CRR) associated with earthquakes of magnitude 7.5;

2. Geometrical uncertainty, in the form of uncertainty in thickness of potentially liquefiable layers and location of ground water table; and

3. Random measurement errors, such as those associated with sleeve friction resistance of cone penetration test.